



University of Pretoria

Department of Civil Engineering

The Influence of Fibre Spatial Characteristics on the Flexural Performance of SFRC

Tiaan Bosman

November 2018

The Influence of Fibre Spatial Characteristics on the Flexural Performance of SFRC

Tiaan Bosman

A project report in partial fulfilment of the requirements for the degree of

MASTER OF ENGINEERING (STRUCTURAL ENGINEERING)

In the

FACULTY OF ENGINEERING

UNIVERSITY OF PRETORIA

November 2018

PROJECT REPORT SUMMARY

THE INFLUENCE OF FIBRE SPATIAL CHARACTERISTICS ON THE FLEXURAL PERFORMANCE OF SFRC

T BOSMAN

Supervisor: **Professor Doctor E.P. Kearsley**
Department: **Civil Engineering**
University: **University of Pretoria**
Degree: **Master of Engineering (Structural Engineering)**

The addition of discontinuous discrete fibres to concrete has repeatedly been shown as an effective method to overcome the inherently brittle nature of concrete. The resulting composite has enhanced toughness and impact resistance and is broadly referred to as Fibre-Reinforced Concrete (FRC). Although the benefits of implementing FRC are evident, the high variability associated with FRC has frequently been cited as a characteristic stunting vast structural application of the material. This research is focussed on the spatial distribution of fibres and the way it affects flexural performance. A thorough understanding of the influence of fibre spatial distribution on composite performance is the first step in incorporating fibre distribution into material and structural design procedures and aids the pursuit of effective and optimal implementation of FRC in practice.

The study was aimed at not only investigating the influence of fibre distribution on flexural performance but also evaluating the effect of fibre length and volume content on the fibre spatial characteristics.

The experimental framework considered two hook-ended steel fibres with different lengths incorporated into a 50 MPa concrete mixture at volume contents ranging from 40 kg/m³ to 120 kg/m³. Flexural response was obtained using three-point bending tests on notched specimen, after which each specimen was cut adjacent to the crack plane and prepared for image analysis. An image processing algorithm was developed to automatically extract the fibre locations that were used to describe the fibre spatial characteristics.

Spatial distribution was explored by evaluating the uniformity of fibres across a section, the inter-batch variability of fibre distribution, and the degree of clustering. A geometric descriptor of fibre spacing was defined using Voronoi diagrams generated from image data and employed in a unique approach developed for quantifying fibre spatial characteristics. An alternative approach was developed and used to compare the spatial metrics resulting from the Voronoi approach.

The findings of the study highlight the role of fibre length and content on the spatial distribution of fibres and it is revealed that the sectional uniformity, inter-batch spatial variability, and degree of clustering are dependent on the number of fibres in the cross section.

Furthermore, the results demonstrate the substantial influence of fibre distribution on the flexural performance of FRC. It is concluded that the variability in flexural strength reduces as the variation in fibre spatial distribution reduces and that extensive clustering has an adverse effect on the effective resistance provided by fibres.


DECLARATION

I, the undersigned hereby declare that:

- I understand what plagiarism is and I am aware of the University's policy in this regard;
- The work contained in this thesis is my own original work;
- I did not refer to work of current or previous students, lecture notes, handbooks or any other study material without proper referencing;
- Where other people's work has been used this has been properly acknowledged and referenced;
- I have not allowed anyone to copy any part of my thesis;
- I have not previously in its entirety or in part submitted this thesis at any university for a degree.

DISCLAIMER:

The work presented in this report is that of the student alone. Students were encouraged to take ownership of their projects and to develop and execute their experiments with limited guidance and assistance. The content of the research does not necessarily represent the views of the supervisor or any staff member of the University of Pretoria, Department of Civil Engineering. The supervisor did not edit the final report and is not responsible for any technical inaccuracies, statements or errors. The conclusions and recommendations given in the report are also not necessarily that of the supervisor, sponsors or companies involved in the research.

Signature of student: 

Name of student: **Tiaan Bosman**

Student number: **11166348**

Date: **2018/11/13**

Number of words in report: 29812 words

ACKNOWLEDGEMENTS

This research was carried out under the supervision of *Professor E.P. Kearsley* to whom the author would like to express his sincere gratitude for her continued guidance and constructive contributions towards this study. The author wishes to commend and convey his appreciation to all those who have been part of this dissertation and would like to recognise the following persons in particular:

- The *Concrete Institute* for their financial support provided over the course of the author's postgraduate studies,
- *Mr. Derek Mostert* for his advice and assistance regarding the mix designs as well as his valued contributions towards preparing the specimens for image analysis,
- *The concrete laboratory staff* for their support during the production of specimens without whom this experimental undertaking would have been insurmountable,
- *Mr. Jaco Botha* and *Mr. Johan Scholtz* for their technical and practical input regarding the strength testing carried out as part of this study.

Finally, I would like to acknowledge the encouragement, enthusiasm, love, support, and patience provided by my parents, brothers, friends, family, and most of all my wife. Thank you all for the sacrifices you have made so I could pursue my interest. This work would not have realised without the substantial contributions made by each of you.

Tiaan Bosman

November, 2018

TABLE OF CONTENTS

CHAPTER 1. Introduction	1
1.1 Background	1
1.2 Research Statement and Objectives.....	2
1.3 Scope of the Study.....	3
1.4 Methodology	3
1.5 Organisation of the Report	4
CHAPTER 2. Literature Review	6
2.1 Background	6
2.2 Post-Cracking Tensile Behaviour of FRC.....	6
2.3 Factors Affecting Pull-Out Response	7
2.3.1 Fibre shape	7
2.3.2 Fibre material	8
2.3.3 Fibre diameter.....	9
2.3.4 Fibre embedded length	9
2.3.5 Fibre orientation	10
2.3.6 Water/binder ratio of matrix.....	12
2.3.7 Filler content.....	12
2.4 Fibre Orientation	12
2.4.1 Introduction	12
2.4.2 Orientation factor	13
2.4.3 Estimating fibre orientation and distribution.....	14
2.4.4 Dupont and Vandewalle (2005) orientation model	17
2.4.5 Influence of fibre effectiveness on tensile behaviour.....	17
2.5 Spatial Distribution of Fibres	19
2.6 Evaluating Fibre Orientation and Distribution	24
2.6.1 Photometric methods.....	24
2.6.2 X-ray computed tomography.....	26
2.6.3 Indirect methods for conductive fibre-reinforced composites.....	28
2.7 Strength Testing Methods	29
2.7.1 RILEM TC 162-TDF (2002) calculation procedure.....	31
2.8 Discussion on Reviewed Literature.....	34
CHAPTER 3. Methodology.....	36
3.1 Background	36
3.2 Experimental Programme and Constituent Materials.....	37
3.3 Production Method	38
3.3.1 Mixing procedure	38
3.3.2 Casting procedure.....	38
3.3.3 Specimen curing and preparation for testing.....	39
3.4 Compressive Strength Tests	39
3.5 Flexural Strength Test: Setup and Procedure	41
3.6 Image Acquisition and Feature Extraction	42
3.6.1 Sample Preparation and Image Acquisition	43
3.6.2 Image Processing Algorithm	45
3.6.3 Feature Extraction: The Voronoi Diagram.....	48

3.7	Fibre Orientation	49
3.8	Quantifying Spatial Distribution with Fibre Count	51
3.8.1	Degree of clustering	51
3.8.2	Fibre homogeneity and variability.....	53
3.9	Quantifying Spatial Distribution with Voronoi Data	54
3.9.1	Random point process	54
3.9.2	Degree of clustering	57
3.10	Discussion on Methodology	60
CHAPTER 4. Experimental Results		62
4.1	Background	62
4.2	Flexural Response Results.....	62
4.3	Flexural Strength Design Parameters	67
4.4	Fibre Count and Spatial Distribution Results	71
4.5	Relating Orientation Theory and Fibre Count	77
4.6	Discussion on Results.....	80
CHAPTER 5. Statistical Analysis of Image Data.....		82
5.1	Background	82
5.2	Statistical Analysis of Fibre Count Distribution	82
5.2.1	Degree of clustering	82
5.2.2	Fibre homogeneity and variability.....	86
5.3	Statistical Analysis of Fibre Spatial Distribution	89
5.3.1	Fibre dispersion and variation	89
5.3.2	Degree of clustering	94
5.4	Comparing the Output Metrics of the Two Approaches	96
5.5	Discussion on Image Analysis Results.....	99
CHAPTER 6. Relating Mechanical Properties and Fibre Distribution Characteristics.....		101
6.1	Background	101
6.2	Evaluating Flexural Strength with Respect to Fibre Count.....	101
6.3	Influence of Fibre Dispersion on Strength and Variability	104
6.4	Influence of Clustering on Equivalent Fibre Resistance	108
6.5	Discussion on the Identified Relationships	109
CHAPTER 7. Conclusions and Recommendations		111
7.1	Conclusions	111
7.2	Influence of Fibre Length and Content on Spatial Distribution	111
7.3	Effect of Fibre Spatial Distribution on Mechanical Performance	112
7.4	Recommendations for Future Research.....	113
CHAPTER 8. References		115
APPENDIX A - Specimen Results		123
A.1	Stress-CMOD Curves.....	123
A.2	Specimen Strength and Spatial Results: 30mm Mixtures	138
A.3	Specimen Strength and Spatial Results: 60mm Mixtures	145
APPENDIX B - Batch 80-60-a Results		152
B.1	Chapter 4	152
B.2	Chapter 5	152
B.3	Chapter 6	153

LIST OF TABLES

Table 3-1: Mixture components by mass	38
Table 3-2: Elastic modulus and cylinder strength of plain concrete mixture	41
Table 3-3: MOR results of beams without fibres	42
Table 3-4: Results from simulations of random spatial patterns with varying point densities.....	56
Table 4-1: Equivalent flexural strength and LOP results	68
Table 4-2: Residual flexural strength results.....	68
Table 4-3: Average of fibre count and spatial CDF parameter results	75
Table 4-4: Power fit equations of spatial CDF parameters	76
Table 4-5: Orientation factor results calculated with empirical approach.....	77
Table 5-1: Results from fibre distribution analysis using standardised grid dimensions	86
Table 5-2: Results of fibre distribution analysis using grid sizes of 2x2 and 10x10.....	88
Table 5-3: Variation in the fibre homogeneity of a batch of specimens	88
Table 5-4: Results of fibre dispersion and Nakagami fit parameters from Voronoi spacing data	91
Table 5-5: Mean degree of clustering for each batch	95
Table 6-1: Mean equivalent fibre resistance for each batch.....	108

LIST OF FIGURES

Figure 2-1: Typical profiles of fibres commonly used in concrete (Löfgren, 2005).....	7
Figure 2-2: Typical fibres and micro-fibres used in cementitious composites (Naaman, 2008).....	9
Figure 2-3: Fibre orientation angle convention (after Brandt (1985)).....	11
Figure 2-4: Fibre orientation states: (a) Discontinuous 1D ideal; (b) Discontinuous planar-random; (c) Discontinuous body-random (Löfgren, 2005).....	14
Figure 2-5: Two-dimensional fibre orientation system (after Kooiman (2000)).....	15
Figure 2-6: Three-dimensional fibre orientation system (after Kooiman (2000)).....	16
Figure 2-7: Beam cross section illustrating the different orientation zones (after Dupont and Vandewalle (2005)).....	17
Figure 2-8: Influence of maximum aggregate size on fibre distribution (after Johnston (1996))	20
Figure 2-9: (a,b) Fibre-matrix interface of embedded fibres; (c,d) Fibre protrusion lengths (Akkaya et al., 2000a).....	22
Figure 2-10: Effect of fibre clumping at the first crack section on composite toughness (Akkaya et al., 2001).....	24
Figure 2-11: Example of photometric method image (a) Grayscale image, (b) Binary image (Abrishambaf et al., 2013).....	25
Figure 2-12: Illustration of fibre orientation calculation (after Lee et al. (2016)).....	26
Figure 2-13: Change in major axis length with increasing fibre orientation (after Lee et al. (2016))... ..	26
Figure 2-14: Example of μ CT output (a) Original μ CT image, (b) Fibre segmenting, (c) Binary image, (d) Reconstructed 3D fibre image (Liu et al., 2013)	27
Figure 2-15: Schematic of flexural beam tests	29
Figure 2-16: Splitting tensile tests.....	31
Figure 2-17: Evaluation of $f_{eq,2}$ and $f_{R,1}$ as recommended by RILEM TC 162-TDF (2002).....	32
Figure 2-18: Evaluation of $f_{eq,3}$ and $f_{R,4}$ as recommended by RILEM TC 162-TDF (2002).....	32
Figure 3-1: Fibre appearance.....	37
Figure 3-2: Slump tests of selected batches	39
Figure 3-3: Cube density relative to the theoretical maximum density.....	40
Figure 3-4: Average compressive strength results	41
Figure 3-5: Three-point bending test setup and instrumentation.....	42
Figure 3-6: Examples illustrating the condition of the fracture surface	43
Figure 3-7: Before and after polishing specimens (120 kg/m^3 dosage).....	44
Figure 3-8: Polishing operation.....	44
Figure 3-9: Camera and lighting setup used to capture images.....	45
Figure 3-10: Example of original RGB image and corresponding grayscale input image.....	46
Figure 3-11: Top hat filtering (left) and contrast enhancement (right)	47

Figure 3-12: Morphological noise removal (left) and Otsu thresholding binary image (right).....	47
Figure 3-13: Original binary image (left), distance transform (centre), and watershed segmentation (right).....	48
Figure 3-14: Components and characteristics of a Voronoi diagram.....	49
Figure 3-15: Pixels required to detect fibre orientation angle from image data.....	50
Figure 3-16: Simulated point patterns demonstrating clustering, CSR, and regularity.....	52
Figure 3-17: Probability distributions of simulated clustered, CSR, and regular patterns.....	52
Figure 3-18: Example of the influence of coarse aggregate particles on the distribution of fibres.....	55
Figure 3-19: Histogram and Nakagami fit of Voronoi spacing for CSR point patterns of varying density.....	56
Figure 3-20: Distribution of variance in Voronoi spacing of CSR point simulations.....	57
Figure 3-21: PDFs and Voronoi diagrams of simulated clustered, CSR, and regular patterns.....	58
Figure 3-22: Nakagami shape factor distribution of 2500 random point simulations with 100 and 1000 points.....	59
Figure 4-1: Envelope and average Stress-CMOD curves for 40 kg/m ³ fibre dosage.....	63
Figure 4-2: Envelope and average Stress-CMOD curves for 60 kg/m ³ fibre dosage.....	63
Figure 4-3: Envelope and average Stress-CMOD curves for 80 kg/m ³ fibre dosage (Batch a).....	63
Figure 4-4: Envelope and average Stress-CMOD curves for 80 kg/m ³ fibre dosage (Batch b).....	64
Figure 4-5: Envelope and average Stress-CMOD curves for 100 kg/m ³ fibre dosage.....	64
Figure 4-6: Envelope and average Stress-CMOD curves for 120 kg/m ³ fibre dosage (Batch a).....	64
Figure 4-7: Envelope and average Stress-CMOD curves for 120 kg/m ³ fibre dosage (Batch b).....	65
Figure 4-8: Average flexural response for various dosages of 30 mm fibres.....	66
Figure 4-9: Average flexural response for various dosages of 60 mm fibres.....	66
Figure 4-10: Rejected test where the crack initiated outside the notch.....	67
Figure 4-11: Examples of various observed crack patterns.....	67
Figure 4-12: $f_{ct,L}$ results box plot.....	69
Figure 4-13: $f_{eq,2}$ results box plot.....	69
Figure 4-14: $f_{eq,3}$ results box plot.....	70
Figure 4-15: $f_{R,1}$ results box plot.....	70
Figure 4-16: $f_{R,4}$ results box plot.....	71
Figure 4-17: Examples of Voronoi diagrams for different fibre counts.....	72
Figure 4-18: Box plot of the number of fibres detected for the various fibre dosages.....	73
Figure 4-19: Average fibre spatial cumulative distribution plot.....	74
Figure 4-20: Average fibre spatial cumulative distribution plot (Logarithmic x-axis).....	74
Figure 4-21: Spatial CDF parameter results.....	76
Figure 4-22: Determining the orientation factor through linear regression.....	78
Figure 4-23: Contours illustrating sectional variation in fibre density.....	79

Figure 4-24: Relation of the average number of 30 mm and 60 mm fibres	80
Figure 5-1: Distribution of fibres throughout a cross section.....	84
Figure 5-2: Fitted Poisson distributions of each batch	85
Figure 5-3: Increase in average CoV of standardised fibre grid count distribution with average total fibre count	86
Figure 5-4: CoV of fibre grid count distribution for designated grid dimensions.....	87
Figure 5-5: Surface fit illustrating the general response of the grid fibre count CoV to grid size and average total fibre count	87
Figure 5-6: Variation of fibre homogeneity with average fibre count	89
Figure 5-7: Histogram and Nakagami fit of Voronoi spacing for selected batches	90
Figure 5-8: Nakagami distribution fits for all fibre dosages	91
Figure 5-9: Similarity between mean Voronoi spacing of fibre – and random patterns	92
Figure 5-10: Similarity between dispersion of fibre – and random patterns	93
Figure 5-11: Comparison of random and experimental Nakagami fits	93
Figure 5-12: Standard deviation of dispersion for fibre – and random patterns.....	94
Figure 5-13: Number of clustered samples with the average batch fibre count	95
Figure 5-14: Equivalence of dispersion and homogeneity	96
Figure 5-15: Equivalence of variation of dispersion and homogeneity.....	97
Figure 5-16: Equivalence of the degree of clustering obtained from the two approaches	98
Figure 6-1: Relationship of flexural strength to the number of 30 mm fibres.....	102
Figure 6-2: Relationship of flexural strength to the number of 60 mm fibres.....	102
Figure 6-3: Average Stress-CMOD response for varying 30 mm fibre dosages.....	103
Figure 6-4: Average Stress-CMOD response for varying 60 mm fibre dosages.....	103
Figure 6-5: Comparing the flexural strength with respect to $N_{f,30}$	104
Figure 6-6: Relating equivalent flexural strength to dispersion of 30 mm fibres.....	105
Figure 6-7: Relating equivalent flexural strength to dispersion of 60 mm fibres.....	106
Figure 6-8: Linear relationship between the variability of flexural strength and – fibre dispersion ...	107
Figure 6-9: Power relationship between the variability of flexural strength and – fibre dispersion ...	107
Figure 6-10: Relationship between equivalent fibre resistance and clustering	109

NOTATIONS

Upper case letters

A_f	Cross-sectional area of a single fibre
A_s	Specimen cross-sectional area
$CL_{Vor,i}$	The degree of clustering of sample i based on the Voronoi approach
$CL_{cnt,i}$	The degree of clustering for specimen i based on the fibre count approach
D_{BZ}^f	Energy absorption capacity provided by fibre reinforcement mechanisms
D_{BZ}^b	Energy provided by matrix cracking
F_L	Load at the limit of proportionality
$L_{f,xy}$	Fibre length projected to the x-y plane
L_f	Fibre length
L	Length of loading span
N_b	Number of fibres intersecting a plane of unit surface area
N_{ideal}	Theoretical number of ideally aligned fibres intersecting a plane of unit surface area
N_f	Number of fibres intersecting a crack plane
$N_{s,j}$	Number of samples in batch j
V_f	Volume fraction of fibres

Lower case letters

b	Width of specimen
d	Minor axis length of fibre
d_f	Fibre diameter
f_{eq}	Equivalent flexural tensile strength
f_R	Residual flexural tensile strength
$f_{fct,L}$	Flexural tensile strength at the limit of proportionality
h	Height of specimen
h_{sp}	Effective specimen height from the notch tip
$h_{grid,i}$	Number of grid tiles for sample i
l	Major axis length of fibre
$\bar{n}_{f,i}$	The mean number of fibres inside a grid square of specimen i
n_f	The number of fibres inside a grid square
$n_{f,std}$	The number of fibres counted inside a grid square of standardised grid
z_i	The standard normal random variable calculated for sample i

Greek letters

α_x	The Voronoi spacing at which x proportion of fibres are spaced closer
------------	---

δ	Deflection
η_{θ}	Fibre orientation factor
$\eta_{\theta 2D}$	Fibre orientation factor in a two-dimensional system
$\eta_{\theta 3D}$	Fibre orientation factor in a three-dimensional system
θ_i	Inclination angle of fibre i
θ_{Ave}	Average fibre inclination angle
κ	Unit proportion of a rectangle attributed to a single fibre
μ	Statistical mean
ξ	Gradient of the straight portion of the Voronoi spacing CDF
σ^2	Statistical variance
σ	Statistical sample standard deviation
τ_{eq}	Resistance provided by an equivalent number of 30 mm fibres
ψ	Fibre orientation angle relative to the z-axis

Abbreviations

3PBT	3-Point Bending Test
4PBT	4-Point Bending Test
AC-IS	Alternating Current Impedance Spectroscopy
CDF	Cumulative Distribution Function
CMOD	Crack Mouth Opening Displacement
CoV	Coefficient of Variation
CSR	Complete Spatial Randomness
CT	Computed Tomography
μ CT	Micro-Computed Tomography
FRC	Fibre-Reinforced Concrete
ITZ	Interfacial Transition Zone
LVDT	Linear Variable Differential Transformer
MOR	Modulus of Rupture
PDF	Probability Density Function
PVA	Polyvinyl Alcohol
RGB	Red Green Blue
SFRC	Steel Fibre-Reinforced Concrete
UHPRFC	Ultra-High-Performance Fibre-Reinforced Concrete
w/c	Water/Cement

GLOSSARY

- Fibre orientation:* The angle between the fibre's longitudinal axis and a vector that is orthogonal to the cut-plane.
- Grid size:* The dimension m of a grid consisting of $m \times m$ squares imposed over a $150 \text{ mm} \times 150 \text{ mm}$ cross section.
- Fibre grid count:* The number of fibres counted inside a single grid square.
- Fibre count:* The total number of fibres detected over a cross section of a given specimen.

CHAPTER 1. Introduction

1.1 Background

The versatility and practicality of concrete as a construction material has been demonstrated repeatedly throughout history and its importance and applicability in all forms of construction continue to increase in the present day. Although concrete is strong when loaded in compression, the material has poor tensile strength, toughness and impact resistance due to its inherently brittle nature. This drawback makes concrete susceptible to cracking and ineffective in resisting local transient overloads. The addition of discontinuous discrete fibres to the brittle concrete matrix can produce a material with enhanced toughness and impact resistance. The composite material is referred to as Fibre-Reinforced Concrete (FRC).

The advantage attained by adding fibres to concrete is most evident in the post-peak tensile behaviour of the composite. Several experimental studies have shown that the ultimate compressive strength of FRC does not show substantial improvement over conventional concrete at fibre volumes that can be conveniently incorporated into the mix. However, considerable improvement in the tensile strain at rupture and residual tensile strengths were observed in the FRC mixes. This property of FRC results in significantly enhancing the ability of structures to control crack widths, reduce reinforcement congestion, and several other properties that can be exploited by practitioners to provide efficient design solutions (Mehta and Monteiro, 1993).

Various mechanical properties can be enhanced by the addition of fibres to concrete depending on the volume fraction of fibres added, the type of fibres, and matrix properties. By varying these parameters, the flexural performance may be improved, and the failure mode of the composite may be altered. This provides the engineer with the ability to design an FRC mixture by selecting the most efficient combination of parameters that will result in acceptable performance as required by specifications. Relating structural requirements to mixture design is, however, no elementary undertaking. The post-peak behaviour of the composite can vary immensely depending on the combination of fibre volume, fibre type, and matrix properties (Bentur and Mindess, 2006).

The variability associated with FRC members has repeatedly been cited as a characteristic stunting the vast structural application of the material (Laranjeira et al., 2011; Parmentier et al., 2008). The reliability and scattering of test results tend to be the primary concern as they have a direct influence on the safety factors to be used for design purposes. The effectiveness of a fibre-reinforced composite element is strongly dependent on the orientation of fibres with respect to the orthogonal direction of the principal tensile stress in the member. Fibre orientation and spatial distribution can be highly variable and in order to assume homogeneous and isotropic material behaviour, large safety factors are required to account for such variability (Di Prisco et al., 2009).

In this study, the spatial distribution of steel fibres is investigated, and the fibre distribution is related to the post-cracking performance of the composite material. Spatial distribution is evaluated using photometric techniques for two types of hook-ended steel fibres with similar aspect ratios but different lengths at various volume contents. The results highlight the unique relationship between fibre spatial distribution and fibre dosage as well as demonstrate the correlation between fibre spatial variability and flexural strength variability. In addition, the influence of fibre clustering on the effective resistance provided by the fibres is investigated.

The demand for material efficiency in construction is perpetually increasing and requires greater ingenuity and creativity from the designer. The thorough investigation and characterisation of FRC broadens the practitioner's understanding of the composite and allows the effective application of the material to provide enhanced structural performance or reduced construction costs without having to compromise on performance.

1.2 Research Statement and Objectives

The purpose of the research is to understand the influence of fibre spatial characteristics on the flexural performance of Steel Fibre-Reinforced Concrete (SFRC). This is based on the premise that the spatial distribution of fibres has a considerable impact on the variability and performance of composite elements. In order to evaluate such a proposition, a set of three main hypotheses are formulated to be investigated in this work:

1. *The flexural response of a SFRC specimen is related to a descriptor quantifying the spatial distribution of fibres.*
2. *The variability in flexural response is positively related to the variability of the parameter describing fibre spatial distribution.*
3. *The effective resistance provided by fibres reduces as the extent of fibre clustering increases.*

The first objective of this research is to study the effect of fibre spatial characteristics on the flexural performance of SFRC by investigating these three primary hypotheses.

Each of the three main hypotheses have sub-hypothesis relating to the number of fibres intersecting a cross section, which is a function of the fibre length and fibre volume content. These sub-hypotheses are:

1. *The spatial distribution of fibres is strongly related to the number of fibres intersecting a plane and the relative fibre dispersion uniformity increases as the number of intersecting fibres increases.*
2. *The variability of fibre spatial distribution within a batch reduces as the number of fibres increases.*
3. *The presence of fibre clustering becomes more prevalent as the number of fibres increases.*

Testing these three sub-hypotheses forms part of the second objective of this study which is to evaluate the influence of fibre length and fibre volume content on the spatial characteristics of steel fibres intersecting a plane.

1.3 Scope of the Study

The scope of work covered by this research is related to the experimental quantification of the flexural behaviour of SFRC specimens and the manner in which it is correlated to fibre spatial distribution. The work includes:

- a) A literature review summarising published research on the influence of fibre orientation and fibre spatial distribution on composite performance as well as the properties affecting the pull-out response of single fibres. The techniques employed to quantify fibre distribution are reviewed and a critical discussion on the available testing methods for evaluating the post-cracking strength of a composite is provided;
- b) Experimental evaluation of the effect of fibre length and fibre volume content on the flexural response and fibre spatial characteristics of the composite by providing experimental results for specimen where these parameters were individually varied;
- c) A processing algorithm was developed to extract the centroidal locations of fibres from an image and an objective geometric descriptor is proposed for quantifying the spatial distribution of fibres;
- d) Metrics that were derived to characterise the uniformity of fibre distribution as well as the degree of clustering, and
- e) An investigation of trends exhibited in flexural and spatial results for varying fibre length and fibre volume content and a study of the relation between the flexural response and a metric describing an element of the fibre spatial distribution.

The following points will not be considered in this study:

- a) The influence of material properties such as varying aggregate type, size, and quantity, different fibre materials, and the effect of admixtures;
- b) The effect of specimen size and testing method on experimental results;
- c) Assessing fibre distribution at multiple locations along a specimen or at geometric planes other than the plane orthogonal to the principal tensile stress direction;
- d) Formulating expressions that can be used to estimate the influence of fibre spatial distribution on the flexural response, and
- e) Experimentally determining the fibre orientation angle distribution from image data.

1.4 Methodology

The work completed in this study can be divided into three phases:

1. Experimental phase;
2. Data processing phase, and
3. Analysis phase.

The experimental phase consisted of concrete mix design and sample production as well as the subsequent preparation and testing of the specimen. The variables can be categorised as fibre length and fibre volume content. Normal strength concrete, designed to attain a nominal compressive strength of 50 MPa, was used and reinforced with hook-ended steel fibres of 30 mm and 60 mm lengths and aspect ratios of 60 and 65, respectively. The steel fibres have an ultimate tensile strength of 1100 MPa and they were incorporated into the mixture at volume contents ranging from 40 kg/m³ (0.5%) to 120 kg/m³ (1.5%) in intervals of 20 kg/m³. A batch of concrete consisting of 9 flexural specimens and 3 compressive cube specimens was cast for each fibre length at the various dosages. A control mixture of plain concrete containing no fibres was also produced and tested. Following flexural testing, each specimen was cut adjacent to the crack location and the cut surface was polished in preparation of capturing an image of the cross section.

The data processing phase consisted of using experimental flexural results to characterise the post-cracking response of the composite specimen as well as developing an image analysis algorithm for extracting the centroidal location of each fibre.

The analysis phase included the development of metrics that quantify the fibre spatial characteristics and relating these metrics to the flexural performance of composite specimen with the objective of identifying correlations between the variables.

1.5 Organisation of the Report

This introductory chapter is followed by a discussion of the current state of knowledge in Chapter 2 on aspects that are relevant to the present study. The literature review comprises of a brief discussion on the pull-out behaviour of single fibres as well as the influence of fibre orientation and spatial distribution on the performance of fibre-reinforced composite members. The chapter concludes with an overview of popular techniques for evaluating fibre distribution as well as a review of available strength testing methods.

The research methodology and procedures employed to gather experimental data and evaluate the formulated hypotheses are presented in Chapter 3. The details regarding mix design and specimen preparation, test methods and procedures, and image analysis are discussed in this chapter. Furthermore, two approaches are proposed for quantifying the fibre spatial characteristics from image analysis data.

Experimental results from the flexural testing and image analysis are presented in Chapter 4 and the general trends observed in the results are discussed on an individual basis.

The approaches developed in Chapter 3 for quantifying fibre spatial characteristics are implemented on image analysis results in Chapter 5 and used to assess the three sub-hypotheses of this study. The

resulting metrics of both approaches are compared and evaluated, and the more suitable approach is decided on for further analysis.

The metrics describing fibre spatial distribution are related to the mechanical performance of flexural specimens in Chapter 6. The three main hypotheses of this work are evaluated by assessing correlations exhibited by the results.

The conclusions drawn throughout the research are summarised in Chapter 7 along with recommendations for future work in the field of study.

CHAPTER 2. Literature Review

2.1 Background

This chapter presents a theoretical framework on fibre-reinforced cementitious composites that is based on decades of research aimed at gaining insight and developing the material. The objective of the chapter is to provide a sense of understanding into the mechanisms and material characteristics that dictate composite performance. In addition, the available methods for evaluating the strength of a composite element as well as the fibre distribution are briefly reviewed.

The chapter commences with a discussion on the factors influencing the pull-out response of single fibres. This is followed by Section 2.4 with an overview of fibre orientation distribution in a matrix, models for predicting fibre orientation, as well as a brief review of the influence of orientation effectiveness on composite performance. The spatial distribution of fibres is discussed in Section 2.5 with emphasis on experimental observations relating fibre distribution to composite response. The methods employed to determine fibre orientation and spatial distribution are discussed in Section 2.6. This is followed by Section 2.7 with a review of the available methods for characterising the post-cracking response of FRC. The chapter concludes with a discussion summarising the main findings of the theoretical framework in Section 2.8.

2.2 Post-Cracking Tensile Behaviour of FRC

The enhanced mechanical properties provided by the addition of steel fibres to a brittle concrete matrix are most evident after the composite member has cracked. This is due to the fibre bridging action which allows tensile stresses to be transferred across cracks, thus preventing brittle failure and increasing the tensile deformation capacity of the specimen. This has the effect of increasing the toughness which is represented by the area under the load-deflection curve. Therefore, toughness is dependent on the amount of energy dissipated during the fracture process (Mehta and Monteiro, 1993). The amount of energy dissipated due to the addition of fibres is in turn dependent on several characteristics related to the matrix, fibres, loading arrangement, fibre orientation, and member geometry.

The pull-out behaviour of single fibres is widely accepted to provide an approximate indication of the post-cracking response of a fibre-reinforced composite element (Kooiman, 2000). The pull-out behaviour of a single fibre can, however, only provide an estimate of the efficiency of the fibres in the crack bridging process. The fibre efficiency in this context can be said to depend on the compatibility and coherence between the selected fibre and the surrounding concrete matrix (Marković, 2006). Experimental and analytical results have shown that to achieve efficient performance in a concrete matrix, the following fibre properties are required (Naaman, 2003):

1. A tensile strength that is two to three orders of magnitude greater than that of the concrete;
2. Bond that is equal to or greater than the tensile strength of the matrix;
3. An elastic modulus in tension that is three times greater than that of the concrete matrix, and

4. Sufficient ductility to avoid fibre fracture due to bending or abrasion.

Other fibre properties that are also important to consider are the Poisson's ratio and coefficient of thermal expansion of the fibre, which should preferably be of the same order of magnitude as the concrete matrix. The potential negative influence of a mismatch of these two properties can, however, be overcome by providing alternative strengthening mechanisms such as surface deformation to create mechanical anchorage.

The factors affecting the pull-out behaviour of a single fibre are briefly discussed in the following section to provide an insight on the effects and interrelations of fibre and matrix properties on the post-cracking behaviour of FRC.

2.3 Factors Affecting Pull-Out Response

2.3.1 Fibre shape

The geometry of steel fibres can be altered to improve fibre-matrix bond and result in more efficient fibre performance. The cross-sectional shapes of fibres can be circular, diamond, triangular, rectangular, square, flat, polygonal, or any substantially polygonal shape. Bond strength can further be improved by modifying the longitudinal shape of the fibre or by roughening its surface (Naaman, 2003). Examples of typical fibre profiles are shown in Figure 2-1.

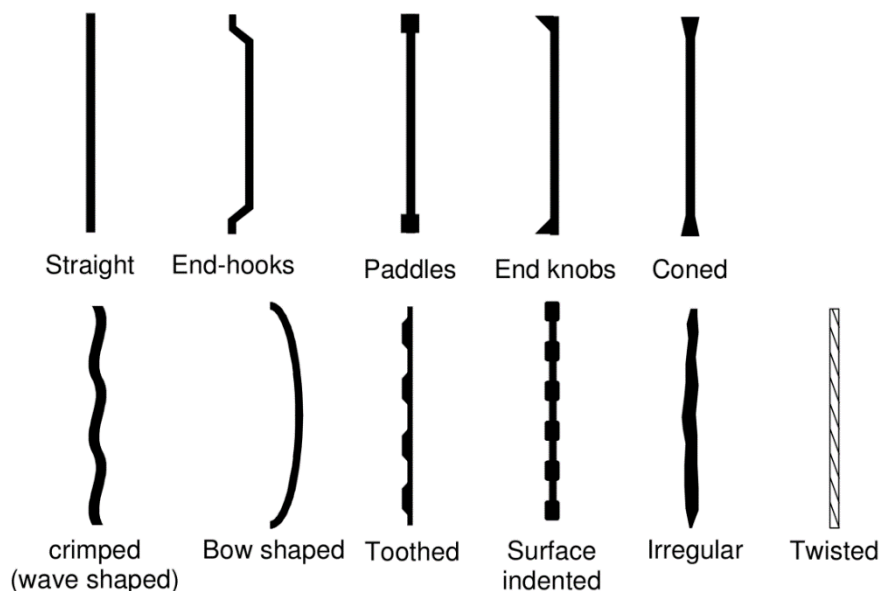


Figure 2-1: Typical profiles of fibres commonly used in concrete (Löfgren, 2005).

The efficiency of the cross-sectional shape can be evaluated by considering the ratio of the perimeter of the fibre to its cross-sectional area. A square and triangular cross section, for example, has a perimeter that is 1.12 and 1.28 times, respectively, greater than a circular cross section for the same cross-sectional area. The increase in the ratio of perimeter to cross-sectional area leads to a direct increase in the post-

cracking strength of the composite by improving the frictional and adhesive components of bond (Naaman, 2003).

The adhesive and frictional bond provided by conventional fibres, of diameters in the order of 0.1 mm or greater, is not sufficient for providing effective reinforcing (Bentur and Mindess, 2006). This is overcome by utilising deformed fibre shapes that provide mechanical bond through anchoring effects. The mechanical bonding achieved by the anchoring action has been shown to contribute significantly more to the total bond than those achieved by interfacial effects. Chin and Xiao (2012) conducted a comprehensive experimental and numerical study evaluating the complete bond-slip response of deformed metallic fibres and reported that the pull-out resistance is significantly influenced by fibre geometry.

If all other influencing factors, such as fibre length, fibre strength, etc., are identical, the ultimate resistance of hook-ended steel fibres are significantly greater than straight fibres due to the plastic deformation of the fibre hooks acting as anchoring mechanisms (Chanvillard and Aitcin, 1990; Naaman and Najm, 1991).

2.3.2 Fibre material

The properties of the fibre are inherently dependent on the fibre material. Properties such as strength, stiffness, specific gravity, surface texture, corrosion resistance, and several other properties can have a considerable effect on the performance of the composite. The appropriate fibre material is highly dependent on the required application. The extent to which the strength of the fibre can enhance the toughness of a composite can be considered in terms of the degree to which the fibre strength is utilised. In a weak matrix, plastic hinges may not form with high-strength fibres and the inclusion of fibres can instead lead to fracture of the wedge of the matrix behind a shallow embedded hook or excessive matrix spalling where the fibre exits the matrix (Naaman, 2004). These effects are likely to be less pronounced in the case of intermediate-strength fibres. In the case of a high-strength matrix, the beneficial effects of high-strength fibres are significantly more evident (Aydin, 2013). A photograph depicting various fibres commonly used in cement composites is shown in Figure 2-2.

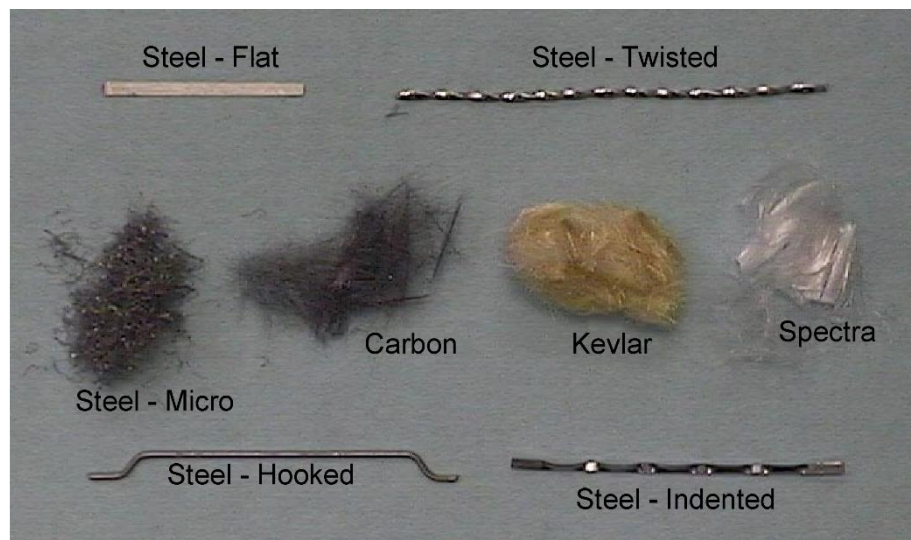


Figure 2-2: Typical fibres and micro-fibres used in cementitious composites (Naaman, 2008)

2.3.3 Fibre diameter

The bending stiffness and therefore the amount of energy required to form a plastic hinge is directly related to the diameter of the fibre. Generally, the maximum tensile stress in a brittle fibre is lower for a smaller diameter fibre for the same crack opening distance, fibre angle, and matrix – and fibre properties (Katz and Li, 1995). However, Brandt (1985) showed that this is not necessarily valid for ductile fibres, where a plastic hinge may form to redistribute the stresses. A larger diameter may therefore be desirable in hook-ended fibres due to the additional energy required to deform the hooks. A study by Betterman et al. (1995) on flexible Polyvinyl Alcohol (PVA) micro-fibres presented experimental results that indicated that the first peak strength increases with increasing fibre content as well as decrease in fibre diameter for a constant aspect ratio. These findings demonstrate the unique response of implementing different fibres and the manner in which similar factors affect the response.

2.3.4 Fibre embedded length

The strength and toughness of cementitious composites have repeatedly been shown to be affected by fibre length (Bentur and Mindess, 2006). Robins et al. (2002) showed that the magnitude and toughness of the pull-out response of hook-ended steel fibres increases with increasing embedment length. The authors also pointed out that full straightening of the hooked-end can only occur if the length of the hooked-end is less than the total embedment length of the fibre. The influence of fibre length is usually considered with regard to a critical length which is dependent on fibre-matrix bond characteristics. The critical length is the minimum length required for a fibre to develop its full-strength capacity. Fibres with shorter lengths will fail by pulling out, since the fibres are not long enough to generate stresses that will cause fracture. Conversely, the full fibre strength can be attained for fibre lengths longer than the critical length and in such cases, failure is governed by fibre fracture (Abbas and Iqbal Khan, 2016). Generally, longer fibres are advantageous for generating high strengths, however, increasing the fibre

length beyond the critical length can be detrimental to the toughness of the composite (Akkaya et al., 2000a).

2.3.5 Fibre orientation

The orientation of a fibre with respect to the direction of the primary tensile force has a significant effect on the mechanical performance of the composite. An important distinction must be made between three different situations related to fibre orientation in cementitious composites:

1. Fibres in an uncracked composite;
2. Ductile fibres bridging cracks in a more brittle matrix, and
3. Brittle fibres bridging cracks in a more ductile matrix.

Analysing the effect of orientation on a fibre bridging over a crack requires the consideration of fibre bending due to local geometrical constraints. A complex stress state is developed involving local flexural stresses in the fibre and compressive stresses in the surrounding matrix (Bentur et al., 1996). The overall behaviour is dependent to a large extent on the balance between the rigidity of the matrix and the ductility of the fibre (Bentur and Mindess, 2006). A distinction between two different situations can be made within this context:

1. Ductile fibres with low modulus of elasticity, and
2. Brittle fibres with higher modulus of elasticity.

A more ductile fibre with a low modulus will allow more plastic rotation and potentially induce a dowel action which may increase the pull-out resistance of the fibre and have greater fibre efficiency at inclined angles than would be predicted for a fibre that is not inclined. Li et al. (1990) showed that the force and energy of fibre pull-out generally tend to increase as the inclination angle increases; however, the increase in pull-out force and energy is limited at high inclination angles due to matrix spalling. A fibre which is more brittle with a higher elastic modulus may experience local flexural stress in addition to the axial tensile stress and lead to premature failure of the fibre and a lower efficiency than would be expected when considering an inclined straight fibre, assuming only axial stresses (Katz and Li, 1995; Leung and Li, 1992). The response is also dependent on the properties of the matrix in the vicinity of the fibre. A weak matrix is more prone to spalling and local damage due to concentrated stresses induced by the bending fibre. A high-strength matrix, however, has been shown to increase the likelihood of undesirable fibre fracture (Banthia and Trottier, 1994).

In general, it has been found that stiff but ductile fibres, such as steel fibres, tend to yield rather than break due to local bending and increase in pull-out load up to an inclination angle of 45°, after which the pull-out loads decrease (Morton and Groves, 1974). Brandt (1985) extended the analysis of flexural stresses in ductile fibres with the objective of calculating the optimum orientation of steel fibres. He stated that the optimal fibre inclination angle is a function of the energy consumed by five processes:

- Debonding of fibres from the matrix;

- Pull-out of fibres from the matrix;
- Plastic deformation of the fibres;
- Crushing of the matrix in compression near the exit point of the fibre, and
- Complementary friction between the fibre and the matrix due to local compression at the bend.

Brandt (1985) concluded that the maximum pull-out energy of steel fibres was at an intermediate angle of approximately $35\text{-}50^\circ$ with respect to the applied tensile force as given in Figure 2-3. A parametric study of the proposed method for 1D systems of fibres revealed the following: (i) The optimum angle decreases considerably as the aspect ratio increases and is in the range of $43\text{-}46^\circ$ for short and thick fibres and $18\text{-}21^\circ$ for long and thin fibres; (ii) Fibres with higher tensile yield strength have larger optimum inclination angles; (iii) The optimum angle decreases as the fibre-matrix bond stress increases. Although Brandt does not explicitly consider the influence of matrix strength in the parametric study, possibly due to the high interrelation of strength and other parameters, the results suggest that the optimum angle of inclination should decrease as matrix strength increases. Experimental results from research by Robins et al. (2002) showed that the magnitude of the pull-out response is directly related to matrix strength at fibre orientations less than 10° . This may also suggest that the optimum orientation angle decreases with increasing matrix strength.

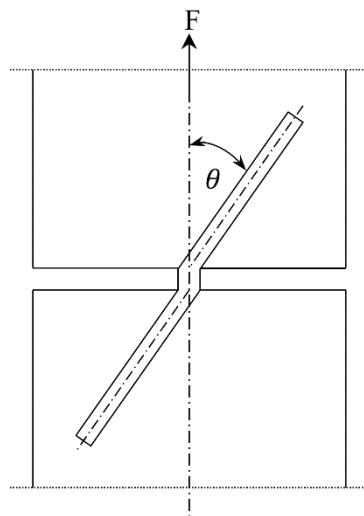


Figure 2-3: Fibre orientation angle convention (after Brandt (1985))

From the brief discussion on single fibre inclination angle, the influence of fibre orientation is not immediately apparent and a broad number of influencing factors have to be considered. Banthia and Trottier (1994) conducted a study to evaluate the pull-out response of three deformed fibres for different concrete strengths and fibre inclination angles. The study showed that the peak pull-out load of hook-ended fibres was not highly dependent on the fibre inclination angle. This finding is in accordance with research done on straight fibres by Naaman and Shah (1976); however, it is in contradiction of the findings of Morton and Groves (1974) and Brandt (1985). The shapes of the remaining two fibres tested in the study were crimped and cone-ended (see Figure 2-1). The results of both fibres indicated that the

peak loads supported by the fibres as well as the energy absorbed during pull-out are greater when the fibres are aligned in the direction of loading. Furthermore, all cone fibres ruptured before pulling out of the matrix and the hook-ended fibres ruptured at inclination angles of 45° and 60° in the 85 MPa concrete mix. Grünewald (2004) has pointed out that increasing matrix strength increases the probability of matrix spalling and/or fibre rupture. Abu-Lebdeh et al. (2011) reported that the total pull-out energy and maximum pull-out load of deformed steel fibres increases as matrix strength increases and that straight fibres are less affected by matrix strength.

2.3.6 Water/binder ratio of matrix

It is generally known that several properties of concrete are related to the water/cement ratio of the mixture, the most common of which is compressive strength. The influence of matrix strength on the pull-out behaviour of a single fibre has been briefly discussed in the previous section. Results from a study by Wei et al. (1986) showed that the microhardness of the matrix surrounding a steel fibre increases with decreasing water/binder ratio. Matrix shrinkage induces normal stresses around the fibre which increase the frictional slip resistance during fibre pull-out (Bentur and Mindess, 2006). A study by Shoya (1979) showed that shrinkage of hydrated cement paste tends to decrease with decreasing w/c ratio. This is because the w/c ratio determines the amount of evaporable water and the rate at which the water can move towards the surface (Neville, 2011). Park et al. (2014) investigated the effect of shrinkage reducing agent on the pull-out resistance of high-strength steel fibres in ultra-high-performance concrete and found a noticeable reduction in pull-out resistance due to the reduced confining stress provided by matrix shrinkage. The potential significance of shrinkage confining stresses on fibre-matrix bonding behaviour was also shown by Stang (1996) who developed a method for estimating clamping pressure in cementitious composites.

2.3.7 Filler content

The presence of fine filler materials such as silica fume, fly ash, metakaolin, etc., influence the pull-out behaviour of fibres through enhancing the properties of the Interfacial Transition Zone (ITZ) and consequently improving adhesive and frictional bonding (Bentur et al., 1996). The sizes of these particles are considerably smaller than that of cement grains and can therefore fill empty spaces around aggregate particles and fibres more effectively. Silica fume in particular substantially enhances the strength of the ITZ as a result of the secondary pozzolanic reaction and the high packing density achievable through extremely fine particle size (Neville, 2011).

2.4 Fibre Orientation

2.4.1 Introduction

The previous section was concerned with the ability of fibres to transfer stresses across a crack and improve the energy absorption capacity of a composite member. Energy absorption and toughness have been shown to be highly dependent on the number of fibres effectively bridging a crack (Barr et al.,

2003b). The number of effective fibres have been found to be dependent on the fibre dosage, fibre orientation, and length efficiency of the fibre (Dupont and Vandewalle, 2005). The high dependency of the post-cracking response on the number of effective fibres bridging the crack can be considered as a major factor contributing to the inherent variability associated with FRC.

The influence of fibre orientation angle within the context of fibre pull-out behaviour was discussed in the previous section. It was found that the efficiency of a fibre is related to the inclination of the fibre with respect to the direction of the principal tensile force. The definitions of fibre efficiency and fibre effectiveness adopted and applied throughout this study are in accordance to those provided by Kameswara Rao (1979). The efficiency of a fibre refers to its individual performance with a specific orientation relative to the direction of the principal tensile stress or crack plane. The fibre effectiveness is obtained as the average value of fibre efficiency considering all possible orientations the fibres can occupy. This section is concerned with the latter: the relation between fibre orientation and the number of fibres intersecting a cross section.

The probability of a fibre intersecting a cross section is related to the orientation of the fibre. A fibre that is aligned to the tensile force has a greater probability of intersecting a crack than a fibre which is inclined. Therefore, the number of fibres intersecting a given cross section is a function of the orientation of the fibres. The probability of a fibre achieving a specific orientation may also be considered as a function of geometric constraints. This means that fibres which are located near boundaries have fewer geometrically possible orientations and therefore the probability of a fibre aligning in a specific direction is increased.

This is considered as one of the primary aspects influencing fibre orientation and is referred to as wall-effects introduced by the formwork (Dupont and Vandewalle, 2005; Kooiman, 2000). Fibre orientation is, however, also significantly dependent on the method of placement (Vandewalle et al., 2008; Zerbino et al., 2012; Yoo et al., 2014; Alberti et al., 2016; Gettu et al., 2005) and the fresh-state properties of the mixture (Alberti et al., 2017; Marković, 2006; Ferrara et al., 2017).

2.4.2 Orientation factor

It was shown by Krenchel (1975) that the unit number of fibres that actually intersect an arbitrary crack plane, N_b , can be related to the theoretical unit number of ideally aligned fibres, N_{ideal} , through an orientation factor, η_θ , as shown in Equation 2.1. The orientation factor is commonly used to characterise the average orientation of fibres in a cross section. The theoretical number of fibres is the case of a one-dimensional system with all fibres orientated in the direction of the load and can be expressed as the ratio of the volume fraction of fibres, V_f , to the cross-sectional area of a single fibre, A_f .

$$\eta_\theta = \frac{N_b}{N_{ideal}} = N_b \frac{A_f}{V_f} = \frac{N_f A_f}{A_s V_f} \quad (2.1)$$

Where:

N_f = The number of fibres intersecting the crack plane

A_s = The total cross-sectional area of the specimen

The orientation factor for the one-dimensional system, where all fibres are perfectly aligned orthogonal to the crack plane (as indicated in Figure 2-4 (a)), represents the optimal scenario and is equal to 1. The orientation of discrete short fibres in a matrix can be characterised by body-random orientation or plane-random orientation depending on the dimensions of the component. Body-random orientation represents the case with equiprobable and unlimited distribution of fibres within the boundaries of a 3-dimensional space, whereas the same is true for plane-random orientation in a 2-dimensional space. The schematics depicted in Figure 2-4 illustrate these states of fibre orientation.

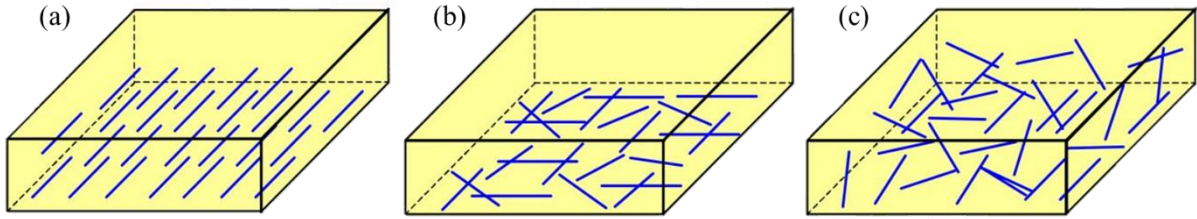


Figure 2-4: Fibre orientation states: (a) Discontinuous 1D ideal; (b) Discontinuous planar-random; (c) Discontinuous body-random (Löfgren, 2005)

The orientation factor can therefore be better understood as the average ratio of the projected fibre length along the orthogonal axis of the section to the total fibre length, as indicated by Equation 2.2:

$$\eta_{\theta} = \frac{1}{N_f} \sum_{i=1}^{N_f} \cos \theta_i \quad (2.2)$$

An approximated average fibre inclination angle, θ_{Ave} , may then be calculated using Equation 2.3 from the orientation factor as given by Equation 2.2 (Laranjeira, 2010):

$$\theta_{Ave} = \cos^{-1}(\eta_{\theta}) \cdot \frac{180}{\pi} \quad (2.3)$$

The orientation factor may be interpreted as providing a measure of fibre effectiveness in terms of the amount of fibres likely to bridge a crack. The orientation factor is, however, entirely unrelated to the *efficiency* of a fibre with regard to its pull-out resistance at various inclination angles.

2.4.3 Estimating fibre orientation and distribution

The number of fibres bridging a crack plane can be estimated with probability theory, however, several assumptions are involved in the calculation. These assumptions commonly relate to the shape and distribution of the fibres, the placement and compaction of the specimen, rheology and composition of the mixture, and aspects related to geometrical considerations (Alberti et al., 2017; Bi et al., 2017; Dupont and Vandewalle, 2005; Laranjeira, 2010).

Methods which only consider the influence of wall-effects on fibre effectiveness have been thoroughly investigated in the past. Three cases are commonly distinguished from one another in the calculations:

1. Fibre effectiveness without restrictions on fibre orientation;
2. Fibre effectiveness restricted by a single geometrical boundary, and
3. Fibre effectiveness restricted by two geometrical boundaries.

In the case of a one-dimensional system, similar to that depicted in Figure 2-4 (a), the fibre efficiency is always optimal since there is only one possible orientation the fibre can assume and must theoretically result in a fibre effectiveness equal to 1. In a two-dimensional system without restrictions, as in Figure 2-4 (b), it is assumed that all fibres are randomly orientated in a plane and that the orientation angle between the fibre embedded length and crack line can vary between 0 and 90°. To determine the effectiveness of the fibres, the mean orientation of fibres has to be projected on the axis that is orthogonal to the crack line, i.e. the axis that represents the direction of the tensile stress (Figure 2-5). The effectiveness may now be calculated as follows:

$$\eta_{\theta 2D} = \int_0^{\pi} \frac{\cos \theta \cdot d\theta}{\pi} = \frac{2}{\pi} \quad (2.4)$$

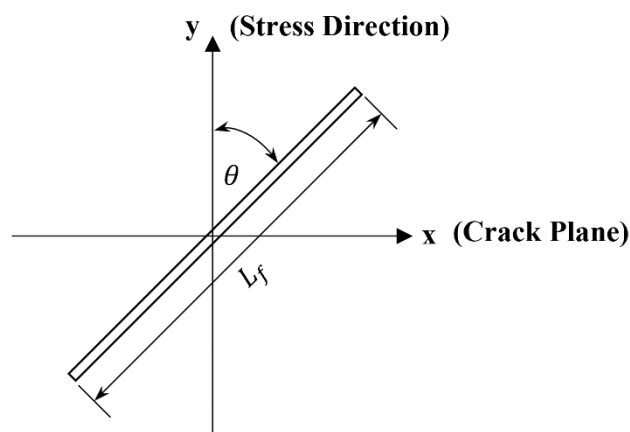


Figure 2-5: Two-dimensional fibre orientation system (after Kooiman (2000))

In the case of a three-dimensional system without orientation restrictions, the end points of the fibres cover the circumference of a sphere with a diameter equal to the fibre length, L_f . Romualdi and Mandel (1964) assumed that the randomly orientated fibres have a uniform probability and calculated the 3D fibre effectiveness, $\eta_{\theta 3D}$, to be equal to $\frac{4}{\pi^2}$. Their assumption was, however, proven to be incorrect by Stroeven (1978), who calculated the fibre effectiveness based on geometric probability theory. Stroeven determined the average projected length of the fibres in the x-y plane by multiplying the individual fibre projections with their contributions to these projections, which is a function of the fibre's orientation relative to the z-axis as depicted in Figure 2-6.

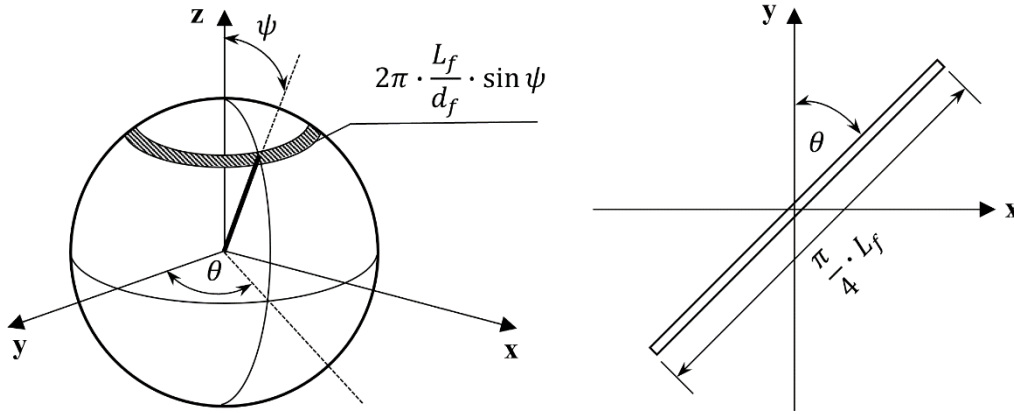


Figure 2-6: Three-dimensional fibre orientation system (after Kooiman (2000))

These contributions have a circular shape with a radius dependent on the orientation angle relative to the z -axis, ψ . As this angle increases, the contribution of the fibre to the projected length increases because the radius of the circle increases and therefore a larger number of fibre end-points form this circle. Stroeven's approach can then be used to determine the average projected fibre length as follows:

$$L_{f,xy} = \frac{\int_0^{\pi/2} L_f \cdot \sin \psi \cdot 2\pi \cdot \frac{L_f}{2} \cdot \sin \psi \cdot d\psi}{2\pi \cdot \frac{L_f}{2}} = \frac{\pi}{4} L_f \quad (2.5)$$

The fibre effectiveness is then calculated with a similar approach as used by Kameswara Rao (1979) in the two-dimensional case where the projected fibre length, $L_{f,xy}$, is projected to the axis which is orthogonal to the crack plane. The fibre effectiveness in three-dimensions is then:

$$\eta_{\theta 3D} = \int_0^{\pi/4} \frac{\pi \cos \theta \cdot d\theta}{\pi} = \frac{1}{2} \quad (2.6)$$

In determining these fibre effectiveness factors, it was assumed that the fibres can orientate themselves freely in space. The proximity of a fibre to a boundary limits the available orientations and therefore increases the fibre effectiveness. By limiting the number of available orientations that a fibre can occupy, the dispersion or variation of orientation angles also decreases. Hence, the dispersion of fibre orientation can be expected to be a maximum under isotropic conditions allowing free rotation of a fibre and to progressively reduce as the fibres tend to assume preferential orientations due to the presence of a boundary.

The effect of geometrical boundaries on the orientation factor has been investigated by several researchers and the underlying theory involved in the models is not included in this study. Comprehensive discussion on the subject can be found in the publications of Alberti (2015), Dupont and Vandewalle (2005), Kameswara Rao (1979), Kooiman (2000), Laranjeira et al. (2011), and Stroeven (1978). Reference can also be made to the work of Bi et al. (2017) and Ferrara et al. (2017) who used

numerical modelling to simulate the distribution and orientation of steel fibres in self-compacting concrete.

2.4.4 Dupont and Vandewalle (2005) orientation model

The method proposed by Dupont and Vandewalle (2005) was selected to estimate the orientation factor due to the simplicity of the procedure. Dupont and Vandewalle derive three orientation factors relating to boundary conditions present at specific zones of the cross section as illustrated in Figure 2-7. The overall orientation factor is then calculated as the geometrical average over the section as follows:

$$\eta_{\theta} = \frac{\eta_1(b-L_f)(h-L_f) + \eta_2 L_f [(b-L_f) + (h-L_f)] + \eta_3 L_f^2}{bh} \quad (2.7)$$

Where:

- η_1 = Orientation factor in zone 1 of Figure 2-7 (= 0.5)
- η_2 = Orientation factor in zone 2 of Figure 2-7 (= 0.6)
- η_3 = Orientation factor in zone 3 of Figure 2-7 (= 0.84)
- b, h = Width and height of the cross section (mm)
- L_f = Fibre length (mm)

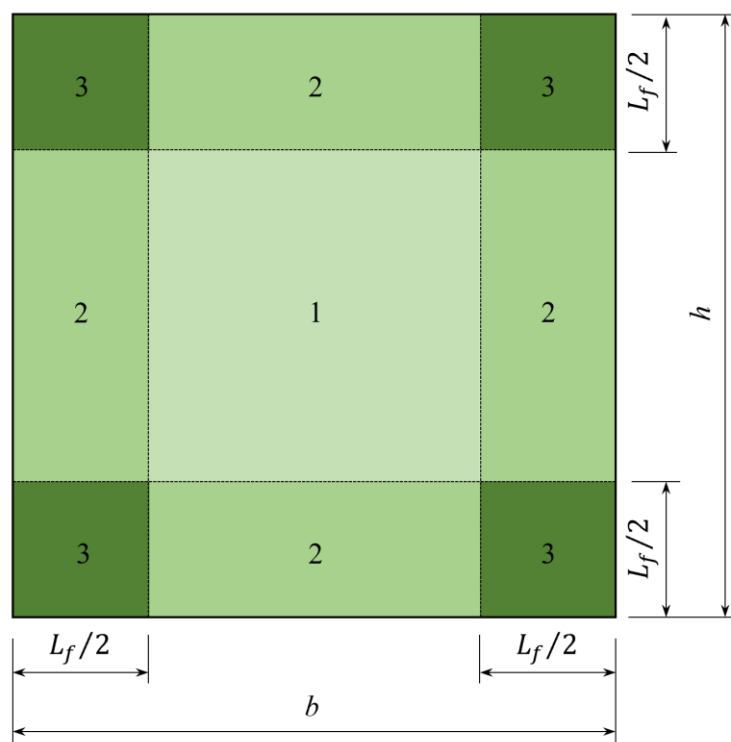


Figure 2-7: Beam cross section illustrating the different orientation zones (after Dupont and Vandewalle (2005))

2.4.5 Influence of fibre effectiveness on tensile behaviour

It is clear from the foregoing discussions that the post-cracking behaviour is highly dependent on the orientation of the fibres in the matrix and that post-cracking behaviour is generally enhanced for fibres that are favourably aligned with respect to the principal tensile stress. Ferrara et al. (2011) presented

results demonstrating the dependency of toughness properties on the fibre orientation factor derived using image analysis. The authors concluded that by tailoring the casting procedure and the fresh state properties of the mixture, fibres can be effectively orientated along the direction of the tensile stresses.

A study by Zhou and Uchida (2017) presented results showing that the number of fibres near a fracture surface is linearly dependent on fibre orientation, while the post-cracking flexural strengths exhibited a perfect linear dependence on the effective number of fibres near the crack surface. This result agrees with the theory presented in the previous sections where the number of effective fibres is a function of the fibre orientation, Equation 2.2. The tensile strength of the composite, as calculated with the law of mixtures (see Equation 2.8), is a function of the fibre effectiveness (Bentur and Mindess, 2006):

$$\sigma_{cu} = \eta_{\theta} \cdot V_f \cdot \tau_{fu} \cdot \frac{L_f}{d_f} \quad (2.8)$$

where σ_{cu} is the tensile strength of the composite in the post-cracking zone; τ_{fu} is the interfacial frictional shear bond strength; and d_f is the diameter of the fibre.

Similar conclusions were obtained by Abrishambaf et al. (2013) in a study evaluating the influence of fibre orientation on the tensile response of steel fibre-reinforced self-compacting concrete. The coefficient of variation in the experimental results of residual flexural strength – and toughness parameters was also found to be significantly lower for the samples with favourable fibre alignment. Abrishambaf et al. (2013) further showed that the scatter of results may be reduced by categorising experimental results in terms of their orientation factor and the number of effective fibres intersecting the crack plane. The trend shown in the stress-Crack Mouth Opening Displacement (CMOD) results indicated that the post-cracking strength is most sensitive to the orientation factor at CMOD values less than 1 mm.

Barragán et al. (2003) conducted uniaxial tensile tests on hook-ended steel fibres and found that the stress at a CMOD of 2 mm and the number of fibres that have effectively pulled out (straightened anchoring hooks) exhibited a linear relationship. The authors reported test results with coefficients of variation of up to 30% and attributed this high scatter to the randomness of the number of effective fibres bridging the crack. Laranjeira et al. (2011) investigated the correlation between the variation of the distribution of fibre orientation and the strength of the composite material. They found that the frequency distribution of orientation angles follows the Gaussian law and suggested a relationship between orientation factor and the standard deviation of the orientation factor, $\sigma(\eta_{\theta})$, as well as the standard deviation of the orientation angles in degrees, $\sigma(\theta)$, as given by Equation 2.9 and Equation 2.10, respectively.

$$\sigma(\eta_{\theta}) = \eta_{\theta} \cdot (1 - \eta_{\theta}) \quad (2.9)$$

$$\sigma(\theta) = 90 \cdot \eta_{\theta} \cdot (1 - \eta_{\theta}) \quad (2.10)$$

Laranjeira et al. (2011) concluded that scatter in material properties is reduced at large orientation factors and this can be attributed to two main reasons: (1) smaller dispersion of the orientation of single fibres around the average orientation angle increases the homogeneous behaviour of the material; (2) based on results presented by Robins et al. (2002), scattering on the pull-out of individual fibres is reduced for smaller inclination angles with respect to the principal tensile stress direction.

A study by Yoo et al. (2014) investigated the effect of fibre length and placement method on the flexural behaviour and fibre distribution characteristics of Ultra-High-Performance Fibre-Reinforced Concrete (UHPFRC). When comparing the results of 19.5 mm and 30 mm fibres, both having an aspect ratio of 100, they noted that the flexural response of the 30 mm fibres demonstrated greater scatter than the specimens containing 19.5 mm fibres. Image analyses of the samples also indicated that the 30 mm fibres were less uniformly distributed across a section when compared to the 19.5 mm samples. The results from their study suggest that variation in flexural behaviour of SFRC may be more dependent on uniformity of fibre distribution than on the magnitude of the fibre orientation factor.

2.5 Spatial Distribution of Fibres

The reinforcing ability of fibres have been shown by several researchers to relate to the spatial distribution of fibres throughout a composite member. Members with poorly dispersed fibres contain regions with low fibre concentrations which require less energy for a crack to initiate, and once a crack has formed, it can easily propagate through the unsupported matrix. Whereas, a composite section with uniformly dispersed fibres minimises the size of such regions, increasing the possibility of bridging a crack, and consequently maximising the reinforcement efficiency.

Studies are generally focussed on investigating preferential fibre orientation caused by casting, processing, rheology, and wall-effects. The influence of fibre distribution is generally assessed by comparing the flexural response of composite members with equal fibre content but different orientation factors resulting from some mechanism affecting fibre orientation. The apparent common conclusion is that the specimen with a higher orientation factor demonstrated superior performance than the specimen with lower fibre effectiveness.

Blanco et al. (2015) showed the effect of varying the width and length of SFRC slabs on the structural response of the members. It was observed that a fibre network forms as a result of flowing concrete during the casting process and that the fibre network enhances the sectional response as the width to length ratio of the slab increases. The influence of flow on fibre orientation and composite performance was also demonstrated by Yoo et al. (2015) by comparing the influence of fibre length and casting location on fibre spatial distribution. The results indicated that the biaxial flexural strength of circular specimen is higher for samples where the pouring of concrete occurred in the centre of the panel compared to pouring at the edge of the mould. Preferential fibre alignment was observed for the specimen cast in the centre and resulted in greater fibre effectiveness. Similar findings were presented

by Abrishambaf et al. (2013) stating that fibres tend to align perpendicular to the radial flow due to the uniform flow profile velocity that defuses outward radially from the centre of the specimen.

Jasiūnienė et al. (2018) investigated the influence of mixture rheological properties on the distribution of steel fibres in self-compacting concrete. The study found that mixtures with low dynamic viscosity exhibited the highest degree of fibre concentration variability and inhomogeneity as well as a more pronounced tendency for fibres to orientate parallel to the casting direction.

The effect of mould surface roughness on steel fibre orientation and the residual flexural tensile strength of composite members was investigated by Žirgulis et al. (2016) by considering fibre orientation angle distribution. High residual flexural strengths corresponded to fibre angle distribution peaks in the range of 10° - 35° , while beam specimens with low residual flexural strengths had peaks in the range of 40° - 60° . The authors also noted that the variation in fibre orientation over the member thickness was well reflected in the variation in flexural strength.

Liu et al. (2013) investigated the 3-dimensional spatial distribution of steel fibres in specimen with varying coarse aggregate contents and sizes. The results demonstrated reduced mean fibre spacing and wider spacing distributions for specimen containing large coarse aggregates which implies a greater degree of fibre clustering. However, the authors concluded that the influence of aggregate size on fibre dispersion could not be decisively established. In an earlier study, Liu et al. (2011) investigated the influence of aggregate size on the fibre orientation factor and reported that increasing aggregate size reduces the orientation factor. The maximum coarse aggregate size should not exceed the fibre length and it is generally recommended that the fibre length should be 2-4 times that of the maximum aggregate size (Bentur and Mindess, 2006; Grünwald, 2004; Johnston, 1996). Figure 2-8 illustrates diagrammatically the effect of maximum aggregate size on the distribution and orientation of fibres.

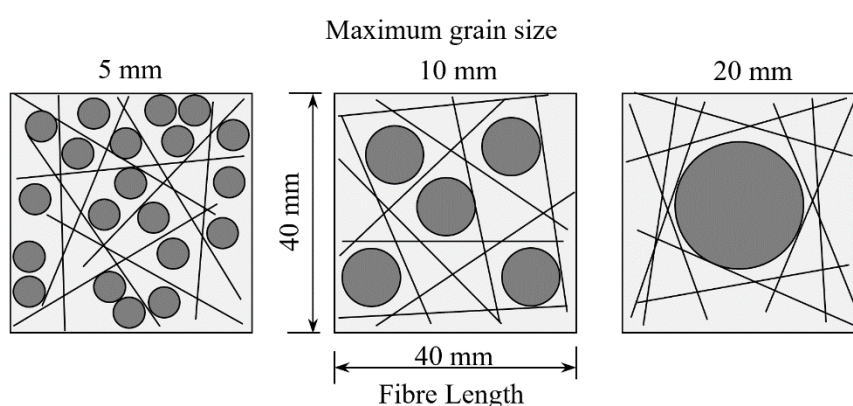


Figure 2-8: Influence of maximum aggregate size on fibre distribution (after Johnston (1996))

The anisotropy commonly encountered with sprayed SFRC was investigated by Segura-Castillo et al. (2018) by assessing fibre distribution and its influence on the residual tensile strength of sprayed SFRC. The authors found that the spraying process did indeed induce a strong preferential alignment of fibres perpendicular to the spraying direction. The orientation factor in this direction was 3 times greater than

the orientation factor in the plane parallel to the spraying direction. The significant anisotropy was also reflected in residual tensile strength results with the strength of specimen loaded parallel to the spraying direction reaching residual loads 3.5 times greater than those loaded perpendicularly.

Caverzan et al. (2015) investigated the influence of fibre dispersion on the dynamic behaviour of high-performance fibre-reinforced cementitious composites. The study revealed that the peak strength of aligned fibres increased by 40% and 30% under static and dynamic loading, respectively, compared to the reference mixture containing no fibres. The specimens with random fibre dispersion and alignment did not favour stable crack propagation and acted as defects in the matrix resulting in a reduction in the peak strength of approximately 30% with respect to the reference mixture.

The effect of fibre length on the tensile and flexural response of extruded and cast PVA fibre-reinforced cement composite specimens was investigated by Akkaya et al. (2000a). PVA fibres of 14 microns in diameter were used with lengths of 2 mm, 4 mm, and 6 mm. The tensile and flexural strengths of the extruded composite members exceeded that of the cast specimen for all fibre lengths, with the 2 mm fibres enhancing composite performance the most. The strength and toughness of the extruded specimens improved as fibre length decreased. Contrary to this behaviour, increasing fibre length improved toughness and strength in the cast specimens. This was considered to be related to the fibre failure mechanisms and the improved fibre-matrix bond attained from the extrusion process, as illustrated in Figure 2-9 (a) and Figure 2-9 (b). The authors observed that long fibres tended to fracture in the extruded system, whereas the dominant failure mechanism of the short 2 mm fibres was pull-out, as shown in Figure 2-9 (c) and Figure 2-9 (d). In the cast system, the dominant failure mechanism of both fibre lengths was fibre pull-out with the longer pull-out length of the 6 mm fibres resulting in improved mechanical performance.

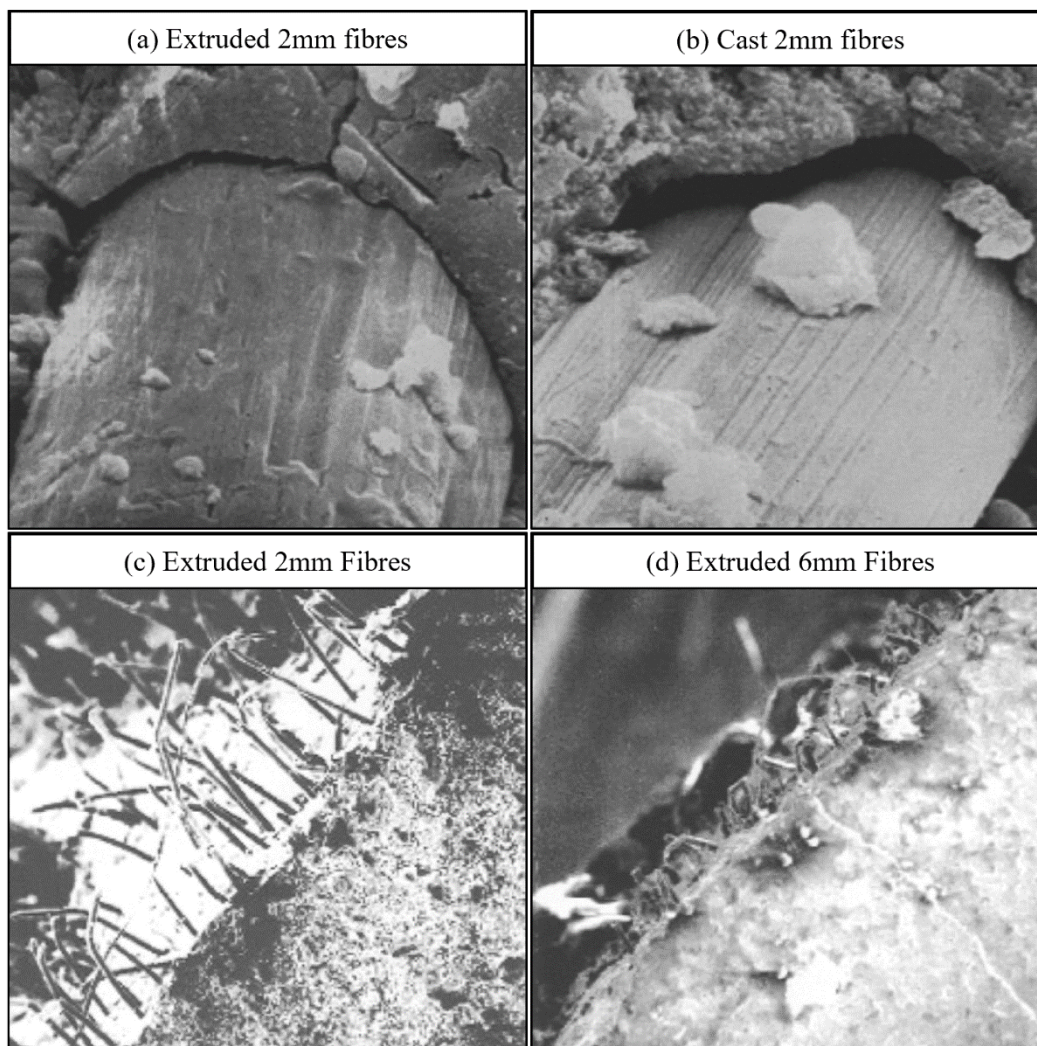


Figure 2-9: (a,b) Fibre-matrix interface of embedded fibres; (c,d) Fibre protrusion lengths (Akkaya et al., 2000a)

As part of an experimental programme aimed at evaluating the notched 3-Point Bending Test (3PBT) proposed in RILEM TC 162-TDF (2002), specimens with varying concrete strength and fibre content were produced and tested by Barr et al. (2003a). As part of the study, the fibre distribution was assessed at the cracked section by Barr et al. (2003b). The results revealed that toughness increased with the number of fibres across the critical section and that the variation in the total number of fibres increased as fibre content decreased. The authors reported that the variability of the normal strength concrete beams generally decreased as the fibre content increased. It was said that achieving a uniform fibre distribution is more difficult with low fibre contents, which possibly contributed to the observed behaviour.

In a study investigating hybrid fibre-reinforced concrete, Sorelli et al. (2005) compared the flexural and uniaxial tensile response of 30 mm steel macro-fibres, 12 mm steel micro-fibres, and a hybrid combination of the two fibres. The authors reported that the Coefficient of Variation (CoV) of the number of fibres intercepting a crack as well as the CoV of tensile and flexural strength is less for the specimens containing micro-fibres. The larger scatter demonstrated by the specimens containing macro-

fibres was attributed to the smaller cracked surfaces where a higher degree of variation in macro-fibre density was observed. It was concluded that the addition of micro-fibres slightly reduces the dispersion in results.

Another consequence of poor fibre dispersion is the high local fibre concentrations associated with local unsupported regions. These effects synergistically interact to reduce the strength of a composite member. Local fibre concentrations are generally referred to as clumps or clusters and the proximity or density of fibres tend to reduce the fibre bond efficiency (Bentur and Mindess, 2006; Bentur et al., 1996; Marković, 2006). Naaman and Shah (1976) investigated the pull-out of aligned and orientated steel fibres and varied the number of fibres that are simultaneously pulled out of a 625 mm² area. A decline in pull-out resistance with increasing fibre density was reported for both orientations. The pull-out resistance of the specimen with the highest fibre density was 86% and 63% of the single fibre resistance, for fibre orientations of 0° and 60°, respectively.

The concept of defect introduction associated with increasing fibre volume content has long been experimentally observed and findings suggest a competing process of strength enhancement and degradation. Strength degradation is considered to be related to an increase in pores or microcrack density brought about by the addition of fibres. Li (1992) speculated that the increase in pores may be due to insufficient compaction and the additional microcracks arise from contacting fibres, unbonded fibre end cracks, or weak fibre-matrix bonding.

The tensile properties of cement mortars reinforced with different-sized PVA fibres and varying volume fractions were studied by Betterman et al. (1995). Fibres with similar aspect ratios but different lengths and diameters were used in the experiment. The results indicated that smaller fibres contributed to higher first-peak tensile strengths, whereas the longer fibres improved the post-peak toughness. The authors performed image analyses on polished sections of specimen and obtained a spacing distribution of fibres. It was observed that the first-peak strength is related to fibre spacing and tended to decrease as the fibre spacing increased.

The spatial distribution of aligned PVA fibres in extruded cement composites was studied by Akkaya et al. (2000b) for different fibre lengths. The authors implemented point process statistics to examine the spatial characteristics of the fibre patterns of each fibre length. Functions were derived for describing the degree of fibre clumping, the size of fibre-free regions, and the number of isolated fibres. It was observed that the 2 mm fibres are distributed more uniformly across the cross section than the 4 mm and 6 mm fibres. The size and amount of the fibre-free regions decreased with fibre length and was found to contribute significantly to the initiation and advance of cracks in the composite. In addition, the authors stated that the presence of clumping in the 6 mm fibre specimens reduced the effectiveness of fibres to resist crack propagation and the initiation of these cracks are more likely due to the larger fibre-free areas associated with specimens containing longer fibres.

The effect of fibre dispersion on composite performance was further studied by Akkaya et al. (2001) by considering the distribution of 2 mm PVA fibres at multiple crack locations of an individual specimen. The authors observed that cracks form sequentially depending on the size of the fibre-free areas and the degree of clumping. Cross sections with a higher degree of clumping tended to crack before cross sections with more uniformly distributed fibres and the toughness of the composite is dependent on the degree of clumping at the cross section of the first crack, as shown in Figure 2-10. A strong correlation was found between the cracking load and the size of the fibre-free regions. It was concluded that the cracking stress is reduced by the fibre-free areas which act as flaws in the composite material.

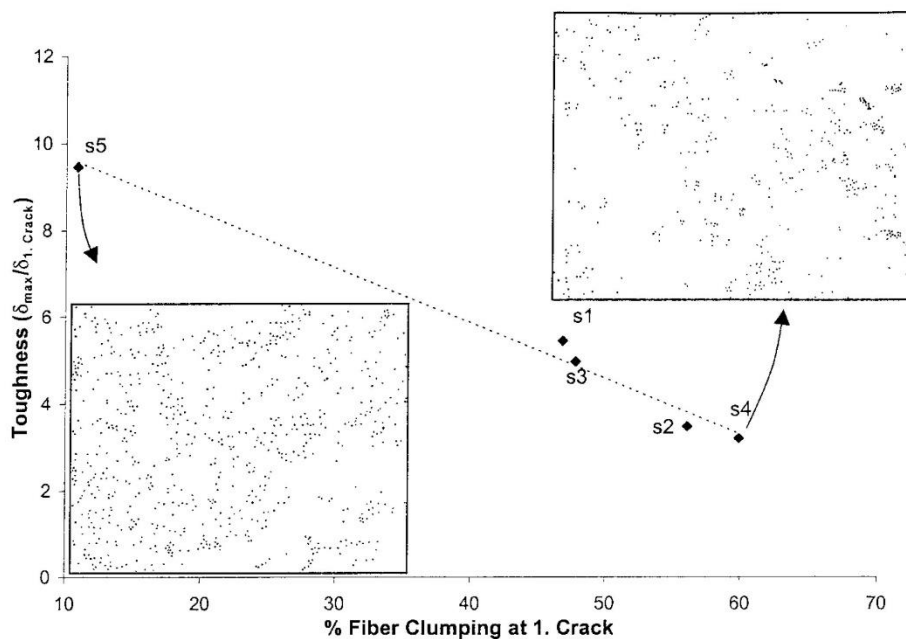


Figure 2-10: Effect of fibre clumping at the first crack section on composite toughness (Akkaya et al., 2001)

2.6 Evaluating Fibre Orientation and Distribution

Various techniques have been developed and proposed in recent years for measuring the orientation and spatial distribution of fibres. These methods include photometric analysis, X-ray computed tomography, and methods based on different physical phenomena such as electrical conductivity and magnetism.

2.6.1 Photometric methods

Photometric analysis usually involves slicing a composite specimen, polishing and preparing the surface, acquiring the images, and extracting and processing the results. Photometric methods can generally be applied to organic and inorganic fibres and can be implemented using a digital camera (Liu et al., 2011), optical microscope (Zhou et al., 2012; Zhou and Uchida, 2017; Ferrara et al., 2011), scanning electron microscopy (Felekoğlu et al., 2015; Akkaya et al., 2000b), and fluorescence microscopy (Torigoe et al., 2003; Lee et al., 2009). An example of a typical image resulting from implementing a photometric technique is shown in Figure 2-11.

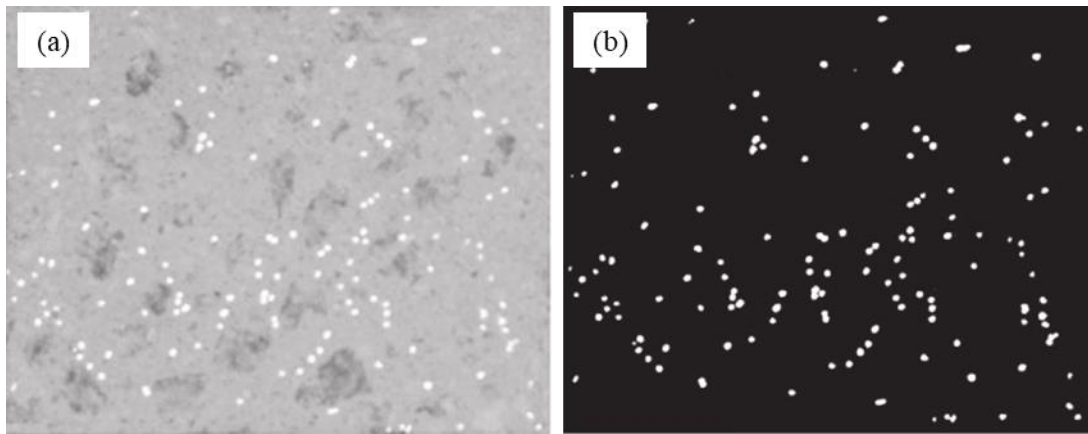


Figure 2-11: Example of photometric method image (a) Grayscale image, (b) Binary image (Abrishambaf et al., 2013)

Fibres with circular cross sections intersecting the cut-plane are seen as elliptical-shaped footprints due to the inclination angles of the fibres in the matrix. Measuring this ellipticity allows for determining the orientation of each fibre. Fibre orientation is commonly defined as the angle between the fibre's longitudinal axis and a vector that is orthogonal to the cut-plane. The angle can be determined using Equation 2.11 by identifying the minor and major axis of the ellipse from image analysis. The calculation is illustrated in Figure 2-12 and Figure 2-13.

$$\theta = \cos^{-1}\left(\frac{d}{l}\right) \quad (2.11)$$

Where:

θ = Fibre angle

d = Minor axis length of fibre (Theoretically equal to the fibre diameter)

l = Major axis length of fibre

A shortcoming of implementing this method to evaluate fibre orientation distribution is illustrated in Figure 2-13. The figure demonstrates the small change in the major axis length for inclination angles below 30° . Consequently, estimation errors are unavoidable when calculating fibre orientations below 30° based on the l/d ratio of the detected ellipses. To prevent false detection, a high-resolution image in relation to the fibre size is required as well as meticulous sample preparation (Lee et al., 2016).

In addition, photometric methods generally involve developing sophisticated image processing algorithms for extracting data from images. Lee et al. (2009) developed an algorithm for automatically detecting PVA fibres from images captured using the fluorescence microscopy technique. The procedure incorporates an artificial neural network that is trained to correctly distinguish between single fibres and potentially aggregated fibres. In addition, the authors proposed the use of the watershed distance transform and morphological reconstruction operations to enhance the fibre-detection capability of the algorithm. Morphological reconstruction is useful to remove small noise spots without altering the overall shape of objects in an image and can be used to extract marked objects, detect or remove objects

touching the image border, detect or fill object holes, and filter out spurious high or low points (Gonzalez et al., 2009).

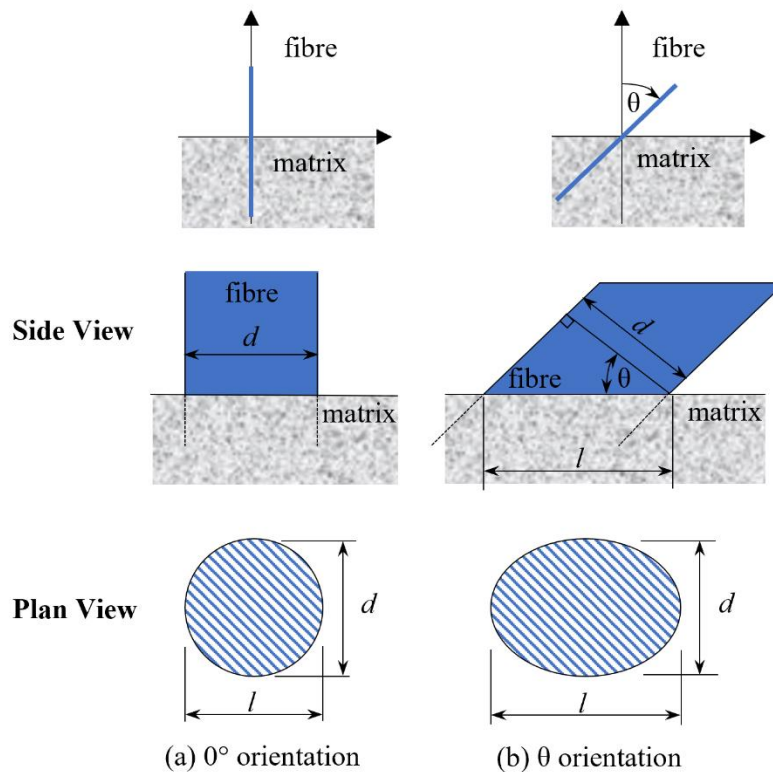


Figure 2-12: Illustration of fibre orientation calculation (after Lee et al. (2016))

Fibre Orientation ($^{\circ}$)	Fibre Cross Section
0	
15	
30	
45	
60	
75	
85	

Figure 2-13: Change in major axis length with increasing fibre orientation (after Lee et al. (2016))

2.6.2 X-ray computed tomography

X-ray Computed Tomography (CT) has emerged as an effective means for non-destructive 3D visualisation of the microstructural features of objects. CT has also been used to quantitatively assess and study the spatial distribution and orientation of steel fibres in cement composite materials (Ponikiewski et al., 2015; Ponikiewski and Katzer, 2016; Liu et al., 2013; Zhou and Uchida, 2017). X-ray Micro-Computed Tomography (μ CT) is essentially based on the same principle as conventional CT, with the primary distinction being that the specimen is rotated while the X-ray source and detector remain stationary and the resolution of the result is commonly in the micrometre range (Eik, 2014). However,

due to the μ CT process and the high-resolution output, the sizes of specimens are limited and therefore the method is generally only partially non-destructive (Bernasconi et al., 2012). Examples demonstrating the segmentation and reconstruction of steel fibre μ CT images are shown in Figure 2-14.

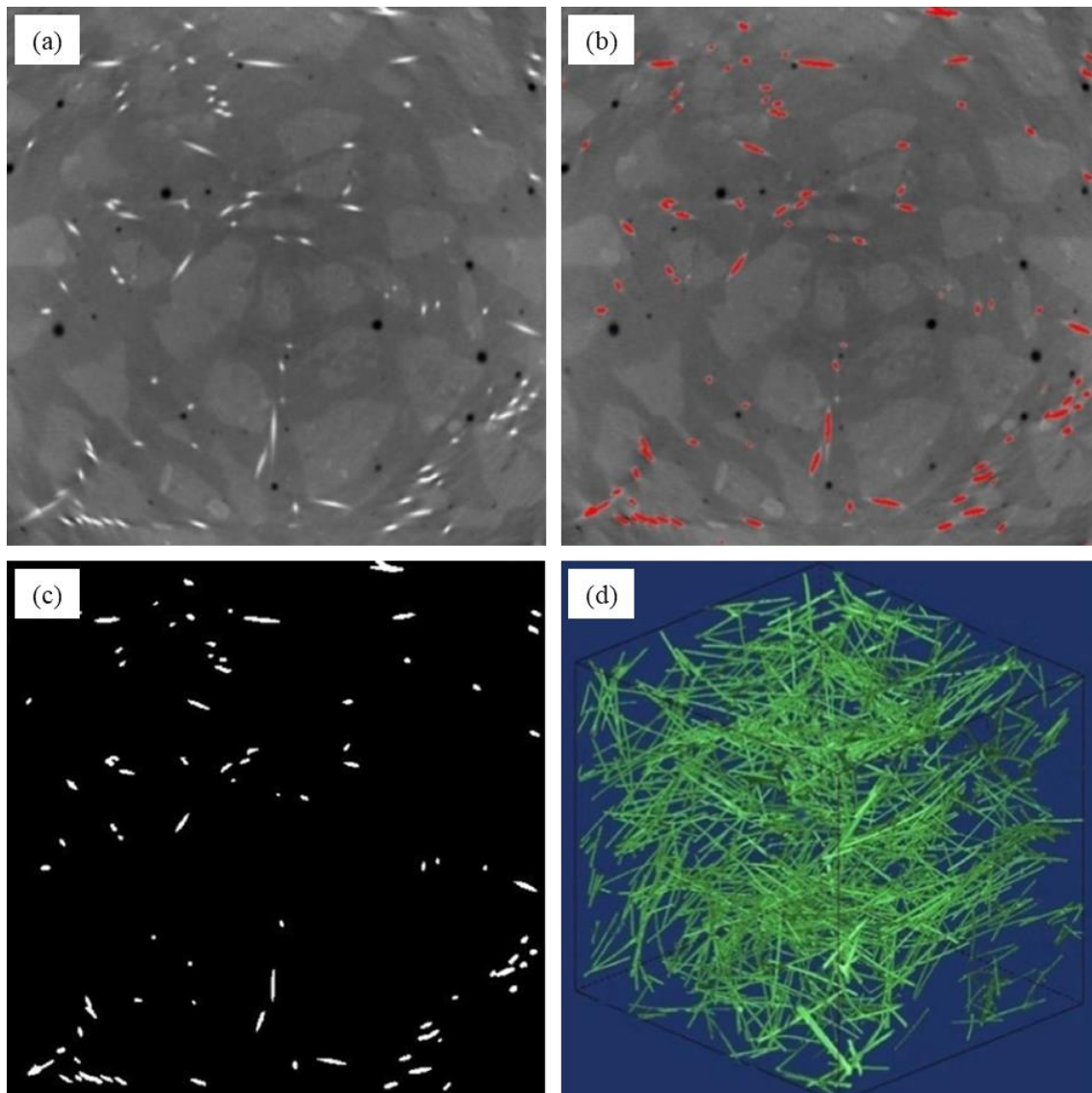


Figure 2-14: Example of μ CT output (a) Original μ CT image, (b) Fibre segmenting, (c) Binary image, (d) Reconstructed 3D fibre image (Liu et al., 2013)

Bernasconi et al. (2012) analysed fibre orientation distribution using photometric and μ CT techniques and compared the results obtained from the two methods. It was concluded that the two methods can provide very similar results in terms of fibre orientation. Analogous observations were found in a study by Andries et al. (2015). Bernasconi et al. (2012) also reported the reduced accuracy of the optical method in measuring low fibre angles. It was ultimately stated that when selecting a technique, one must consider the simpler experimental setup, but fully destructive nature of the optical method and the partially non-destructive, but expensive experimental facilities related to the μ CT approach.

2.6.3 Indirect methods for conductive fibre-reinforced composites

Indirect methods based on measuring either electrical or magnetic properties of fibre-reinforced cementitious composites have been proposed as non-destructive methods for evaluating fibre dispersion. These methods mainly rely on the electro-magnetic properties of fibres and are well suited for fibres that are conductive and have strong ferromagnetic behaviour such as steel fibres (Faifer et al., 2013). A drawback of these techniques is that they are only able to assess general tendencies, such as the average fibre spacing and the average fibre orientation and alignment, rather than providing the orientation of individual fibres (Eik, 2014).

The effective magnetic permeability of a composite material is affected by the presence of steel fibres in a cementitious matrix. Non-destructive measuring techniques, which employ a probe that is sensitive to the magnetic properties of steel fibres, exploit this phenomenon and have been developed for analysing fibre dispersion and orientation in FRC elements (Faifer et al., 2011; Torrents et al., 2012; Ferrara et al., 2012; Ferrara et al., 2017). The path of magnetic field lines, generated by the winding of a probe, is modified by the presence and arrangement of steel fibres and produces variation in the measured impedance of the probe (Faifer et al., 2013). By calibrating the method for the aspect ratio and dosage of a specific fibre, the fibre concentration can be quantitatively assessed and preferential fibre orientation can be estimated (Ferrara et al., 2012).

Alternating Current Impedance Spectroscopy (AC-IS) is an alternative non-destructive technique for investigating microstructural features such as fibre dispersion, fibre orientation, clumping, and segregation (Faifer et al., 2013; Woo et al., 2005; Ozyurt et al., 2004). The dual-arc response of conductive FRC allows for obtaining parameters that describe fibre dispersion. The dual-arc response refers to the unique frequency-dependent behaviour of the composite material where conductive fibres (such as steel and carbon fibres) are insulating under low AC frequencies while under high frequencies they are conductive. Therefore, by applying an excitation voltage to the specimen over a range of frequencies and measuring the phase and amplitude of the output current, the conductivity can be calculated for the composite when fibres are conducting (high frequencies) as well as the conductivity of the matrix (low frequencies) to result in a parameter that describes fibre dispersion (Ferrara et al., 2008).

Ozyurt et al. (2007) investigated the correlation between fresh state properties and mechanical performance of steel fibre-reinforced composites using AC-IS to monitor fibre segregation non-destructively. The results indicated that the fresh state properties affected fibre dispersion and mechanical properties. In a previous study, Ozyurt et al. (2006) implemented AC-IS together with image analysis to demonstrate the capability of AC-IS to monitor fibre dispersion and it was concluded that the results from both methods agreed well (within experimental uncertainty).

2.7 Strength Testing Methods

Several test methods are available for experimentally evaluating the post-cracking behaviour of fibre reinforced composite materials. Selecting the most suitable method depends on factors such as the complexity of the test setup, specimen preparation, and execution, as well as the cost, reproducibility, and general acceptance of the method by researchers and practitioners (Kooiman, 2000). The available methods may be categorised as bending tests, splitting tests, and uniaxial tensile tests.

The most recognised and widely used bending tests are the 4-Point Bending Test (4PBT) and the 3-Point Bending Test (3PBT). Figure 2-15 illustrates the difference between the two tests, which is that the 3PBT is loaded at mid span, while the 4PBT is loaded at two locations with each load applied a third of the span away from the supports on either side. In both tests the specimen can be shaped to have a notch, although it is more common for the 3PBT to be notched.

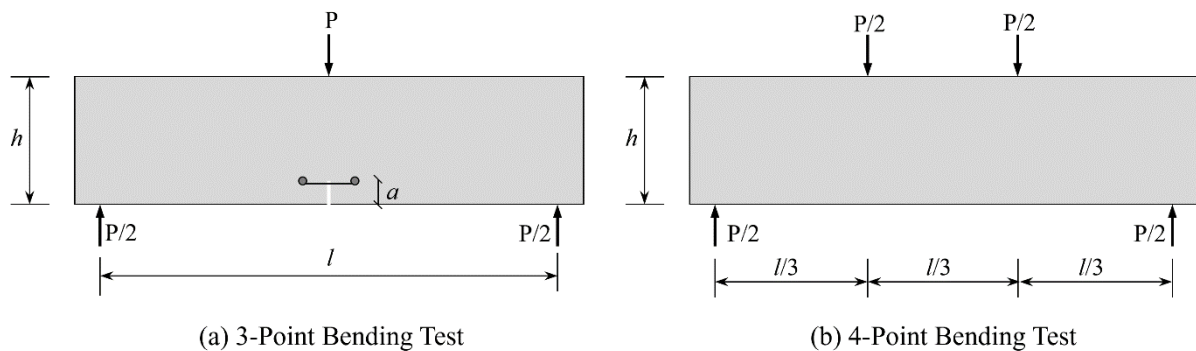


Figure 2-15: Schematic of flexural beam tests

The 4PBT was developed to incorporate the effect of variation in material strength by applying the load such that a constant bending moment occurs in the central section of the beam and the first crack will therefore initiate at the weakest cross section. The position of discrete cracks cannot be predicted and consequently complicates the measurement of Crack Mouth Opening Displacements (CMOD). The mid-span deflection is usually measured and can be utilised to calculate the area under the load-displacement curve to acquire a measure of the composite's energy absorption capacity. ASTM C1609/C1609M-12 (2013), JCI-S-003-2007, and several other standards are available that use 4PBT to characterise the flexural behaviour of FRC.

In the 3PBT, the first crack will always be in the vicinity of the beam's centre, although the exact location is uncertain. Specimen are often notched at mid-span so that a crack may initiate at a known location, which then permits the measurement of CMOD. This allows establishing a direct relationship between the bending moment and the crack width of the sample. The disadvantage is that the crack is forced to localise at the notch which may not necessarily be the weakest cross section. Furthermore, although there are no shear stresses in the vertical plane located at the central loading point, the shear stresses are at a maximum directly adjacent to the plane. The implication of such a condition in a material like concrete is that shear stresses may contribute to the initiation of fracture should a fracture form on a

plane other than the central vertical plane. In order to assume the primary failure comes from tensile or compression stress, the shear stress in the section must be minimised. In the 4PBT, the central loaded region is free from shear stresses and has non-zero shear stress values in the spans adjacent to the central loading span. Consequently, the material in the central region is in a simpler stress state and should fracture occur within the central region it may be regarded as occurring primarily due to the tensile and compressive stresses exceeding the material capacity. The 3PBT generally specify that a notch be cut at the centre loading point of the beam ensure that failure occurs at the location of minimum shear stress and maximum bending moment. Additionally, the standards specify that should a specimen fail outside of the notch, the test must be disregarded. Standards that have adopted the use of notched 3PBT to quantify the flexural strength of FRC include RILEM TC 162-TDF (2002), *fib* Model Code 2010 (2013), EN 14651 (2005), and JCI-S-002-2003.

A round panel test has also been proposed in ASTM C1550-12a that can be used to determine the flexural toughness of FRC by centrally loading a statically determinate round panel. Paegle and Fischer (2013) reported that the round panel test is a reasonable alternative FRC flexural test that not only accounts for multiple cracking but also reduces the variability in test results.

Splitting tests have been used extensively with plain concrete as a method for indirectly determining the tensile strength of a specimen. The Brazilian splitting test is a load-controlled test on a cylinder and is one of the most well-known splitting tests. Denneman et al. (2011) proposed a methodology for a modified Brazilian splitting tensile test procedure that successfully provided improved estimates of the true tensile behaviour of FRC. The wedge-splitting test is alternative method that involves splitting a cube or cylinder from one side by a wedge. Löfgren et al. (2004b) and Löfgren et al. (2004a) used the wedge-splitting test method to determine the fracture properties of FRC and investigated the applicability and repeatability of the method. The authors reported that the results demonstrated lower scatter than the notched 3PBT and that the test method is suitable for assessing the fracture properties of FRC. Both tests are generally carried out using a closed-loop testing system to enable deformation-controlled testing of the post-cracking behaviour of the composite. The configurations of the tests are shown in Figure 2-16.

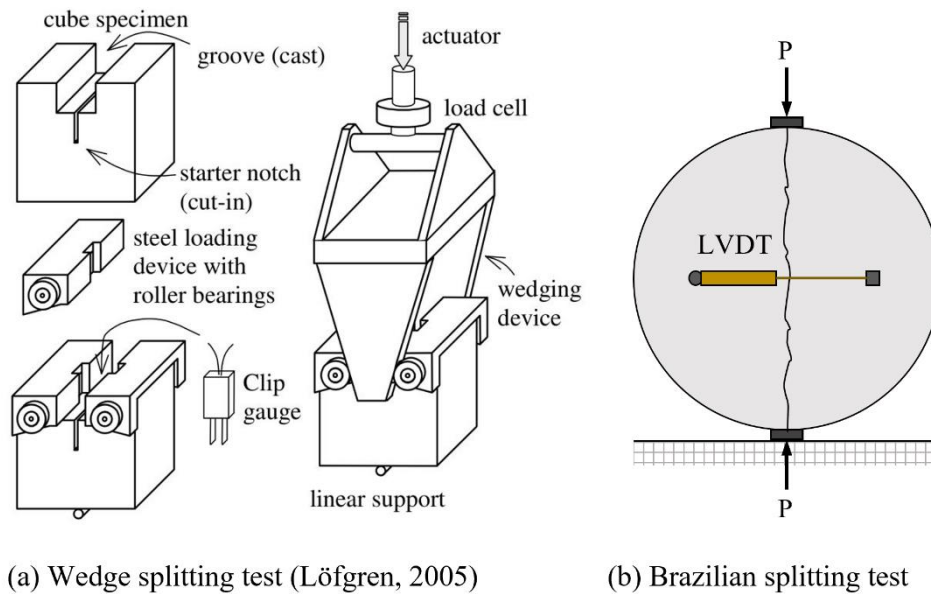


Figure 2-16: Splitting tensile tests

The uniaxial tensile test is theoretically the most appropriate method to determine the post-cracking tensile response of FRC, due to the ability of directly translating test results into a uniaxial material relation. The disadvantages associated with the method generally relate to the complexity of the test setup. Therefore, conducting the test demands highly trained and experienced personnel and the required preparation is usually more time consuming than bending or splitting tests; consequently, the experimental costs are relatively high.

Within the scope of this research, the notched 3PBT was selected to evaluate the post-cracking behaviour of FRC. The method was found to be well established and known in the field of FRC and constituted a simple, cost-effective, and reliable procedure for experimental testing. Furthermore, the formation of a single crack localised at the notch enables investigating fibre spatial characteristics at one location adjacent to the crack as opposed to multiple cracks potentially forming in the 4PBT. The recommendations and procedures provided in RILEM TC 162-TDF (2002) was adopted for conducting the 3PBTs in this study.

2.7.1 RILEM TC 162-TDF (2002) calculation procedure

The RILEM TC 162-TDF (2002) final recommendation for the bending test provides two different approaches for deriving flexural strength parameters from test data. The first approach involves calculating the equivalent flexural tensile strengths ($f_{eq,2}$ and $f_{eq,3}$) and the second approach the residual flexural tensile strengths ($f_{R,1}$ and $f_{R,4}$). In both cases it is assumed that the stress distribution in the cross section is linear elastic. Additionally, RILEM TC 162-TDF (2002) proposed that the load at the limit of proportionality (F_L) should be taken as the highest load recorded up to a deflection of 0.05 mm. The RILEM TC 162-TDF (2002) final recommendation for the bending test ultimately culminated into the *fib* Model Code 2010 (2013) with some alterations. The *fib* Model Code 2010 (2013) adopted the

use of residual flexural strength parameters to quantify the post cracking flexural tensile strength of fibre reinforced beam specimen instead of the equivalent flexural strength parameters. The equivalent flexural strength concept is a function of the energy dissipated up to a given deflection and is presumed to only account for the energy absorption capacity provided by the fibre mechanisms. The concept of the residual flexural tensile strength gives the stress for distinct displacements or CMOD. It is possible that the residual flexural strength approach was adopted by the *fib* Model Code 2010 (2013) due to the advantage of being easier to evaluate than the equivalent flexural strength approach. The force-deflection relationship that is typically obtainable from a bending test is shown in Figure 2-17 and Figure 2-18 (adapted from Barros et al. (2005)).

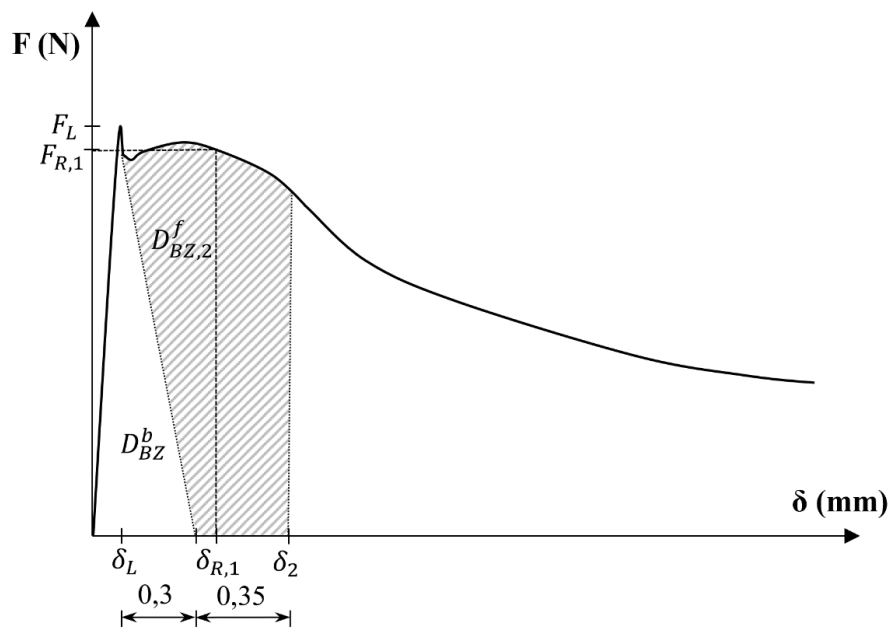


Figure 2-17: Evaluation of $f_{eq,2}$ and $f_{R,1}$ as recommended by RILEM TC 162-TDF (2002)

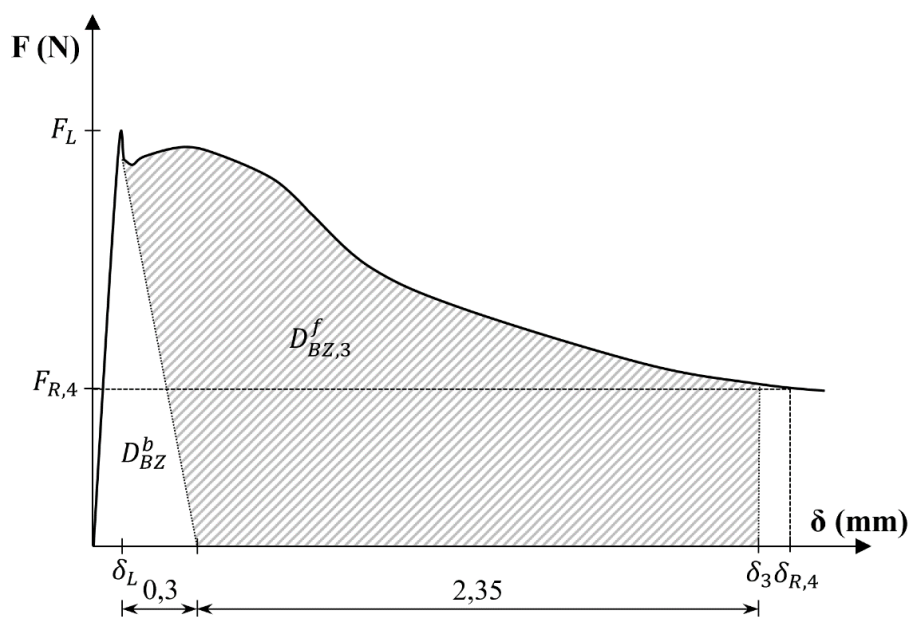


Figure 2-18: Evaluation of $f_{eq,3}$ and $f_{R,4}$ as recommended by RILEM TC 162-TDF (2002)

2.7.1.1 Equivalent flexural tensile strength

The equivalent flexural strength parameters $f_{eq,2}$ and $f_{eq,3}$ are related to the energy absorption capacity provided by the fibre reinforcement mechanisms $D_{BZ,2}^f$ and $D_{BZ,3}^f$ up to deflections δ_2 and δ_3 where:

$$\delta_2 = \delta_L + 0.65 \text{ mm} ; \text{ (see Figure 2-17)}$$

$$\delta_3 = \delta_L + 2.65 \text{ mm} ; \text{ (see Figure 2-18)}$$

δ_L = Deflection corresponding to F_L , and

$D_{BZ,2}^f$ and $D_{BZ,3}^f$ are the areas under the $F - \delta$ curve up to deflections δ_2 and δ_3 as depicted in Figure 2-17 and Figure 2-18.

The parcel of energy provided by cracks forming in the matrix, D_{BZ}^b , is not included in the evaluation of the equivalent flexural strength parameters. According to RILEM TC 162-TDF (2002), the equivalent flexural tensile strength parameters and limit of proportionality ($f_{fct,L}$) can be calculated using the following expressions:

$$f_{fct,L} = \frac{3 F_L L}{2 b h_{sp}^2} \quad (2.12)$$

$$f_{eq,2} = \frac{3 D_{BZ,2}^f L}{2 \cdot 0.50 b h_{sp}^2} \quad (2.13)$$

$$f_{eq,3} = \frac{3 D_{BZ,3}^f L}{2 \cdot 2.50 b h_{sp}^2} \quad (2.14)$$

Where b (=150 mm) is the width of the specimen, L (=450 mm) is the loading span, and h_{sp} (=125 mm) is distance from the tip of the notch to the top of the cross section.

2.7.1.2 Residual flexural tensile strength

The residual flexural strength is obtained by taking the load at a certain displacement and calculating the stress using simple beam theory. RILEM TC 162-TDF (2002) states that the loads $F_{R,1}$ and $F_{R,4}$ be determined at $CMOD_1$ (= 0.5 mm) and $CMOD_4$ (= 3.5 mm) or at displacements $\delta_{R,1}$ (= 0.46 mm) and $\delta_{R,4}$ (= 3.00 mm) (see Figure 2-17 and Figure 2-18). Assuming a linear elastic stress distribution, the residual flexural tensile strength parameters can then be calculated using the following expressions:

$$f_{R,1} = \frac{3 F_{R,1} L}{2 b h_{sp}^2} \quad (2.15)$$

$$f_{R,4} = \frac{3 F_{R,4} L}{2 b h_{sp}^2} \quad (2.16)$$

It has been pointed out by some authors (Barros et al., 2005; Nayar et al., 2014) that although the residual flexural strength parameters have the advantage of a more simplified derivation, they are more susceptible to local irregularities in the load-deflection curve and may provide results that show a larger amount of scatter than the equivalent strength parameters.

2.8 Discussion on Reviewed Literature

The principal aim of this chapter was to provide a concise overview of the current state of knowledge regarding the factors that influence fibre pull-out response, the distribution of fibres in a cementitious matrix, and relevant test methods for quantifying composite strength and fibre distribution. The reviewed body of knowledge serves as a guideline defining the direction of this study.

The post-cracking behaviour of fibre-reinforced composites was investigated by exploring the mechanisms and material characteristics that dictate the pull-out response of a single fibre. It was found that composite behaviour is highly complex and is dependent on a multitude of interrelated variables such as fibre geometry, fibre material, matrix characteristics, and fibre inclination angle. The high complexity in composite response constituted a requirement to minimise the number of variables in the experimental framework of this study. This will limit the number of mechanisms possibly contributing towards the observed composite response and facilitate the thorough investigation and understanding of fibre distribution and flexural performance.

Fibre orientation distribution has received much attention by various researchers owing to the significant effect of fibre orientation on composite performance. Extensive studies have revealed that fibre orientation is a function of several variables including fibre geometry, fresh-state properties, mixture composition, and wall-induced effects. The effectiveness of a given fibre to orientate itself is expressed as an orientation factor and several models have been developed for estimating fibre orientation distribution. The model proposed by Dupont and Vandewalle (2005) was selected due to the simplicity of implementing the method.

Experimental studies investigating fibre spatial distribution were reviewed and the results demonstrated an evident influence on the behaviour of FRC. It was shown that uniformly distributed fibres enhance the strength of a composite member by effectively sharing the crack-bridging load. Furthermore, evidence was presented suggesting that variability in mechanical response is related to fibre spatial distribution. The unfavourable influence of fibre clustering and dense fibre concentrations on composite toughness and fibre pull-out resistance was also shown.

The methods commonly implemented to obtain the distribution of fibres at a cross section were reviewed. It was found that photometric methods are perceived as the most conventional and simple approach to obtain fibre spatial information. However, the method has the disadvantage of low accuracy in determining fibre orientation at low inclination angles as well as ambiguity in the angular direction of the fibre. In addition, in order to avoid extraneous manual selection of fibres, the approach requires advanced image processing techniques to segment fibres automatically.

The test methods available for characterising the post-cracking response of FRC specimen were discussed. It was found that there is no general consensus on the most suitable test method and the preferred method is primarily dependent on the available resources of the laboratory. For the purpose of

quantifying the post-cracking response of SFRC, the notched 3PBT recommended by RILEM TC 162-TDF (2002) was selected for experimental testing.

A recurring theme noticed during the literature review was the large degree of variation generally associated with FRC which was frequently considered to be strongly correlated with fibre spatial characteristics. However, limited studies were found which investigated such a hypothesis. Researchers also continually emphasised the importance of considering fibre orientation and spatial distribution when designing composite elements. No prominent studies were found that simultaneously assessed the influence of fibre type and dosage on the spatial distribution of fibres and subsequently relating the findings to the mechanical response and variability of laboratory specimen. Investigating fibre spatial characteristics in conjunction with composite performance is a natural step that will contribute towards the thorough understanding of fibre-reinforced composites.

CHAPTER 3. Methodology

3.1 Background

Testing the hypotheses posed in Chapter 1 requires the experimental evaluation of two unknown material characteristics: strength and fibre spatial distribution. Determining these variables requires the development of a specialised methodology that is formulated taking cognizance of current practice and the state of knowledge presented in Chapter 2. This chapter discusses the elements associated with the experimental phase which consists of the following:

- Experimental design;
- Sample production;
- Strength testing;
- Image acquisition and processing, and
- Quantifying fibre spatial characteristics.

The first section of this chapter serves to outline the experimental programme and contains details relating to material testing, mixture design, and the proposed experimental variables. The methodology applied in the production of laboratory specimens is described in Section 3.3 and includes discussions on relevant procedural aspects related to mixing, casting, and curing of samples. Compressive strength and density results are presented in Section 3.4 and the observed trends are briefly discussed. The setup and instrumentation used in the adopted flexural strength testing method is described in Section 3.5.

The methodology involved in sample preparation and image acquisition is discussed in Sub-section 3.6.1. An algorithm for extracting the centroidal coordinates of each fibre from image data is developed in Sub-section 3.6.2. These results are then used in Sub-section 3.6.3 to generate a Voronoi diagram to provide the geometric descriptors necessary to quantify the spatial distribution of the fibres. Section 3.7 contains a discussion on fibre orientation and an empirical approach is proposed to determine the orientation factor from image data.

Section 3.8 and Section 3.9 are dedicated to establishing suitable measures that describe fibre spatial characteristics. The first approach is presented in Section 3.8 and is based on specifying a square raster size and counting the number of fibres inside each raster tile. A second approach that employs Voronoi data as a geometric descriptor is proposed in Section 3.9. Random point patterns are also simulated in Sub-section 3.9.1 and are used as an objective reference condition for quantifying fibre clustering as well as for comparing the distribution process of fibres to that of a random Poisson process.

Section 3.10 concludes the chapter with a discussion on the main findings and observations concerning the formulated methodology.

3.2 Experimental Programme and Constituent Materials

The objective of the study is to quantify the fibre spatial characteristics for various fibre contents and fibre lengths and to evaluate the influence of fibre spatial distribution on the flexural performance of a notched composite beam under three-point loading. Two different lengths of hook-ended steel fibres with similar aspect ratios were sourced from a local supplier. The fibre lengths were 30 mm and 60 mm with wire diameters of 0.5 mm and 0.9 mm, respectively, and the nominal tensile strength is stated as 1100 N/mm² for both fibres. The appearance of each fibre is shown in Figure 3-1.

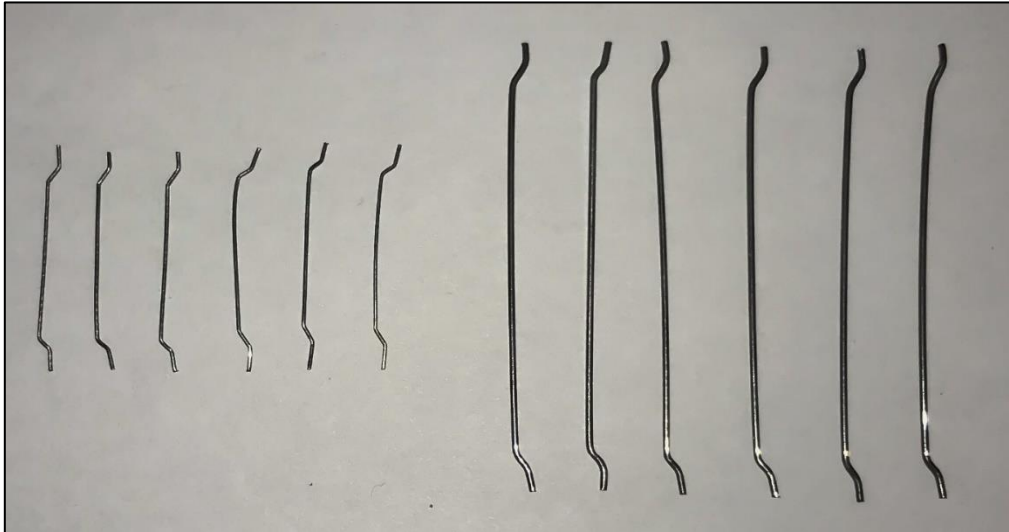


Figure 3-1: Fibre appearance

The fibre dosage for each fibre length ranged from 40 kg/m³ to 120 kg/m³ in intervals of 20 kg/m³. These dosages roughly translate to fibre volume contents of 0.5, 0.75, 1.0, 1.25, and 1.5 per cent. Double batches were cast for fibre dosages of 80 kg/m³ and 120 kg/m³, resulting in a total of 7 batches for each fibre geometry. The double batches were cast with the intent of evaluating the consistency between batches. Each batch comprised of nine 150 mm x 150 mm x 600 mm flexural beams and three 150 mm x 150 mm x 150 mm cubes for compressive strength testing. Furthermore, a control mix containing no fibres was cast with an additional three 150 mm x 300 mm cylinders used to determine the elastic modulus of the concrete.

The name convention followed throughout this study allows each batch to be identified by two numbers separated by a dash; the first number indicates the dosage and the second the fibre length used in the batch. A third letter is added in the case of the 80 kg/m³ and 120 kg/m³ double batches to distinguish between the batches.

The mixture proportions were selected to achieve a target mean compressive strength of 50 MPa after water curing the specimens for 28 days. A conventional mixture with a w/c ratio of 0.5 was designed and each batch was mixed according to the proportions provided in Table 3-1. The coarse aggregate fraction was adjusted to account for increasing fibre content.

Table 3-1: Mixture components by mass

Material	Unit	Relative Density	Fibre Content (kg/m ³)					
			0	40	60	80	100	120
Cement (CEM I 52.5N)	kg/m ³	3.14	460	460	460	460	460	460
Water	kg/m ³	1.00	230	230	230	230	230	230
Dolomite 9.5 mm aggregate	kg/m ³	2.85	897	883	876	868	861	854
Dolomite sand	kg/m ³	2.85	880	880	880	880	880	880
Steel fibre	kg/m ³	7.87	0	40	60	80	100	120
Theoretical Density	kg/m ³	-	2467	2493	2506	2518	2531	2544

3.3 Production Method

3.3.1 Mixing procedure

A standard sequence of consecutive mixing steps was followed for every batch. First, the dry materials were transferred to a skip which was then emptied into a 300 ℓ pan mixer and mixed for 30-45 seconds. At this stage water was gradually added to the mixture over a period of approximately 90 seconds and allowed to properly integrate into the mix for an additional 60 seconds. Thereafter, the fibres were gradually introduced by hand until all fibres were thoroughly dispersed throughout the mixture. The duration of this step depended on the fibre dosage as well as the fibre length.

It was observed that at volume contents above 80 kg/m³, the 60 mm fibres started balling and required that the mixer be periodically stopped in order to break apart the accumulations. The 30 mm fibres showed little tendency for balling at similar volume contents.

3.3.2 Casting procedure

The production method as recommended by RILEM TC 162-TDF (2002) was adopted for casting the flexural beam specimens. Prior to casting, all moulds were cleaned and prepared with oil to facilitate easy demoulding. As prescribed by the recommendation, the moulds were filled in two portions in a single layer up to approximately 90% of the specimen height. The moulds were then further filled and levelled off while being compacted. Compaction continued until no air bubbles were visible on the concrete surface. No indication of significant bleeding or segregation was observed during compaction.

Slump tests were carried out for every batch to provide an indication of the workability of the mixture. Photographs of slump tests of selected batches are shown in Figure 3-2. Although increased fibre content or length reduced the workability, all mixtures were sufficiently workable as to allow the facile placement and compaction of concrete specimens.



Figure 3-2: Slump tests of selected batches

3.3.3 Specimen curing and preparation for testing

Shortly after casting, the samples were covered with plastic sheeting for 24 hours before demoulding commenced. The samples were then placed in temperature-controlled water curing tanks for a period of 28 days until testing. The RILEM TC 162-TDF (2002) recommendation specifies that a 25 mm notch be cut at the centre of each beam perpendicular to the top surface at casting. This process was performed using a wet cutting circular diamond blade 7 to 14 days prior to testing; thereafter, the samples were returned to the curing tanks until testing commenced. The batch with no fibres was not notched in order to avoid risking accidental fracture at the notch while handling the samples.

3.4 Compressive Strength Tests

Three 150 mm cubes were cast for each batch of concrete and prepared as described in the previous section. After water curing for 28 days, the weights of the cubes were measured in air and under water

and used to calculate the density of each cube before being crushed. Figure 3-3 shows the ratio of mean cube density to maximum theoretical density of each batch as given in Table 3-1. Although the figure indicates that a lower degree of compaction was generally achieved for the mixtures containing 60 mm fibres, it can be concluded that the unintentional entrapment of air voids should not have a significant effect on the properties measured for any of the mixes cast.

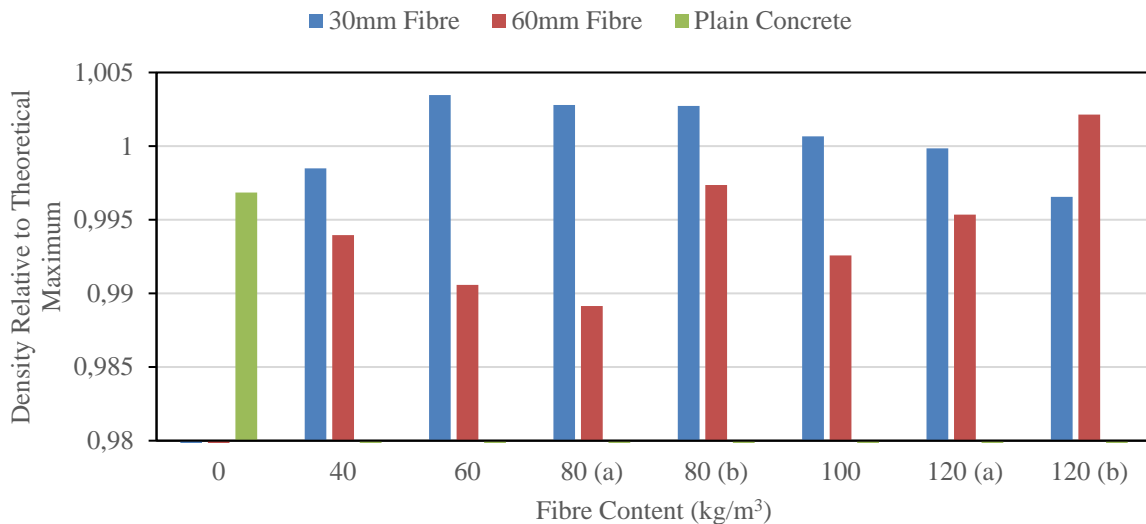


Figure 3-3: Cube density relative to the theoretical maximum density

The average compressive strength results are presented in Figure 3-4. The compressive strength of mixtures containing 30 mm fibres demonstrated an increase in strength with increasing fibre content, whereas the 60 mm fibre mixtures showed limited dependency of strength on fibre content. This may potentially be due to the lower degree of compaction generally achieved for the 60 mm fibre mixtures as depicted in Figure 3-3. In addition, it has also repeatedly been shown in literature that an increase in compressive strength can be achieved with micro-fibres at high fibre volumes (> 1%). The higher strengths attained by the mixtures containing 30 mm fibres is therefore likely due to the higher number of fibres that offer resistance against longitudinal crack growth through the matrix.

Although all the mixtures containing fibres had higher compressive strengths than the reference mixture, the increase in strength is limited to less than 10 MPa and would not serve as an economical solution for improving the compressive strength of concrete. The figure demonstrates that the difference in strength of the double cast batches is generally low, with the largest variation exhibited by the 60 mm batches with fibre dosages of 120 kg/m³. The difference is possibly due to the higher degree of compaction achieved with the 120-60-b batch, however, the material is known to be inherently variable and the difference may be due to the variable nature of the composite.

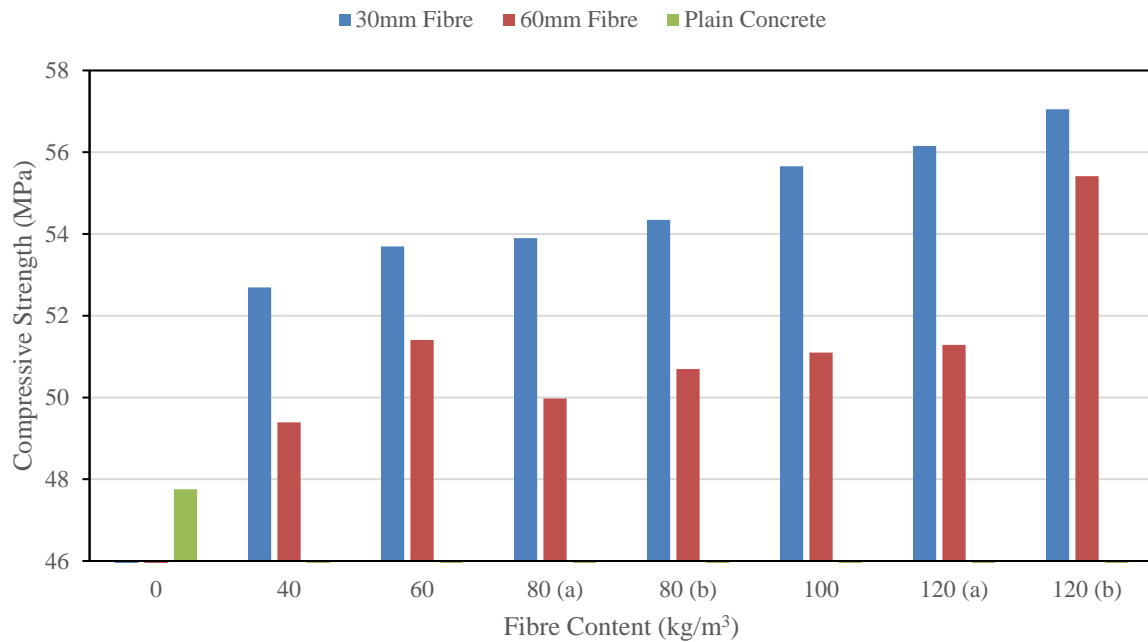


Figure 3-4: Average compressive strength results

For the sake of completeness, the modulus of elasticity was evaluated using the 3 cylinders of the mixture containing no fibres by applying 3 load cycles within the elastic range of the concrete. The cylinders were subsequently loaded up to failure to provide an additional measure of compressive strength for the plain concrete. The results are presented in Table 3-2.

Table 3-2: Elastic modulus and cylinder strength of plain concrete mixture

	Unit	Cylinder A	Cylinder B	Cylinder C	Average
Elastic Modulus	GPa	41.4	39.3	45.5	42.1
Cylinder Strength	MPa	45.4	45.5	43.3	44.7

3.5 Flexural Strength Test: Setup and Procedure

The 3-Point Bending Tests (3PBT) were carried out as recommended by RILEM TC 162-TDF (2002) with a slight modification to the length of the loading span. The recommendation specifies that the supports be positioned 500 mm apart, however, due to limited experimental equipment availability a distance of 450 mm was used for all beams tested in this study. Each specimen was instrumented with 2 Linear Variable Differential Transformers (LVDTs), one on either side of the mid-span, and a clip gauge placed over the centre of the notch underneath the beam. To avoid the effects of extraneous deformation measurements due to local crushing at the supports and loading point, the vertical deflection was measured with respect to the specimen. This was achieved by clamping yoke frames to the specimen at mid-height above the supports and mounting the LVDTs on a horizontal bar resting on the yokes. The test setup and instrumentation are shown in Figure 3-5.



Figure 3-5: Three-point bending test setup and instrumentation

The tests were performed under displacement control such that the average mid-span deflection increased at a constant rate of 0.2 mm/min. The load was applied with the direction of casting perpendicular to the loading direction until a minimum CMOD of 5.5 mm was recorded by the clip gauge. Prior to testing, the dimensions of each beam were measured using a digital vernier caliper. The height of the unnotched section was measured on either side as well as the average width of the specimen at the notch. The depth of the notch was measured at three locations to ensure that the specimen was cut evenly and within the tolerance prescribed by RILEM TC 162-TDF (2002).

The batch containing no fibres was tested at the same displacement rate as recommended by RILEM TC 162-TDF (2002); however, the beams were not notched as explained in Section 3.3.3 and therefore CMOD readings are not available. The Modulus of Rupture (MOR) results for the batch of plain concrete beams are given in Table 3-3.

Table 3-3: MOR results of beams without fibres

Minimum (MPa)	Maximum (MPa)	Average (MPa)	Coefficient of Variation (%)
6.15	7.21	6.60	5.20

3.6 Image Acquisition and Feature Extraction

Image analysis refers to the process of objectively assessing an image by firstly processing an image to extract specific information and subsequently analysing this information in a quantitative manner.

Within the scope of this dissertation, the primary data to be extracted is the location of each fibre in an image of a composite beam's cross section. This requires the progression of three operations: sample preparation, image acquisition, and feature extraction.

3.6.1 Sample Preparation and Image Acquisition

Preparing the samples involves two primary stages: cutting the samples from the beam specimen and polishing the surfaces that will be used for image analysis. This is a vital step in the process as it may cause significant complications during the subsequent phases if not carried out meticulously. If the samples are not carefully cut, they may require excessive polishing to obtain a smooth and level surface. If the samples are not adequately polished, fibres may not be recognized by the segmentation algorithm or a cluster of several fibres may be erroneously identified as a single entity.

The beam specimens were firstly cut through the centre of the fracture surface, predominantly located at the notch, and secondly as close as possible to the fracture surface without intersecting a crack, which was generally 40 mm – 60 mm away from the first cut location. Initially it was postulated that image analysis of the fracture surface may be possible if the surface could be levelled off with grout and polished smooth. It was later observed that a substantial amount of fibres was lost either through pulling out or while cleaning the friable fracture surface. This led to the conclusion that image analysis data collected at the crack location will not provide a representative indication of the true fibre content and fibre spatial distribution. Examples illustrating the condition of the fracture surface are shown in Figure 3-6.

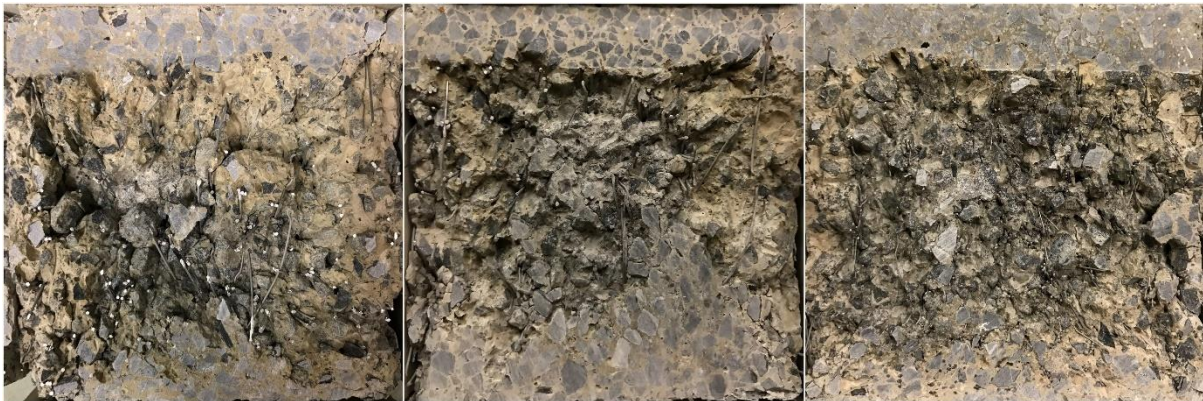


Figure 3-6: Examples illustrating the condition of the fracture surface

The significant importance of polishing is illustrated in Figure 3-7 showing examples of the specimen surface before and after polishing. A photo of the polishing operation is shown in Figure 3-8. The sample preparation phase was concluded with wiping the smooth surface of each specimen with methanol to remove any remaining residue.

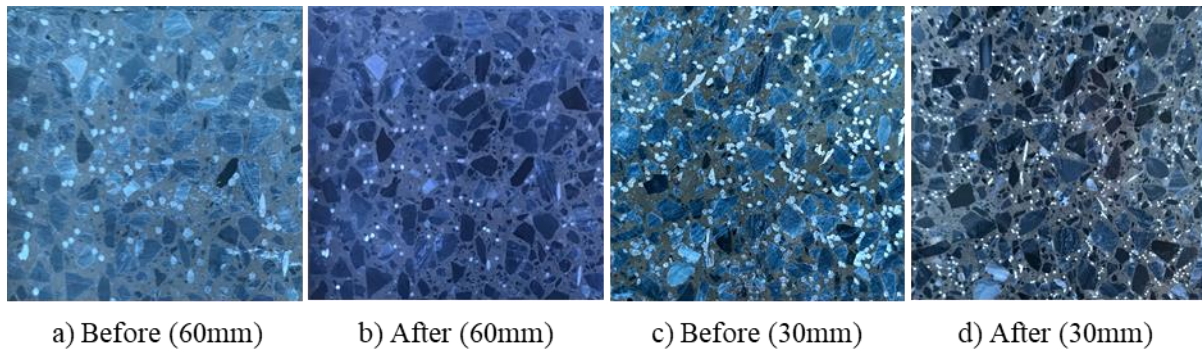


Figure 3-7: Before and after polishing specimens (120 kg/m^3 dosage)



Figure 3-8: Polishing operation

Images of the prepared specimen were captured with a Nikon D7100 digital camera equipped with a Nikon 18 – 140 mm zoom lens. The setup is shown in Figure 3-9. The camera settings and lighting remained constant throughout the duration of the process.

The lens that was used is known to result in optic distortion of the images. This was corrected by post-processing the images in Adobe Lightroom for the specific lens profile.



Figure 3-9: Camera and lighting setup used to capture images

3.6.2 Image Processing Algorithm

As stated in the previous section, the primary objective of the image processing algorithm is to extract the centroidal coordinates of each fibre in the image. Image processing is the final step in the image data extraction phase and involves performing a sequence of steps to obtain results that may then be analysed. The code for the algorithm was written in MATLAB and can be summarised to consist of the following steps:

1. Convert the RGB image to a grayscale image;
2. Scale and crop the image;
3. Top-hat filtering and contrast enhancement;
4. Morphological noise removal;
5. Segmentation by thresholding, and
6. Watershed segmentation using the distance transform.

The initial RGB image and grayscale input image are shown in Figure 3-10 for specimens from batches 100-30 (top 2 images) and 100-60 (bottom 2 images).

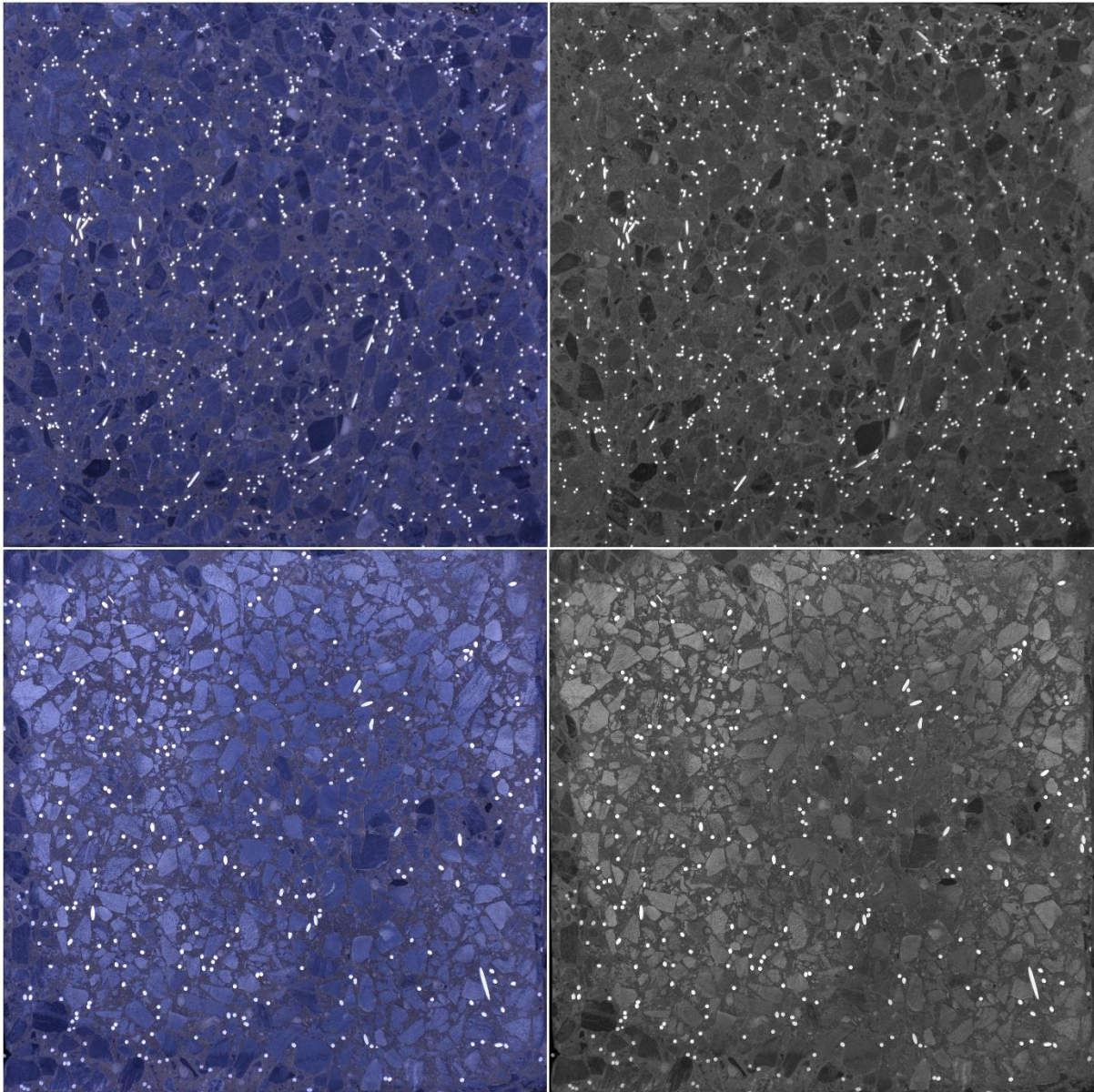


Figure 3-10: Example of original RGB image and corresponding grayscale input image

The objective of the white top-hat transform in the third step is to correct for possible nonuniform illumination across the image and was implemented in the algorithm as a disk-shaped structuring element (Heilbronner and Barrett, 2013). This is followed by adjusting the contrast to saturate the bottom 85% of the pixel intensity values to black and the pixel values above 220 to white. This provides high contrast between the fibres and the surrounding material. The output of step 3 is shown in Figure 3-11 for a sample from batch 100-30.

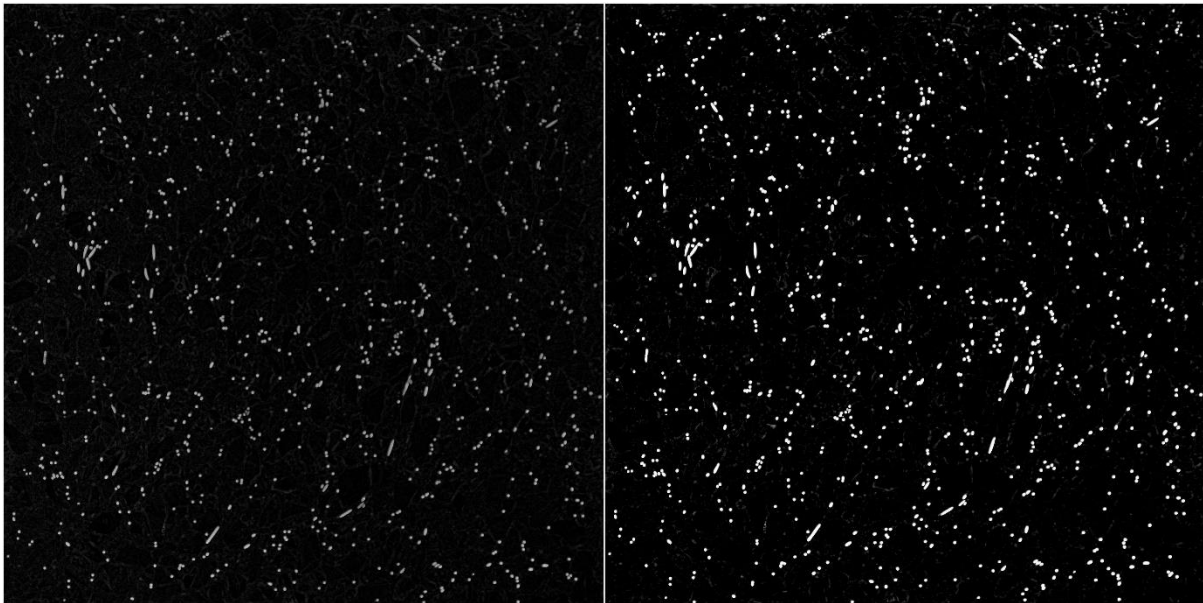


Figure 3-11: Top hat filtering (left) and contrast enhancement (right)

The morphological operations that were implemented removed small noise spots without altering the overall shape of the objects in the image (Jähne, 2005). The morphological techniques used in step 4 are called “opening-by-reconstruction” followed by “closing-by-reconstruction”. Opening-by-reconstruction is an erosion operation followed by a morphological reconstruction, while closing-by-reconstruction is a dilation operation followed by a morphological reconstruction. A disk-shaped structuring element was used in both morphological techniques. Otsu thresholding is then used in step 5 to create a binary image. The resulting images of steps 4 and 5 are shown in Figure 3-12.

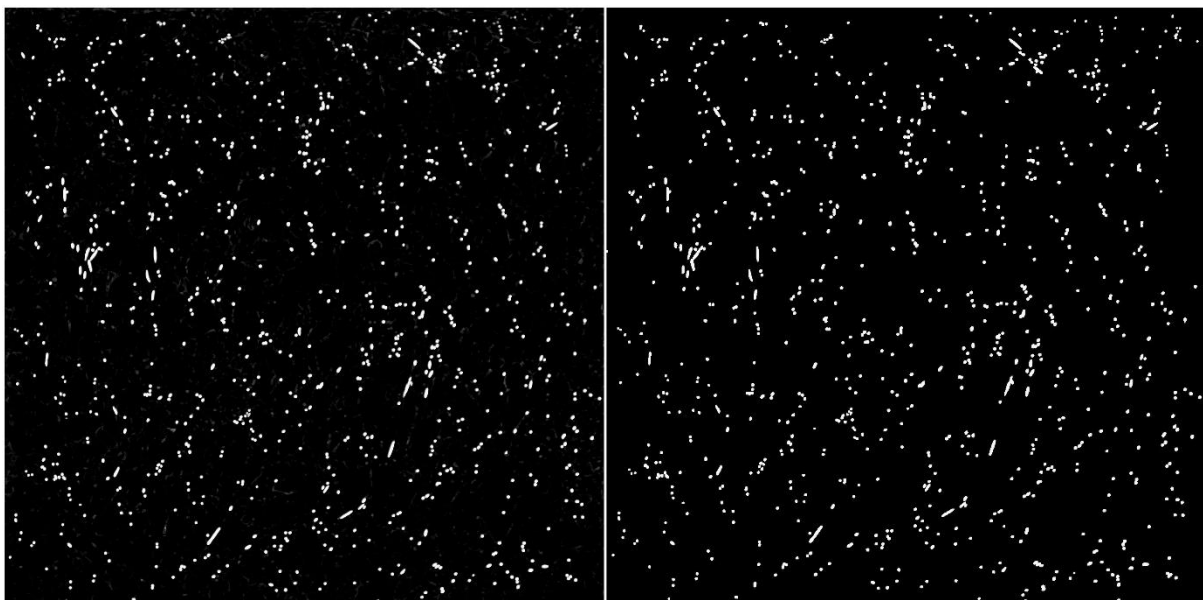


Figure 3-12: Morphological noise removal (left) and Otsu thresholding binary image (right)

The final step is necessary for separating multiple adjacent fibres that were segmented as a single object. This was accomplished by using the distance transform of the binary image as an input to the watershed transform algorithm. The underlying idea of the watershed transform intuitively originates from

geography. The watershed algorithm identifies “catchment basins” by treating an image as a topographical surface with low pixel-intensity values representing low elevations and high pixel values as high elevations. A detailed discussion of the watershed transform is given by Roerdink and Meijster (2000). The distance transform of the binary image provides a metric of separation of points by calculating the distance between each background pixel and the nearest foreground pixel. The resulting transform is a grayscale image with the intensity of pixels in the foreground objects altered to reflect the distance of each point to the closest boundary. Figure 3-13 illustrates the distance transform of the binary image and segmented image resulting from the subsequent watershed transform.



Figure 3-13: Original binary image (left), distance transform (centre), and watershed segmentation (right)

3.6.3 Feature Extraction: The Voronoi Diagram

The first objective of performing image analysis was to extract the centroidal location of each fibre and was accomplished by the designed algorithm. The second objective involves quantitatively characterising the spatial distribution of the fibres using the data obtained from the image processing algorithm. The Voronoi method was selected for this purpose and is briefly discussed in this section.

A Voronoi diagram is constructed from a given set of “sites” to form a collection of regions that divide up the plane. Each site corresponds to one of the regions and all points within a region is closer to the corresponding generator site than any other site. Where a point is equidistant to two sites, there is a boundary line that delineates two regions. Boundary lines intersect to form vertices, which are points that are equidistant to three or more generator sites (De Berg, 2008). These concepts are illustrated in Figure 3-14.

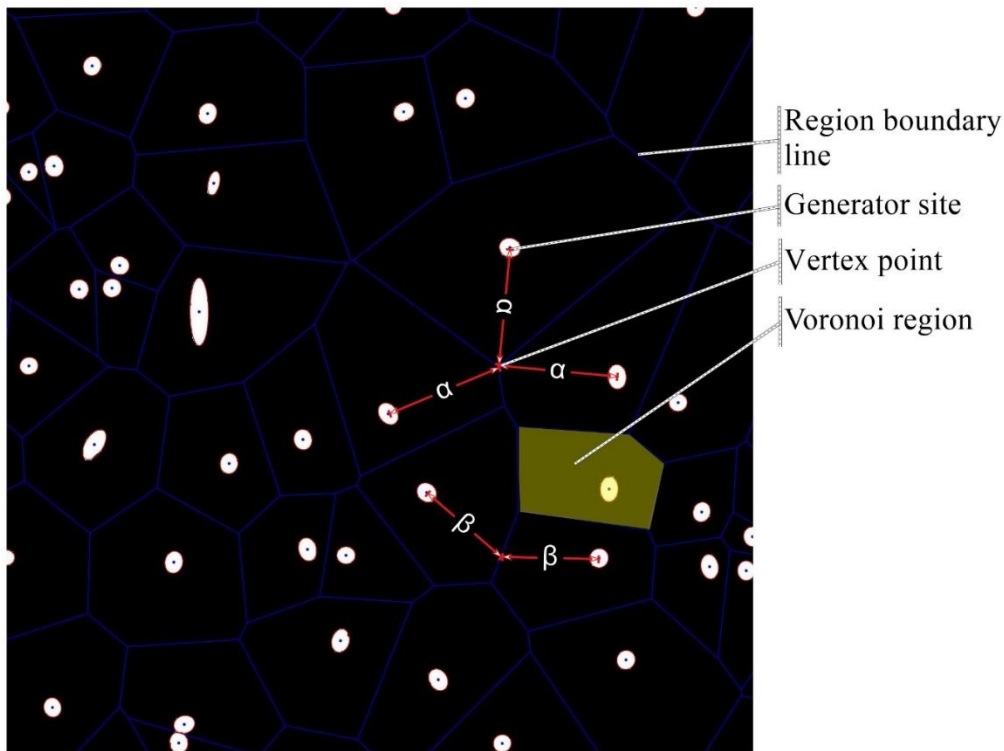


Figure 3-14: Components and characteristics of a Voronoi diagram

The concept underlying a Voronoi diagram may also be explained as an analogy where each generator site is imagined as an island. Each island has a boat and all boats are capable of travelling the same speed. Then, let every point that is reached by a boat from island x before any other boat be associated with island x . The region of points associated with island x is referred to as the Voronoi region of x (De Berg, 2008).

The measure that was ultimately selected to define the spatial distribution of fibres is the distance between a vertex and the nearest fibre(s), indicated in Figure 3-14 as α . The distance represents the radius of the largest circle bordering three or more fibres that does not contain any fibres. An alternative measure that could have sufficed is the area attributed to each fibre. However, this measure was expected to reflect the clustering of fibres less effectively. The sizes of Voronoi regions do not adequately reflect the spacing between fibres because fibres are not necessarily located near the centre of the region nor is the region regularly shaped. Therefore, clusters of fibres may not be identified due to the misinterpretation of the size of their regions.

3.7 Fibre Orientation

The principles of fibre orientation theory, discussed in Chapter 2, can roughly be described as quantifying the effectiveness of fibres in terms of the number of fibres intersecting a plane. The fibre effectiveness is said to increase as the fibres tend to align perpendicular to the intersecting plane, increasing the probability of a fibre being intersected. Fibre effectiveness is generally quantified in the form of an orientation factor, η_θ , and image processing results can be utilised in various fashions to determine the orientation factor of a given specimen.

The orientation of an individual fibre is frequently determined from image data as the inverse cosine of the ratio of the minor to the major axis of the ellipse formed by the fibre intersecting the cutting plane (see Figure 2-12 and Equation 2.11). The result is then used to calculate the orientation factor as in Equation 2.2. For this approach to provide reasonable results, sharp high-resolution images are required as well as meticulous surface preparation of each specimen. Determining fibre orientation from image analysis is not included in the scope of this study; therefore, the experimental setup was not designed to accomplish such an objective.

Attempting to derive fibre orientation from images with insufficient resolution will produce significant underestimation of the fibre orientation angles and consequently an overestimation of the orientation factor. This phenomenon may be better understood by considering the graphs shown in Figure 3-15. The figure illustrates the change in major axis length corresponding to fibre orientation angle as well as the number of pixels required to detect the change. Reference can also be made to Figure 2-13 which visually depicts the change in major axis length with increasing fibre orientation angle. Figure 3-15 was constructed using a fibre diameter of 0.9 mm and a scale of 21 pixels/mm as achieved on average from the images captured in this study. Orientation angle is therefore highly susceptible to large errors due to the low number of pixels available to accurately detect slight changes in fibre orientation.

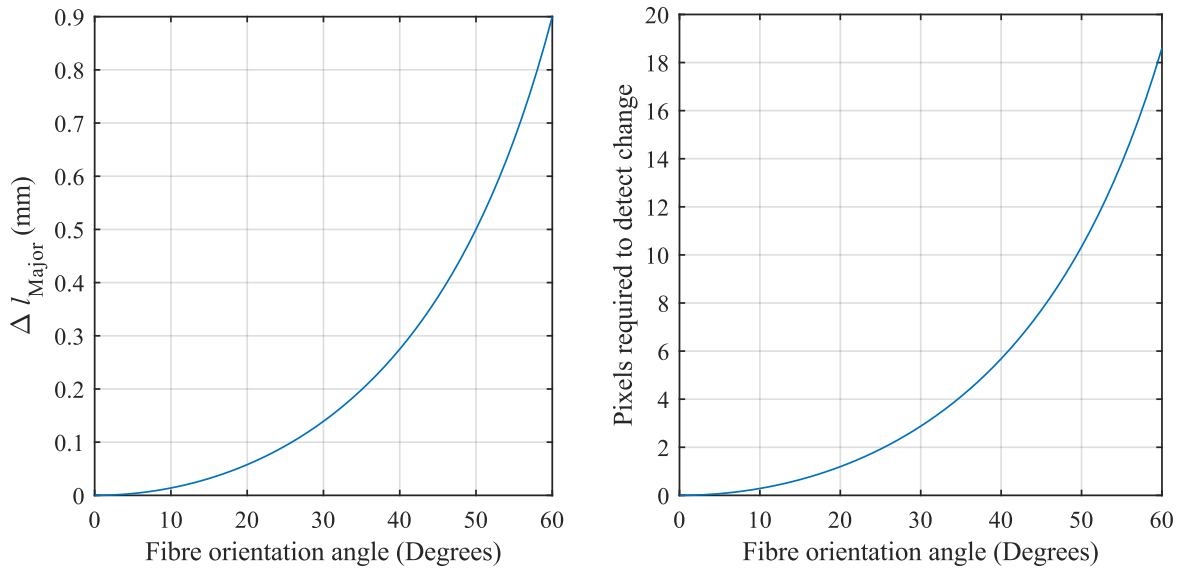


Figure 3-15: Pixels required to detect fibre orientation angle from image data

An alternative method involves calculating the orientation factor as initially expressed in Equation 2.1:

$$\eta_{\theta} = \frac{N_f}{N_{ideal}} = N_f \frac{A_f}{A_s V_f} \quad (3.1)$$

Where:

N_f = Number of fibres intersecting the crack plane

N_{ideal} = Number of ideally aligned fibres intersecting the crack plane

A_f = Cross-sectional area of a single fibre (mm)

$$A_s = \text{Cross-sectional area of the specimen (mm}^2\text{)}$$

$$V_f = \text{Volume content of fibres (Dosage}/\rho_{\text{steel}}\text{)}$$

Equation 3.1 is used in Chapter 4 to empirically calculate the orientation factor from the fibre count obtained from image analysis results.

A second alternative involves determining the theoretical orientation factor based on stereological principles using the fibre geometry and specimen dimensions as inputs to the calculation. The underlying theory of these methods were briefly discussed in Chapter 2 for fibres that are not restricted by geometrical boundaries. The model developed by Dupont and Vandewalle (2005) is implemented in Chapter 4 to theoretically derive orientation factors for the two fibre lengths.

3.8 Quantifying Spatial Distribution with Fibre Count

Two distinct approaches are developed for quantifying fibre spatial distribution:

1. The fibre count approach, and
2. The Voronoi approach.

The distribution of fibres across a section is described with the following three metrics:

1. The uniformity of fibre distribution in a section;
2. The variability of this distribution within a batch, and
3. The degree of fibre clustering.

The aspects involved in deriving each metric according to the fibre count approach is discussed in this section.

3.8.1 Degree of clustering

This first approach entails specifying an $m \times m$ grid dimension and counting the number of fibres within each grid square. The grid size or grid dimension refers to the number of $m \times m$ grid squares imposed over a 150 mm \times 150 mm cross section, whereas the fibre grid count, n_f , is defined as the number of fibres counted inside an individual grid square. Calculating the grid dimension in terms of the total number of fibres in the specimen, results in all specimens having approximately the same fibre density regardless of the fibre length or dosage. Plotting the probability distribution of fibre grid count, should theoretically produce identical probability distributions for all fibre contents if the fibres are distributed according to the same process. These are referred to as the standardised probability distributions of fibre grid count.

The standardised probability distributions provide an objective criterion that can be used to evaluate the relative dispersion of fibres by considering the spread of the distribution for different total fibre counts. A property of the standardised probability distribution is that the mean of the distribution remains constant irrespective of total fibre count, but the spread of the distribution varies depending on the characteristics of the pattern. A distribution with a large spread of data represents a point pattern

exhibiting clustering, whereas a distribution with a narrow spread of data constitutes a point pattern with regularly spaced points. A point process exhibiting Complete Spatial Randomness (CSR) results in a distribution with a spread that is larger than a regular pattern but less than a clustered pattern. Figure 3-16 depicts simulated point patterns of the same point density demonstrating clustering, complete spatial randomness, and regularity. The standardised probability distributions of each pattern are provided in Figure 3-17.

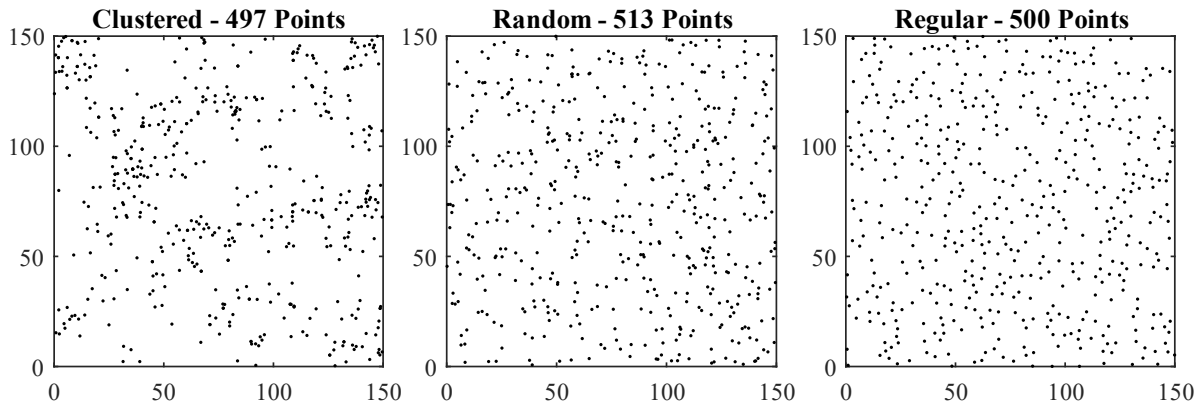


Figure 3-16: Simulated point patterns demonstrating clustering, CSR, and regularity

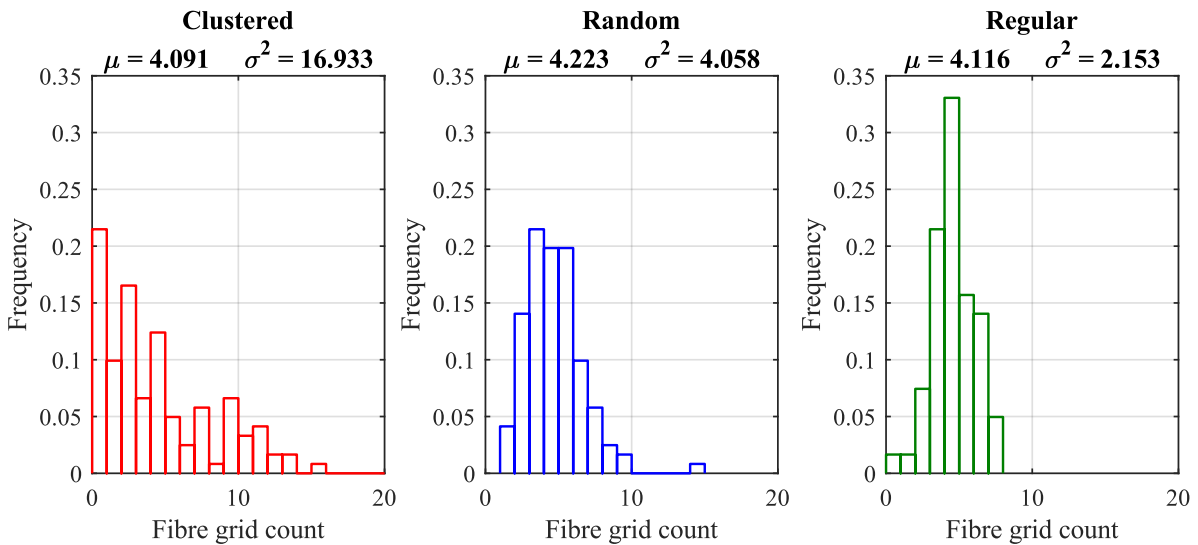


Figure 3-17: Probability distributions of simulated clustered, CSR, and regular patterns

The first step required to obtain the standardised probability distribution is calculating the grid dimension with respect to the total number of fibres. The standardised grid dimension was calculated using Equation 3.2 and rounded to the nearest integer value.

$$h_{grid,i} = 0.5\sqrt{N_{f,i}} \tag{3.2}$$

Where:

$h_{grid,i}$ = The $m \times m$ number of grid squares for sample i

$N_{f,i}$ = The total fibre count of sample i

The standardised grid dimension obtained from Equation 3.2, $h_{grid,i}$, represents the number of grid tiles along a single cross-sectional dimension of the specimen. The total number of grid tiles would therefore be equal to $h_{grid,i} \times h_{grid,i}$. Equation 3.2 was adapted from Equation 3.3 which can be used to calculate the unit proportion of a rectangle attributed to a single fibre.

$$\kappa = \frac{1}{\sqrt{N_f}} \quad (3.3)$$

Multiplying κ with the width of the cross section produces the equidistant spacing length between fibres for the given number of fibres in the section. The standardised grid dimension is equal to twice this value as stated in Equation 3.2.

To assess the effect of clustering on the performance of a composite, the metric has to account for the distance between fibres which is a function of the total fibre count. The adverse influence of low fibre spacing on the effective pull-out strength of fibres was discussed in Chapter 2. It is therefore postulated that the impact of clustering on the flexural response is more severe for specimens with high fibre counts due to the proximity of fibres associated with such specimens. Assuming that the number of fibres can be used to account for the influence of fibre spacing, the degree of clustering of a single specimen may be calculated as follows:

$$CL_{cnt,i} = N_{f,i} \cdot \frac{\sigma_{nf,i}}{\bar{n}_{f,i}} \quad (3.4)$$

Where:

$CL_{cnt,i}$ = The degree of clustering for specimen i based on the fibre count approach

$N_{f,i}$ = The total number of fibres intersecting the cross section of specimen i

$\sigma_{nf,i}$ = The sample standard deviation of fibre grid count of specimen i

$\bar{n}_{f,i}$ = The mean number of fibres inside a grid square of specimen i

If the extent of clustering does indeed have a negative effect on the mechanical properties of the composite, a relationship should exist between the degree of clustering and the resistance provided by fibres. This hypothesis is further investigated in Chapter 6.

3.8.2 Fibre homogeneity and variability

Comparing the fibre distribution using a standardised grid dimension does not, however, reflect the relative degree of homogeneity over the cross section. Comparing homogeneity requires that the degree of variation be evaluated at the same grid size. Equation 3.5 is proposed for calculating the mean batch homogeneity as the mean CoV for designated grid dimensions, with high CoV results representing poor homogeneity.

$$Homogeneity_j = \frac{1}{N_{s,j}} \sum_{i=1}^{N_{s,j}} \frac{\sqrt{\sigma_{nf,i}^2}}{\bar{n}_{f,i}} \cdot 100 = \frac{1}{N_{s,j}} \sum_{i=1}^{N_{s,j}} Homogeneity_{j,i} \quad (3.5)$$

Where:

$Homogeneity_j$ = The mean fibre homogeneity of batch j (%)

$\bar{n}_{f,i}$ = The mean number of fibres inside a grid square of sample i in batch j

$N_{s,j}$ = The number of samples in batch j

$\sigma_{nf,i}^2$ = The variance in fibre grid count of sample i in batch j

$Homogeneity_{j,i}$ = The fibre homogeneity of sample i in batch j (%)

The influence of varying grid dimensions on the mean homogeneity is investigated in Chapter 5 with the objective of selecting the most appropriate grid dimension.

The uniformity of fibre distribution in a cross section is expected to influence the mechanical performance of the composite. This implies that the variability of fibre homogeneity in a batch should have a corresponding influence on the variability in the flexural response of specimens in a batch. Equation 3.5 provides a measure of the mean fibre homogeneity for a batch of specimens. To evaluate the variability of fibre homogeneity within a batch, the fibre homogeneity of a single specimen is required. Following from Equation 3.5, the fibre homogeneity of a single specimen is calculated as follows:

$$Homogeneity_i = \left(\frac{\sigma_{nf,i}}{\bar{n}_{f,i}} \right) \cdot 100 \quad (3.6)$$

Where:

$Homogeneity_i$ = The fibre homogeneity of sample i (%)

$\sigma_{nf,i}$ = The standard deviation of fibre grid count for sample i

$\bar{n}_{f,i}$ = The mean fibre grid count for sample i

The variation in homogeneity of a batch can then be calculated as the standard deviation of the results obtained from Equation 3.6.

3.9 Quantifying Spatial Distribution with Voronoi Data

3.9.1 Random point process

Naaman (1972) proposed that the distribution of fibres can be adequately modelled as a Poisson process, which is a fibre pattern that is completely random and has no systematic tendencies for fibres to avoid each other or form clusters. However, literature presented in the previous chapter suggest that fibres are not spatially randomly distributed. The presence of boundaries certainly challenges the assumption of CSR as factors such as the size of the coarse aggregate particles may significantly influence the distribution of fibres at high fibre counts as shown in Figure 3-18. The mould walls should theoretically also have an effect caused by varying density of fibres across the section as indicated in Figure 2-7.

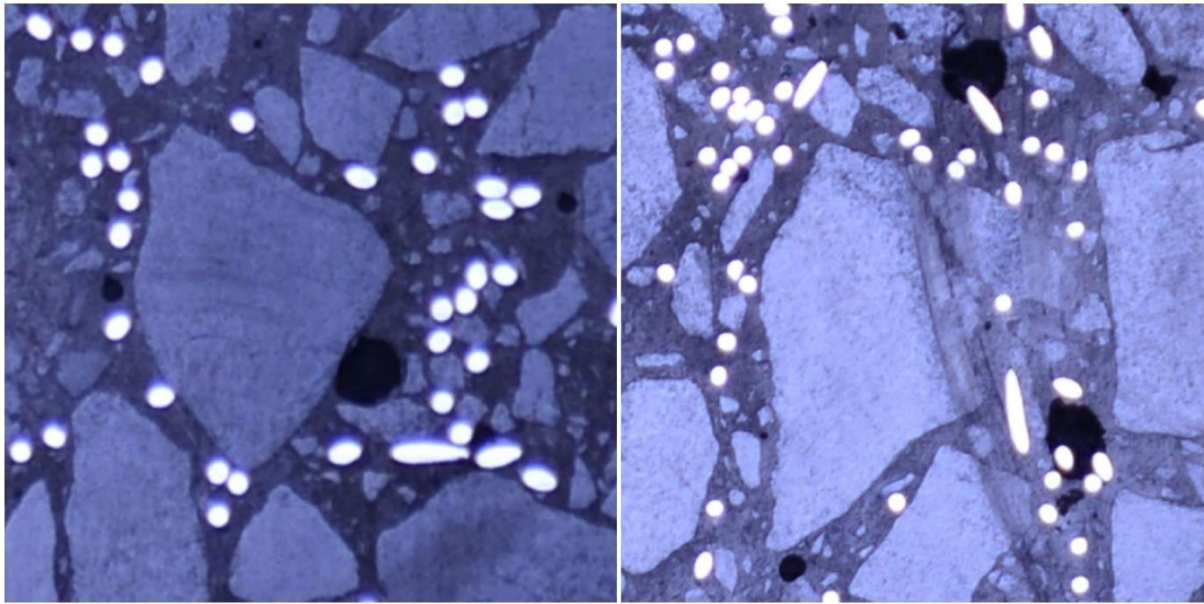


Figure 3-18: Example of the influence of coarse aggregate particles on the distribution of fibres

Although it is reasonably evident that additional factors are involved in the process governing fibre distribution, it is assumed that fibre spatial distribution can be modelled using the same distribution *type* as a CSR point pattern. A Nakagami distribution was identified as the most suitable fit to the Voronoi spacing results of CSR patterns. The histograms of Voronoi spacing of selected CSR point patterns are given in Figure 3-19 along with the Nakagami distribution fit for each data set.

The Nakagami distribution was originally introduced by Nakagami (1960) and is described by two parameters: the shape parameter which affects the shape of the distribution and the scale parameter which controls the spread. The Nakagami distribution is related to the Gamma distribution and is mostly used for modelling small scale fading of dense radio signal scatters (Ahmad, 2016). The Nakagami distribution has also successfully been implemented in many other fields for modelling right-skewed, positive data sets. Sarkar et al. (2009) and Sarkar et al. (2010) found that the Nakagami distribution performs well in constructing unit hydrographs which can be used in hydrology to estimate runoff. Tsui et al. (2006) applied the Nakagami distribution to ultrasound data to characterise tissue and Carcolé and Sato (2009) and Nakahara and Carcolé (2010) demonstrated the utility of the distribution to characterise small scale fluctuations in seismic velocity from high frequency seismogram envelopes.

Results from the CSR simulations for different fibre counts are presented in Table 3-4. The results indicate that the mean and spread of data reduces as the number of fibres increase and that the shape parameter remains approximately constant with fibre count.

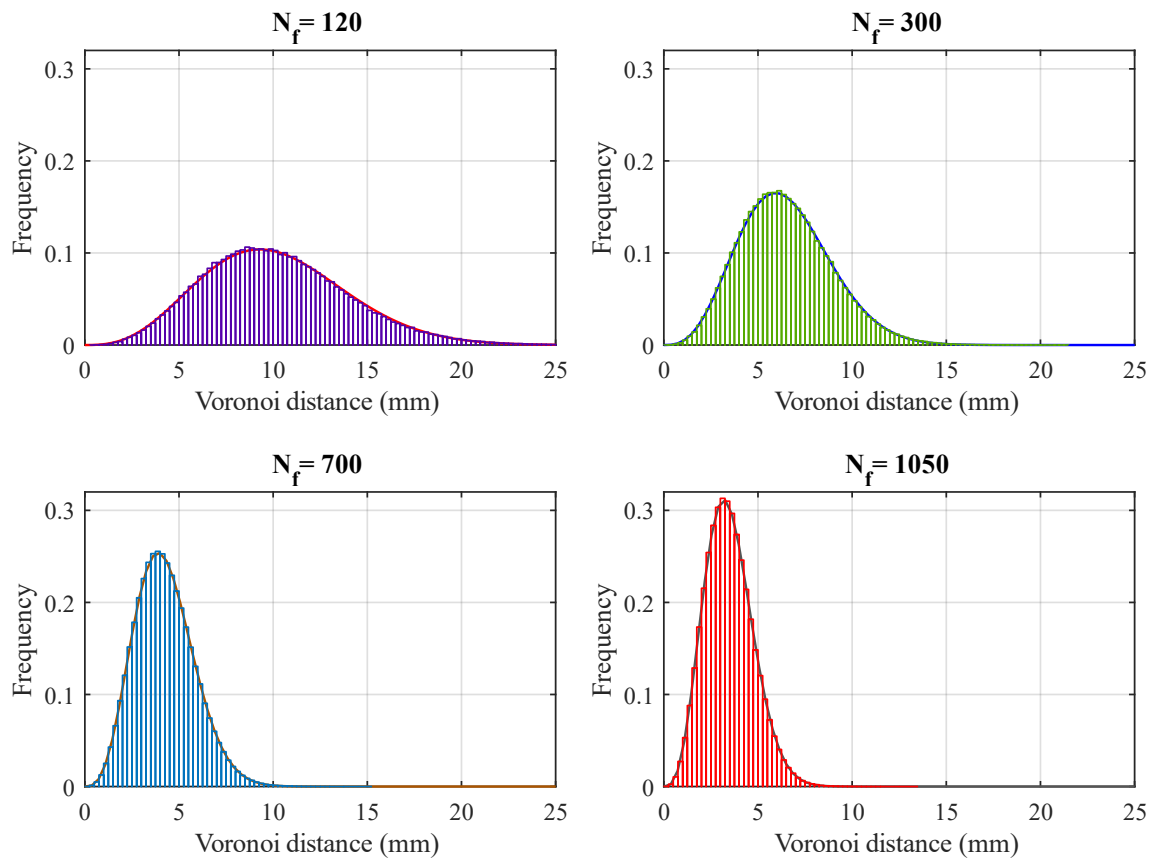


Figure 3-19: Histogram and Nakagami fit of Voronoi spacing for CSR point patterns of varying density

Table 3-4: Results from simulations of random spatial patterns with varying point densities

N_f	Shape parameter	Scale parameter	Mean Voronoi spacing (mm)	Dispersion	Variance of dispersion
120	1.973	117.77	10.16	14.56	8.8607
175	1.962	81.25	8.44	9.94	2.6873
225	1.955	63.26	7.45	7.68	1.1754
300	1.971	47.43	6.45	5.77	0.4908
360	1.972	39.51	5.89	4.77	0.2809
500	1.959	28.54	5.01	3.42	0.1068
700	1.968	20.36	4.23	2.43	0.0363
830	1.975	17.20	3.89	2.05	0.0231
1050	1.969	13.59	3.46	1.62	0.0111

The statistical variance of the data is equivalent to the spread of the distribution and will be used to quantify the dispersion of fibres in the composite. The dispersion of fibres is suspected to correlate with the flexural strength of specimens as stated in the first main hypothesis presented in Chapter 1. Based on such a proposition, the second hypothesis formulated in Chapter 1 states that the variation in dispersion should correlate with the variation in flexural strength. Fibre dispersion and variation of dispersion is quantified in a similar manner and compared to the CSR results in Chapter 5.

Histograms illustrating the distribution of dispersion for 2500 simulations are shown in Figure 3-20. Note that the scales of the various axes differ to avoid excessive distortion of the shape of each distribution. The figures indicate that the variation in dispersion, i.e. the variation in the variance of Voronoi spacing, reduces as the number of points increase.

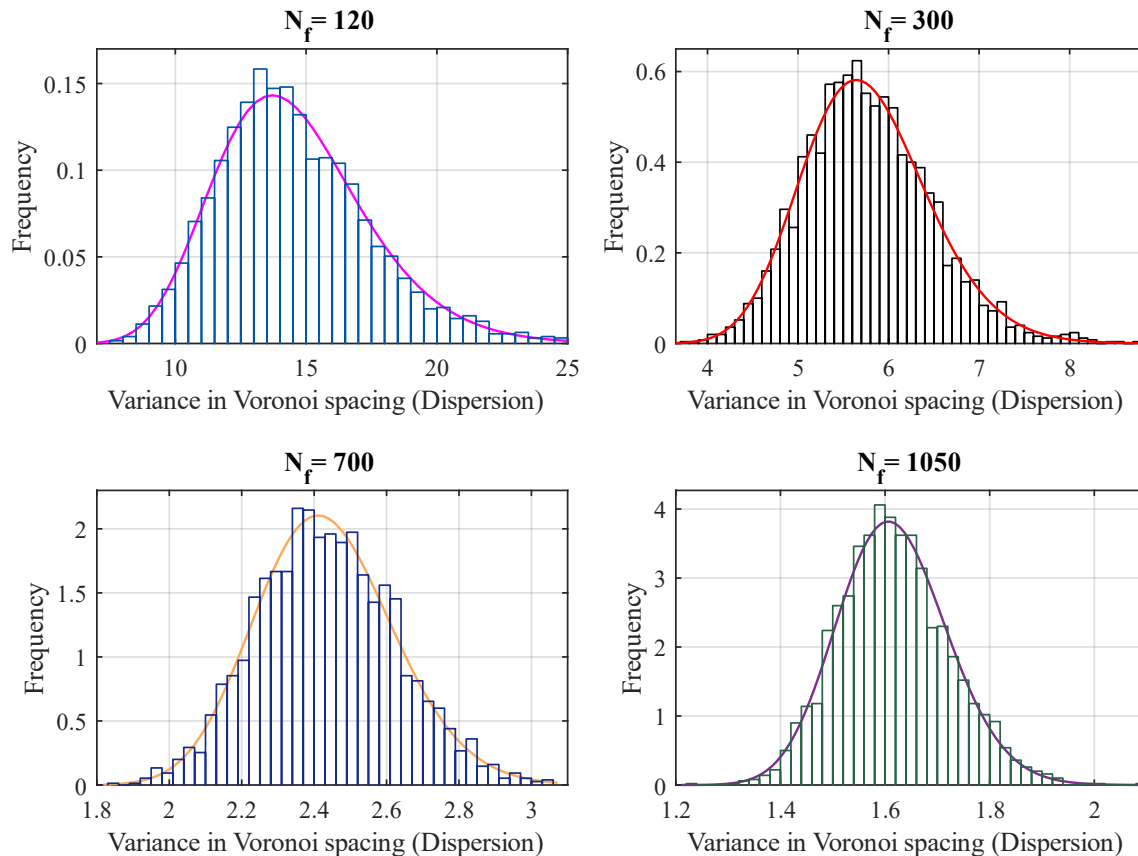


Figure 3-20: Distribution of variance in Voronoi spacing of CSR point simulations

3.9.2 Degree of clustering

Although simulating CSR point patterns and comparing the results to that obtained for fibres can offer some insight on the distribution processes, the primary use of the CSR pattern data relates to quantifying the degree of clustering of fibres. As discussed previously, CSR provides an objective criterion for assessing whether a point pattern exhibits clustering.

The probability distribution and Nakagami fits for simulated patterns exhibiting clustering, CSR, and regularity are shown in Figure 3-21 along with the Voronoi diagram generated for each pattern. The figure demonstrates the increase in shape factor and decrease in variance as the pattern becomes increasingly regular while the mean Voronoi spacing remains approximately constant.

The shape factor was identified as a suitable measure to evaluate whether the fibre distribution is random or clustered. For the random point patterns, the mean shape factor remained constant as the number of points increased while the variance of the shape factor decreased. This is illustrated by the probability

distributions shown in Figure 3-22. The shape factor distributions were obtained for various point densities by simulating 2500 CSR patterns at each point density increment.

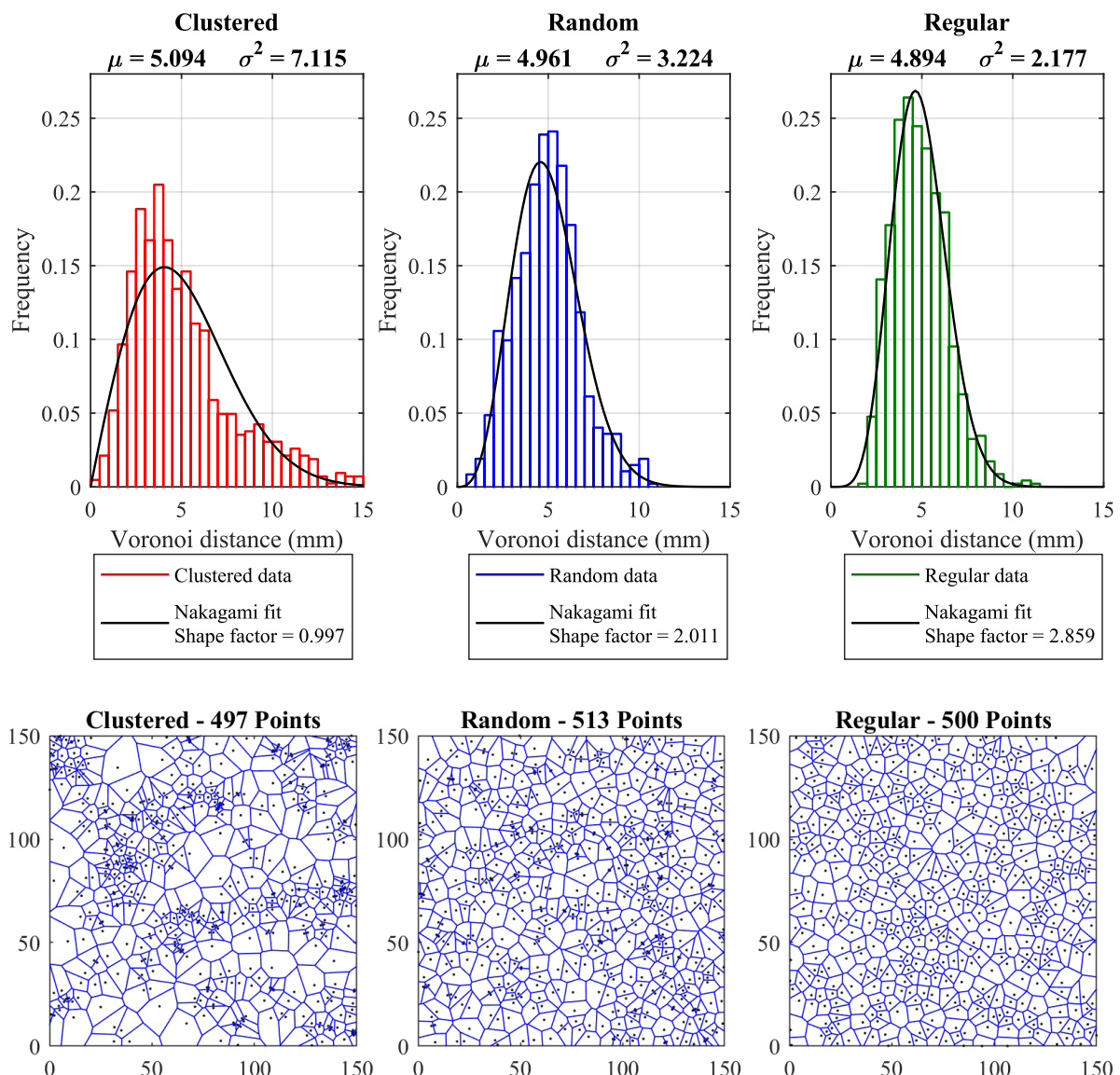


Figure 3-21: PDFs and Voronoi diagrams of simulated clustered, CSR, and regular patterns

The properties of a Nakagami type distribution constitutes that a low shape factor is generally associated with a clustered pattern. However, depending on the variance of the random pattern shape factor distribution, a low shape factor may still be within the probable range of shape factors. Considering the distributions shown in Figure 3-22, for a fibre count of 100, a shape factor equal to 1.5 is within the range of values obtained from a random pattern and it is therefore statistically probable that the fibres are randomly distributed. Whereas for a fibre count of 1000, it is highly improbable that a shape factor of 1.5 will result from a random pattern and that the fibres are likely exhibiting a more clustered distribution. This implies that the shape factor alone does not provide a sufficient indication of clustering and that the distribution of possible CSR shape factors must first be considered.

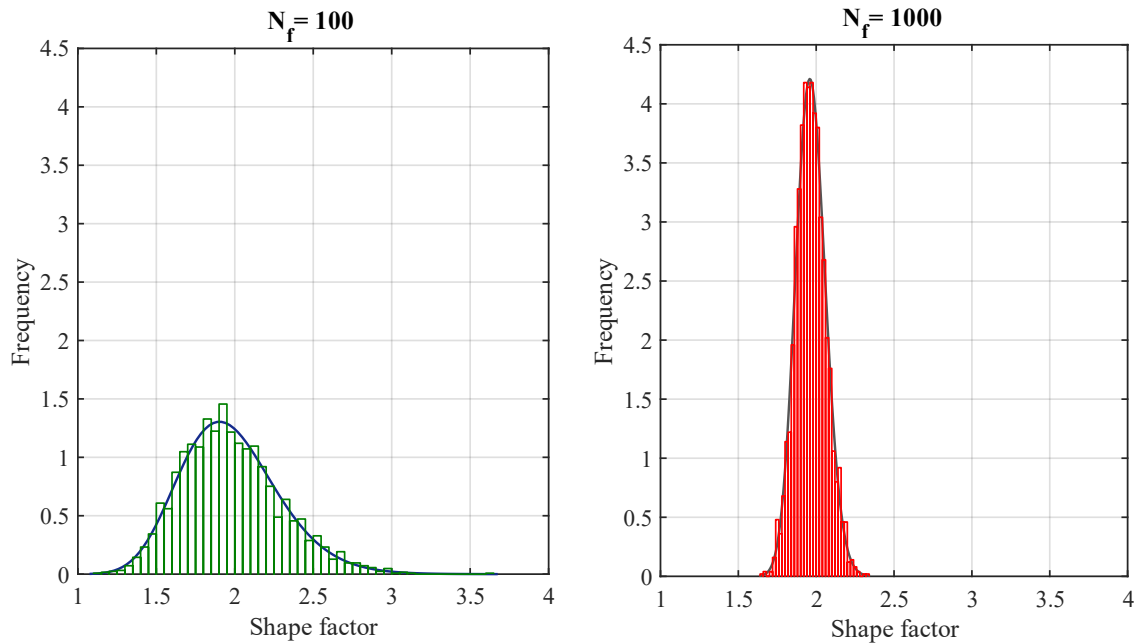


Figure 3-22: Nakagami shape factor distribution of 2500 random point simulations with 100 and 1000 points

Assuming that the shape factor for a random point process is distributed according to a lognormal distribution, the probability that a given shape factor forms part of such a distribution can be determined and used to assess whether the fibre distribution is characteristic of a random pattern or a clustered pattern. This involves the following sequence of steps:

1. Obtain the lognormal distribution for the shape factors of a specified fibre density from several simulations of random point patterns (Figure 3-22);
2. Transform the lognormally distributed variable, X , to the normally distributed variable, W , using the transformation $\ln(X)=W$;
3. Using the mean θ and variance ω^2 of the transformed data, the standard normal random variable is calculated as $z = \frac{\ln(x)-\theta}{\omega}$, and
4. The standard normal random variable is then used to determine the probability that a shape factor of a random process is less or equal to the shape factor considered.

A pattern can then be classified as random if the probability of a random process to generate a shape factor lower than the provided shape factor is less than a specified probability, which was selected as 0.005 in this study.

If it can be said that the standard normal random variable, z , provides a measure of clusteredness with respect to a random point process of the same point density, the relative degree of clustering with respect to the number of fibres affected can be defined as follows:

$$CL_{Vor,i} = |z_i \cdot N_{f,i}| \quad (3.7)$$

Where:

$CL_{Vor,i}$ = The relative degree of clustering of sample i based on the Voronoi approach

z_i = The standard normal random variable calculated for sample i

$N_{f,i}$ = The total number of fibres in the section of sample i

The $N_{f,i}$ term is also included in Equation 3.7 to account for the influence of fibre proximity on the effective resistance provided by the fibres.

3.10 Discussion on Methodology

The primary objective of this chapter was to formulate an appropriate methodology for producing and testing of laboratory specimens, acquiring and extracting image data, and developing suitable parameters that characterise fibre spatial distribution. The main conclusions drawn throughout the chapter are summarised and briefly discussed in the following paragraphs.

The experimental variables and methodology were selected based on considerations of the research in the literature review. Two lengths of hook-ended steel fibres with similar aspect ratios were chosen and seven batches of each fibre length were cast with fibre dosage varying from 40 kg/m³ to 120 kg/m³. This will enable identifying the influence of fibre length and fibre content on the spatial characteristics and the manner in which this potentially affects the flexural response.

A consistent production process based on the recommendations by RILEM TC 162-TDF (2002) was implemented for all batches. During the mixing operation it was observed that batches containing 60 mm fibres started to exhibit balling at dosages of 80 kg/m³ and required that the mixer periodically be stopped to break apart the accumulations.

Density measurements collected from cubes indicated that the mixtures with 30 mm fibres generally achieved a marginally higher degree of compaction than the 60 mm fibre mixtures. The compressive cube strength of the 30 mm fibre mixtures exceeded that of the 60 mm fibre mixtures for all fibre dosages. Furthermore, an increasing trend of compressive strength with fibre content was observed for the 30 mm fibre mixtures whereas no discernible trend was evident in the 60 mm fibre batches.

Notched 3-Point Bending Tests were carried out according to the recommendations by RILEM TC 162-TDF (2002) with a slight modification to the specified loading span from 500 mm to 450 mm.

Sample preparation, image capturing, and image processing were identified as the critical operations dictating the accuracy of image analysis results. The procedures in each phase were discussed with emphasis on the value of meticulous surface preparation, even lighting, and correcting for optic lens distortion. An image processing algorithm was developed using MATLAB and the primary steps involved in the algorithm were discussed with examples of the output of each step. The concept of Voronoi diagrams were briefly covered and it was proposed to implement Voronoi diagrams as a consistent means of evaluating the spatial distribution of fibres. Fibre coordinates are used to delineate the cross section in the form of a Voronoi diagram and the measure α (Figure 3-14) was selected as the geometric descriptor of fibre spatial distribution.

Two approaches are proposed for quantifying the spatial characteristics of fibres, with each approach providing three metrics to describe fibre distribution. The first approach involves dividing the cross section into a specified grid size and counting the number of fibres inside each square. Point patterns were simulated to exhibit clustering, CSR, and regularity and it was found that the mean density of fibres over a section is approximately equal for all simulations, however, the variance in density increases as the pattern becomes more clustered. A measure for the degree of clustering was proposed with Equation 3.4 taking into consideration the effect of fibre proximity on fibre pull-out effectiveness. Homogeneity was defined according to Equation 3.6 and the variation of homogeneity within a batch was calculated as the sample standard deviation of a set of homogeneity values.

The second approach obtains a geometric descriptor from a Voronoi diagram of the fibre coordinates and was used to quantify fibre spatial distribution. This approach was implemented on points obtained from using a Poisson process to simulate spatially random point patterns of various point densities with the objective of investigating the behaviour of CSR patterns and using the results to compare to fibre distribution in Chapter 5. The probability density function of Voronoi spacing of the random simulations was found to follow a Nakagami type distribution and it was assumed that the same distribution can be fitted to the spatial distribution of fibres. The possible factors relating to the validity of the assumption were also briefly discussed. Equation 3.7 was proposed for calculating the degree of clustering from the Nakagami shape parameter and taking cognisance of effect of fibre proximity. Fibre dispersion was defined as the variance in Voronoi spacing and the variation in dispersion of a batch of specimens was calculated as the sample standard deviation of a set of dispersion values.

CHAPTER 4. Experimental Results

4.1 Background

This chapter contains the results and analysis of experimental work performed according to the research methodology presented in the previous chapter. The results from flexural strength testing and image analysis are presented and discussed independently. The primary objectives of the chapter are to determine the flexural strength parameters, investigate the influence of fibre length and fibre content on the flexural response, to explore fibre spatial arrangement from Voronoi data, and to evaluate the fibre orientation factor.

The 3PBT results are presented in Section 4.2 and observations regarding flexural strength and variability are briefly discussed. The results are used in Section 4.3 to derive the flexural strength design parameters according to the RILEM TC 162-TDF (2002) calculation procedure laid out in Chapter 2.

The general relationship of the number of fibres as well as the spatial distribution of fibres with regard to fibre type and content are presented in Section 4.4. Section 4.5 contains discussions on fibre orientation and the number of fibres in a specimen. These results are then used to establish a relationship between the number of 30 mm and 60 mm fibres. The chapter is concluded on Section 4.6 with a discussion summarising the main findings of the experimental work.

4.2 Flexural Response Results

The Stress-CMOD curves for all 14 batches of FRC cast are presented in Figure 4-1 to Figure 4-7. The curves shown in the figures represent the envelope of minimum and maximum flexural responses of a batch of 9 beams with the blue curve indicating the average flexural response. The individual Stress-CMOD curves for each batch as well as the calculated design parameters of each specimen are given in Appendix A. In order to account for the possible influence of slight variations in notch depth and beam dimensions, the force was converted to a flexural stress using simple beam theory similar to Equation 2.15.

The figures demonstrate an evident increase in flexural strength for increasing fibre content, with the highest flexural strengths generally achieved by the 60 mm fibre batches. In addition, the figures suggest that the range of flexural responses is lower for the 30 mm fibre batches.

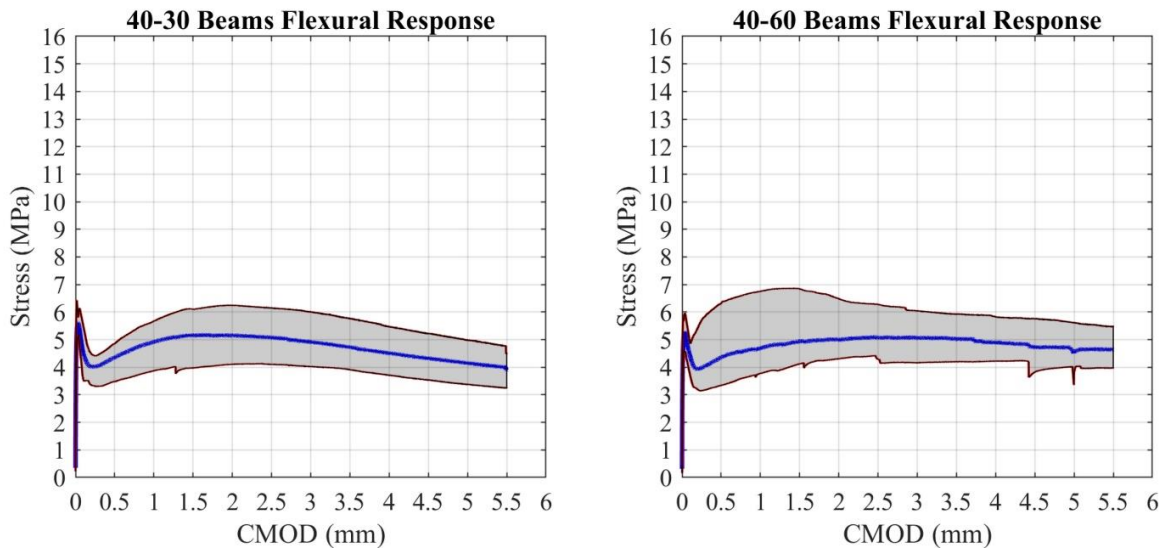


Figure 4-1: Envelope and average Stress-CMOD curves for 40 kg/m³ fibre dosage

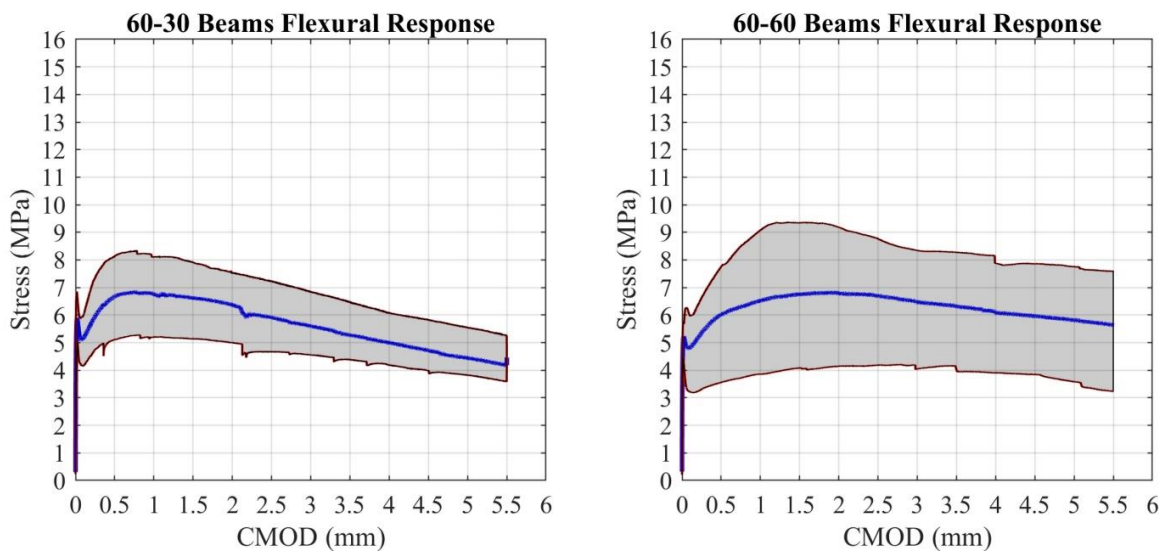


Figure 4-2: Envelope and average Stress-CMOD curves for 60 kg/m³ fibre dosage

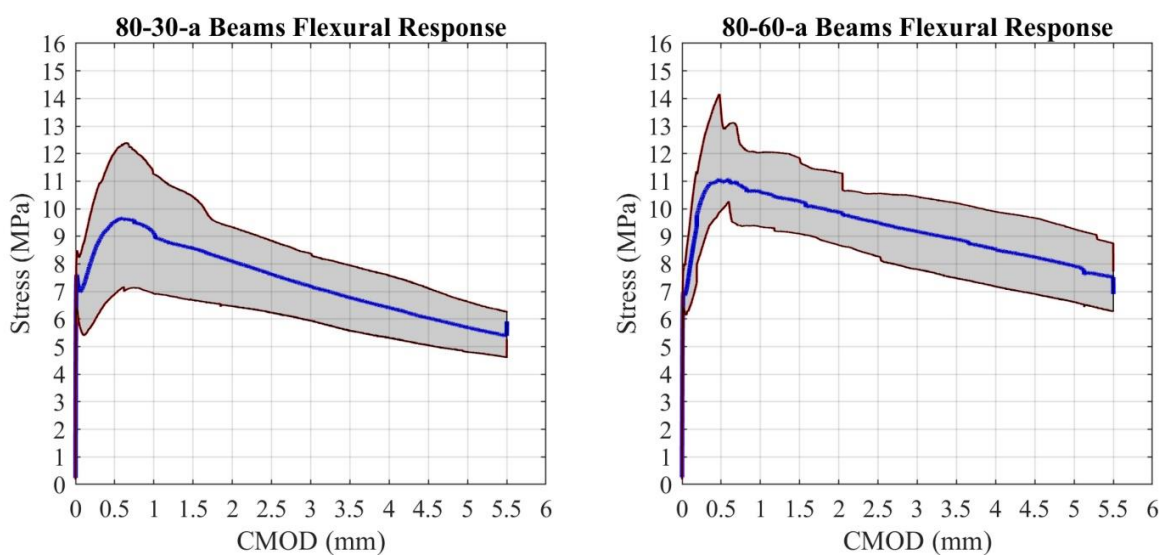


Figure 4-3: Envelope and average Stress-CMOD curves for 80 kg/m³ fibre dosage (Batch a)

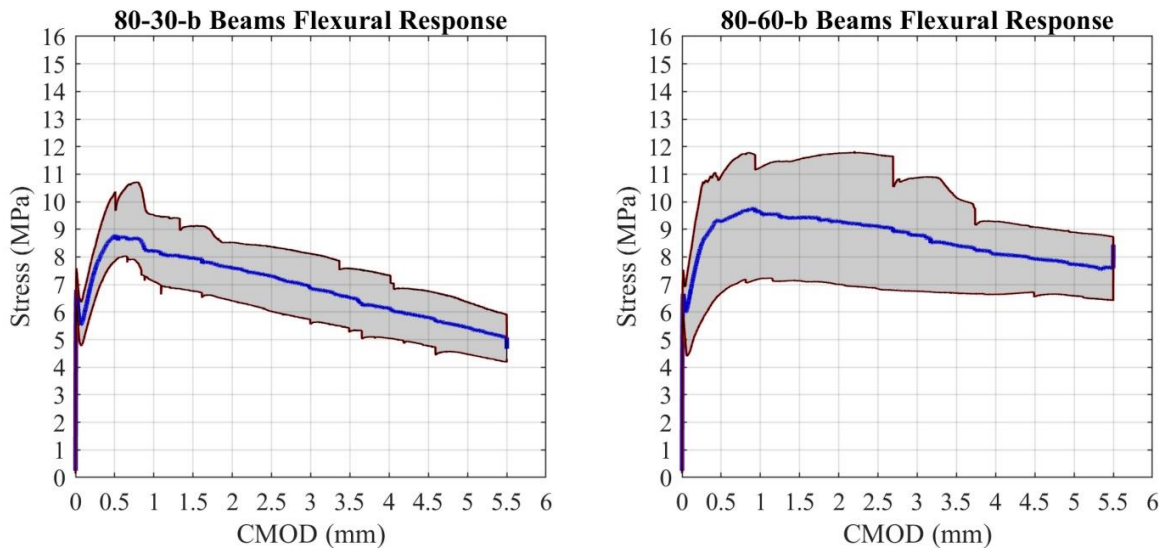


Figure 4-4: Envelope and average Stress-CMOD curves for 80 kg/m³ fibre dosage (Batch b)

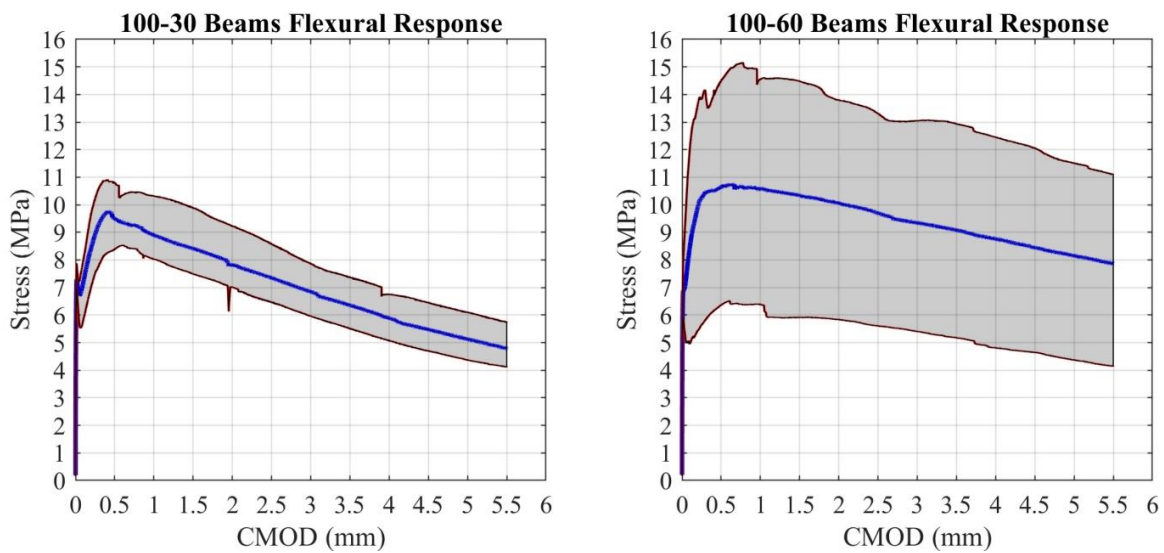


Figure 4-5: Envelope and average Stress-CMOD curves for 100 kg/m³ fibre dosage

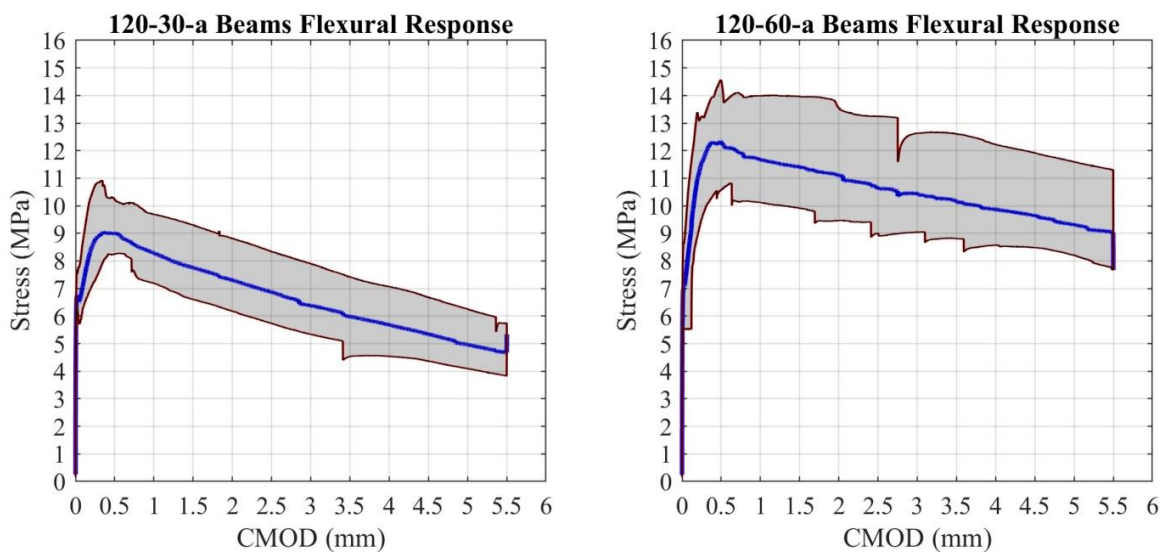


Figure 4-6: Envelope and average Stress-CMOD curves for 120 kg/m³ fibre dosage (Batch a)

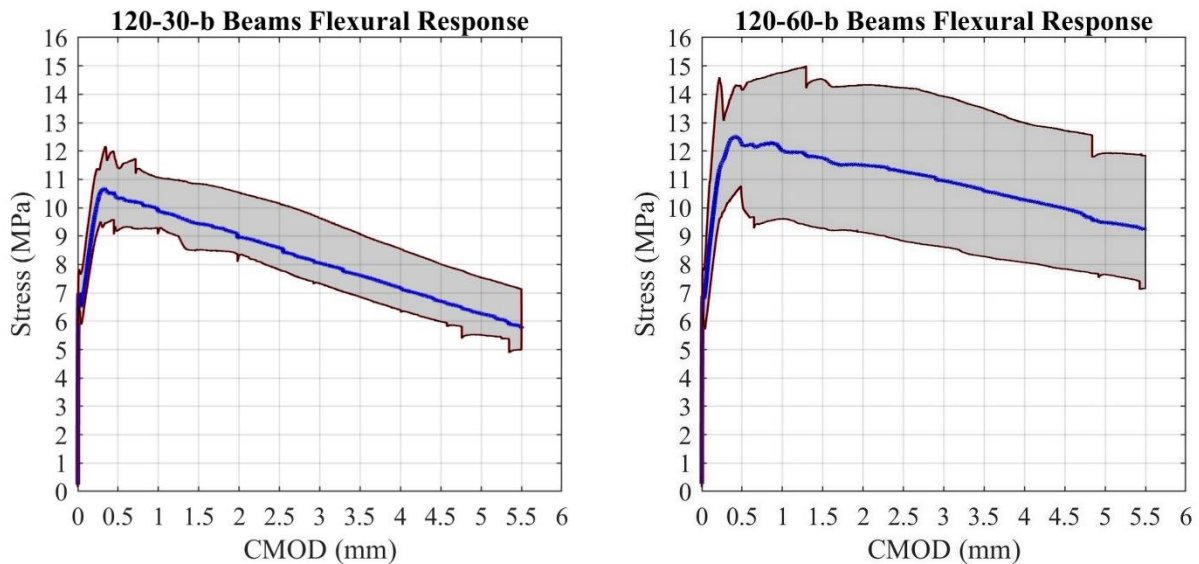


Figure 4-7: Envelope and average Stress-CMOD curves for 120 kg/m³ fibre dosage (Batch b)

It should be noted that during the mixing process of batch 80-60-a it was found that the 60 mm fibres were contaminated with an unknown quantity of 30 mm fibres. It was decided to continue with the operation rather than disposing of the 160 ℓ batch of concrete in the mixer. Although all results relating to this batch are presented in Appendix B, they are disregarded and do not form part of any data analyses in subsequent chapters. It is, however, interesting to note the performance of this *hybrid* batch with regard to strength and variability in comparison to the other batches.

The figures indicate that the double cast batches, with the exception of batch 80-60-a, demonstrated similar flexural behaviour in terms of the peak flexural strength as well as the degree of variation within a batch.

The average flexural response of specimens with varying fibre content is shown in Figure 4-8 and Figure 4-9 for 30 mm and 60 mm fibres, respectively. The results in Figure 4-8 indicate that the improvement in average flexural response of the 30 mm fibres is inconsequential for fibre dosages of 80 kg/m³ and greater. The trend illustrated by the results in Figure 4-9 exhibits a more substantial improvement in the average flexural response as the dosage of 60 mm fibres is increased.

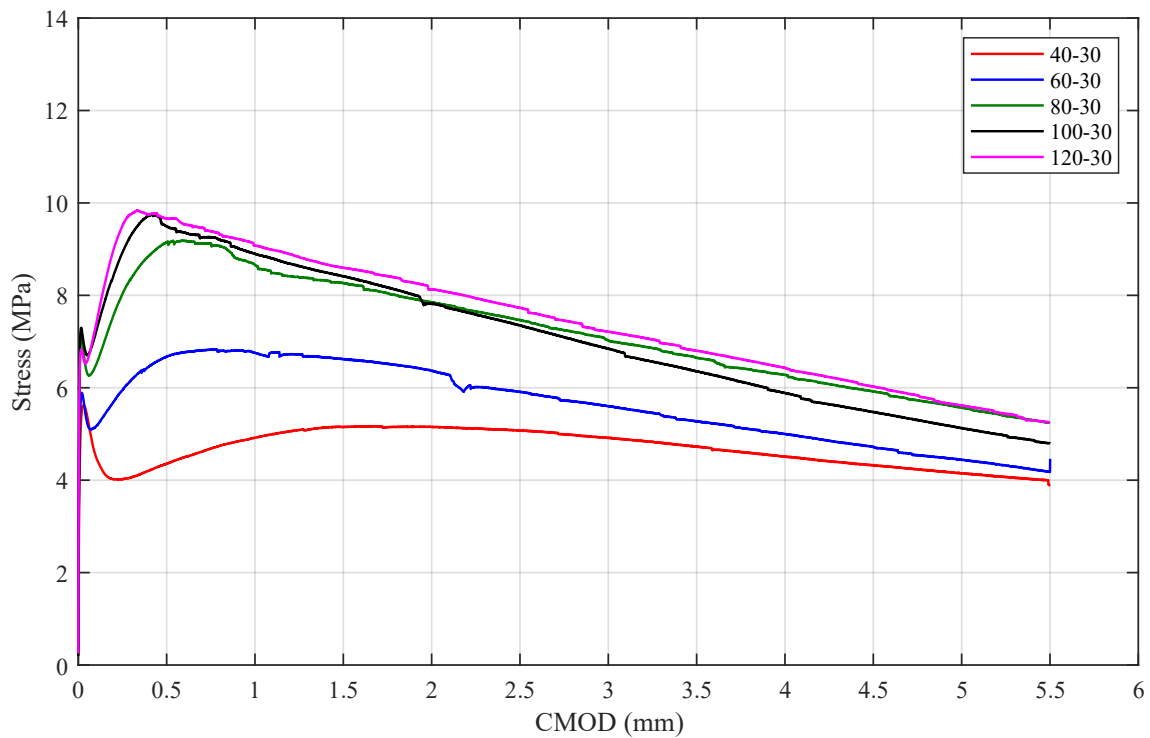


Figure 4-8: Average flexural response for various dosages of 30 mm fibres

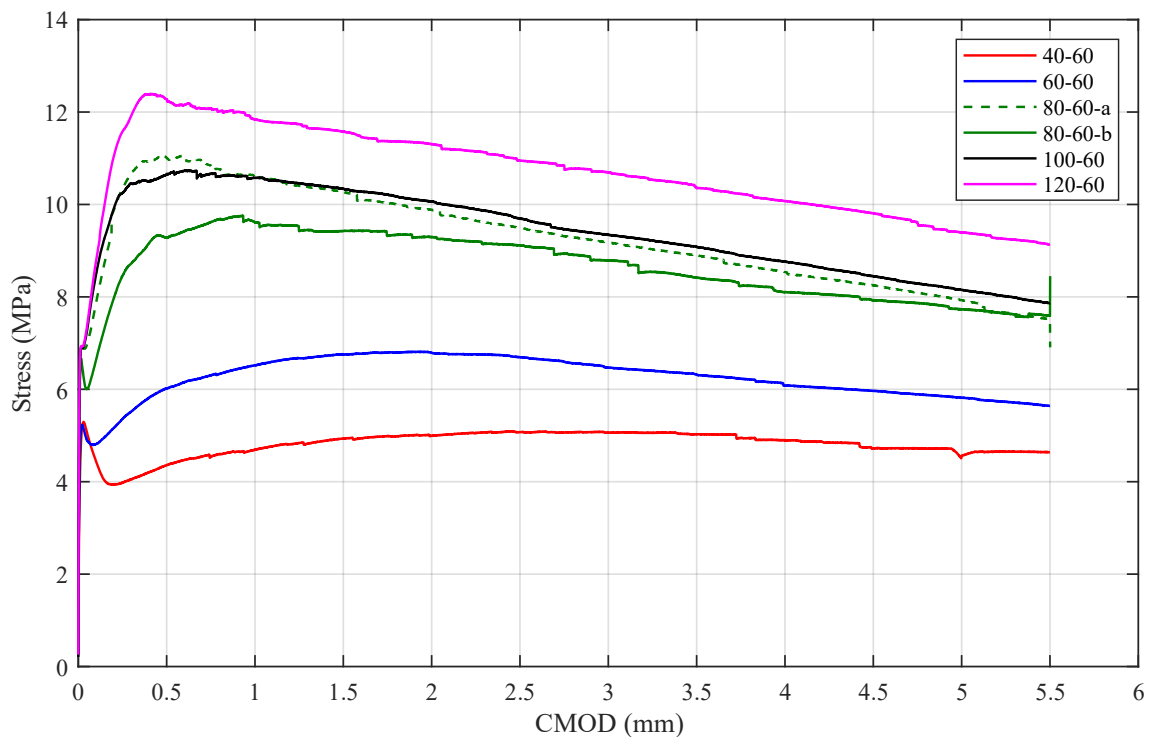


Figure 4-9: Average flexural response for various dosages of 60 mm fibres

RILEM TC 162-TDF (2002) specifies a condition that if a crack should initiate outside the notch, the test must be rejected. This occurred once out of the 126 tests that were performed. The sample that failed this condition formed part of batch 120-60-a and is shown in Figure 4-10. Some more typical crack patterns are depicted in Figure 4-11.



Figure 4-10: Rejected test where the crack initiated outside the notch



Figure 4-11: Examples of various observed crack patterns

4.3 Flexural Strength Design Parameters

The calculations involved in obtaining the flexural strength design parameters were given in Sub-section 2.7.1 and the results of implementing those procedures on the experimental data are presented in this section. The average equivalent flexural strengths and limit of proportionality of each batch are provided in Table 4-1. The average residual strengths are presented in Table 4-2. The equivalent strength was calculated from the individual $F - \delta$ curves, whereas the $F - CMOD$ data of each test were used to determine the residual strengths. The residual strength parameters are only presented in this section for the sake of completeness. Only the equivalent flexural tensile strength parameters are used in subsequent chapters to relate to fibre distribution characteristics; however, using residual strength parameters would have provided similar results due to the equivalence between the two parameters. The ultimate decision of selecting the equivalent strength parameters as the flexural tensile strength descriptor in this research

was discussed in the literature review. It was said that the residual flexural strength parameters are more susceptible to local irregularities in the load-displacement curve than the equivalent flexural strength parameters.

Table 4-1: Equivalent flexural strength and LOP results

Fibre Content (kg/m ³)	Fibre Type	$f_{fct,L}$		$f_{eq,2}$		$f_{eq,3}$	
		Average (MPa)	CoV (%)	Average (MPa)	CoV (%)	Average (MPa)	CoV (%)
40	30 mm	5.94	6.37	4.17	13.37	4.79	12.94
	60 mm	5.45	8.62	4.08	25.55	4.85	15.87
60	30 mm	6.06	8.95	5.99	17.11	6.25	15.01
	60 mm	5.44	10.41	5.73	28.24	6.42	24.95
80	30 mm (a)	7.68	10.13	8.36	16.14	8.73	14.65
	30 mm (b)	6.87	6.45	7.28	8.63	7.83	6.88
	60 mm (b)	6.76	8.09	8.27	21.50	9.20	15.26
100	30 mm	7.39	4.09	8.75	10.81	8.62	8.66
	60 mm	7.54	16.30	10.32	27.36	10.31	22.94
120	30 mm (a)	6.86	8.39	8.67	11.73	8.14	8.64
	60 mm (a)	7.59	14.70	11.83	12.93	11.54	11.34
	30 mm (b)	7.03	5.96	9.87	7.53	9.54	7.36
	60 mm (b)	7.37	12.53	11.62	12.47	11.68	13.60

Table 4-2: Residual flexural strength results

Fibre Content (kg/m ³)	Fibre Type	$f_{R,1}$		$f_{R,4}$	
		Average (MPa)	CoV (%)	Average (MPa)	CoV (%)
40	30 mm	4.36	9.96	4.73	14.37
	60 mm	4.36	26.73	5.03	11.12
60	30 mm	6.68	17.30	5.28	15.16
	60 mm	6.02	23.73	6.32	25.23
80	30 mm (a)	9.53	15.54	6.78	11.65
	30 mm (b)	8.77	9.57	6.52	12.16
	60 mm (b)	9.28	16.08	8.42	11.44
100	30 mm	9.50	7.96	6.35	10.26
	60 mm	10.64	22.60	9.08	23.46
120	30 mm (a)	8.99	6.51	5.98	13.56
	60 mm (a)	12.32	11.24	10.13	12.00
	30 mm (b)	10.33	7.43	7.61	9.28
	60 mm (b)	12.22	10.87	10.57	18.14

Box plots of the various flexural strength parameters are shown for 30 mm and 60 mm fibres in Figure 4-12 to Figure 4-16. The trends displayed by the data in the box plots indicate that a lower dispersion of results was generally observed for the mixtures containing 30 mm fibres compared to the mixtures with 60 mm fibres. Apart from the $f_{fct,L}$ results, a distinct increase in strength with increasing fibre content is evident from the figures, with the 60 mm mixtures achieving the greatest flexural strengths. In addition,

the 30 mm fibre results exhibit a similar trend to what was observed in Figure 4-8 in that increasing 30 mm fibre dosages beyond 80 kg/m³ provides limited increase in composite flexural strength.

The results from the double cast batches did not vary substantially from one another and the deviations are considered to be within bounds of the expected degree of experimental variation.

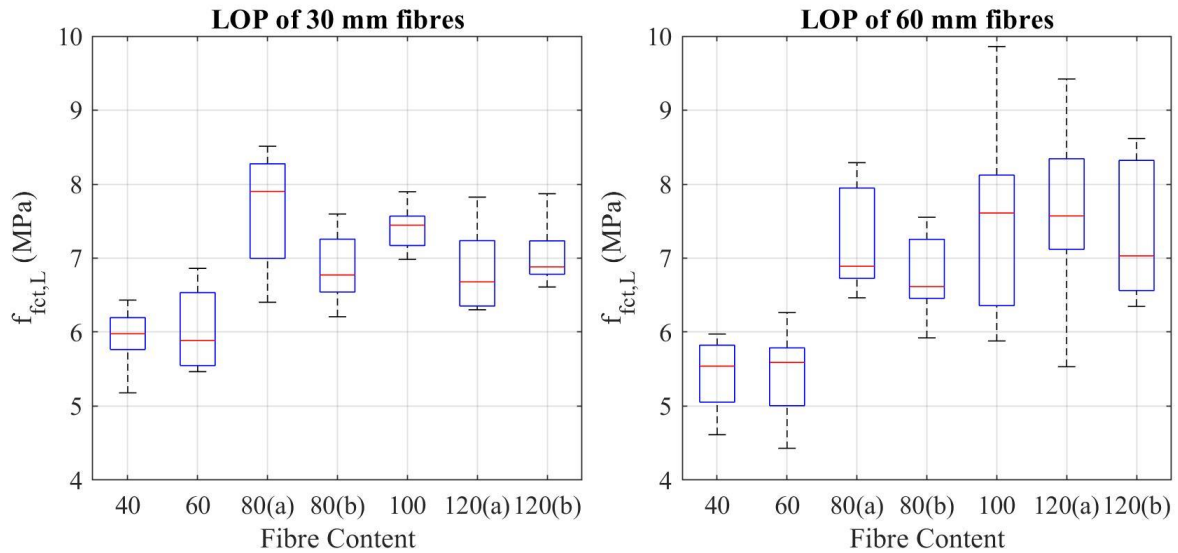


Figure 4-12: $f_{fct,L}$ results box plot

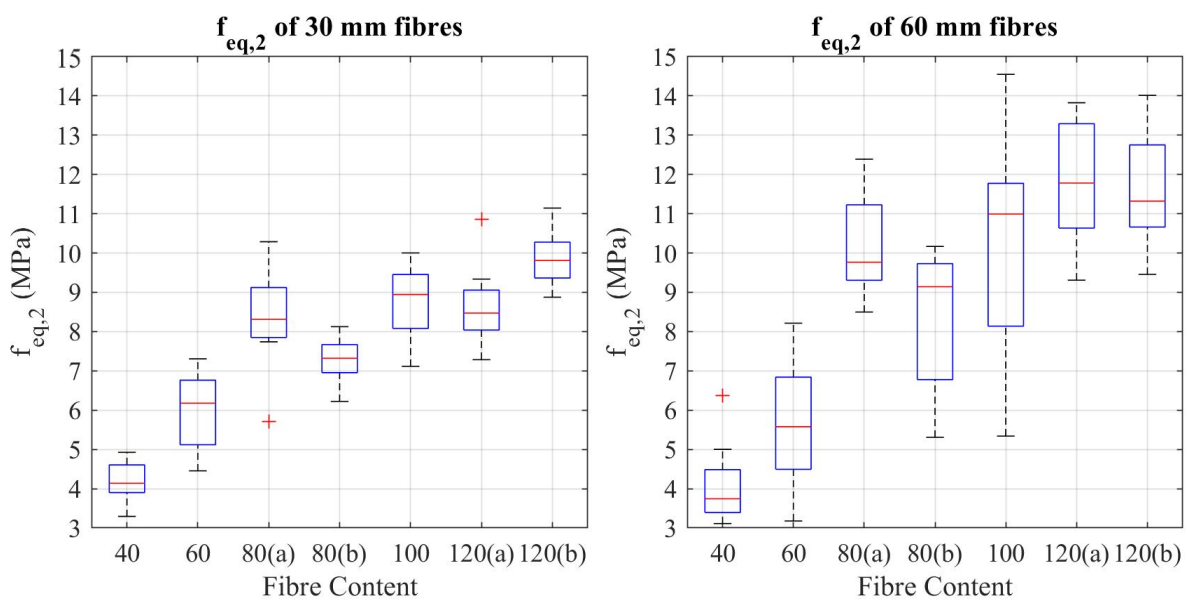


Figure 4-13: $f_{eq,2}$ results box plot

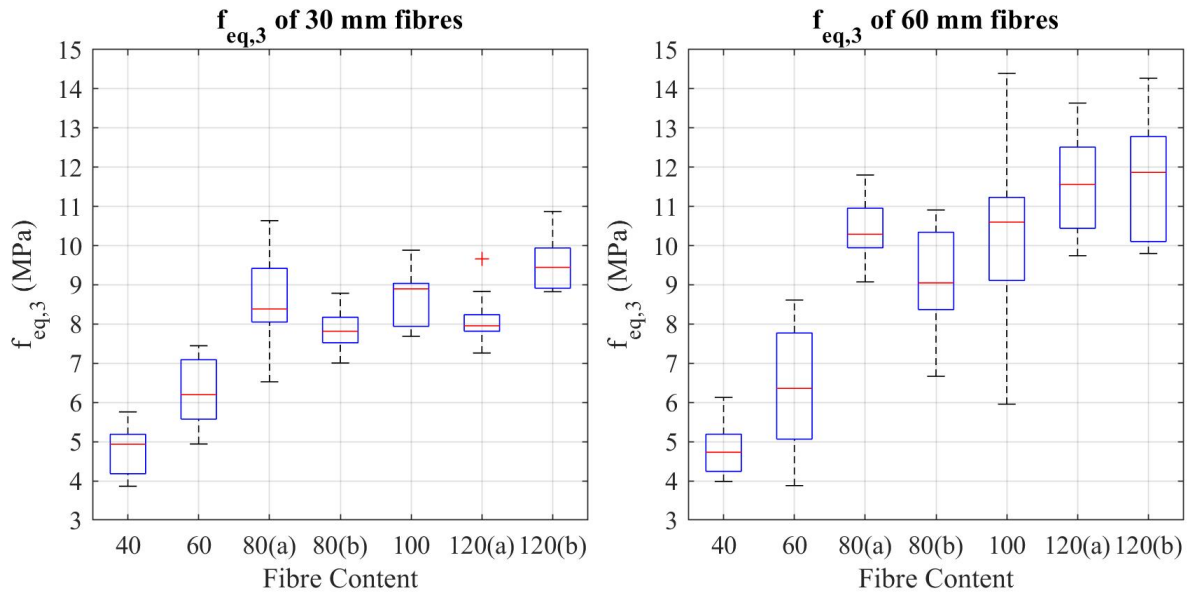


Figure 4-14: $f_{eq,3}$ results box plot

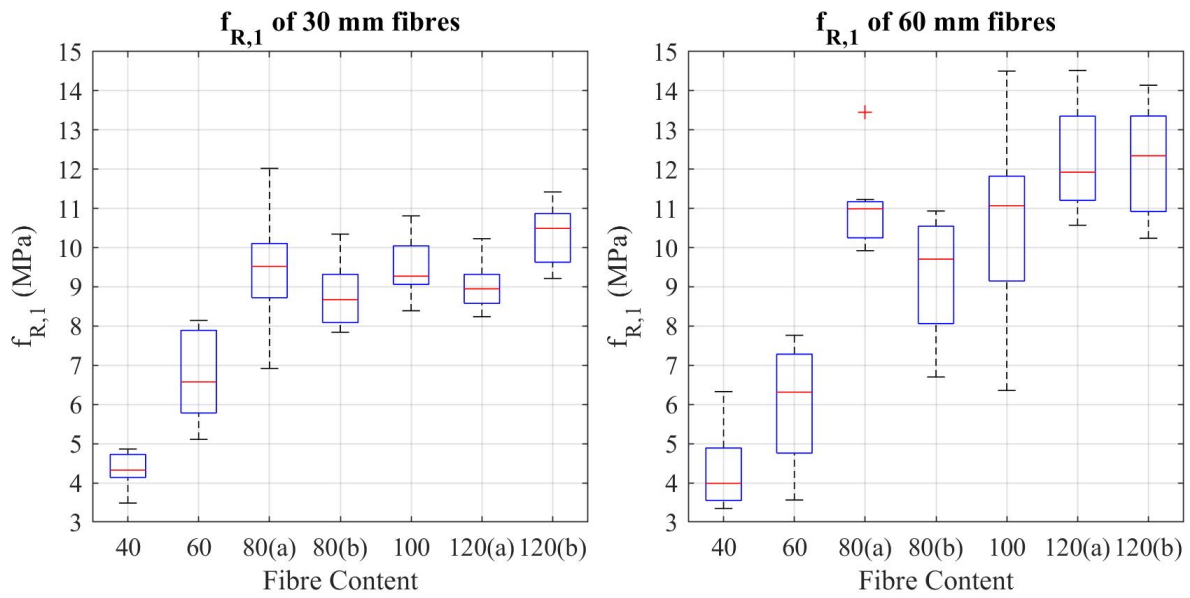
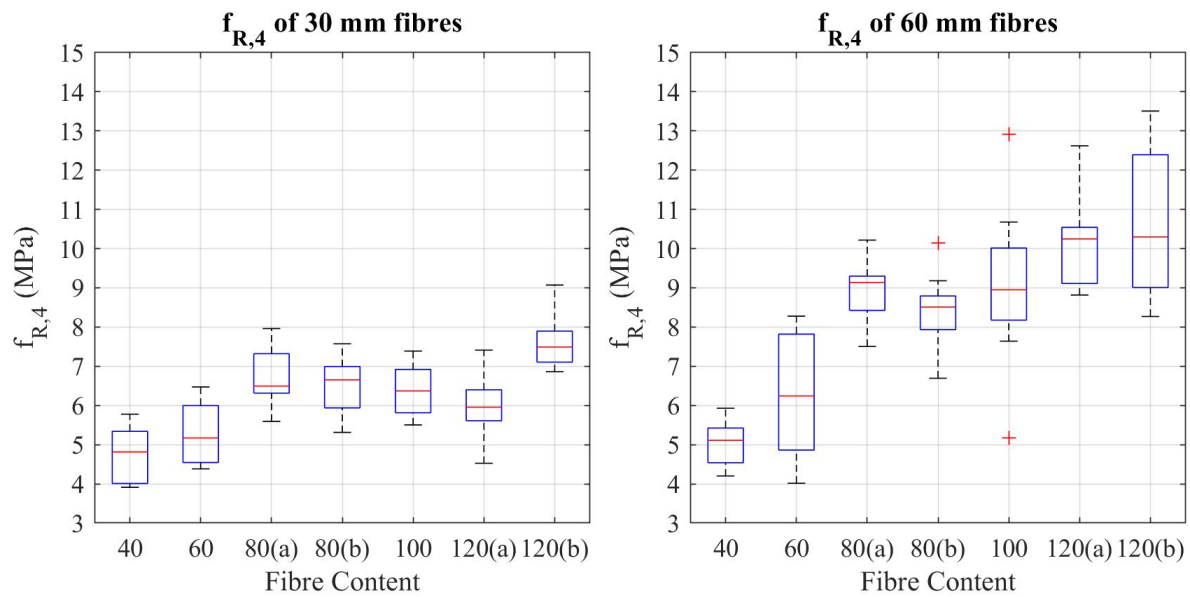


Figure 4-15: $f_{R,1}$ results box plot

Figure 4-16: $f_{R,4}$ results box plot

4.4 Fibre Count and Spatial Distribution Results

The distance between a vertex and the nearest fibre(s) was selected as the geometric descriptor used to quantify the spatial distribution of fibres. This was designated as the dimension α in Figure 3-14. The parameter provides an indication of the average spacing between a group of three or more fibres and can therefore be used to determine an overall frequency distribution describing the proximity of fibres towards one another. Examples of Voronoi diagrams generated for selected batches are shown in Figure 4-17.

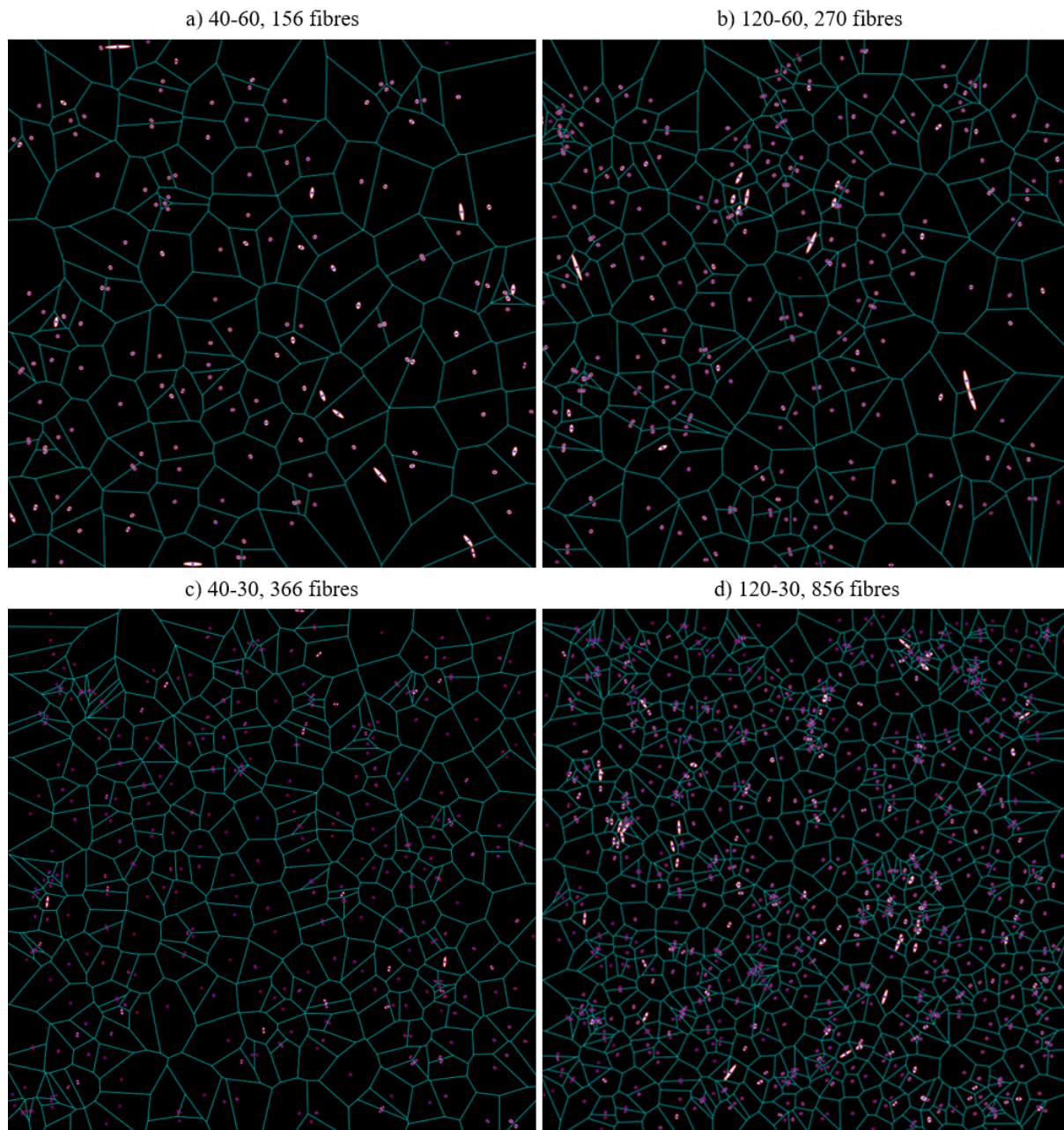


Figure 4-17: Examples of Voronoi diagrams for different fibre counts

The following parameters were extracted from the image processing results to obtain a preliminary understanding of the mechanisms that influence the spatial arrangement of fibres.

1. The number of fibres intersecting the cross section, N_f .
2. The Voronoi distance at which 95% of fibres are closer spaced, a_{95} .
3. The Voronoi distance at which 50% of fibres are closer spaced, a_{50} .
4. The Voronoi distance at which 5% of fibres are closer spaced, a_5 .
5. The gradient of the straight portion of the Cumulative Distribution Function (CDF) of the Voronoi spacing, ξ .

A box plot of the number of fibres with volume content is shown in Figure 4-18 for 30 mm and 60 mm fibres. The average number of fibres counted for each fibre content follows a distinct linear trend.

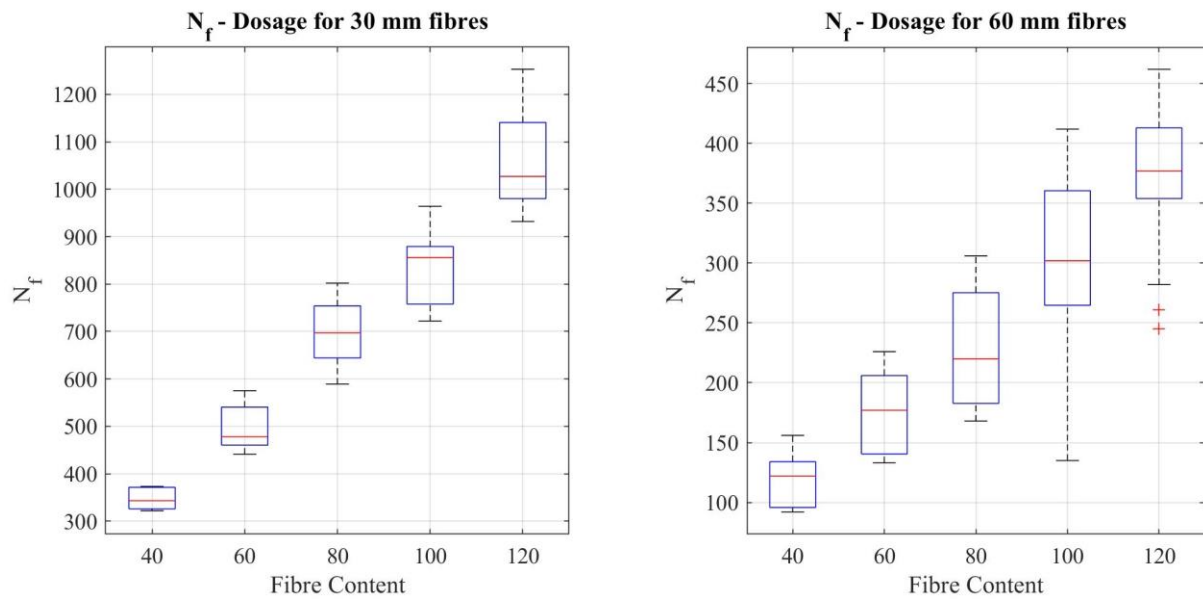


Figure 4-18: Box plot of the number of fibres detected for the various fibre dosages

The average CDF's describing fibre spacing of selected batches are given in Figure 4-19. The average, minimum, and maximum CDF graphs for each batch are provided in Appendix A. The figure illustrates how the range of fibre spacing becomes progressively narrower with increasing fibre count. Furthermore, the distribution of fibre spacing below α_{50} tends to be more continuous relative to the range of spacings for the batches with high fibre counts. This observation is better illustrated with the fibre spacing CDF's plotted on an x-axis with a logarithmic scale as shown in Figure 4-20.

Considering the similarity in the CDF shapes of the two fibre types, Figure 4-19 and Figure 4-20 imply that the fibre spatial distribution is highly dependent on the number of fibres as opposed to the fibre length. However, this may not be the case for exceedingly high fibre contents where the fibre spacing distribution may be more dependent on the fibre diameter. Theoretically, the spatial distribution has a limiting minimum distance equal to the diameter of the specific fibre; therefore, a matrix fully saturated with 0.5 mm diameter fibres will have a highly uniform CDF initiating at 0.5 mm, whereas a fibre diameter of 1.0 mm will initiate at a distance of 1.0 mm.

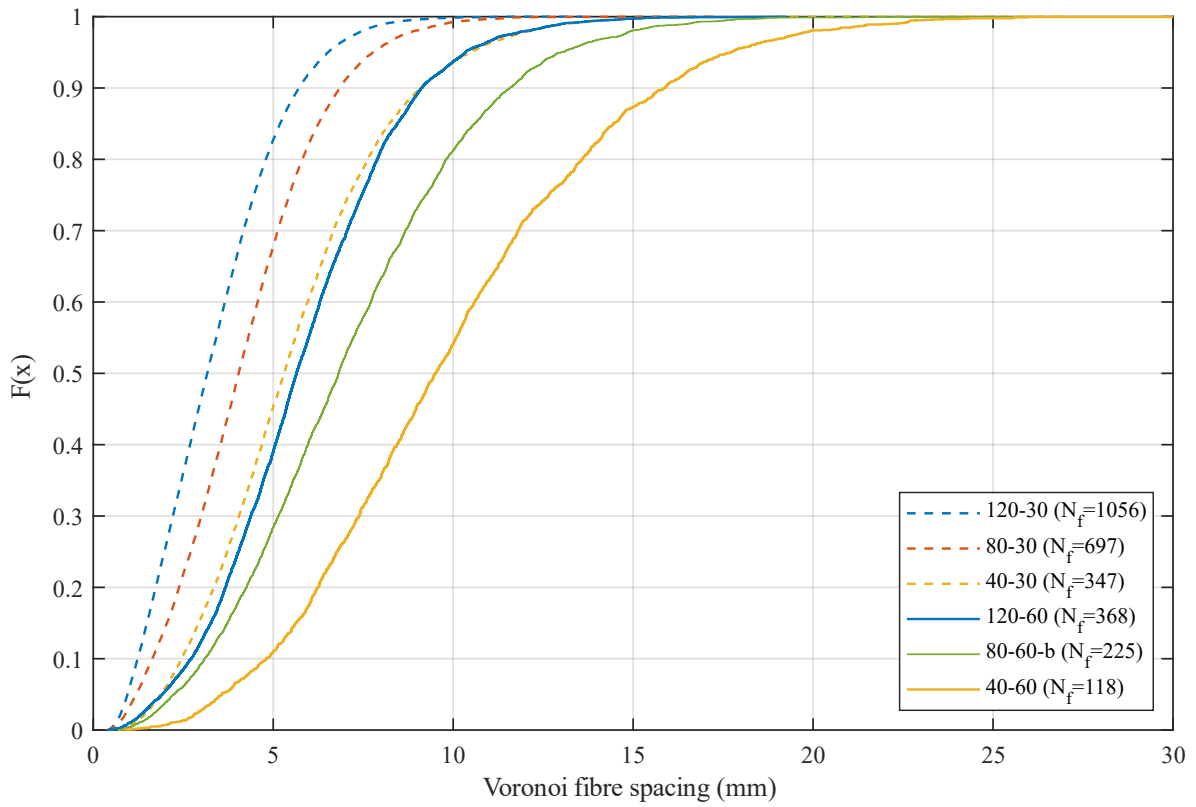


Figure 4-19: Average fibre spatial cumulative distribution plot

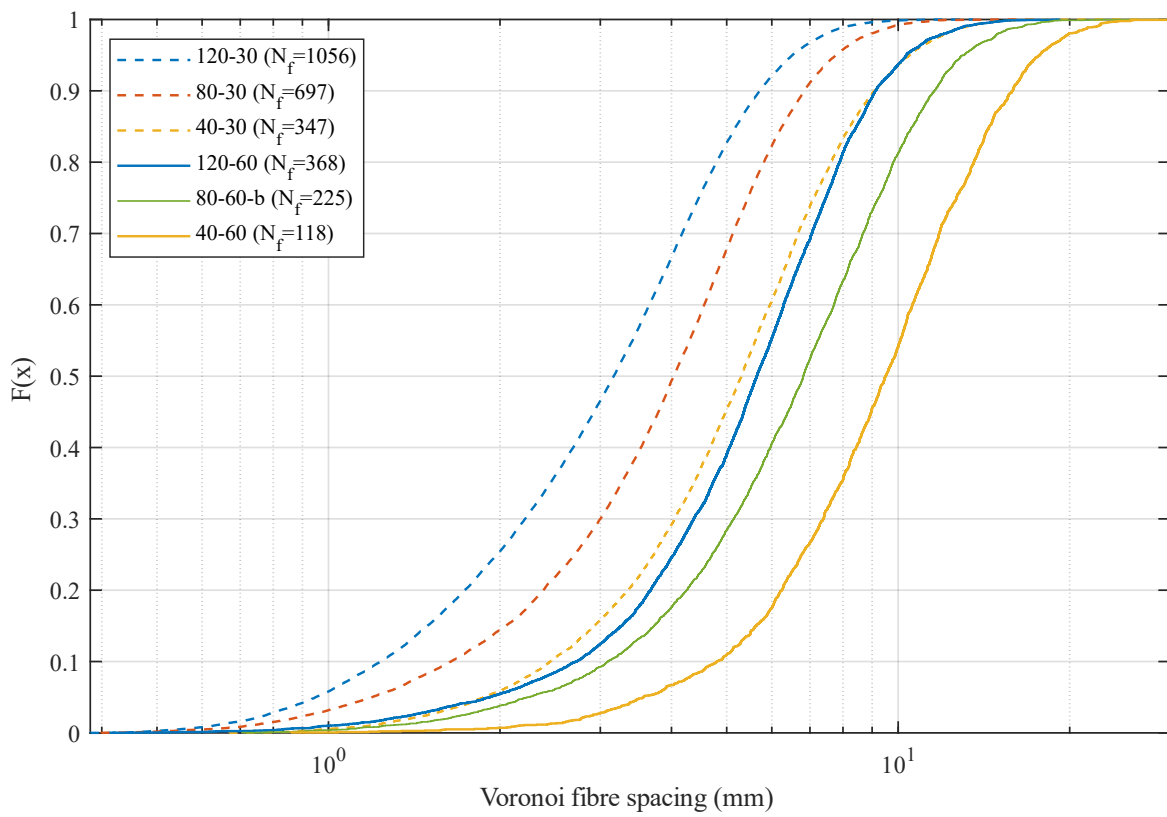


Figure 4-20: Average fibre spatial cumulative distribution plot (Logarithmic x-axis)

The average number of fibres as well as the average of the parameters obtained from the spacing CDFs are presented in Table 4-3 for each batch.

Table 4-3: Average of fibre count and spatial CDF parameter results

Fibre	Dosage (kg/m ³)	N _f	α_{95} (mm)	α_{50} (mm)	α_5 (mm)	Slope (ξ)
60mm	40	119	17.6	9.7	3.8	0.085
	60	174	15.0	8.0	3.0	0.102
	80-b	225	13.1	7.0	2.4	0.114
	100	299	11.8	6.3	2.1	0.128
	120-a	371	10.7	5.4	2.0	0.147
	120-b	367	10.4	5.5	2.0	0.146
30mm	40	347	10.3	5.7	1.9	0.148
	60	501	8.8	4.7	1.4	0.170
	80-a	716	7.7	4.0	1.2	0.186
	80-b	678	7.8	4.1	1.2	0.183
	100	829	7.2	3.7	1.1	0.194
	120-a	1028	6.6	3.3	1.0	0.198
	120-b	1089	6.5	3.1	1.0	0.204

The various CDF spacing parameters are plotted against fibre count in Figure 4-21. The data have been fitted using a power series model and the equations for each trendline are given in Table 4-4 along with the R-squared value of each fit. The results in Figure 4-21 serve as further confirmation of the strong correlation between the spatial distribution of fibres and fibre count. In addition, the continuity present at the overlap between the 60 mm and 30 mm fibre results indicates the insensitivity of spatial characteristics towards fibre length and diameter.

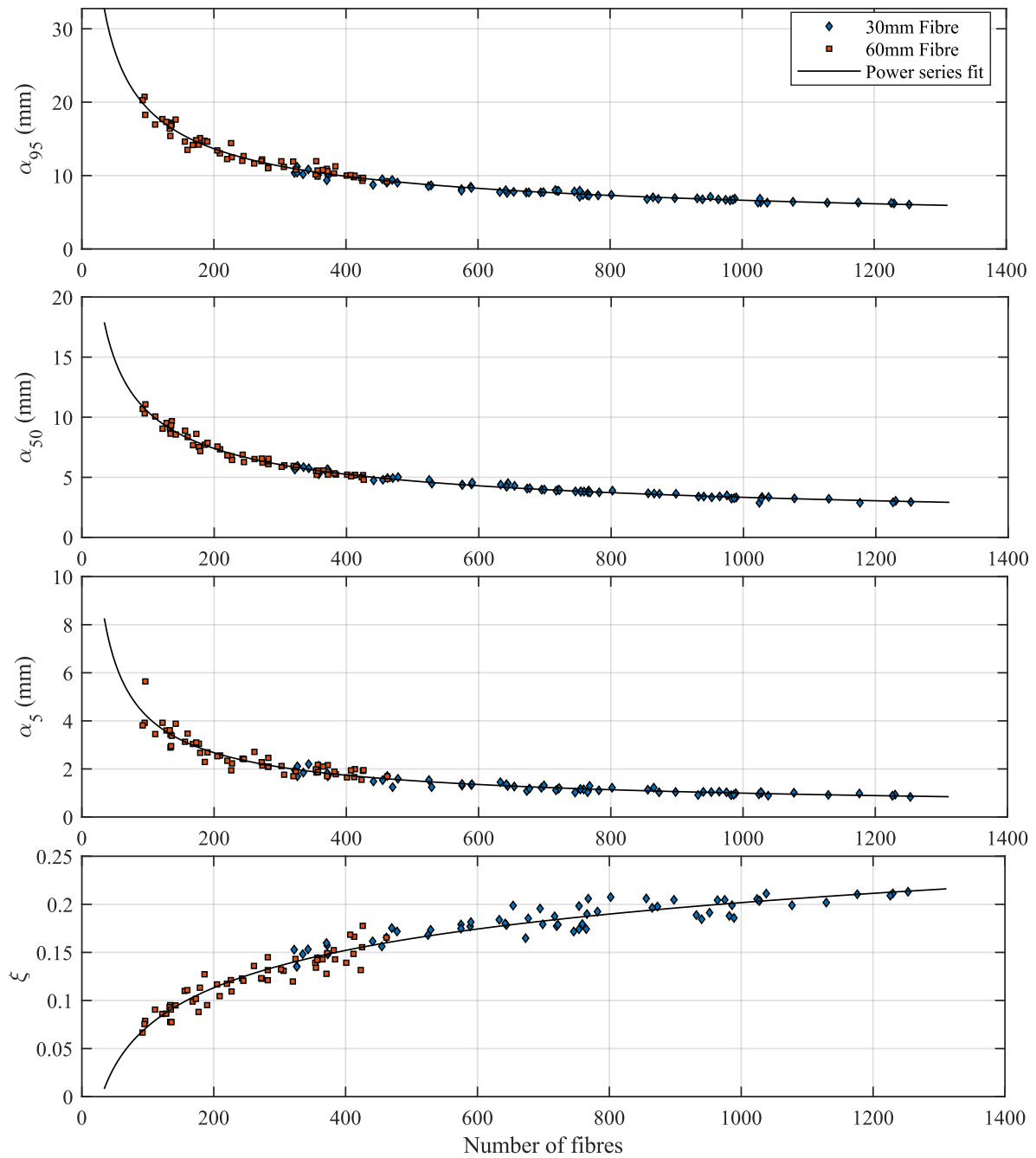


Figure 4-21: Spatial CDF parameter results

Table 4-4: Power fit equations of spatial CDF parameters

Parameter	Power fit equation	R ²
α_{95}	$f(x)=202.6x^{-0.5295}+1.416$	0.98
α_{50}	$f(x)=103.8x^{-0.4996}+0.04457$	0.99
α_5	$f(x)=79.78x^{-0.649}+0.07291$	0.93
ζ	$f(x)=-1.653x^{-0.04337}+1.427$	0.94

4.5 Relating Orientation Theory and Fibre Count

Recall that the orientation factor is defined as the ratio of the actual number of fibres intersecting an arbitrary crack plane to the theoretical number of ideally aligned fibres. An orientation factor approaching 1 represents the case of fibres predominantly aligned orthogonal to the crack plane, whereas a value of 0.5 represents isotropic conditions with fibres freely able to orientate themselves in space.

The theoretical orientation factors can be estimated using Equation 2.7 developed by Dupont and Vandewalle (2005). Applying the model produces the orientation factors $\eta_{\theta,30} = 0.546$ and $\eta_{\theta,60} = 0.602$ for 30 mm and 60 mm fibres, respectively. The effect of boundary conditions to cause preferential fibre alignment is more pronounced for the 60 mm fibres due to the larger influence zones associated with the longer fibre.

The orientation factor can be determined empirically from image analysis results by employing two equivalent approaches based on Equation 3.1. In the first approach, the orientation factor for each batch was calculated directly using the average number of fibres and volume content of the specific batch and then determining the orientation factor as the average of these results. The results obtained from implementing the first approach are presented in Table 4-5. Alternatively, N_{ideal} can be calculated for each batch and plotted against the corresponding average number of fibres. Using linear regression, a trendline was then fitted to the data, as shown in Figure 4-22, with the slope of the line representing the orientation factor.

Table 4-5: Orientation factor results calculated with empirical approach

Dosage (kg/m ³)	30mm Fibres			60mm Fibres		
	N_{ideal}	N_f	η_{θ}	N_{ideal}	N_f	η_{θ}
40	582	347	0.596	180	119	0.660
60	874	501	0.574	270	174	0.646
80	1165	697	0.598	360	225	0.626
100	1456	829	0.569	449	299	0.666
120	1747	1057	0.605	539	369	0.684
Average η_{θ}	0.588			0.656		

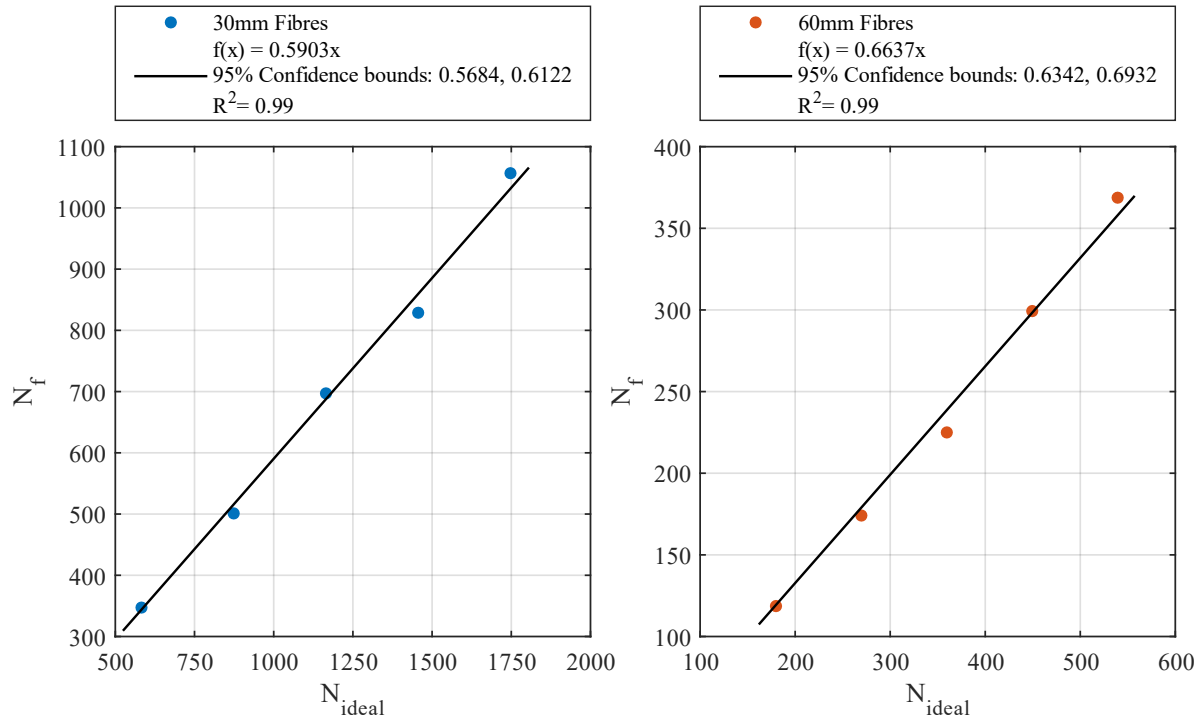


Figure 4-22: Determining the orientation factor through linear regression

As would be expected, the orientation factors calculated with the two approaches are approximately equal to one another. The orientation factors derived using the model proposed by Dupont and Vandewalle are lower than the factors derived from test data and Equation 3.1. The reason for this deviation is unclear; however, it is likely due to model assumptions that are not fully valid as well as the inherent variability associated with the material. Examples of fibre density plots are given in Figure 4-23. The preferential alignment of fibres due to wall-effects is not evident in the fibre density plots.

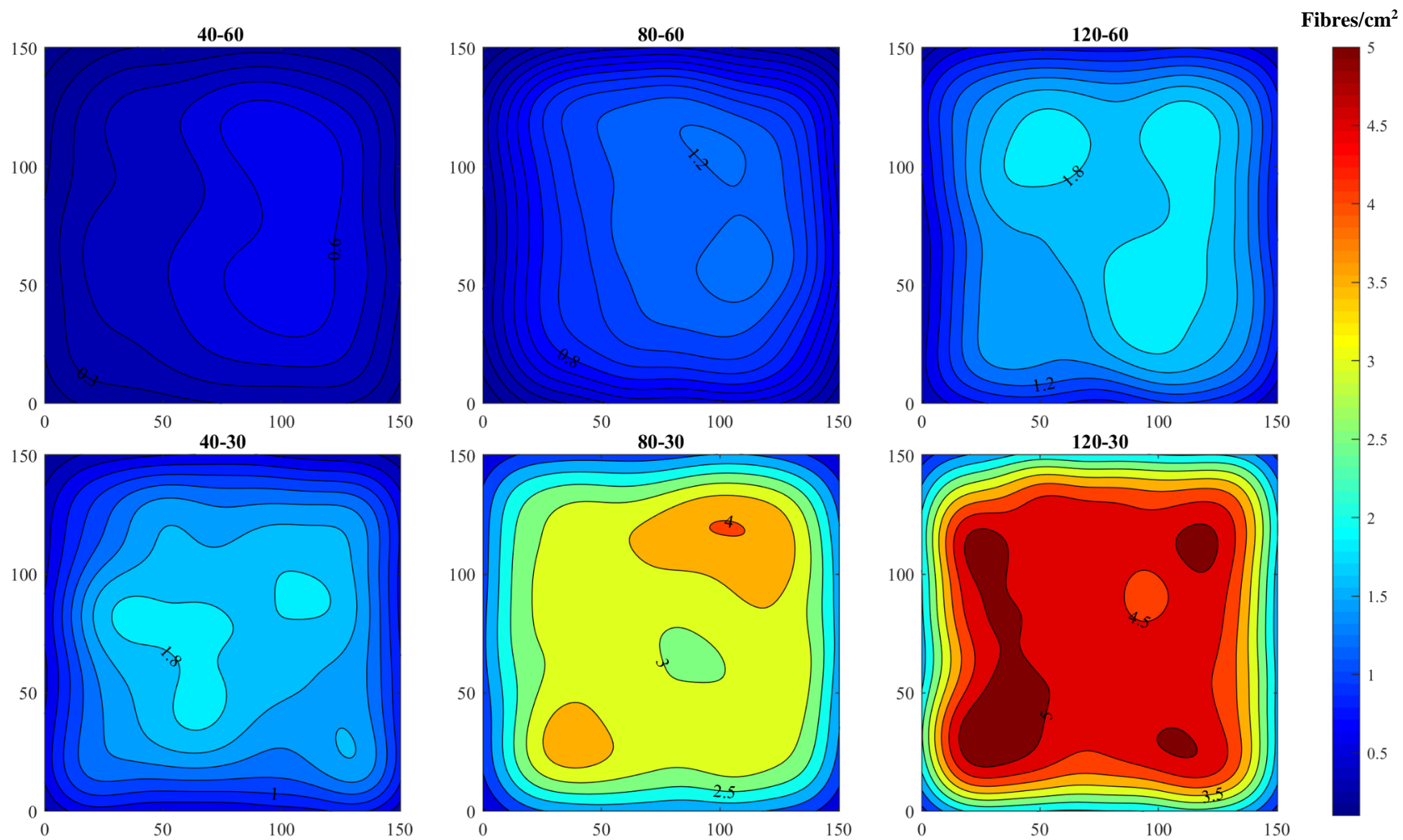


Figure 4-23: Contours illustrating sectional variation in fibre density

Equation 3.1 can also be applied to determine the average ratio of the number of 30 mm fibres to the number of 60 mm fibres using Equation 4.1 as follows:

$$\frac{N_{f,30}}{N_{f,60}} = \frac{\eta_{\theta,30} d_{f,60}^2}{\eta_{\theta,60} d_{f,30}^2} = \frac{0.5903 \cdot 0.9^2}{0.6637 \cdot 0.5^2} = 2.882 \quad (4.1)$$

Plotting the average number of 30 mm fibres against the 60 mm fibres and performing linear regression, as shown in Figure 4-24, yields a similar relation. This factor is used in Chapter 6 to adjust the fibre count of the 60 mm specimens to an equivalent number of 30 mm fibres, allowing improved comparisons of strength and fibre data.

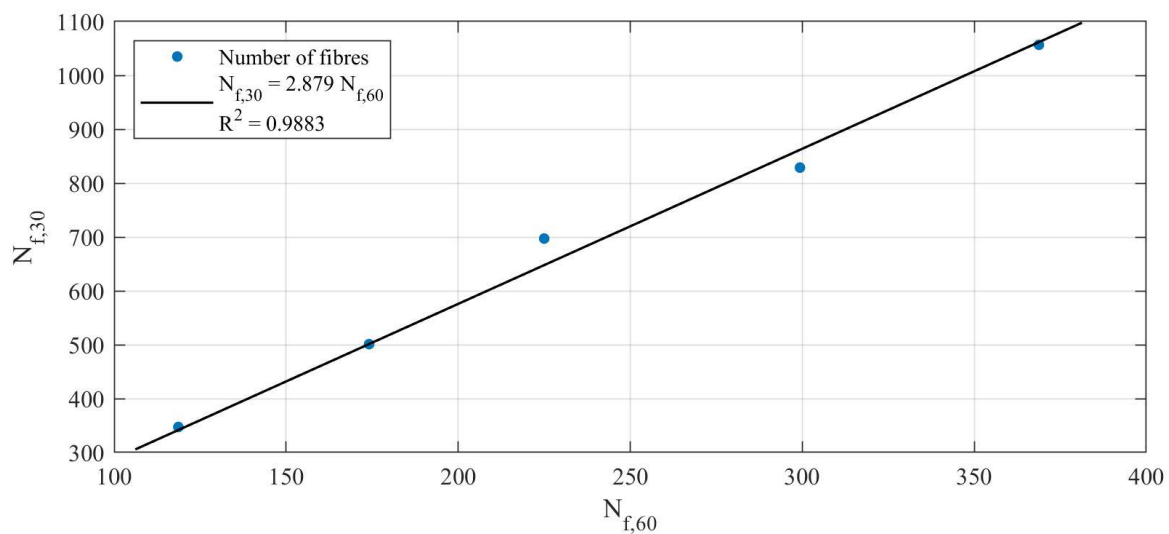


Figure 4-24: Relation of the average number of 30 mm and 60 mm fibres

4.6 Discussion on Results

The objective of this chapter was to present and analyse experimental results from flexural tests and image analysis to independently study the flexural behaviour and spatial arrangement of fibres for varying fibre lengths and dosages.

Summarising Stress-CMOD curves for each batch were presented and it was noted that the 60 mm fibre mixtures achieved more efficient flexural strength improvement with increasing fibre dosage than the 30 mm fibre batches which demonstrated limited increase in strength for fibre dosages above 80 kg/m³. It was pointed out that batch 80-60-a was contaminated with an unknown quantity of 30 mm fibres. The results from the batch are disregarded in all analyses in subsequent chapters and can be found in Appendix B. Boxplots of the data indicated that the batches containing 30 mm fibres generally demonstrated lower dispersion in flexural strength compared to the 60 mm fibre batches.

The fibre spatial arrangement was investigated using the geometric descriptor obtained from the Voronoi diagrams generated for each specimen. The findings highlighted the strong correlation between the number of fibres and the spatial distribution of fibres in a section. Furthermore, it was shown that the number of fibres in a section can be utilised to empirically determine an orientation factor that is

dependent on the fibre length and remains constant for fibre dosage. As expected, the 60 mm fibres had a higher orientation factor than the 30 mm fibres, indicating a higher fibre effectiveness. The theoretical orientation factor for each fibre type was calculated and compared to the empirically determined orientation factor and was found to estimate lower orientation factors. It was also shown that the number of 30 mm and 60 mm fibres are linearly related to one another and the relationship can be implemented to compare flexural strengths with respect to an equivalent number of 30 mm fibres.

CHAPTER 5. Statistical Analysis of Image Data

5.1 Background

The objective of this chapter is to evaluate the three sub-hypotheses formulated as part of the second research statement of this study: *investigating the influence of fibre length and fibre volume content on fibre spatial characteristics*. The three sub-hypotheses were formulated in Chapter 1 as follows:

1. *The spatial distribution of fibres is strongly related to the number of fibres intersecting a plane and the relative fibre dispersion uniformity increases as the number of intersecting fibres increases.*
2. *The variability of fibre spatial distribution within a batch reduces as the number of fibres increases.*
3. *The presence of fibre clustering becomes more prevalent as the number of fibres increase.*

These propositions are assessed in this chapter by using image analysis results and implementing the methods proposed in Section 3.8 and Section 3.9 to derive metrics that quantify the cross-sectional uniformity of a specimen, the consistency of spatial distribution within a batch, and the degree of clustering.

Results obtained from applying the first approach are presented in Section 5.2 and the effect of varying grid size on homogeneity is explored. The second approach, which utilizes the data obtained from Voronoi diagrams, is implemented in Section 5.3 and the results from the analysis are compared to the results obtained from a CSR point process. The qualities of the two approaches are compared in Section 5.4 with the aim of identifying the preferable method for quantifying the fibre spatial descriptors. The chapter is concluded with a discussion on the main findings from analysing the image data in Section 5.5.

5.2 Statistical Analysis of Fibre Count Distribution

Statistical analysis was performed to assess the distribution of fibres across a section with the objective of quantifying the fibre spatial characteristics. The approach implemented in this section is based on constructing a roster of given grid size, counting the fibres inside each grid square, and analysing the result. This is an alternative method for evaluating the fibre spatial characteristics and the resulting descriptors are used later in the chapter to compare to the parameters obtained using Voronoi data.

5.2.1 Degree of clustering

The degree of clustering is calculated with Equation 3.4 using a standardised grid dimension obtained from Equation 3.2. The standardised grid dimension is a function of the number of fibres in an individual specimen and represents the number of m squares in the $m \times m$ grid imposed over the cross section.

Performing the analysis and fitting a Poisson distribution to the data produces the curves shown in Figure 5-1. Two observations are worth noting from the plots:

1. The average fibre density is approximately equal regardless of fibre content, and
2. The data seems to deviate further from a Poisson distribution as the number of fibres increase.

It has been pointed out in Section 3.8 that the first observation is a property of the standardised probability distribution brought about by the calculated grid size and allows for comparing the characteristic shape of each batch's fibre distribution. The result of fitting a Poisson distribution to each batch and plotting the curves on the same axis is shown in Figure 5-2. The curves are practically identical which may prompt the incorrect conclusion that fibres are distributed according to the exact same point process irrespective of fibre content. This leads to the second observation noted from Figure 5-1. A characteristic of a Poisson type distribution is that the variance is equal to the mean which is the case for a point process exhibiting complete spatial randomness (Devore and Berk, 2012). The deviation is suspected to be due to the increasing variance that is characteristic of a more clustered point process as illustrated by the simulated point patterns given in Figure 3-17. Therefore, the spread of the distribution, or the variance, can be used as a measure of clustering with an increase in variance indicating more pronounced clustering in the pattern.

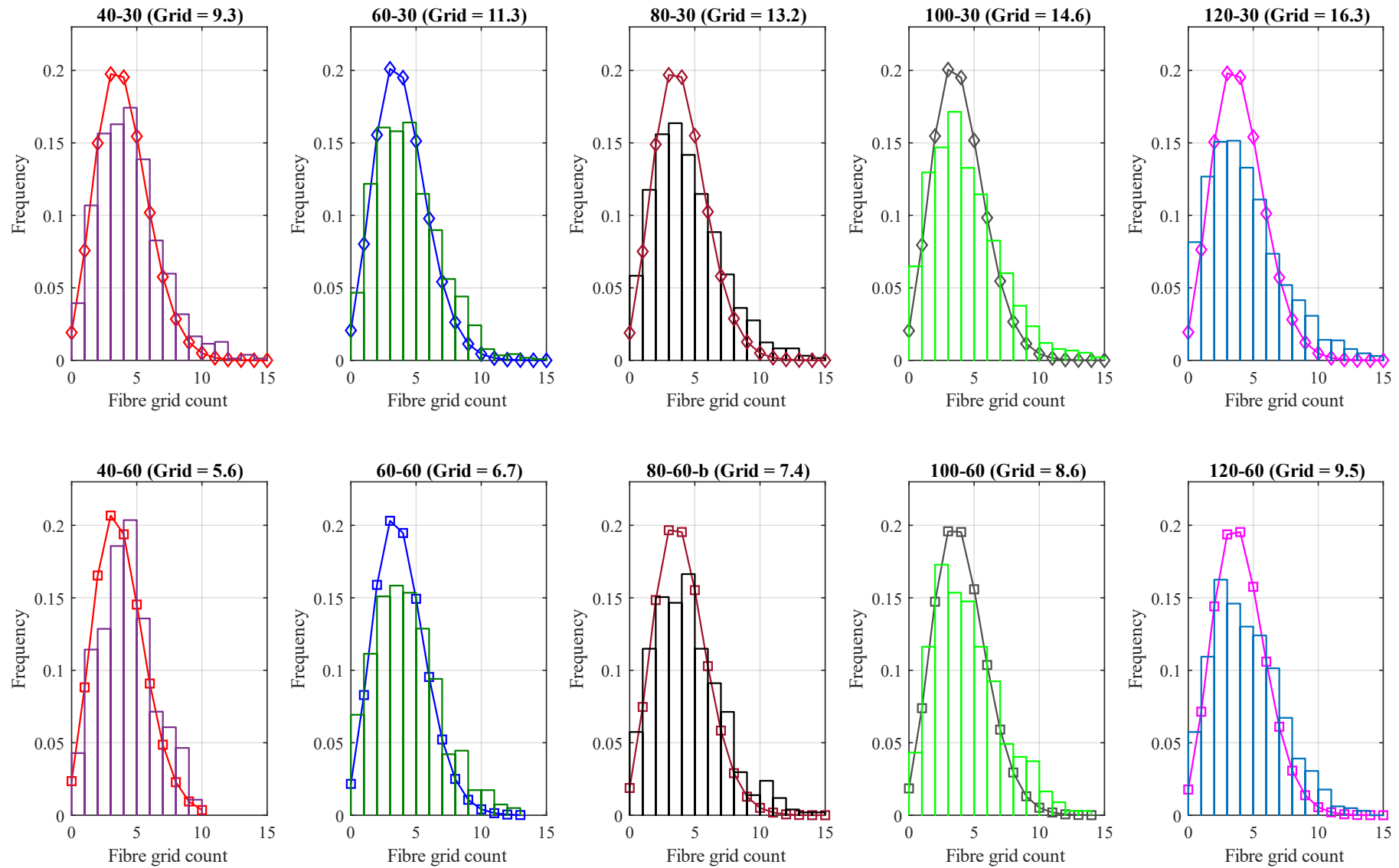


Figure 5-1: Distribution of fibres throughout a cross section

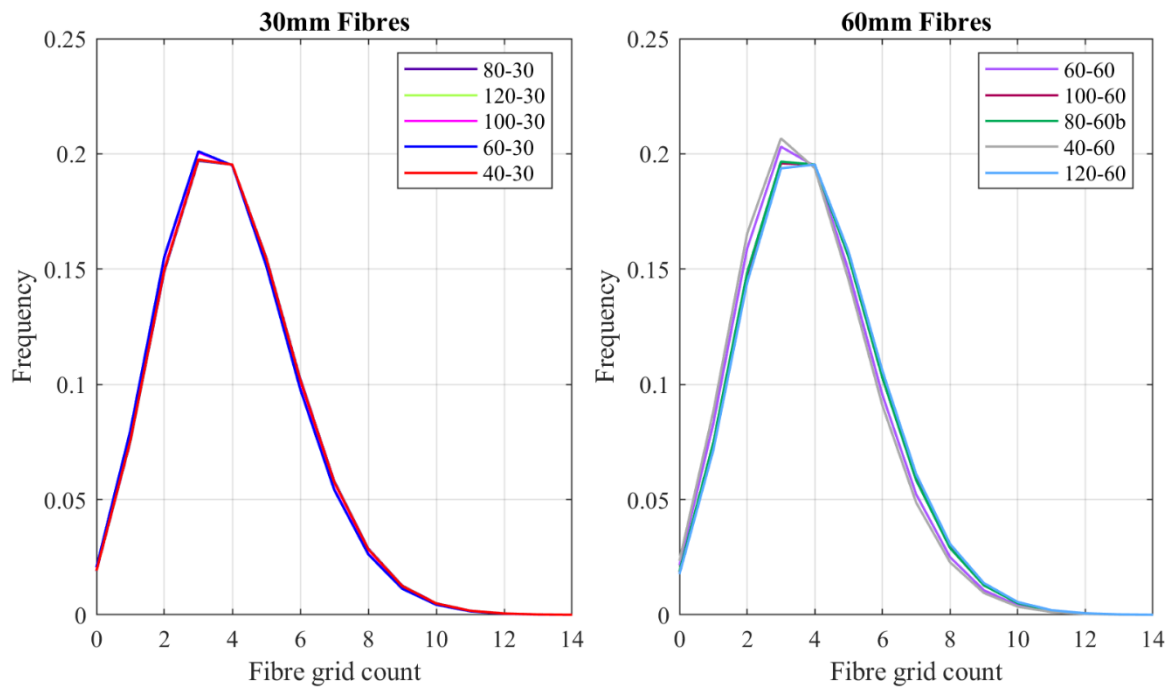


Figure 5-2: Fitted Poisson distributions of each batch

To account for the influence of small fluctuations in the mean number of fibres counted in a grid square, clustering was initially evaluated by calculating the mean Coefficient of Variation (CoV) as in Equation 3.5. The increase in fibre grid count CoV with the average number of fibres in a batch is demonstrated in Figure 5-3. The prevalence of clustering is less prominent for low fibre counts and consequently the increasing trend is less clear at low fibre counts. The results attained from the analysis are given in Table 5-1.

The results presented in Figure 5-3 and Table 5-1 provide evidence that is in support of the third sub-hypothesis of this study in that clustering tends to increase as fibre count increases.

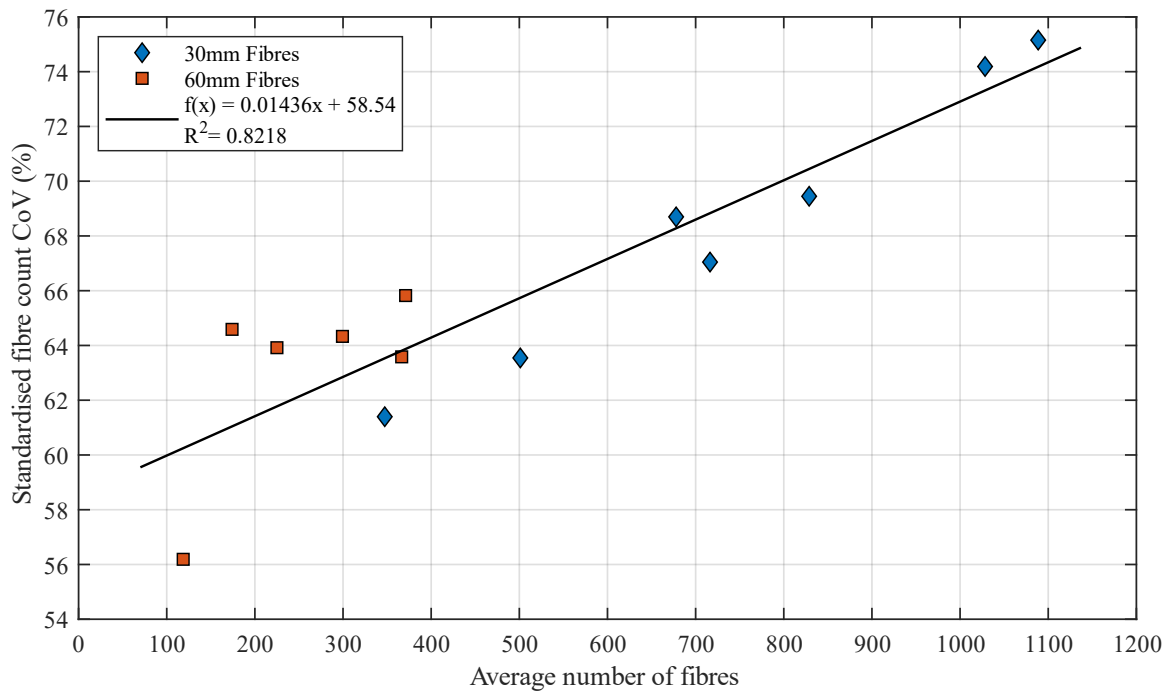


Figure 5-3: Increase in average CoV of standardised fibre grid count distribution with average total fibre count

Table 5-1: Results from fibre distribution analysis using standardised grid dimensions

Fibre Type	Dosage (kg/m ³)	Mean Standardised Grid size	Mean $n_{f, std}$	Mean Variance of $n_{f, std}$	$n_{f, std}$ CoV (%)	Density (Fibres/mm ²)
60	40	5.6	3.8	4.5	56.2	0.0053
	60	6.7	3.9	6.2	64.6	0.0077
	80-b	7.4	4.0	6.5	63.9	0.0101
	100	8.6	4.0	6.6	64.3	0.0132
	120-a	9.7	4.0	6.8	65.8	0.0167
	120-b	9.3	4.1	6.9	63.6	0.0165
30	40	9.3	4.0	6.0	61.4	0.0156
	60	11.3	3.9	6.1	63.5	0.0224
	80-a	13.3	4.0	7.2	67.0	0.0322
	80-b	13.1	3.9	7.3	68.7	0.0301
	100	14.6	3.9	7.3	69.4	0.0369
	120-a	16.0	4.0	8.9	74.2	0.0458
	120-b	16.6	3.9	8.7	75.2	0.0483

5.2.2 Fibre homogeneity and variability

A bar chart illustrating the n_f CoV evaluated using grid dimensions of 2x2, 5x5, and 10x10 is shown in Figure 5-4 for the various fibre dosages. The figure demonstrates that the homogeneity of fibre distribution increases as fibre dosage increases and that the 30 mm fibres have greater spatial uniformity than the 60 mm fibres. The interaction between fibre homogeneity, average fibre count, and grid size is

better visualised by the surface fitted to results shown in Figure 5-5. The results serve to confirm the first sub-hypothesis of this study in that the distribution of fibres in a cross section is more uniform for high fibre contents and small diameter fibres, i.e. a high fibre count. Results obtained from the analysis are presented in Table 5-2. A 10x10 grid was ultimately selected as the most appropriate size to evaluate fibre homogeneity using the fibre count approach. The 10x10 grid size was found to be a good intermediate dimension that can distinguish well between fibre distributions of specimen with high and low fibre counts.

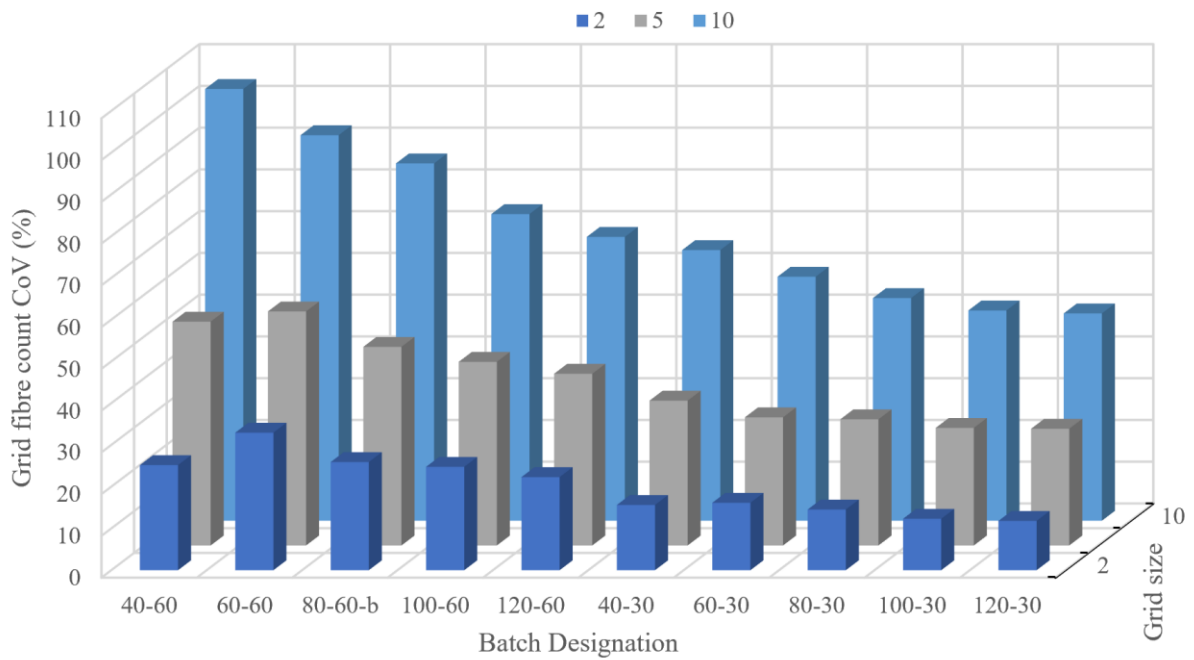


Figure 5-4: CoV of fibre grid count distribution for designated grid dimensions

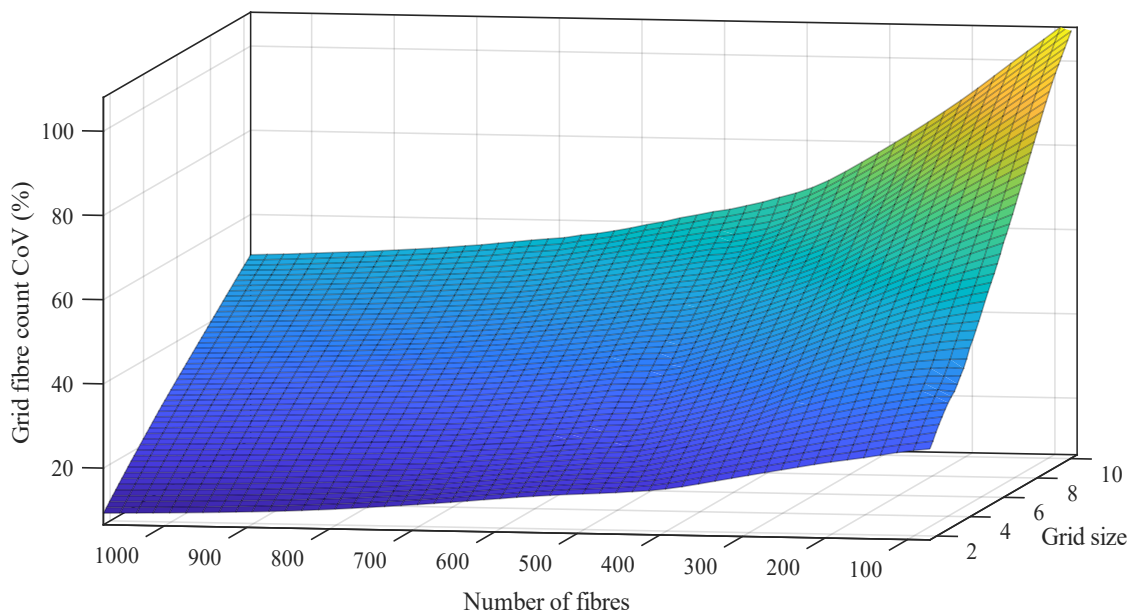


Figure 5-5: Surface fit illustrating the general response of the grid fibre count CoV to grid size and average total fibre count

Table 5-2: Results of fibre distribution analysis using grid sizes of 2x2 and 10x10

Fibre Type	Dosage (kg/m ³)	2 x 2 Roster			10 x 10 Roster		
		Mean n_f	Mean Variance of n_f	Mean n_f CoV (%)	Mean n_f	Mean Variance of n_f	Mean n_f CoV (%)
60	40	29.2	53.9	23.5	1.17	1.46	104.35
	60	43.0	200.9	30.3	1.72	2.53	92.33
	80-b	55.8	208.5	23.5	2.23	3.64	85.52
	100	74.3	338.7	24.1	2.97	4.77	74.15
	120-a	92.3	526.3	21.9	3.69	6.19	67.47
	120-b	91.1	329.2	18.6	3.65	6.32	69.19
30	40	86.3	182.1	14.9	3.45	5.01	64.94
	60	124.8	405.9	15.7	4.99	8.51	58.49
	80-a	178.6	684.3	13.6	7.14	13.47	51.58
	80-b	169.0	593.4	13.1	6.76	13.96	54.71
	100	206.7	648.3	11.9	8.27	17.33	50.53
	120-a	256.6	820.3	10.3	10.26	26.23	50.03
	120-b	271.7	1146.5	11.3	10.87	28.81	49.03

The standard deviation of fibre homogeneity for each batch is given in Table 5-3. The variation in fibre homogeneity tends to decrease as the number of fibres increase as indicated in Figure 5-6. This observation is in support of the second sub-hypothesis of this study stating that the spatial variation within a batch reduces as fibre count increases.

Table 5-3: Variation in the fibre homogeneity of a batch of specimens

60mm Fibres		30mm Fibres	
Dosage (kg/m ³)	Standard deviation of homogeneity	Dosage (kg/m ³)	Standard deviation of homogeneity
40	15.36	40	4.24
60	9.58	60	6.22
80-b	7.67	80-a	5.27
		80-b	3.77
100	10.04	100	5.36
120-a	6.35	120-a	4.20
120-b	7.96	120-b	3.05

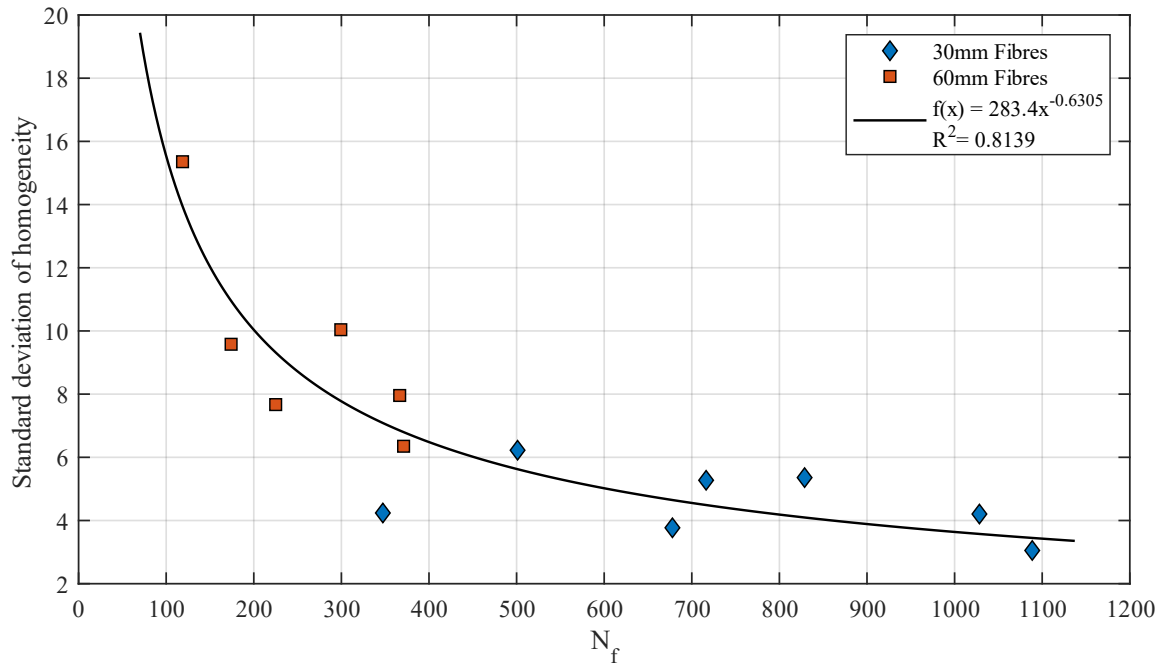


Figure 5-6: Variation of fibre homogeneity with average fibre count

5.3 Statistical Analysis of Fibre Spatial Distribution

In order to evaluate and assess the spatial distribution of fibres, an objective criterion is required to determine the degree of clustering as well as provide insight to the nature of the process. The condition of Complete Spatial Randomness (CSR) was selected as a suitable reference for comparing patterns. In Section 3.9, CSR point patterns were generated assuming that points are distributed according to a random Poisson process. In this section, the results from the CSR point pattern simulations are compared to the actual fibre distributions and the spatial distribution metrics are derived using the Voronoi approach.

5.3.1 Fibre dispersion and variation

While it has been demonstrated that fibres probably do not follow a CSR process, the two processes do behave somewhat similarly, and the same distribution type can be fitted to the results of both processes. The histograms and Nakagami fits of selected fibre dosages are shown in Figure 5-7 and results from the analysis are provided in Table 5-4. The Nakagami fits of each fibre dosage are superimposed in Figure 5-8 to illustrate the change in fibre distribution with fibre count.

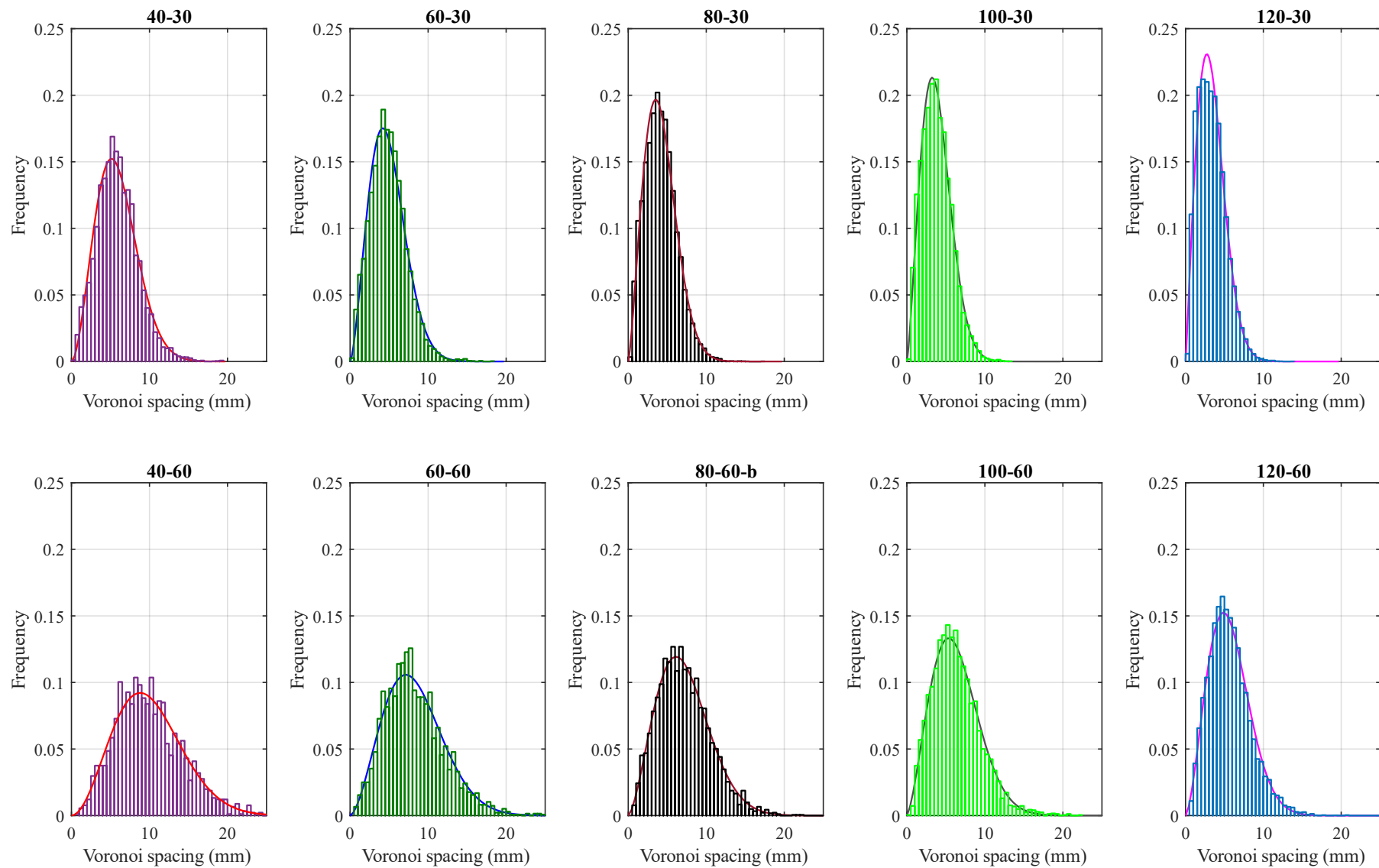


Figure 5-7: Histogram and Nakagami fit of Voronoi spacing for selected batches

Table 5-4: Results of fibre dispersion and Nakagami fit parameters from Voronoi spacing data

Batch	N_f	Shape parameter	Scale parameter	Mean Voronoi spacing (mm)	Dispersion	Variance of dispersion
40-60	119	1.454	118.4	10.15	18.82	28.74
60-60	174	1.313	82.2	8.40	14.12	9.35
80-60-b	225	1.259	62.3	7.32	10.90	3.00
100-60	299	1.219	48.6	6.59	9.12	10.88
120-60-a	371	1.286	39.5	5.74	7.09	1.37
120-60-b	367	1.291	38.3	5.72	6.77	1.50
40-30	347	1.380	41.1	5.89	6.68	0.48
60-30	501	1.258	28.9	4.90	5.07	0.40
80-30-a	716	1.165	21.2	4.17	4.03	0.23
80-30-b	678	1.187	22.2	4.27	4.08	0.04
100-30	829	1.167	18.3	3.86	3.49	0.16
120-30-a	1028	1.073	14.9	3.45	3.10	0.09
120-30-b	1089	1.033	13.8	3.31	3.00	0.07

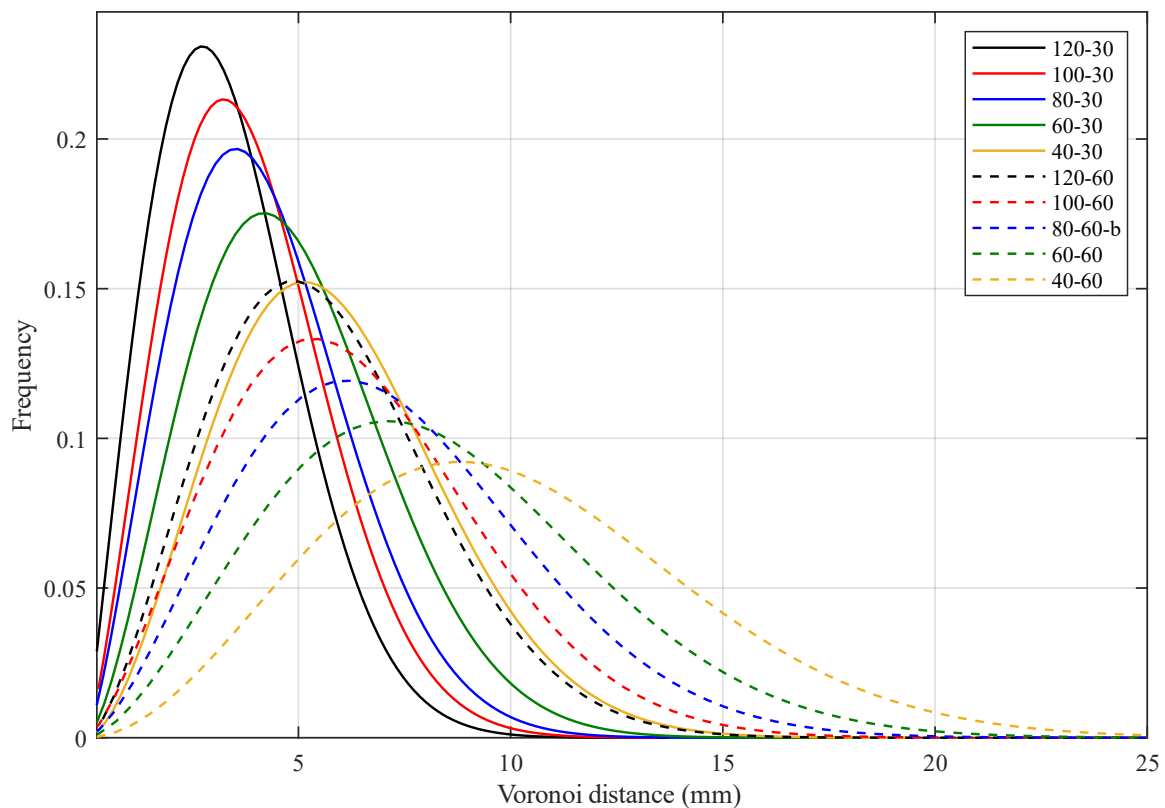


Figure 5-8: Nakagami distribution fits for all fibre dosages

The mean Voronoi spacing as well as dispersion results are compared to the results obtained from random pattern simulations in Figure 5-9 and Figure 5-10. Plotting the Nakagami probability density functions of random and experimental data, as in Figure 5-11, provides insight to the trends observed in the figures.

Figure 5-9 shows the similarity between the mean Voronoi spacing of actual fibres and of the simulated random patterns. The random simulations follow nearly the exact same relationship as the actual fibres. The similarity between the dispersion of the random simulations and of fibre results is shown in Figure 5-10. The figure supports the first sub-hypothesis stating that fibres are more uniformly dispersed over the section for high fibre counts. In addition, the trend in the figure suggests that the dispersion of random points is generally lower than that of the fibres. This implies that the two processes do indeed differ, and the difference is likely brought about by the factors discussed in Section 3.954.

Comparing the Nakagami distribution parameters in Table 3-4 and Table 5-4, the scale factors of the two processes follow a near identical relationship whereas the shape factors of the fibre results tend to decrease as the number of fibres increase. This observation is also illustrated by the probability density functions shown in Figure 5-11. It is therefore possible to apply the shape factor as an indicator to distinguish between a spatially random process and a clustered process.

The standard deviation of dispersion for random point patterns and actual fibres is shown in Figure 5-12. Although no statistically significant conclusions can be made on the difference between the random and actual patterns, a rather clear trend of decreasing variability of dispersion with increasing number of fibres is evident in the figure. This observation is in accordance with the second sub-hypothesis of this work.

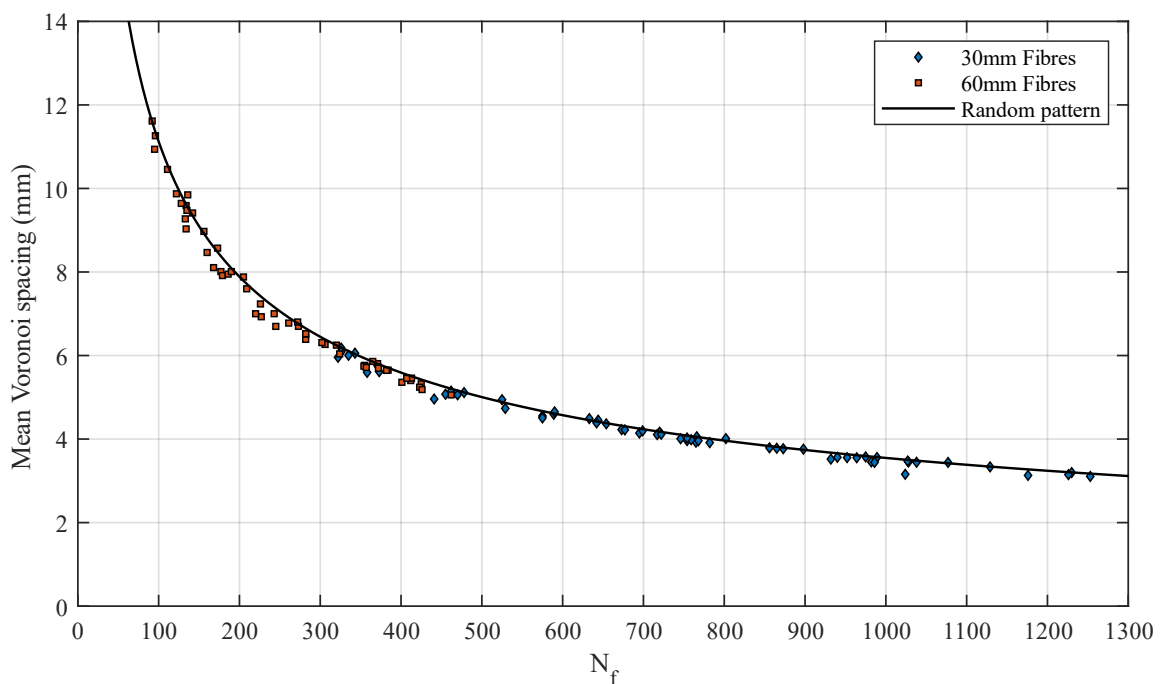


Figure 5-9: Similarity between mean Voronoi spacing of fibre – and random patterns

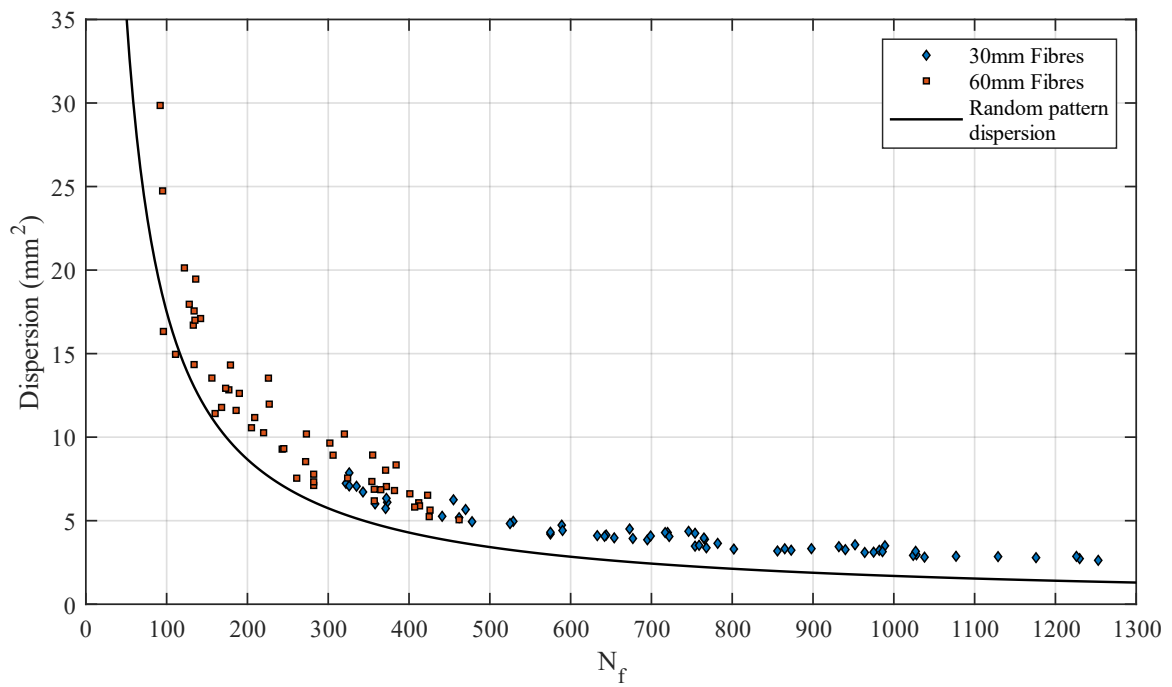


Figure 5-10: Similarity between dispersion of fibre – and random patterns

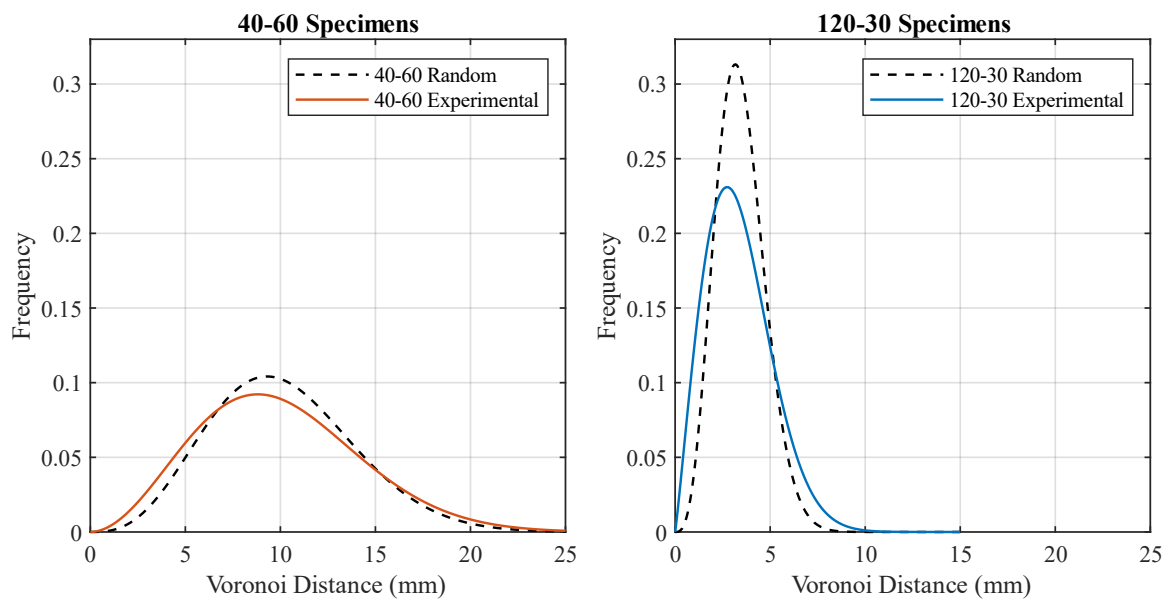


Figure 5-11: Comparison of random and experimental Nakagami fits

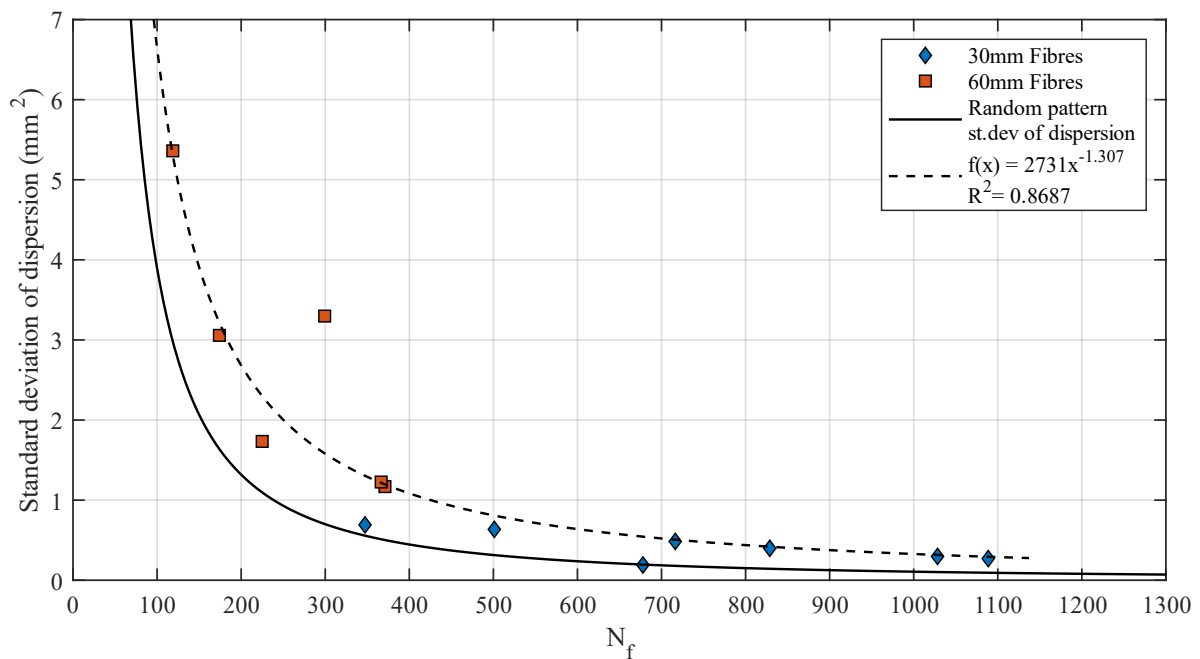


Figure 5-12: Standard deviation of dispersion for fibre – and random patterns

5.3.2 Degree of clustering

In Section 3.9 it was proposed that the clustering in a sample can be evaluated using the shape parameter obtained from fitting a Nakagami distribution to the Voronoi spacing results. A specimen was said to exhibit clustering if the probability of a random process to generate a shape factor lower than the provided shape factor is more than a specified probability, which was selected as 0.005.

The number of clustered samples in a batch can then be plotted against the average number of fibres in the batch as shown in Figure 5-13. The figure substantiates the third sub-hypothesis proposing that clustering is a function of the number of fibres in a section and tends to increase as the fibre count increases.

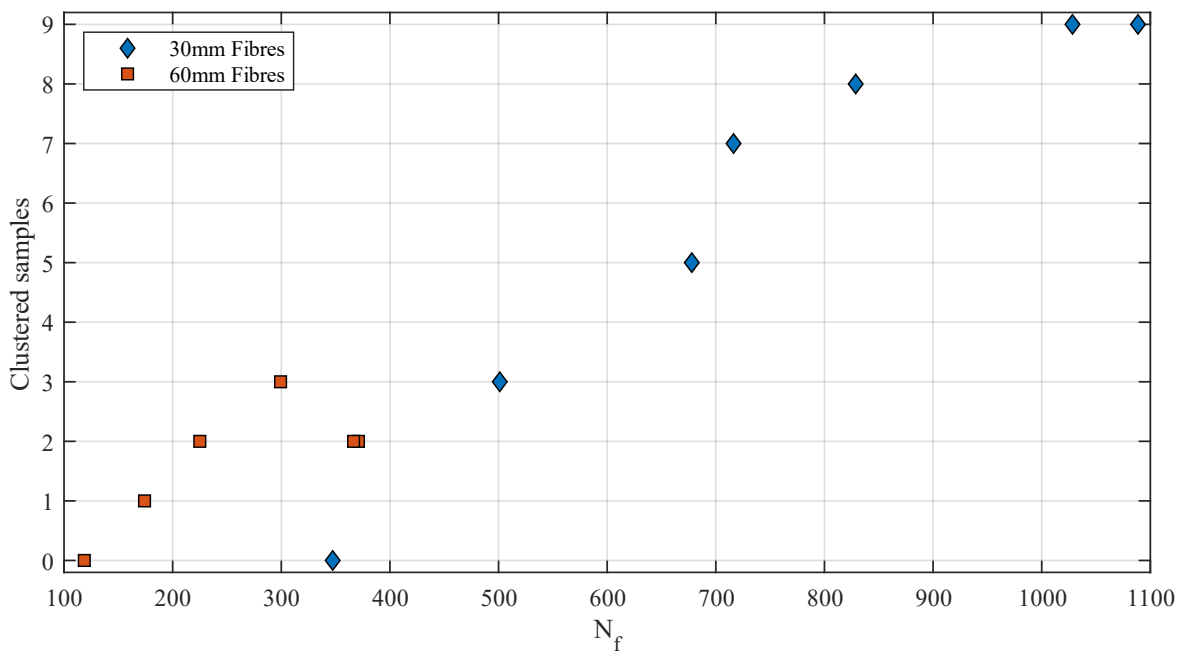


Figure 5-13: Number of clustered samples with the average batch fibre count

All calculated values of z were negative and therefore taking the absolute value of the term, as in Equation 3.7, has no consequence and merely transforms the data to the more familiar domain of natural numbers. The mean batch values for degree of clustering and z are presented in Table 5-5. The degree of clustering is suspected to influence the strength of composite beams by reducing the effective pull-out resistance provided by fibres. This is the third main hypothesis posed in Chapter 1 and is further investigated in the subsequent chapter.

Table 5-5: Mean degree of clustering for each batch

Fibre Type	Dosage (kg/m^3)	Degree of Clustering (CL_{Vor})	z
60	40	169	-1.41
	60	350	-1.95
	80-b	504	-2.18
	100	678	-2.20
	120-a	844	-2.26
	120-b	795	-2.13
30	40	680	-1.96
	60	1232	-2.46
	80-a	2089	-2.92
	80-b	1900	-2.77
	100	2416	-2.91
	120-a	3522	-3.43
	120-b	3926	-3.60

5.4 Comparing the Output Metrics of the Two Approaches

Two approaches for quantifying the characteristics relating to fibre spatial distribution were implemented in this chapter. The first approach, referred to as the *fibre count approach*, involved counting the number of fibres inside a grid square of specified size and analysing the results. The second approach, referred to as the *Voronoi approach*, involved obtaining a geometric descriptor by first delineating the cross section using a Voronoi diagram generated from the fibre coordinates. Fibre spatial arrangement was then evaluated using the geometric descriptor defined as the radius of the largest circle containing no fibres with the radius being equidistant to all fibres intersecting the circle border (see Figure 3-14). Although both approaches are distinctly different, the resulting metrics describe equivalent properties that characterise the spatial distribution of fibres.

Three parameters are obtained from each approach. The first parameter provides a measure that is a function of the number of fibres in the section while accounting for some degree of variation over the cross section. The fibre count approach defines homogeneity as the CoV of the number of fibres counted using a grid size of 10x10. The Voronoi approach defines dispersion as the variance of Voronoi spacing. The correlation between the two metrics is demonstrated in Figure 5-14.

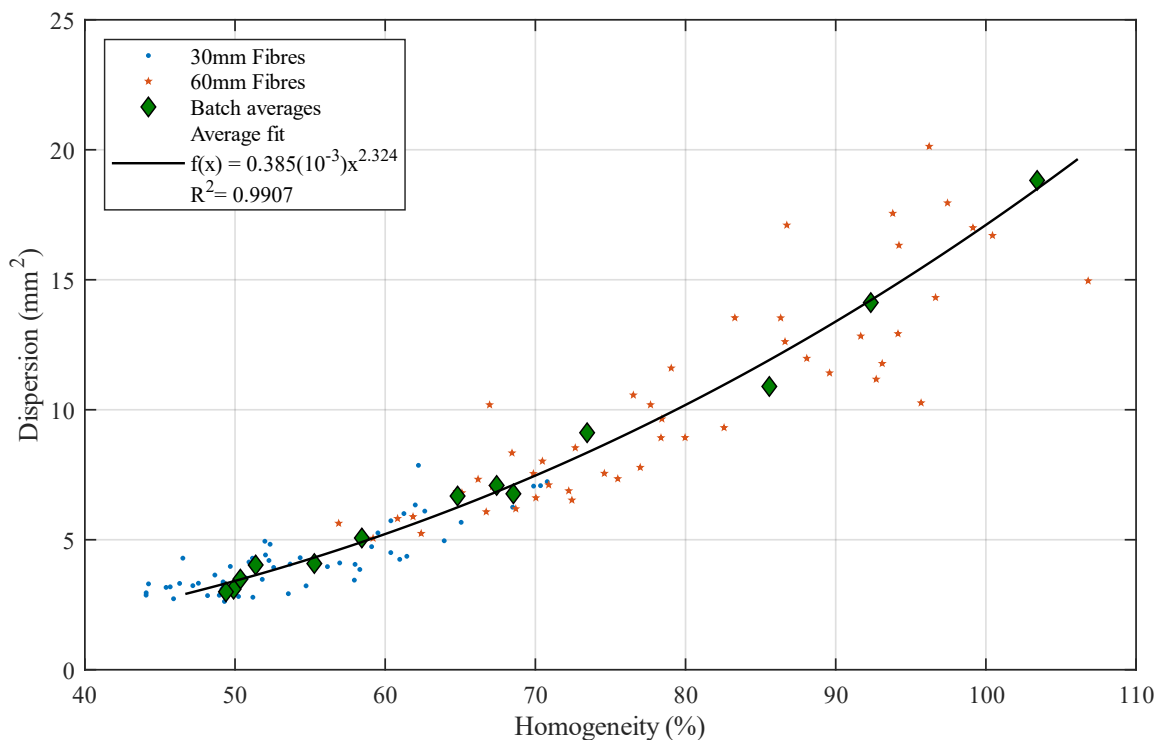


Figure 5-14: Equivalence of dispersion and homogeneity

The second parameter serves to provide a measure of the variability of the first parameter within a batch of samples. In both approaches the second metric is simply the standard deviation of the homogeneity or dispersion values of a batch. The correlation between the second metric provided by the two approaches is depicted in Figure 5-15.

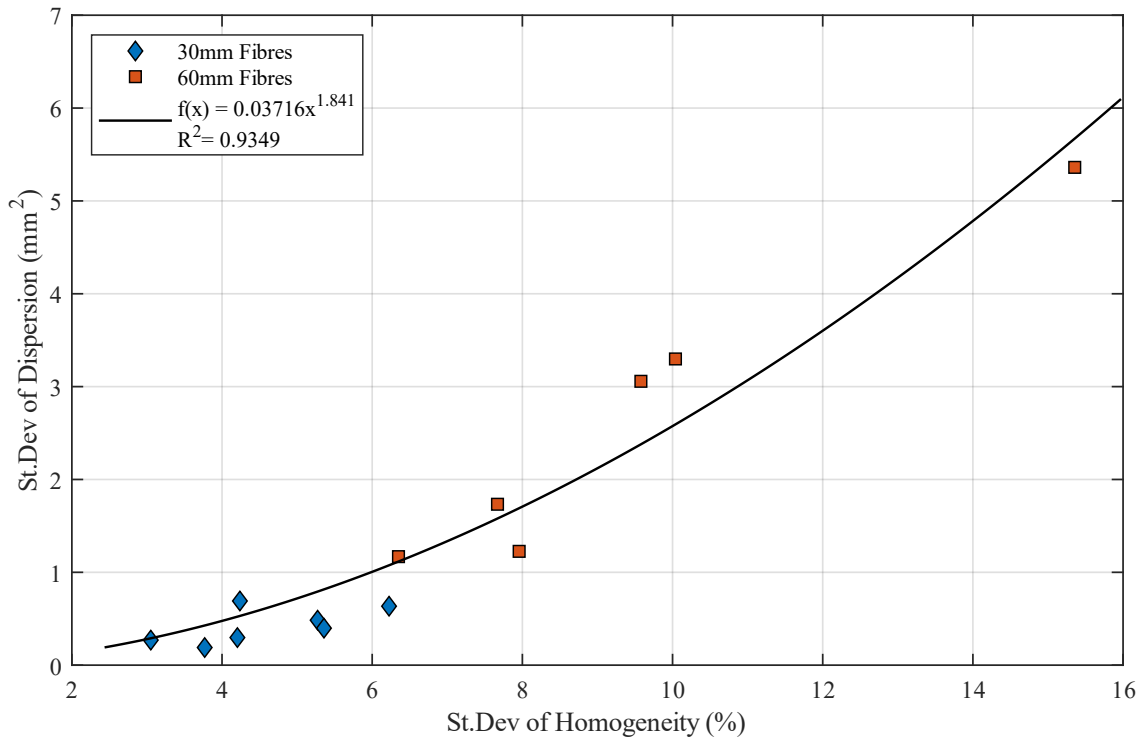


Figure 5-15: Equivalence of variation of dispersion and homogeneity

The third and final metric obtained from the two approaches was used to define the degree of clustering in a specimen. The fibre count approach determined the degree of clustering by first calculating a standardised grid size with respect to the number of fibres, resulting in a grid fibre density that is constant irrespective of the total fibre count. The distribution of fibre grid count then follows a Poisson type distribution if the fibres are randomly distributed over the section. The ratio of standard deviation to the mean number of fibres in a grid is equal to 1 if the fibres are spatially random and greater than 1 if the fibre distribution is clustered. The ratio is multiplied with the total number of fibres intersecting the section to account for the proximity between fibres, presumed to exacerbate the effect of clustering, thus obtaining the degree of clustering, CL_{cnt} .

The Voronoi approach is similar in that a CSR point process is used as a reference condition. In the Voronoi approach, the degree of clustering, CL_{Vor} , was derived using the shape parameter obtained from fitting a Nakagami distribution to the Voronoi spacing results. The standard normal random variable, z , was then calculated from the distribution of shape factors determined from random pattern simulations of the same point density. The standard normal random variable was then also multiplied with the total number of fibres to account for the distance separating fibres. The correlation between the degree of clustering provided by both approaches is illustrated in Figure 5-16.

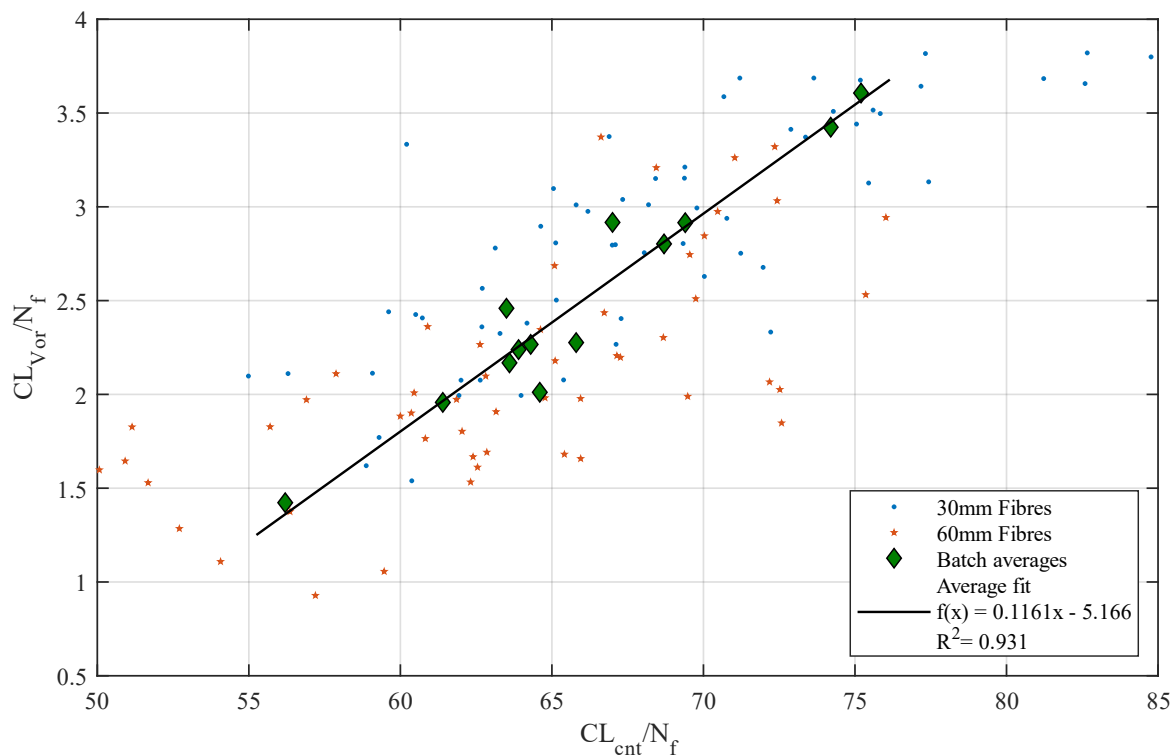


Figure 5-16: Equivalence of the degree of clustering obtained from the two approaches

The strong correlation demonstrated between the parameters derived from the respective approaches implies that using all six metrics to investigate the relation between fibre spatial distribution and flexural response will produce redundant results. Therefore, the fibre spatial distribution metrics of only one approach is implemented in the subsequent chapter: the Voronoi approach. Although the decision was not based on defined criteria, the merits and deficiencies inherent to each approach were evaluated to select the most appropriate method with reasonable objectivity.

The intuitive methodology implicit to the first approach is the essence of method's elegance. The method has the advantage of simplicity in derivation and interpretation of results and the analysis involves techniques that are generally more familiar. In addition, assumptions on the type of probability density function are not required as the degree of clustering is calculated directly from the data. Although the merits of the approach are evident, a significant deficiency is the influence that the selected grid size has on the magnitude of homogeneity and consequently the variation of homogeneity. A grid size of 10x10 was arbitrarily selected in this study without thoroughly investigating whether alternative grid sizes may have been more appropriate. The challenge of selecting the most appropriate grid size lies in the criteria on which the decision is based. The limited analysis that was done on the subject indicated that although the influence of grid size on homogeneity is apparent (as illustrated in Figures 5-4 and 5-5), the relationship is less discernible for variation of homogeneity. Due to the equivalency between homogeneity and dispersion, additional in-depth analysis was deemed superfluous.

The preeminent advantage that the Voronoi approach has over the fibre count approach, is that the method objectively tessellates the cross section without any user input which may induce errors. The method exemplifies the versatility and practicality of Voronoi diagrams which, to the author's opinion, have not been fully exploited in the field of engineering. The relative complexity is likely the primary drawback of the approach. A substantial amount of information can be extracted from a Voronoi diagram generated for given fibre coordinates. The complexity lies in discerning which information can be utilised to provide the most logical characterisation of fibre spatial distribution. The final drawback of the approach is that an assumption on the type of distribution is required to calculate the degree of clustering. Although it is apparent that the selected distribution adequately reflects the spacing of random points, the shape factor may not sufficiently describe the degree of clustering for highly clustered patterns. In such cases, an approach based on conventional spatial statistics, as used by Akkaya et al. (2001), may provide a more effective solution.

5.5 Discussion on Image Analysis Results

In this chapter, statistical analysis was performed to assess the distribution of fibres across a section with the objective of quantifying the distribution of the number of fibres in a section, the variability of this distribution within a batch, and the degree of fibre clustering. The two approaches developed in Chapter 3 for quantifying fibre spatial characteristics were implemented on the image analysis results.

The first approach involved dividing the cross section into a specified grid size and counting the number of fibres inside each square. It was found that the density of fibres over a section approximately followed a Poisson distribution for low fibre counts and tended to deviate from a Poisson distribution as the number of fibres increased due to increasing variance. This behaviour was attributed to clustering of fibres which was shown to increase as the number of fibres increase. The influence of varying grid size on the homogeneity was explored and a grid size of 10x10 was ultimately selected to characterise homogeneity as well as variability in homogeneity. The results demonstrated that variation in homogeneity tended to decrease as the number of fibres in the section increased.

In the second approach a geometric descriptor was obtained from a Voronoi diagram of the fibres which was used to quantify the spatial distribution of fibres. Results from this approach were compared to results obtained from using a Poisson process to simulate spatially random point patterns with various point densities. In Chapter 3 it was found that the probability density function of Voronoi spacing of random point simulations followed a Nakagami type distribution and it was assumed that the same distribution can be fitted to the spatial distribution of fibres. The results indicated that the variance of Voronoi spacing, i.e. fibre dispersion, reduced as the number of fibres increased and that the inter-batch variability of fibre dispersion also reduced as the number of fibres increased. Furthermore, it was demonstrated that the number of samples in a batch exhibiting clustered patterns increased with total fibre count.

Both approaches provided evidence substantiating all three sub-hypotheses formulated as part of the second research objective of this study.

The two approaches were compared in the final section of this chapter and it was shown that although both approaches provide equivalent results, the grid dimensions selected in the first approach introduces uncertainties in the calculated parameters. It was ultimately concluded that the metrics obtained from the Voronoi approach are used in the subsequent chapter to evaluate the influence of fibre spatial characteristics on the flexural performance of the composite beams.

CHAPTER 6. Relating Mechanical Properties and Fibre Distribution Characteristics

6.1 Background

The primary objective of this dissertation is to investigate the influence of fibre distribution on flexural strength by assessing the validity of three main propositions. The first hypothesis states that the flexural response of a composite member is related to a parameter that describes fibre spatial distribution. The second hypothesis is a logical deduction of the first proposition and states that the variability in flexural strength is positively related to the variability of the fibre spatial distribution descriptor. The third and final hypothesis states that fibre clustering reduces the resistance effectively provided by fibres.

The preceding chapter contained the development of a geometric descriptor that quantifies the spatial arrangement of fibres as well as a parameter that provides a measure of clustering. The objective of this chapter is to evaluate the three main hypotheses of this dissertation by investigating the correlation between the proposed parameters and the flexural properties of the composite specimens.

The relationship between selected flexural strength parameters and the number of fibres is investigated in Section 6.2 and the flexural strength of the two fibre types is compared in terms of an equivalent fibre count. The work in Section 6.3 evaluates the relationship between equivalent flexural strength and dispersion as well as the variability of flexural response and standard deviation of dispersion. In Section 6.4, a measure of equivalent fibre resistance is proposed and used to assess the influence of clustering. The chapter is concluded with Section 6.5 containing a discussion summarising the identified relationships and the validity of the formulated hypotheses.

6.2 Evaluating Flexural Strength with Respect to Fibre Count

In Chapter 3, the flexural strength of a composite beam was defined as the residual strength at a specified CMOD or an equivalent strength at a specified vertical deflection. The equivalent flexural strength was selected to evaluate the influence of fibre distribution as it is less susceptible to local irregularities in the load-displacement curve than the residual flexural strength parameters. For the sake of completeness, however, both flexural strength parameters are plotted against the number of 30 mm and 60 mm fibres in Figure 6-1 and Figure 6-2, respectively.

Considering that the image analysis was carried out on a section adjacent to the crack plane, the correlation demonstrated in Figure 6-1 and Figure 6-2 is moderately distinct. This implies that it is reasonable to assume that the fibre distribution in the vicinity of the crack is representative of the actual fibre distribution at the crack plane.

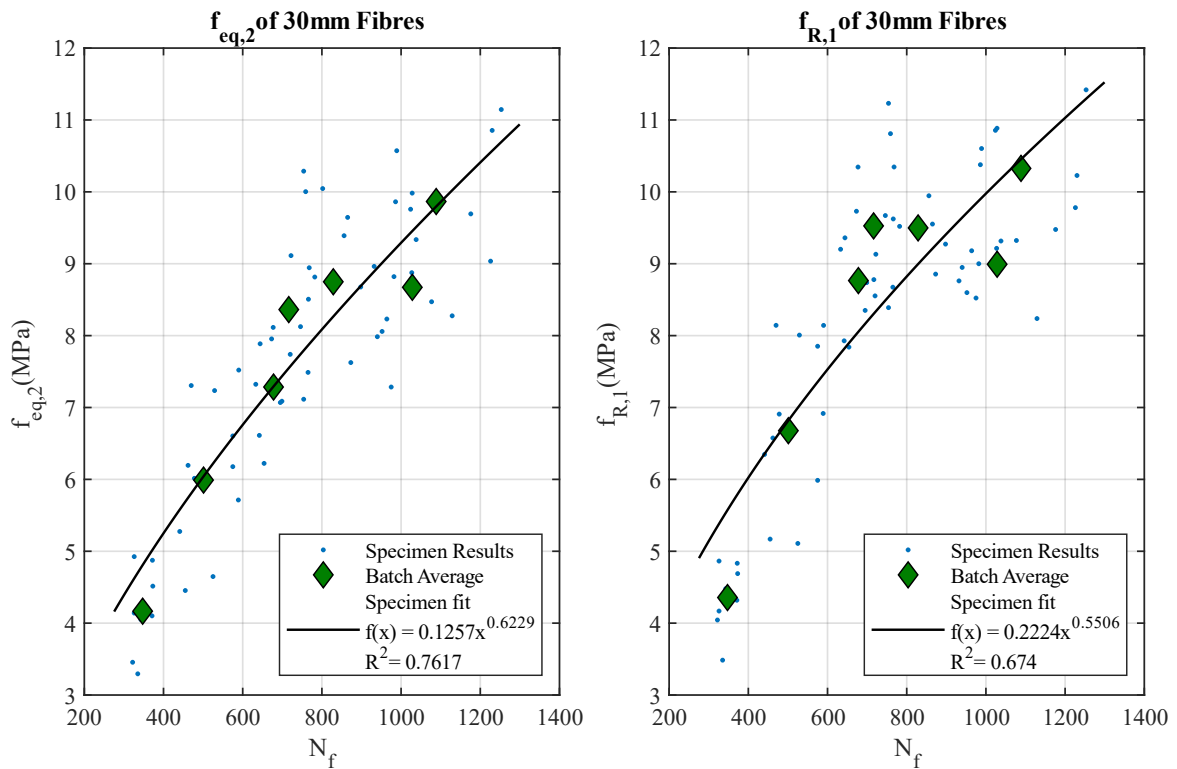


Figure 6-1: Relationship of flexural strength to the number of 30 mm fibres

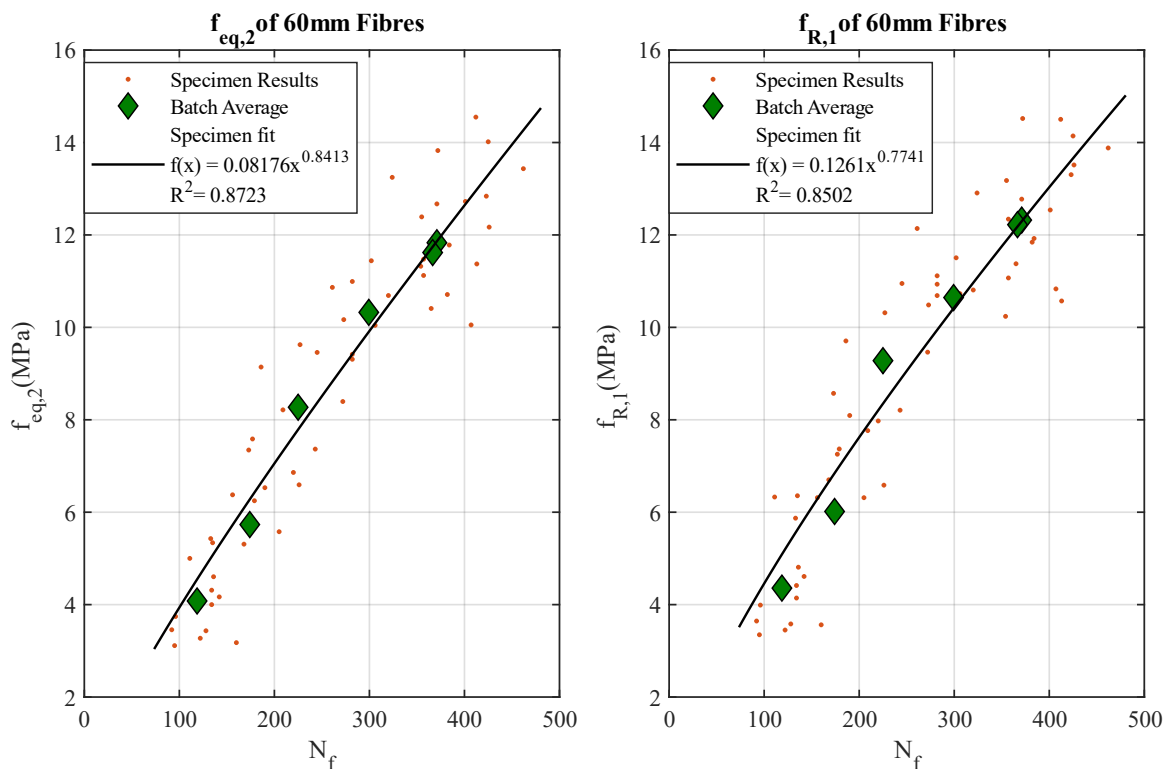


Figure 6-2: Relationship of flexural strength to the number of 60 mm fibres

The average Stress-CMOD curves for the various fibre contents are shown in Figure 6-3 and Figure 6-4 for 30 mm and 60 mm fibres, respectively. A surface has been fitted to the data to provide a more effective visualisation of the results. The figures suggest that a more effective improvement in flexural

strength is achieved by increasing the dosage of 60 mm fibres. The improvement in the average flexural response for increasing 30 mm fibre dosage beyond 80 kg/m^3 is inconsequential compared to the 60 mm mixtures.

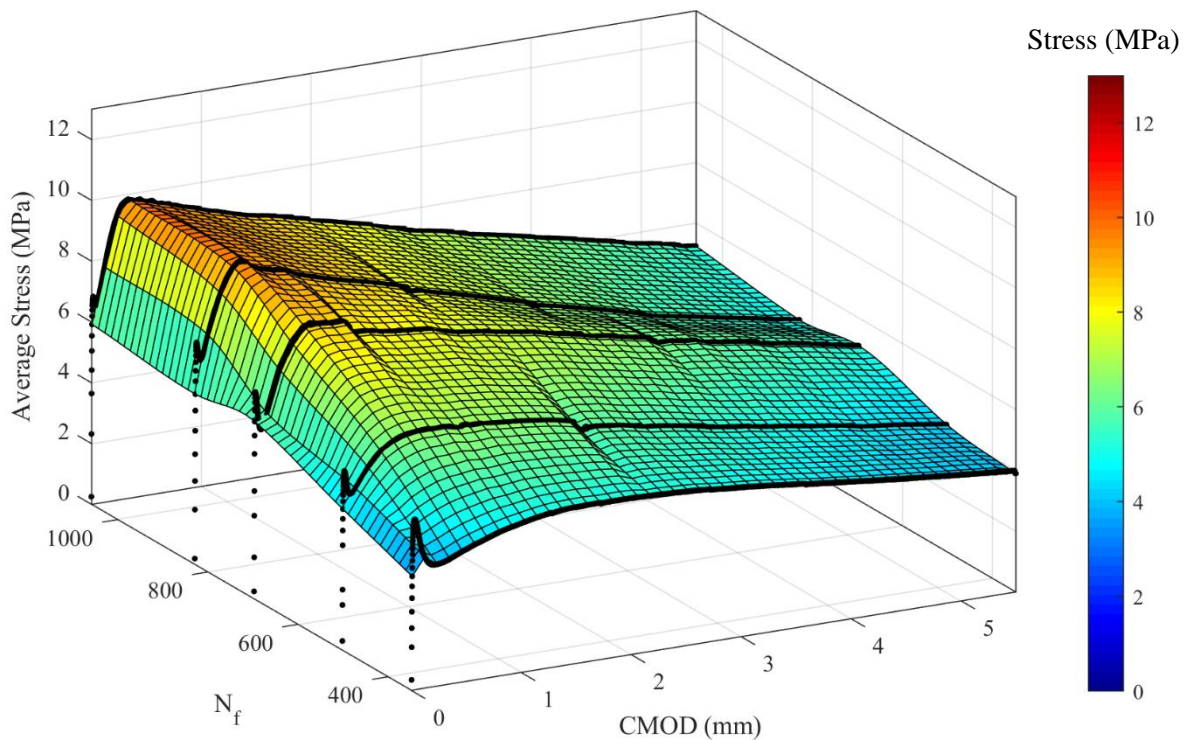


Figure 6-3: Average Stress-CMOD response for varying 30 mm fibre dosages

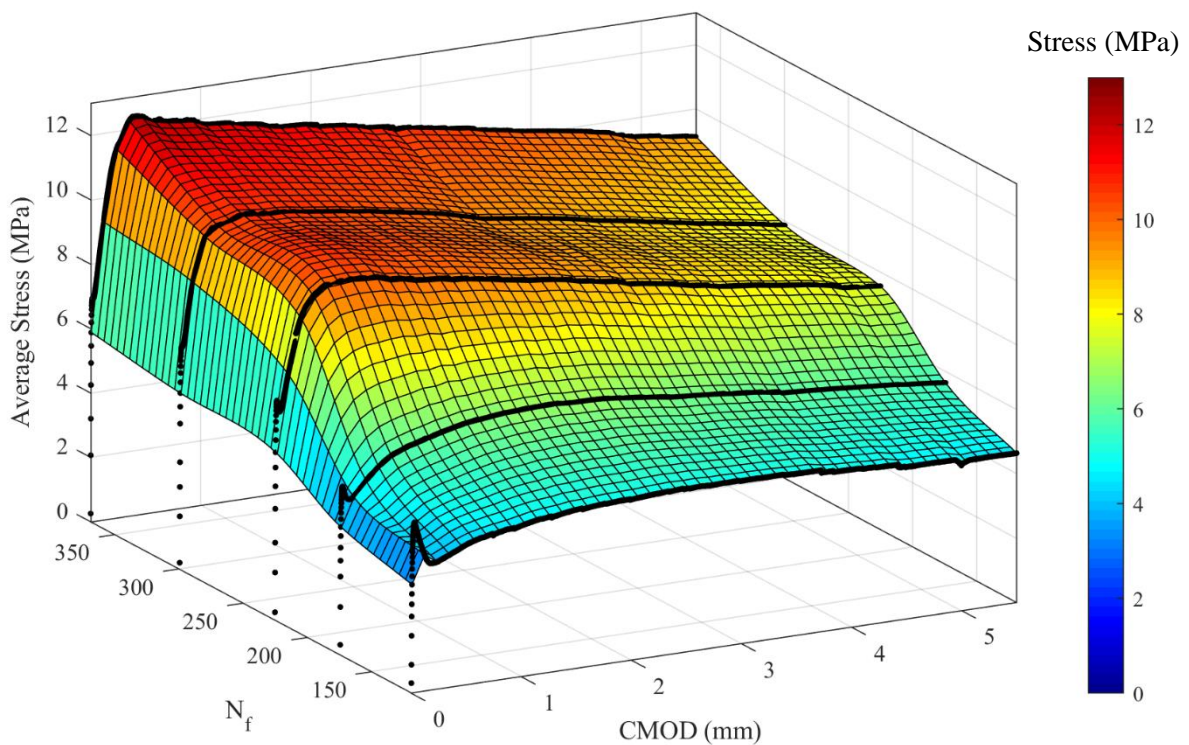


Figure 6-4: Average Stress-CMOD response for varying 60 mm fibre dosages

In Section 4.5, it was shown with Equation 4.1 that the number of 60 mm fibres is related to the number of 30 mm fibres through a factor of 2.882. Applying this factor to the average number of 60 mm fibres in a batch and plotting the result as a function of the average $f_{eq,2}$ for both fibre types produces the plots in Figure 6-5. The trends in the figure suggest that flexural strengths associated with both fibres are approximately equal for dosages up to 80 kg/m^3 ($N_{f,30} \approx 690$), after which the specimens containing 60 mm fibres achieve greater flexural strengths. The reason for such behaviour cannot be conclusively established and is likely a function of several interrelated variables. However, clustering is suspected to reduce the pull-out effectiveness of fibres and possibly negating the improvement in strength by increasing the dosage of 30 mm fibres beyond 80 kg/m^3 .

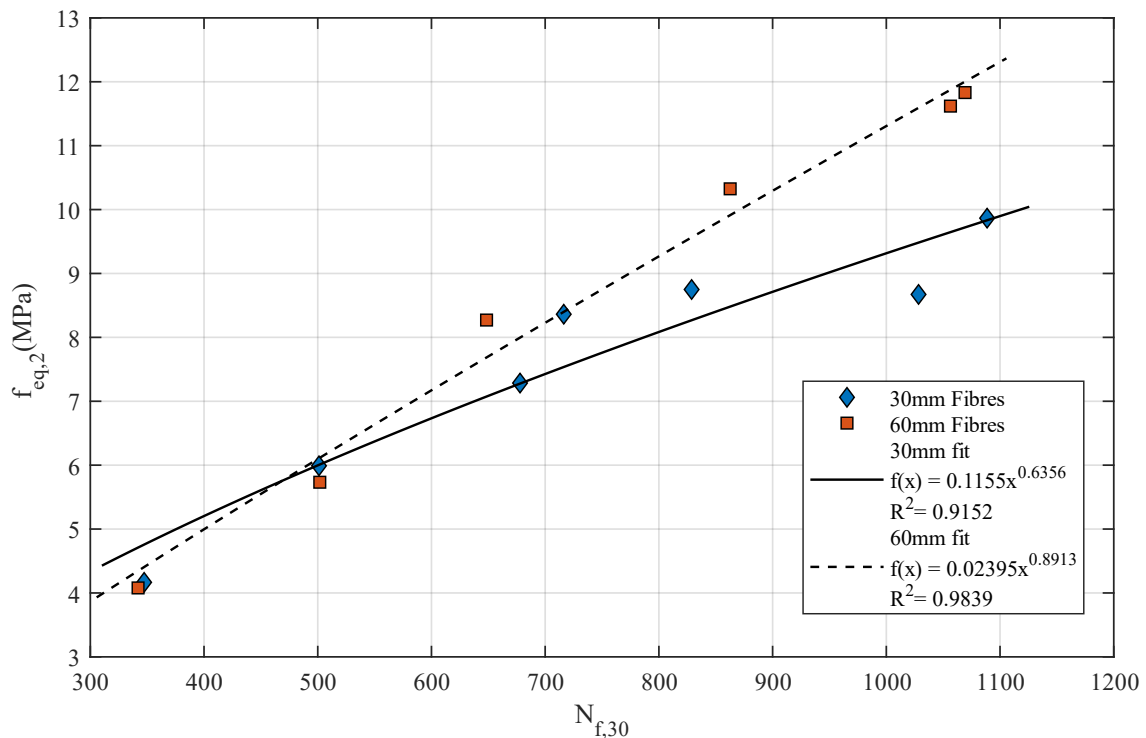


Figure 6-5: Comparing the flexural strength with respect to $N_{f,30}$

6.3 Influence of Fibre Dispersion on Strength and Variability

The results from the previous section indicate that flexural strength is undoubtedly influenced by the number of fibres. The fibre count does not, however, account for the influence of the spatial arrangement of fibres and is therefore not considered to be the most robust descriptor of fibre distribution. Consequently, a more suitable descriptor, termed fibre dispersion, was developed in the preceding chapter and was defined as the variance of Voronoi spacing of a given specimen.

The second proposition of this dissertation states that the variability in flexural response is related to the variability of a parameter that quantifies fibre spatial distribution. The second proposition is a logical deduction of the first proposition stating that a relationship exists between flexural strength and fibre distribution. This relationship is demonstrated in Figure 6-6 and Figure 6-7 showing results of equivalent

flexural strength and fibre dispersion for 30 mm and 60 mm fibres, respectively. The figures provide evidence in support of the first main hypothesis of this work.

Although the exponential fits applied to the data in Figure 6-6 and Figure 6-7 do not reflect the true nature of the relationship, the fits provide a qualitative indication of the strong correlation between flexural strength and fibre dispersion.

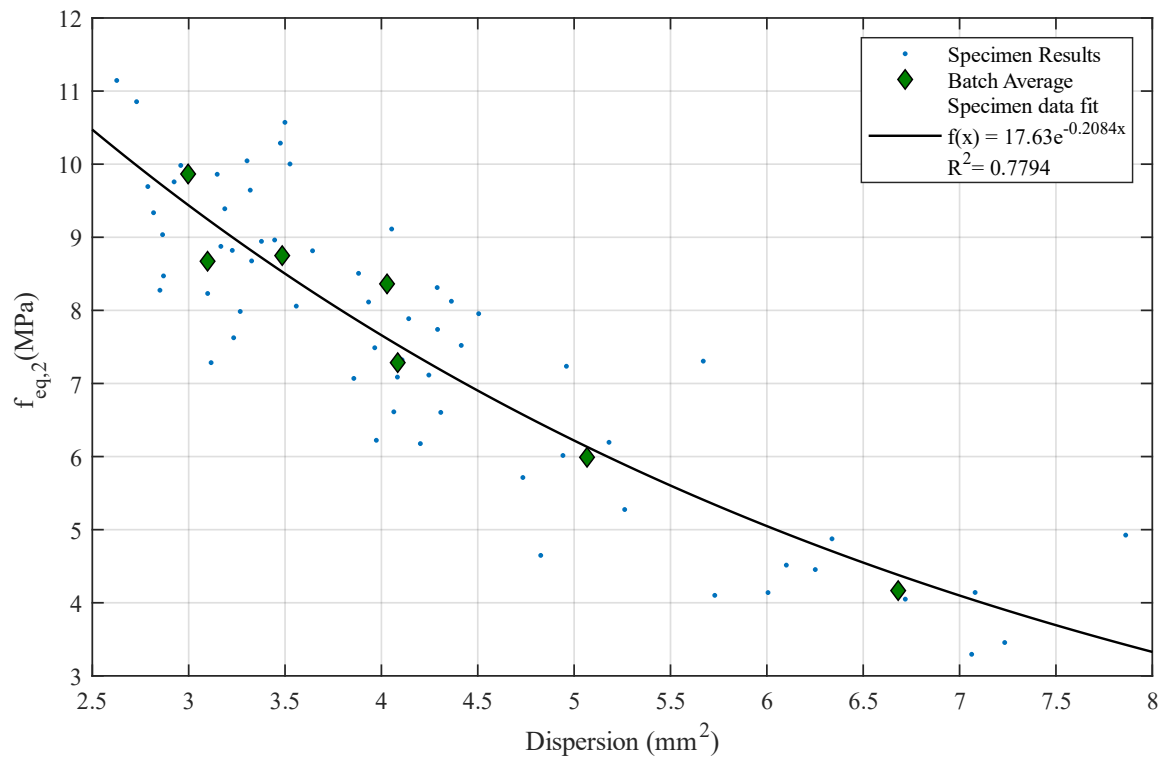


Figure 6-6: Relating equivalent flexural strength to dispersion of 30 mm fibres

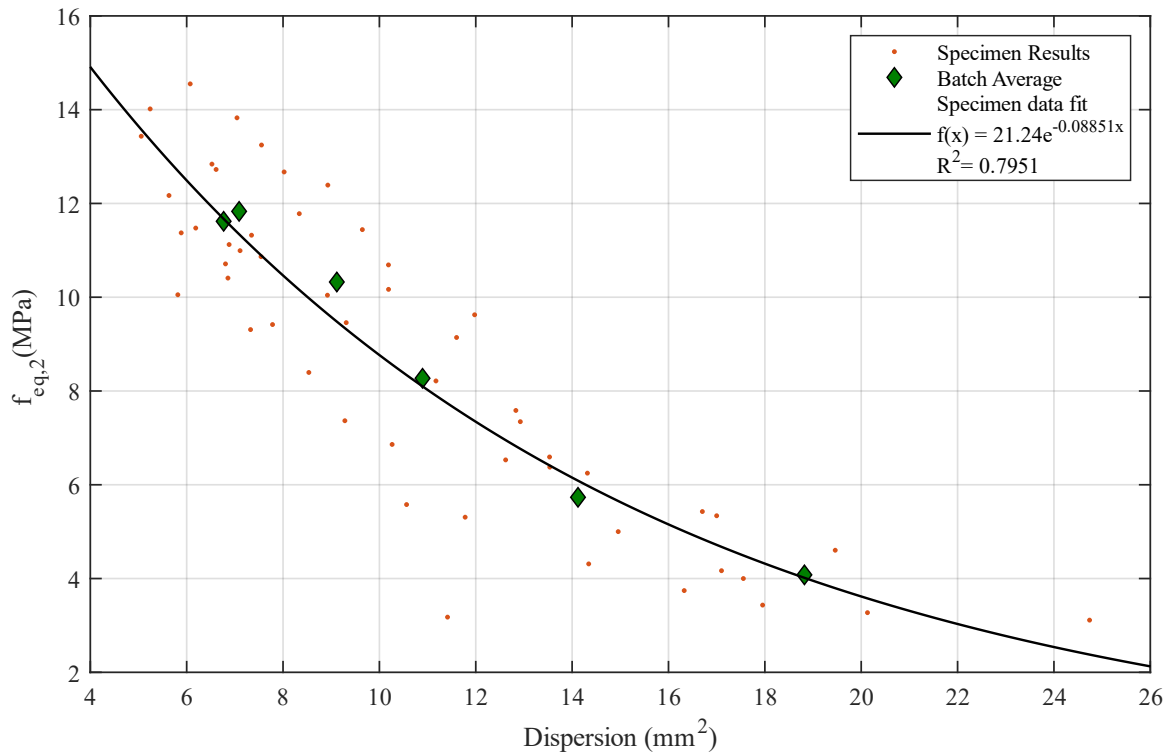


Figure 6-7: Relating equivalent flexural strength to dispersion of 60 mm fibres

The Coefficient of Variation was used in Section 3.5 as a measure to quantify the variability in flexural strength. If the variability in flexural strength can be considered to be additive, then according to the second proposition a relationship exists between the CoV of flexural strength and the variability associated with fibre dispersion. The CoV of equivalent flexural strength is plotted against the standard deviation of dispersion in Figure 6-8.

The figure supports the second main hypothesis stating that a positive correlation exists between the variability in flexural response and the variability of fibre spatial distribution. However, no definitive conclusions regarding the nature of the relationship can be made based on the available data. The result from batch 40-60 was assumed to be an outlier due to the relatively large deviation from the observed trend. The provided linear trend then implies that the variability of the composite is a purely additive function of the variability attributed by the constituent materials. Such a relation is questionable considering the complexity of the various interrelated variables affecting flexural strength. An alternative trend based on a power function can be fitted to the data to include the outlier as shown in Figure 6-9. Both trends are, however, only for demonstrating the correlation between the variability in flexural strength – and fibre dispersion and defining an accurate relationship is beyond the scope of this study.

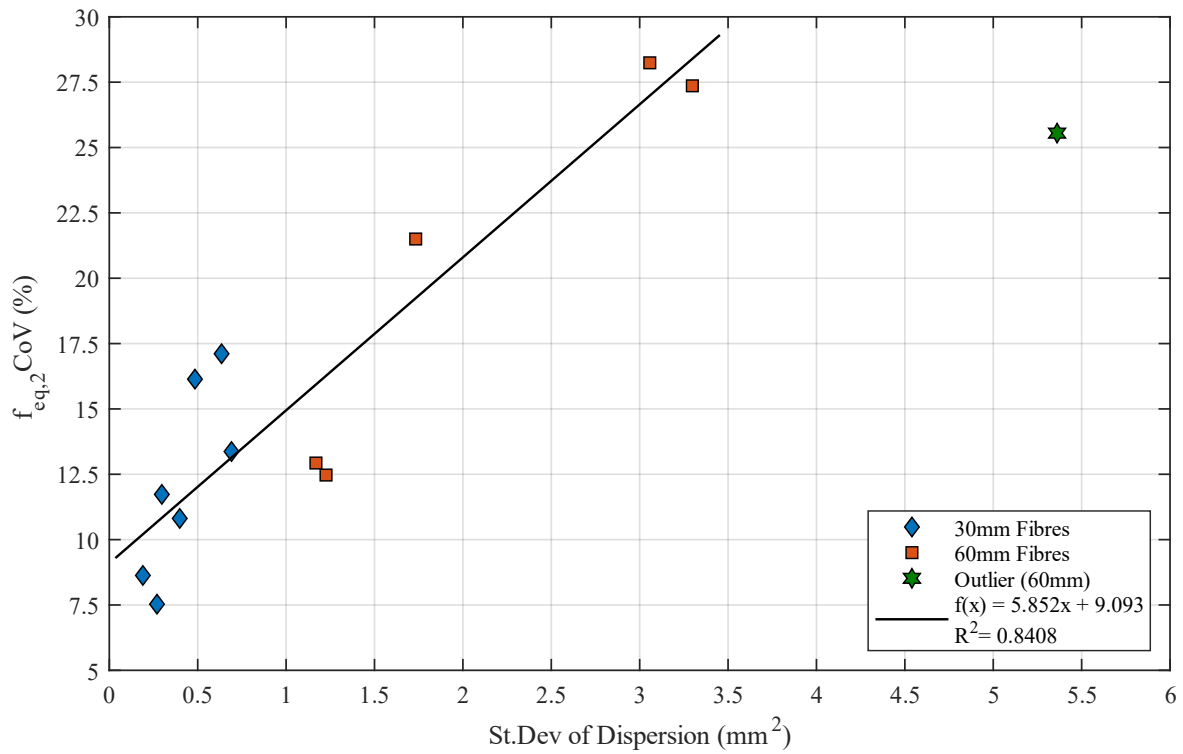


Figure 6-8: Linear relationship between the variability of flexural strength and – fibre dispersion

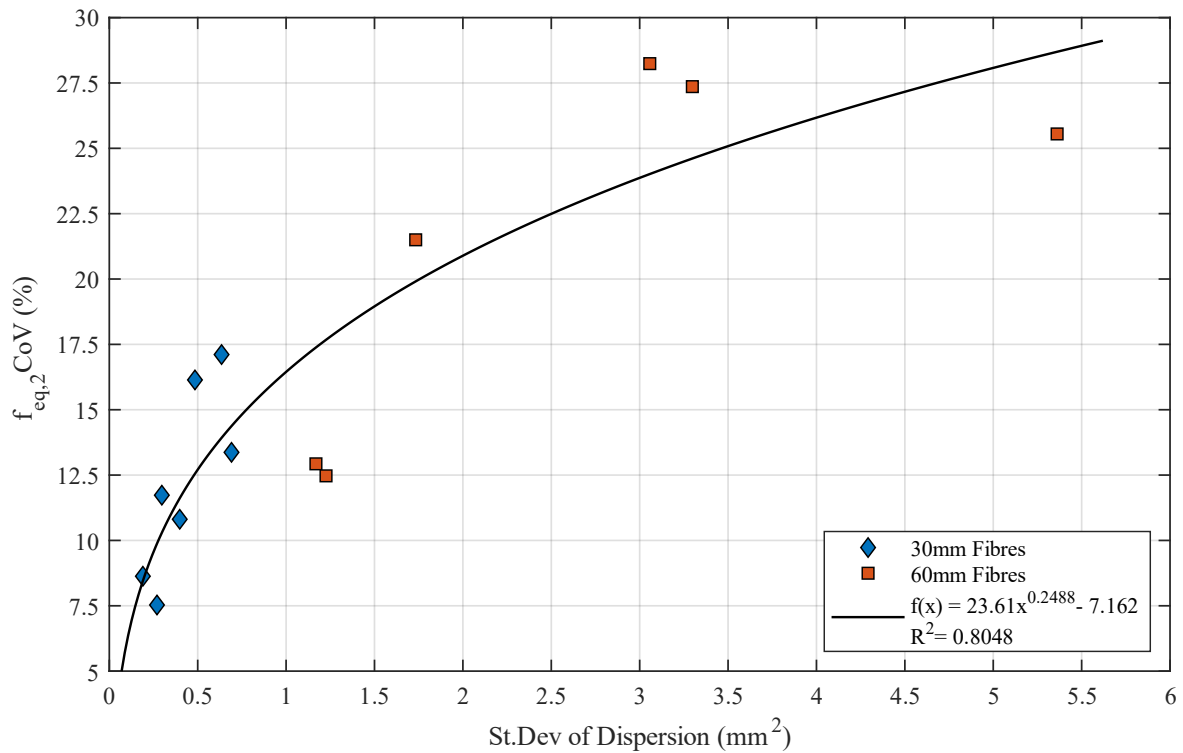


Figure 6-9: Power relationship between the variability of flexural strength and – fibre dispersion

The results presented in this section substantiate the intuitive hypothesis posed by several researchers stating that the variability in flexural response increases as the variability in the spatial distribution of fibres increases. Such a finding aids the thorough understanding of the factors influencing the variability

and performance of a composite member and adds scope for research into possible measures for mitigating the increased variability due to the addition of fibres.

6.4 Influence of Clustering on Equivalent Fibre Resistance

The degree of clustering, CL_{Vor} , was defined in Section 5.3 according to Equation 3.7 and represents the deviation from a random process of the same point density. In order to evaluate whether strength is influenced by fibre clustering, a normalised measure of equivalent flexural strength is required. This is achieved by dividing flexural strength by the number of equivalent 30 mm fibres to provide a value of fibre resistance. It was shown in Section 4.5 that the number of 60 mm fibres is related to the number of 30 mm fibres by a factor of 2.882. This factor is implemented to convert the number of 60 mm fibres to an equivalent number of 30 mm fibres which is then used to calculate the equivalent fibre resistance using Equation 6.1 as follows:

$$\tau_{eq} = \frac{f_{eq,2}}{N_{f,30}} \cdot 1000 \quad (6.1)$$

Where:

τ_{eq} = The equivalent fibre resistance (kPa/fibre)

$f_{eq,2}$ = The equivalent flexural strength (MPa)

$N_{f,30}$ = The equivalent number of 30 mm fibres

The mean equivalent fibre resistance for each batch is presented in Table 6-1 along with the mean degree of clustering and equivalent number of 30 mm fibres.

Table 6-1: Mean equivalent fibre resistance for each batch

Fibre Type	Dosage (kg/m ³)	N _f	N _{f,30}	τ_{eq} (kPa/fibre)	Degree of Clustering (CL_{Vor})
60	40	119	342	11.99	169
	60	174	502	11.46	350
	80-b	225	648	12.90	504
	100	299	863	12.05	678
	120-a	371	1069	11.17	844
	120-b	367	1056	11.25	795
30	40	347	347	12.00	680
	60	501	501	11.95	1232
	80-a	716	716	11.67	2089
	80-b	678	678	10.75	1900
	100	829	829	10.56	2416
	120-a	1028	1028	8.43	3522
	120-b	1089	1089	9.06	3926

The relationship between equivalent fibre resistance and the degree of clustering is demonstrated in Figure 6-10. The trend shown by the data suggests that equivalent fibre resistance decreases as the degree of clustering increases. Research by Naaman and Shah (1976) showed a decline in pull-out resistance with an increase in fibre density which is in agreement with the trend illustrated by the data in Figure 6-10. It is considered that high fibre counts cause microstructural inhomogeneity which deteriorates the mechanical properties of the composite and the increased fibre interactions lead to a less effective stress transferring mechanism. This finding supports the third main proposition of this research.

As expected, the 60 mm fibre results exhibit limited dependency to the degree of clustering and the negative effects of fibre clustering only become evident for the 30 mm fibre mixtures at dosages of 80 kg/m^3 and higher. This behaviour can be explained by the mechanisms presumed to contribute to the degree of clustering. An increase in the degree of clustering corresponds to an increase in the number of fibres in a cluster as well as the spacing of fibres in a cluster. This is an unlikely combination for low fibre counts and a more likely combination for high fibre counts as demonstrated by the results.

A large degree of scatter is displayed by the specimen results with the trend of variation suggesting that the scatter of 60 mm fibre results is more pronounced than the 30 mm fibre results. This observation also supports the findings presented in the preceding section.

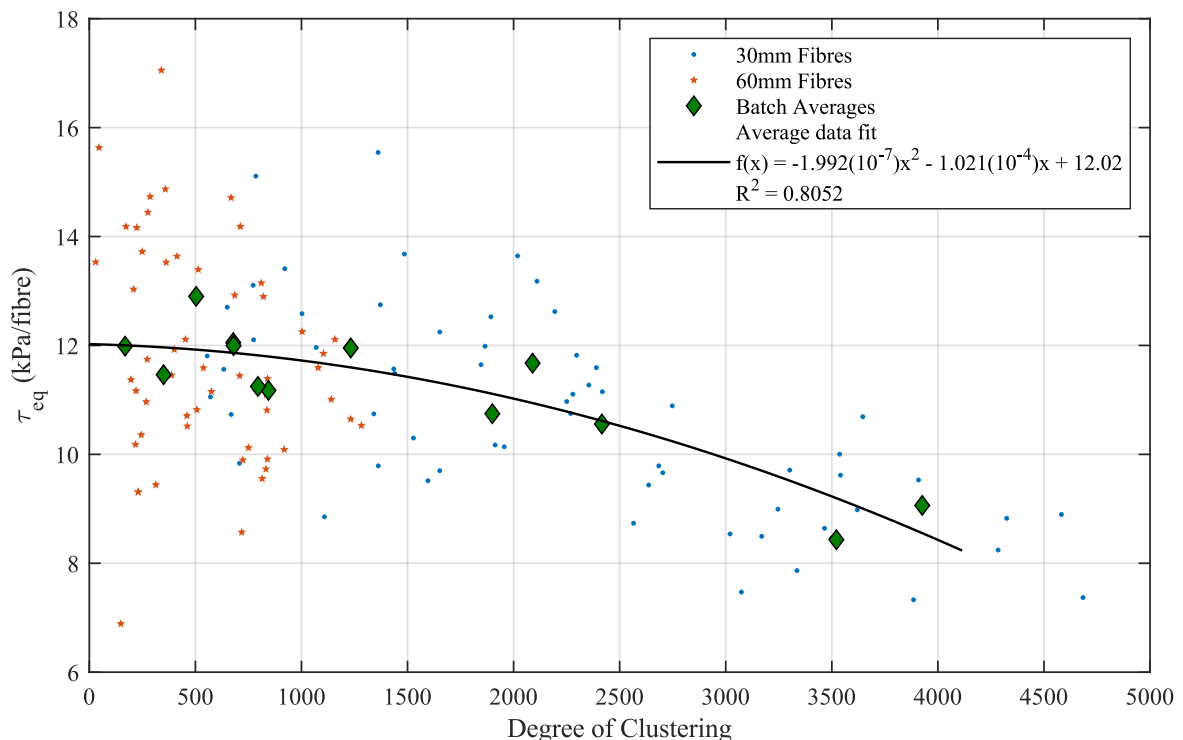


Figure 6-10: Relationship between equivalent fibre resistance and clustering

6.5 Discussion on the Identified Relationships

In this chapter, the descriptors of fibre spatial distribution, calculated in the previous chapter, were related to flexural properties with the objective of evaluating the three main hypotheses of this research.

The number of fibres were related to the equivalent flexural strength and residual flexural strength and produced a trend that indicated a reasonable correlation between fibre count and flexural strength. The equivalent flexural strength was ultimately selected for further analyses involving fibre characteristics as the parameter was less sensitive to local irregularities in the load-displacement curve. The flexural response was plotted as a function of the number of equivalent 30 mm fibres with the aim of comparing the strength provided by the two fibre lengths. The results indicated that the two fibre lengths provided similar flexural strengths for equivalent fibre counts below approximately 650 fibres, after which the flexural strength of the 60 mm fibre specimens exceeded that of the specimens containing 30 mm fibres. A conclusive explanation for the phenomenon could not be established, although it was suggested that the influence of clustering becomes more pronounced at high fibre counts causing a reduction in the pull-out effectiveness of the fibres.

A distinct correlation was found to exist between dispersion and equivalent flexural strength with an increase in equivalent flexural strength corresponding to a decrease in fibre dispersion. This finding is in support of the first main hypothesis of this research. The CoV was used as a measure of variability of the equivalent flexural strength of a batch and compared to the standard deviation of fibre dispersion for each batch. A positive correlation was demonstrated by the trend in the results which substantiates the second main proposition that an increase in the variability of flexural response relates to an increase in the variability of fibre dispersion. This finding also implies that the variability of a composite material is a function of the variability related to the constituent materials; however, the nature of the relation is highly complex and not necessarily purely additive.

To evaluate the effect of clustering on the performance of the composite, equivalent fibre resistance, τ_{eq} , was defined as the flexural strength, $f_{eq,2}$, divided by the equivalent number of 30 mm fibres, $N_{f,30}$, and used as a normalised measure of strength. Although the individual specimen results demonstrated a large degree of variation, the mean batch results produced a definitive trend indicating that fibre resistance decreased as the degree of clustering increased. The reduction of fibre resistance was shown to become apparent at CL_{Vor} values above approximately 1250, suggesting that the performance of the 60 mm fibre specimens was not substantially affected by clustering at the fibre dosages considered. These results are in agreement with the third main proposition stating that fibre resistance decreases as the degree of fibre clustering increases.

This chapter presented evidence in support of all three main hypotheses posed in Chapter 1. The findings demonstrated the relevance of considering the characteristics related to fibre spatial distribution and their implications on the mechanical properties of the composite material. The relationships may ultimately be implemented in composite design to select the fibre length and volume content that provides the optimum effectiveness in terms of fibre resistance or contributes the least to material variability. These findings are an integral component necessary for the thorough understanding of the performance of fibre reinforced composite materials.

CHAPTER 7. Conclusions and Recommendations

7.1 Conclusions

The study set out to investigate *the influence of fibre spatial distribution on the flexural performance of steel fibre-reinforced concrete*. A stepwise approach to the issue was adopted and a set of three main hypotheses were constructed to explore the problem statement. The three main hypotheses are as follows:

1. *The flexural response of a steel fibre-reinforced concrete specimen is related to a descriptor quantifying the spatial distribution of fibres.*
2. *The variability in flexural response is positively related to the variability of the parameter describing fibre spatial distribution.*
3. *The effective resistance provided by fibres reduces as the extent of fibre clustering increases.*

The experimental results presented in Chapter 6 substantiated all three of the main hypotheses.

Three sub-hypotheses were formulated as part of the secondary research statement for *investigating the influence of fibre length and fibre volume content on the spatial distribution of fibres*. These were stated as follows:

1. *The spatial distribution of fibres is strongly related to the number of fibres intersecting a plane and the relative fibre dispersion uniformity increases as the number of intersecting fibres increases.*
2. *The variability of fibre spatial distribution within a batch reduces as the number of fibres increases.*
3. *The presence of fibre clustering becomes more prevalent as the number of fibres increases.*

Experimental evidence in support of all three sub-hypotheses was presented in Chapter 5.

The findings supporting the sub-hypotheses are discussed in detail in Section 7.2. This is followed by a discussion on the findings in support of the three main hypotheses in Section 7.3. In the final section of this document, recommendations are provided with regard to future research on the subject matter presented in this dissertation.

7.2 Influence of Fibre Length and Content on Spatial Distribution

The sub-hypotheses serve to provide an understanding of the factors that influence fibre spatial characteristics and offer a logical foundation which can be used to evaluate the three main hypotheses of this study.

The first sub-hypothesis consists of two statements considering the relation between fibre spatial distribution and the number of fibres, and the number of fibres and the fibre dispersion or homogeneity over a cross section. Parameters relating to the spatial distribution were derived in Section 4.4 using

Voronoi diagrams generated from the centroidal locations of fibres. These parameters demonstrated a strong correlation with the total number of fibres intersecting a plane which validates the first part of this hypothesis. The second part of the proposition involves the uniformity of fibre distribution and was evaluated using the results of fibre dispersion and fibre homogeneity in Chapter 5. The experimental results of both parameters supported the second part of the first sub-hypothesis.

The second sub-hypothesis relates to the degree of variation of the spatial descriptor within a batch of samples. This was assessed using fibre dispersion and fibre homogeneity as spatial descriptors and calculating the sample standard deviation to obtain an indication of the spatial variation within a batch. The results showed an evident decrease in the inter-batch variation of fibre spatial distribution with increasing fibre count. Lower inter-batch variation was observed for the 30 mm fibres compared to the 60 mm fibres due to the larger number of 30 mm fibres intersecting a section at the same volume content.

The third sub-hypothesis concerns the pervasiveness of fibre clustering with regard to the number of fibres intersecting a cross section. The degree of clustering was defined using two approaches: the first was based on a standardised grid size dependent on the fibre count, and the second on the fitted Nakagami shape parameter. The two spatial metrics demonstrated a distinct increase in the degree of fibre clustering with increasing fibre count, adding support to the third sub-hypothesis. Due to the greater number of 30 mm fibres intersecting a given plane, the degree of clustering was greater for the specimens containing 30 mm fibres than for the 60 mm fibre specimens.

7.3 Effect of Fibre Spatial Distribution on Mechanical Performance

The first main hypothesis of this research has been indirectly validated by several other researchers whom have shown that flexural strength strongly correlates with fibre content, which in turn relates to the number of fibres and thereby the spatial distribution of fibres. Evidence in support of the first main hypothesis was presented, although it was observed that each fibre length provided a unique flexural relationship. However, this was not an issue as the purpose of this hypothesis was to demonstrate that flexural strength is influenced by the spatial distribution of fibres and acted as a logical segue to the second main hypothesis. Therefore, if the first main hypothesis was shown to be false, it would be unlikely that the second main hypothesis would be validated.

The second main hypothesis has long been intuitively speculated to be true, however, limited experimental evidence was found on the subject in literature. The proposition was investigated by relating the CoV of equivalent flexural strength to the standard deviation of fibre dispersion. The results indicated a positive correlation between the variables and thereby substantiating the second main hypothesis. The variation in flexural response and fibre dispersion was lower for the 30 mm fibres than the 60 mm fibres and the trend also suggested that variation reduces as the fibre dosage increases.

The third and final main hypothesis tested in this study stated that the effective resistance provided by fibres reduced as the degree of clustering increased. The reasoning underlying the third main hypothesis

was that the effective pull-out resistance of fibres in dense clusters was lower than that of regularly spaced fibres. The degree of clustering was determined using the Nakagami shape parameter fitted to the Voronoi spacing distribution of fibres and adjusted to account for the influence of fibre proximity by considering the number of fibres intersecting the cross section. Fibre resistance was calculated by dividing the equivalent flexural strength by the equivalent number of 30 mm fibres. The results supported the third main hypothesis and demonstrated a decrease in effective fibre resistance as the degree of clustering increased. A notable amount of scatter was observed at low degrees of fibre clustering, which was attributed to the high variation in flexural strength also observed at low fibre counts. The 60 mm fibres showed limited decrease in fibre resistance and the effects of fibre clustering only become evident at 30 mm fibre dosages of 80 kg/m^3 and greater.

7.4 Recommendations for Future Research

In this study, evidence was presented that demonstrate the considerable influence of fibre spatial characteristics on the flexural performance of steel fibre-reinforced concrete beams. Although expressions for estimating the fibre spatial distribution and influence on flexural response were not formulated, the work acts as a preliminary investigation whereupon future research can be built. A thorough understanding of the influence of fibre spatial distribution on composite performance is the first step in incorporating fibre distribution into material and structural design procedures and aids the pursuit towards effective, optimal, and efficient implementation of FRC in practice.

Developing a model that estimates the spatial characteristics of steel fibres is recommended for future research. Although fibre length and diameter may provide a fair estimate, such a model would also have to account for the influence of several other variables, such as the fresh-state mixture properties, wall-effects, and constituent materials, which have all been shown to have a significant effect on the spatial distribution of fibres. The influence of these individual factors can serve as the focus of future research projects on the subject.

The following points are recommended for future work on the matter:

- Investigating the tendency of flexible fibres to form clusters and comparing the results to rigid fibres.
- The spatial behaviour of hybrid fibre combinations and the influence on composite performance with respect to strength and variability.
- The influence of bond strength and fibre-matrix interface properties on the adverse effects of clustering on fibre resistance.
- The influence of fibre length and dosage on the degree of fibre spatial variation throughout an FRC element.

The outcomes of such studies will aid in developing a model which can estimate the influence of fibre distribution on composite performance as well as contribute to the greater body of knowledge and understanding of fibre-reinforced composite material behaviour.

CHAPTER 8. References

- Abbas, Y. M. & Iqbal Khan, M. (2016) Fiber–Matrix Interactions in Fiber-Reinforced Concrete: A Review. *Arabian Journal for Science and Engineering*, Vol 41, No 4, pp 1183-1198.
- Abrishambaf, A., Barros, J. A. & Cunha, V. M. (2013) Relation between fibre distribution and post-cracking behaviour in steel fibre reinforced self-compacting concrete panels. *Cement and Concrete Research*, Vol 51, pp 57-66.
- Abu-Lebdeh, T., Hamoush, S., Heard, W. & Zornig, B. (2011) Effect of matrix strength on pullout behavior of steel fiber reinforced very-high strength concrete composites. *Construction and Building Materials*, Vol 25, No 1, pp 39-46.
- Ahmad, I. (2016) Parameters Estimation of Nakagami Probability Distribution Using Methods of L. Moments. *NUST Journal of Engineering Sciences*, Vol 8, No 1, pp 10-13.
- Akkaya, Y., Peled, A. & Shah, S. (2000a) Parameters related to fiber length and processing in cementitious composites. *Materials and Structures*, Vol 33, No 8, pp 515-524.
- Akkaya, Y., Picka, J. & Shah, S. P. (2000b) Spatial distribution of aligned short fibers in cement composites. *Journal of materials in civil engineering*, Vol 12, No 3, pp 272-279.
- Akkaya, Y., Shah, S. P. & Ankenman, B. (2001) Effect of fiber dispersion on multiple cracking of cement composites. *Journal of engineering mechanics*, Vol 127, No 4, pp 311-316.
- Alberti, M., Enfedaque, A. & Gálvez, J. (2017) On the prediction of the orientation factor and fibre distribution of steel and macro-synthetic fibres for fibre-reinforced concrete. *Cement and Concrete Composites*, Vol 77, pp 29-48.
- Alberti, M., Enfedaque, A., Gálvez, J. & Agrawal, V. (2016) Fibre distribution and orientation of macro-synthetic polyolefin fibre reinforced concrete elements. *Construction and Building Materials*, Vol 122, pp 505-517.
- Alberti, M. G. (2015) Polyolefin fibre-reinforced concrete: from material behaviour to numerical and design considerations.) Technical University Madrid, Madrid, Spain.
- Andries, J., Van Itterbeeck, P., Vandewalle, L. & Van Geysel, A. (2015) Influence of concrete flow on spatial distribution and orientation of fibres in steel fibre reinforced self-compacting concrete. In *fib symposium, Copenhagen, Denmark.*)
- ASTM C1550-12a (2012): Standard Test Method for Flexural Toughness of Fiber Reinforced Concrete (Using Centrally Loaded Round Panel). West Conshohocken, ASTM International.
- ASTM C1609/C1609M-12 (2013): Standard Test Method for Flexural Performance of Fiber-Reinforced Concrete (Using Beam With Third-Point Loading). West Conshohocken, ASTM International.
- Aydin, S. (2013) Effects of fiber strength on fracture characteristics of normal and high strength concrete. *Periodica Polytechnica. Civil Engineering*, Vol 57, No 2, pp 191.
- Banthia, N. & Trottier, J.-F. (1994) Concrete reinforced with deformed steel fibers, part I: bond-slip mechanisms. *Materials Journal*, Vol 91, No 5, pp 435-446.
- Barr, B., Lee, M., De Place Hansen, E. J., Dupont, D., Erdem, E., Schaerlaekens, S., Schnütgen, B., Stang, H. & Vandewalle, L. (2003a) Round-robin analysis of the RILEM TC 162-TDF beam-

- bending test: part 1—test method evaluation. *Materials and Structures*, Vol 36, No 9, pp 609-620.
- Barr, B., Lee, M., De Place Hansen, E. J., Dupont, D., Erdem, E., Schaerlaekens, S., Schnütgen, B., Stang, H. & Vandewalle, L. (2003b) Round-robin analysis of the RILEM TC 162-TDF beam-bending test: Part 3—Fibre distribution. *Materials and Structures*, Vol 36, No 9, pp 631-635.
- Barragán, B. E., Gettu, R., Martín, M. A. & Zerbino, R. L. (2003) Uniaxial tension test for steel fibre reinforced concrete—a parametric study. *Cement and Concrete Composites*, Vol 25, No 7, pp 767-777.
- Barros, J. A., Cunha, V. M., Ribeiro, A. F. & Antunes, J. (2005) Post-cracking behaviour of steel fibre reinforced concrete. *Materials and Structures*, Vol 38, No 1, pp 47-56.
- Bentur, A. & Mindess, S. (2006) *Fibre Reinforced Cementitious Composites*. 2nd edn. Taylor & Francis.
- Bentur, A., Wu, S., Banthia, N., Baggott, R., Hansen, W., Katz, A., Leung, C., Li, V. C., Mobasher, B. & Naaman, A. (1996) Fiber-matrix interfaces. In *High Performance Fiber Reinforced Cement Composites 2*. (Naaman, A., and Reinhardt, H. (eds)) E & FN Spon, London, vol. 2, pp 150-185.
- Bernasconi, A., Cosmi, F. & Hine, P. (2012) Analysis of fibre orientation distribution in short fibre reinforced polymers: A comparison between optical and tomographic methods. *Composites Science and Technology*, Vol 72, No 16, pp 2002-2008.
- Bertoncelj, B., Vojisavljevic, K., Rihtarsic, J., Trefalt, G., Huskic, M., Zagar, E. & Malic, B. (2016) A Voronoi-diagram analysis of the microstructures in bulk-molding compounds and its correlation with the mechanical properties. *Express Polymer Letters*, Vol 10, No 6, pp 493.
- Betterman, L., Ouyang, C. & Shah, S. (1995) Fiber-matrix interaction in microfiber-reinforced mortar. *Advanced Cement Based Materials*, Vol 2, No 2, pp 53-61.
- Bi, J., Bao, C., Xu, D., Guan, J. & Cheng, W. (2017) Numerical simulation of the distribution and orientation of steel fibres in the SCC. *Magazine of Concrete Research*, Vol 69, No 16, pp 811-822.
- Blanco, A., Cavalaro, S., De La Fuente, A., Grünwald, S., Blom, C. & Walraven, J. (2015) Application of FRC constitutive models to modelling of slabs. *Materials and Structures*, Vol 48, No 9, pp 2943-2959.
- Brandt, A. (1985) On the optimal direction of short metal fibres in brittle matrix composites. *Journal of Materials Science*, Vol 20, No 11, pp 3831-3841.
- Carcolé, E. & Sato, H. (2009) Statistics of the fluctuations of the amplitude of coda waves of local earthquakes. In *Seismological Society of Japan, 2009 Fall Meeting, C31-13, Kyoto, Japan.*
- Caverzan, A., Di Prisco, M. & Cadoni, E. (2015) Dynamic behaviour of HPRCC: The influence of fibres dispersion. In *EPJ Web of Conferences.* EDP Sciences, Vol 94, pp 01064.
- Chanvillard, G. & Aitcin, P.-C. (1990) Micro-Mechanical Modeling of the Pull-Out Behavior of Corrugated Wiredrawn Steel Fibers from Cementitious Matrices. *MRS Online Proceedings Library Archive*, Vol 211.

- Chin, C. & Xiao, R. (2012) Experimental and Nonlinear Finite Element Analysis of Fiber-Cementitious Matrix Bond-Slip Mechanism. In *High Performance Fiber Reinforced Cement Composites 6.*) Springer, pp 145-152.
- De Berg, M. (2008) *Computational geometry : algorithms and applications.* 3rd ed. edn. Springer, Berlin.
- Denneman, E., Kearsley, E. P. & Visser, A. T. (2011) Splitting tensile test for fibre reinforced concrete. *Materials and Structures*, Vol 44, No 8, pp 1441-1449.
- Devore, J. L. & Berk, K. N. (2012) *Modern mathematical statistics with applications.*) 2nd ed. edn. Springer, New York, NY.
- Di Prisco, M., Plizzari, G. & Vandewalle, L. (2009) Fibre reinforced concrete: new design perspectives. *Materials and Structures*, Vol 42, No 9, pp 1261-1281.
- Dupont, D. & Vandewalle, L. (2005) Distribution of steel fibres in rectangular sections. *Cement and Concrete Composites*, Vol 27, No 3, pp 391-398.
- Eik, M. (2014) Orientation of short steel fibres in concrete: measuring and modelling. In *Mechanics and Applied Mathematics Department.*) Aalto University, Helsinki, Vol PhD.
- EN 14651 (2005): *Test method for metallic fibered concrete - Measuring the flexural tensile strength (limit of proportionality (LOP), residual)*, Ref. No. EN 14651 : 2005 : E, CEN European Committee for Standardization, Brussels.
- Faifer, M., Ferrara, L., Ottoboni, R. & Toscani, S. (2013) Low Frequency Electrical and Magnetic Methods for Non-Destructive Analysis of Fiber Dispersion in Fiber Reinforced Cementitious Composites: An Overview. *Sensors*, Vol 13, No 1, pp 1300-1318.
- Faifer, M., Ottoboni, R., Toscani, S. & Ferrara, L. (2011) Nondestructive Testing of Steel-Fiber-Reinforced Concrete Using a Magnetic Approach. *IEEE Transactions on Instrumentation and Measurement*, Vol 60, No 5.
- FIB (2013) *fib Model Code for Concrete Structures 2010.* Berlin, Ernst & Sohn, Wiley.
- Felekoğlu, B., Tosun-Felekoğlu, K. & Gödek, E. (2015) A novel method for the determination of polymeric micro-fiber distribution of cementitious composites exhibiting multiple cracking behavior under tensile loading. *Construction and Building Materials*, Vol 86, pp 85-94.
- Ferrara, L., Cremonesi, M., Faifer, M., Toscani, S., Sorelli, L., Baril, M.-A., Réthoré, J., Baby, F., Toutlemonde, F. & Bernardi, S. (2017) Structural elements made with highly flowable UHPFRC: Correlating computational fluid dynamics (CFD) predictions and non-destructive survey of fiber dispersion with failure modes. *Engineering Structures*, Vol 133, pp 151-171.
- Ferrara, L., Faifer, M. & Toscani, S. (2012) A magnetic method for non destructive monitoring of fiber dispersion and orientation in steel fiber reinforced cementitious composites—part 1: method calibration. *Materials and Structures*, Vol 45, No 4, pp 575-589.
- Ferrara, L., Ozyurt, N. & Di Prisco, M. (2011) High mechanical performance of fibre reinforced cementitious composites: the role of “casting-flow induced” fibre orientation. *Materials and Structures*, Vol 44, No 1, pp 109-128.

- Ferrara, L., Park, Y.-D. & Shah, S. P. (2008) Correlation among fresh state behavior, fiber dispersion, and toughness properties of SFRCs. *Journal of materials in civil engineering*, Vol 20, No 7, pp 493-501.
- Gettu, R., Gardner, D., Saldivar, H. & Barragán, B. (2005) Study of the distribution and orientation of fibers in SFRC specimens. *Materials and Structures*, Vol 38, No 1, pp 31-37.
- Grünewald, S. (2004) Performance-based design of self-compacting fibre reinforced concrete.) TU Delft, Delft University of Technology.
- Heilbronner, R. & Barrett, S. (2013) *Image analysis in earth sciences: microstructures and textures of earth materials*. Springer Science & Business Media.
- Jähne, B. (2005) *Digital Image Processing, 6th Revised and Extended Edition*. Springer.
- Jasiūnienė, E., Cicėnas, V., Grigaliūnas, P., Rudžionis, Ž. & Navickas, A. A. (2018) Influence of the rheological properties on the steel fibre distribution and orientation in self-compacting concrete. *Materials and Structures*, Vol 51, No 4, pp 103.
- JCI-S-003-2007 (2007): Method of test for bending moment-curvature curve of fiber-reinforced cementitious composites, Japanese Concrete Institute Standard Committee.
- JCI-S-002-2003 (2003): Method of test for load-displacement curve of fibre reinforced concrete by use of notched beam, Japanese Concrete Institute Standard Committee.
- Johnston, C. D. (1996) Proportioning, mixing and placement of fibre-reinforced cements and concretes. In *International RILEM conference, Production methods and workability of concrete*. (Bartos, P. J. M., Marrs, D. L., and Cleland, D. J. (eds)) E & FN Spon, London, pp 155-180.
- Kameswara Rao, C. V. S. (1979) Effectiveness of Random Fibres in Composites. *Cement and Concrete Research*, Vol 9, No 6, pp 685-693.
- Katz, A. & Li, V. C. (1995) Inclination angle effect of carbon fibers in cementitious composites. *Journal of engineering mechanics*, Vol 121, No 12, pp 1340-1348.
- Kooiman, A. G. (2000) Modelling steel fibre reinforced concrete for structural design.) Delft University of Technology, Delft, Netherlands.
- Krenchel, H. (1975) Fibre spacing and specific fibre surface. In *Fibre reinforced cement and concrete*.) Construction Press, UK.
- Laranjeira, F. (2010) Design-oriented constitutive model for steel fiber reinforced concrete. In *Departament d'Enginyeria de la Construcció*.) Universitat Politècnica de Catalunya.
- Laranjeira, F., Grünewald, S., Walraven, J., Blom, C., Molins, C. & Aguado, A. (2011) Characterization of the orientation profile of steel fiber reinforced concrete. *Materials and Structures*, Vol 44, No 6, pp 1093-1111.
- Lee, B. Y., Kang, S.-T., Yun, H.-B. & Kim, Y. Y. (2016) Improved sectional image analysis technique for evaluating fiber orientations in fiber-reinforced cement-based materials. *Materials*, Vol 9, No 1, pp 42.
- Lee, B. Y., Kim, J.-K., Kim, J.-S. & Kim, Y. Y. (2009) Quantitative evaluation technique of Polyvinyl Alcohol (PVA) fiber dispersion in engineered cementitious composites. *Cement and Concrete Composites*, Vol 31, No 6, pp 408-417.

- Leung, C. K. & Li, V. C. (1992) Effect of fiber inclination on crack bridging stress in brittle fiber reinforced brittle matrix composites. *Journal of the Mechanics and Physics of Solids*, Vol 40, No 6, pp 1333-1362.
- Li, V. C. (1992) A simplified micromechanical model of compressive strength of fiber-reinforced cementitious composites. *Cement and Concrete Composites*, Vol 14, No 2, pp 131-141.
- Li, V. C., Wang, Y. & Backer, S. (1990) Effect of inclining angle, bundling and surface treatment on synthetic fibre pull-out from a cement matrix. *Composites*, Vol 21, No 2, pp 132-140.
- Liu, J., Li, C., Liu, J., Cui, G. & Yang, Z. (2013) Study on 3D spatial distribution of steel fibers in fiber reinforced cementitious composites through micro-CT technique. *Construction and Building Materials*, Vol 48, pp 656-661.
- Liu, J., Li, C., Liu, J., Du, Z. & Cui, G. (2011) Characterization of fiber distribution in steel fiber reinforced cementitious composites with low water-binder ratio.
- Löfgren, I. (2005) Fibre-reinforced Concrete for Industrial Construction—a fracture mechanics approach to material testing and structural analysis.) Chalmers University of Technology, Göteborg, Sweden.
- Löfgren, I., Olesen, J. F. & Flansbjerg, M. (2004a) *Application of WST-method for fracture testing of fibre-reinforced concrete*.
- Löfgren, I., Stang, H. & Olesen, J. F. (2004b) Wedge splitting test—a test to determine fracture properties of FRC. In *Fibre-Reinforced Concretes-BEFIB 2004-Proceedings of the Sixth RILEM symposium/di Prisco, M., Felicetti, R., Plizzari, GA.*) Rilem publications, Vol 1, pp 379-388.
- Marković, I. (2006) High-performance hybrid-fibre concrete: development and utilisation.) Delft University of Technology, Delft, Netherlands.
- Mehta, P. K. & Monteiro, P. J. M. (1993) *Concrete: Structure, Properties, and Materials*. 2nd edn. Prentice Hall.
- Morton, J. & Groves, G. (1974) The cracking of composites consisting of discontinuous ductile fibres in a brittle matrix—effect of fibre orientation. *Journal of Materials Science*, Vol 9, No 9, pp 1436-1445.
- Naaman, A. (2004) 31. Evaluation of steel fibers for applications in structural concrete. In *6th International RILEM Symposium on Fibre Reinforced Concretes.*) RILEM Publications SARL, pp 389-400.
- Naaman, A. E. (1972) A statistical theory of strength for fiber reinforced concrete. In *Massachusetts Institute of Technology. Dept. of Civil Engineering.*) Massachusetts Institute of Technology, pp 196.
- Naaman, A. E. (2003) Engineered steel fibers with optimal properties for reinforcement of cement composites. *Journal of advanced concrete technology*, Vol 1, No 3, pp 241-252.
- Naaman, A. E. (2008) High performance fiber reinforced cement composites. In *High-performance construction materials: Science and applications.* (Shi, C., and Mo, Y. L. (eds)) World Scientific, pp 91-153.
- Naaman, A. E. & Najm, H. (1991) Bond-slip mechanisms of steel fibers in concrete. *Materials Journal*, Vol 88, No 2, pp 135-145.

- Naaman, A. E. & Shah, S. P. (1976) Pull-out mechanism in steel fiber-reinforced concrete. *ASCE J Struct Div*, Vol 102, No 8, pp 1537-1548.
- Nakagami, M. (1960) The m-distribution—A general formula of intensity distribution of rapid fading. In *Statistical methods in radio wave propagation.*) Elsevier, pp 3-36.
- Nakahara, H. & Carcolé, E. (2010) Maximum-likelihood method for estimating coda Q and the Nakagami-m parameter. *Bulletin of the Seismological Society of America*, Vol 100, No 6, pp 3174-3182.
- Nayar, S. K. & Gettu, R. (2014) Characterisation of the toughness of fibre reinforced concrete—revisited in the Indian context. *Indian Concr. J*, Vol 88, No 2, pp 8-23.
- Neville, A. M. (2011) *Properties of Concrete*. 5 edn. Pearson Education Limited.
- Ozyurt, N., Mason, T. O. & Shah, S. P. (2007) Correlation of fiber dispersion, rheology and mechanical performance of FRCs. *Cement and Concrete Composites*, Vol 29, No 2, pp 70-79.
- Ozyurt, N., Woo, L. Y., Mason, T. O. & Shah, S. P. (2006) Monitoring fiber dispersion in fiber-reinforced cementitious materials: comparison of AC-impedance spectroscopy and image analysis. *ACI Materials Journal*, Vol 103, No 5, pp 340.
- Ozyurt, N., Woo, L. Y., Mu, B., Shah, S. P. & Mason, T. O. (2004) Detection of fiber dispersion in fresh and hardened cement composites. In *Advances in Concrete Through Science and Engineering, An International Symposium During the RILEM Spring Meeting.*)
- Paegle, I. & Fischer, G. (2013) Evaluation of test methods used to characterize fiber reinforced cementitious composites. In *International Conference „Innovative Materials, Structures and Technologies”.*)
- Park, S. H., Ryu, G. S., Koh, K. T. & Kim, D. J. (2014) Effect of shrinkage reducing agent on pullout resistance of high-strength steel fibers embedded in ultra-high-performance concrete. *Cement and Concrete Composites*, Vol 49, pp 59-69.
- Parmentier, B., Vandewalle, L. & Van Rickstal, F. (2008) Evaluation of the scatter of the postpeak behaviour of fibre reinforced concrete in bending: A step towards reliability. In *BEFIB 2008: 7th RILEM International Symposium on Fibre Reinforced Concrete.*) RILEM Publications SARL, pp 133-143.
- Ponikiewski, T. & Katzer, J. (2016) X-ray computed tomography of fibre reinforced self-compacting concrete as a tool of assessing its flexural behaviour. *Materials and Structures*, Vol 49, No 6, pp 2131-2140.
- Ponikiewski, T., Katzer, J., Bugdol, M. & Rudzki, M. (2015) X-ray computed tomography harnessed to determine 3D spacing of steel fibres in self compacting concrete (SCC) slabs. *Construction and Building Materials*, Vol 74, pp 102-108.
- RILEM TC 162-TDF (2002) Test and design methods for steel fibre reinforced concrete: Bending test - Final Recommendation. *Materials and Structures*, Vol 35, No 9, pp 579-582.
- Robins, P., Austin, S. & Jones, P. (2002) Pull-out behaviour of hooked steel fibres. *Materials and Structures*, Vol 35, No 7, pp 434-442.
- Roerdink, J. B. & Meijster, A. (2000) The watershed transform: Definitions, algorithms and parallelization strategies. *Fundamenta informaticae*, Vol 41, No 1, 2, pp 187-228.

- Romualdi, J. P. & Mandel, J. A. (1964) Tensile strength of concrete affected by uniformly distributed and closely spaced short lengths of wire reinforcement. In *Journal Proceedings.*, Vol 61, pp 657-672.
- Sarkar, S., Goel, N. & Mathur, B. (2009) Adequacy of Nakagami-m distribution function to derive GIUH. *Journal of Hydrologic Engineering*, Vol 14, No 10, pp 1070-1079.
- Sarkar, S., Goel, N. & Mathur, B. (2010) Performance investigation of Nakagami-m distribution to derive flood hydrograph by genetic algorithm optimization approach. *Journal of Hydrologic Engineering*, Vol 15, No 8, pp 658-666.
- Segura-Castillo, L., Cavalaro, S. H., Goodier, C., Aguado, A. & Austin, S. (2018) Fibre distribution and tensile response anisotropy in sprayed fibre reinforced concrete. *Materials and Structures*, Vol 51, No 1, pp 29.
- Shoya, M. (1979) Drying shrinkage and moisture loss of super plasticizer admixed concrete of low water cement ratio. *Transactions of the Japan Concrete Institute, Technical Report, No. II-5*, pp 103-110.
- Sorelli, L. G., Meda, A. & Plizzari, G. A. (2005) Bending and Uniaxial Tensile Tests on Concrete Reinforced with Hybrid Steel Fibers. *Journal of materials in civil engineering*, Vol 17, No 5, pp 519-527.
- Stang, H. (1996) Significance of shrinkage-induced clamping pressure in fiber-matrix bonding in cementitious composite materials. *Advanced Cement Based Materials*, Vol 4, No 3-4, pp 106-115.
- Stroeven, P. (1978) Morphometry of fibre reinforced cementitious materials. *Matériaux et Construction*, Vol 11, No 1, pp 31-38.
- Torigoe, S.-I., Horikoshi, T., Ogawa, A., Saito, T. & Hamada, T. (2003) Study on evaluation method for PVA fiber distribution in engineered cementitious composite. *Journal of advanced concrete technology*, Vol 1, No 3, pp 265-268.
- Torrents, J. M., Blanco, A., Pujadas, P., Aguado, A., Juan-García, P. & SáNchez-Moragues, M. a. N. (2012) Inductive method for assessing the amount and orientation of steel fibers in concrete. *Materials and Structures*, Vol 45, No 10, pp 1577-1592.
- Tsui, P., Huang, C. & Wang, S. (2006) Use of Nakagami distribution and logarithmic compression in ultrasonic tissue characterization. *Journal of Medical and Biological Engineering*, Vol 26, No 2, pp 69.
- Vandewalle, L., Heirman, G. & Van Rickstal, F. (2008) Fibre orientation in self-compacting fibre reinforced concrete. In *Proc. of the 7th Int. RILEM Symp. on Fibre Reinforced Concrete: Design and Applications (BEFIB2008.)* RILEM Publications SARL, pp 719-728.
- Wei, S., Mandel, J. A. & Said, S. (1986) Study of the interface strength in steel fiber-reinforced cement-based composites. In *Journal Proceedings.*, Vol 83, pp 597-605.
- Woo, L., Wansom, S., Ozyurt, N., Mu, B., Shah, S. & Mason, T. (2005) Characterizing fiber dispersion in cement composites using AC-Impedance Spectroscopy. *Cement and Concrete Composites*, Vol 27, No 6, pp 627-636.

- Yoo, D.-Y., Kang, S.-T. & Yoon, Y.-S. (2014) Effect of fiber length and placement method on flexural behavior, tension-softening curve, and fiber distribution characteristics of UHPFRC. *Construction and Building Materials*, Vol 64, pp 67-81.
- Yoo, D.-Y., Zi, G., Kang, S.-T. & Yoon, Y.-S. (2015) Biaxial flexural behavior of ultra-high-performance fiber-reinforced concrete with different fiber lengths and placement methods. *Cement and Concrete Composites*, Vol 63, pp 51-66.
- Zerbino, R., Tobes, J., Bossio, M. & Giaccio, G. (2012) On the orientation of fibres in structural members fabricated with self compacting fibre reinforced concrete. *Cement and Concrete Composites*, Vol 34, No 2, pp 191-200.
- Zhou, B. & Uchida, Y. (2017) Relationship between fiber orientation/distribution and post-cracking behaviour in ultra-high-performance fiber-reinforced concrete (UHPFRC). *Cement and Concrete Composites*, Vol 83, pp 66-75.
- Zhou, J., Qian, S., Ye, G., Copuroglu, O., Van Breugel, K. & Li, V. C. (2012) Improved fiber distribution and mechanical properties of engineered cementitious composites by adjusting the mixing sequence. *Cement and Concrete Composites*, Vol 34, No 3, pp 342-348.
- Žirgulis, G., Švec, O., Sarmiento, E. V., Geiker, M. R., Cwirzen, A. & Kanstad, T. (2016) Importance of quantification of steel fibre orientation for residual flexural tensile strength in FRC. *Materials and Structures*, Vol 49, No 9, pp 3861-3877.

APPENDIX A - Specimen Results

A.1 Stress-CMOD Curves

40-30

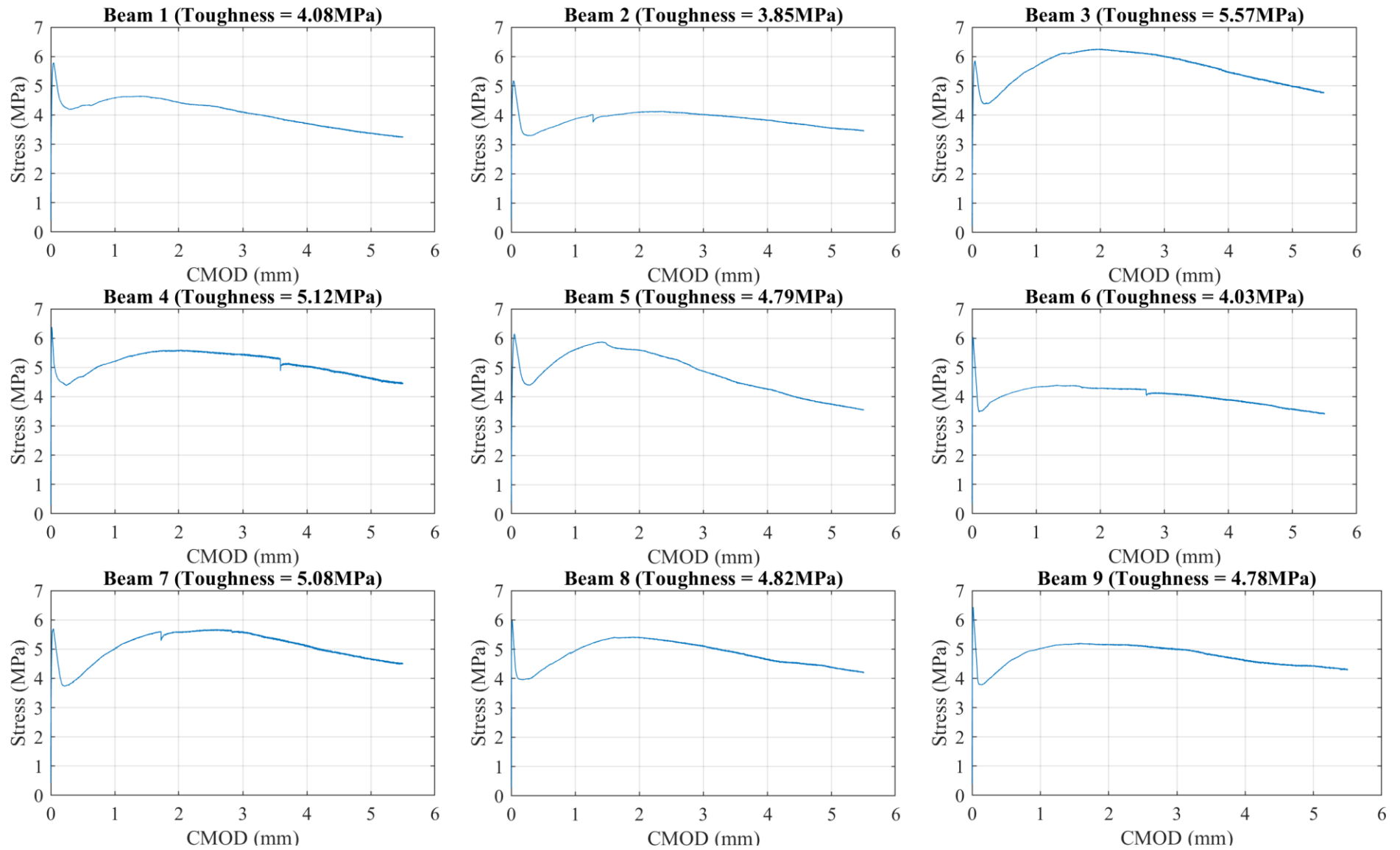


Figure A-1: Batch 40-30 individual Stress-CMOD curves

60-30

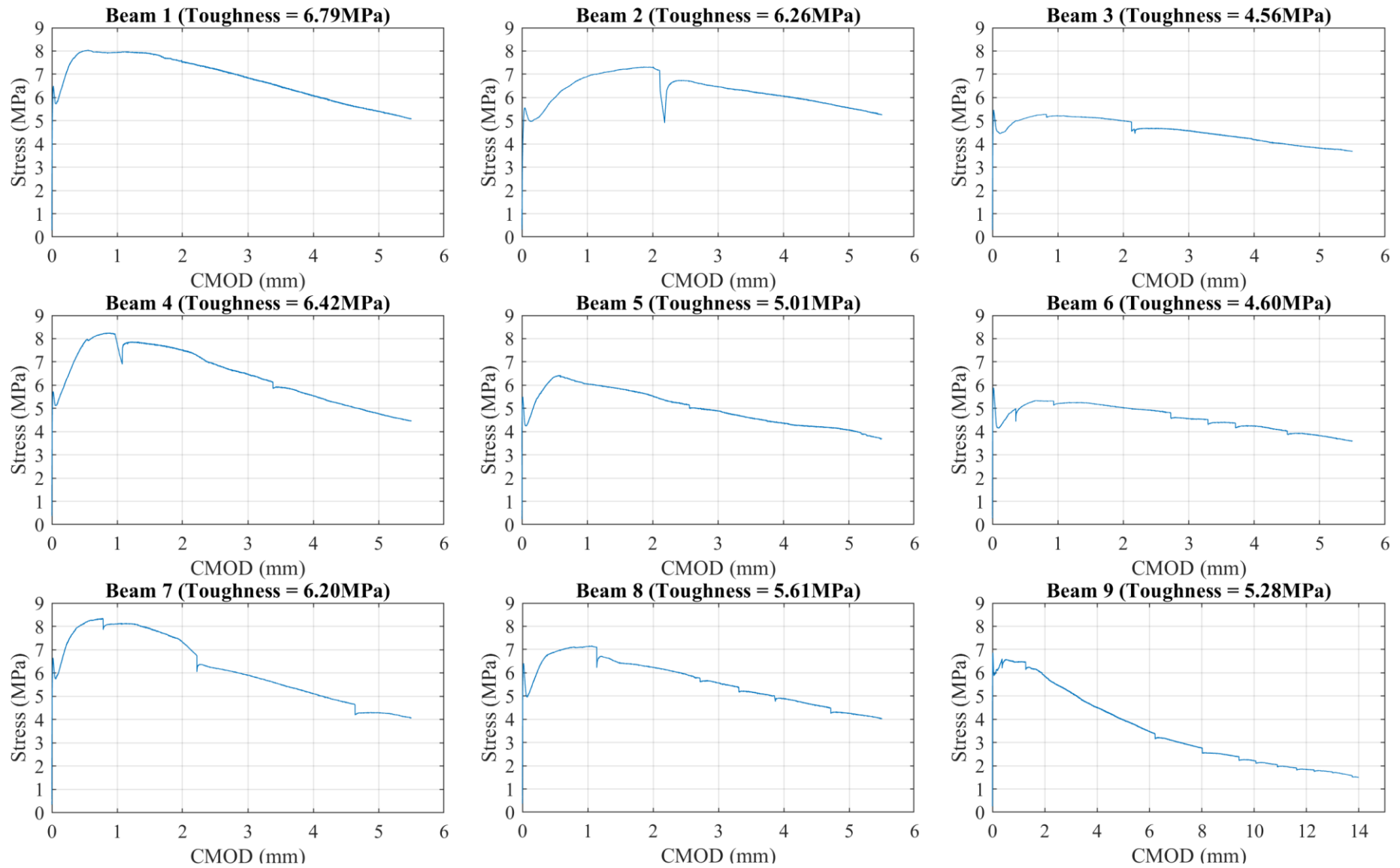
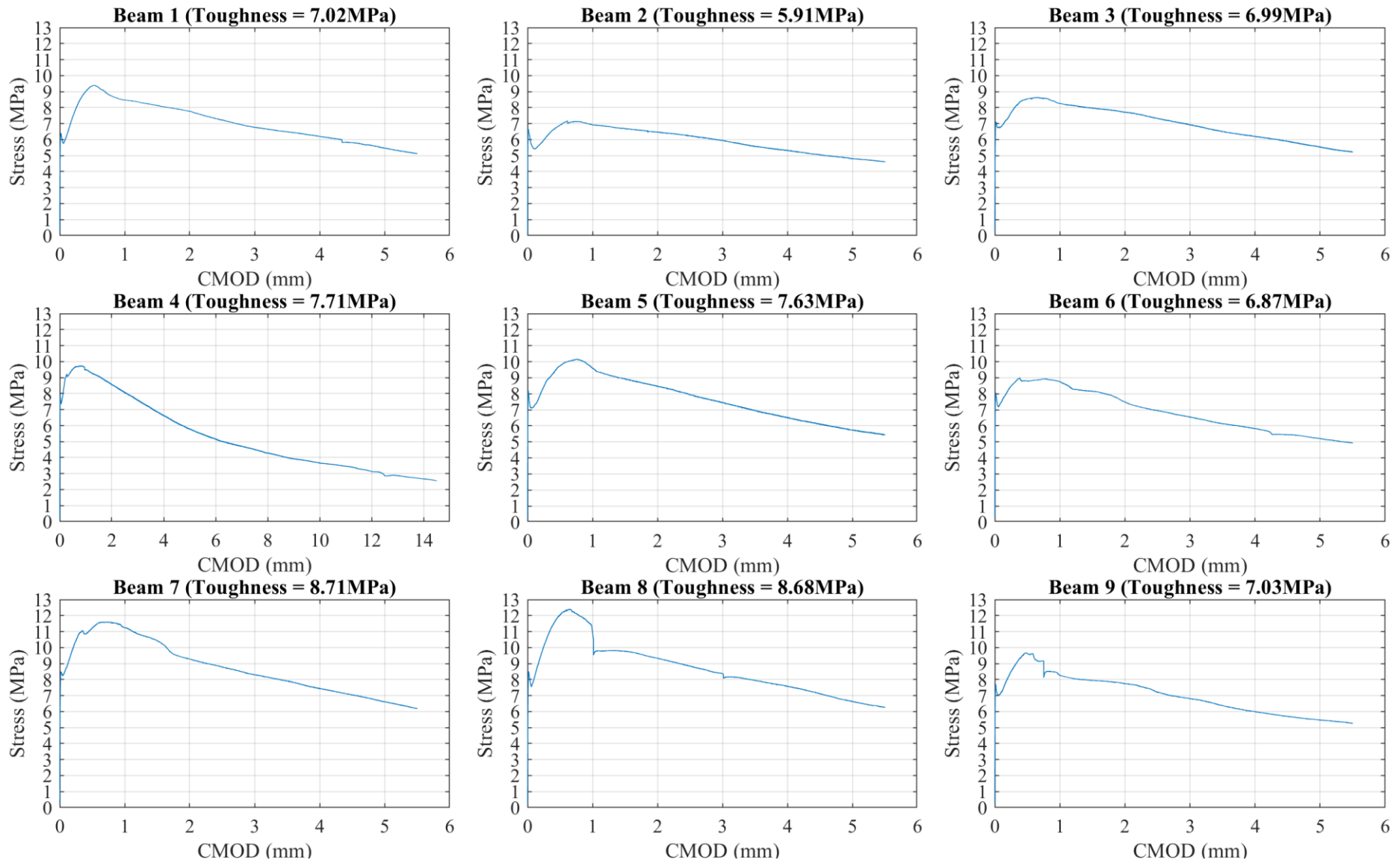


Figure A-2: Batch 60-30 individual Stress-CMOD curves

80-30-a



FigureA-3: Batch 80-30-a individual Stress-CMOD curves

80-30-b

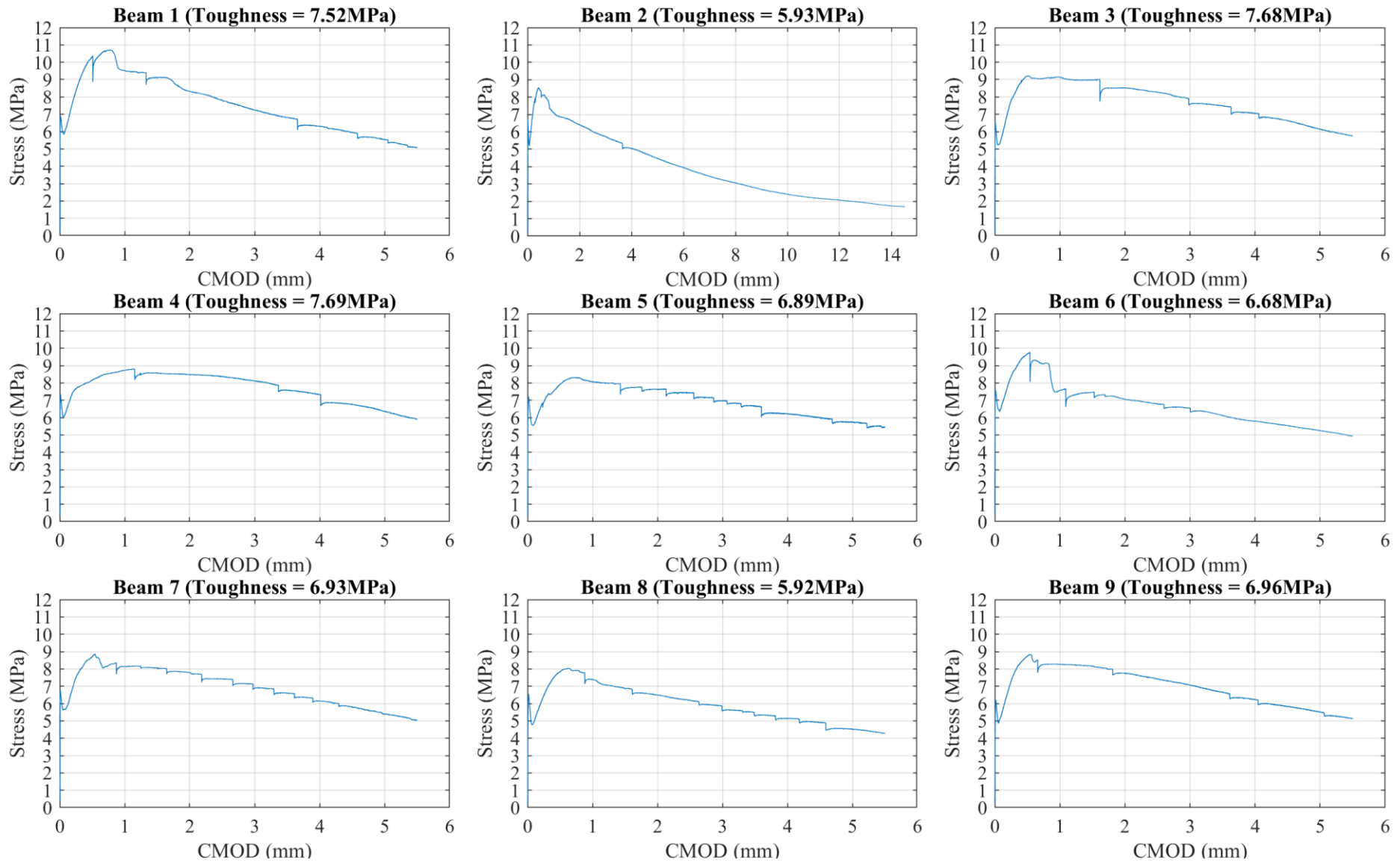


Figure A-4: Batch 80-30-b individual Stress-CMOD curves

100-30

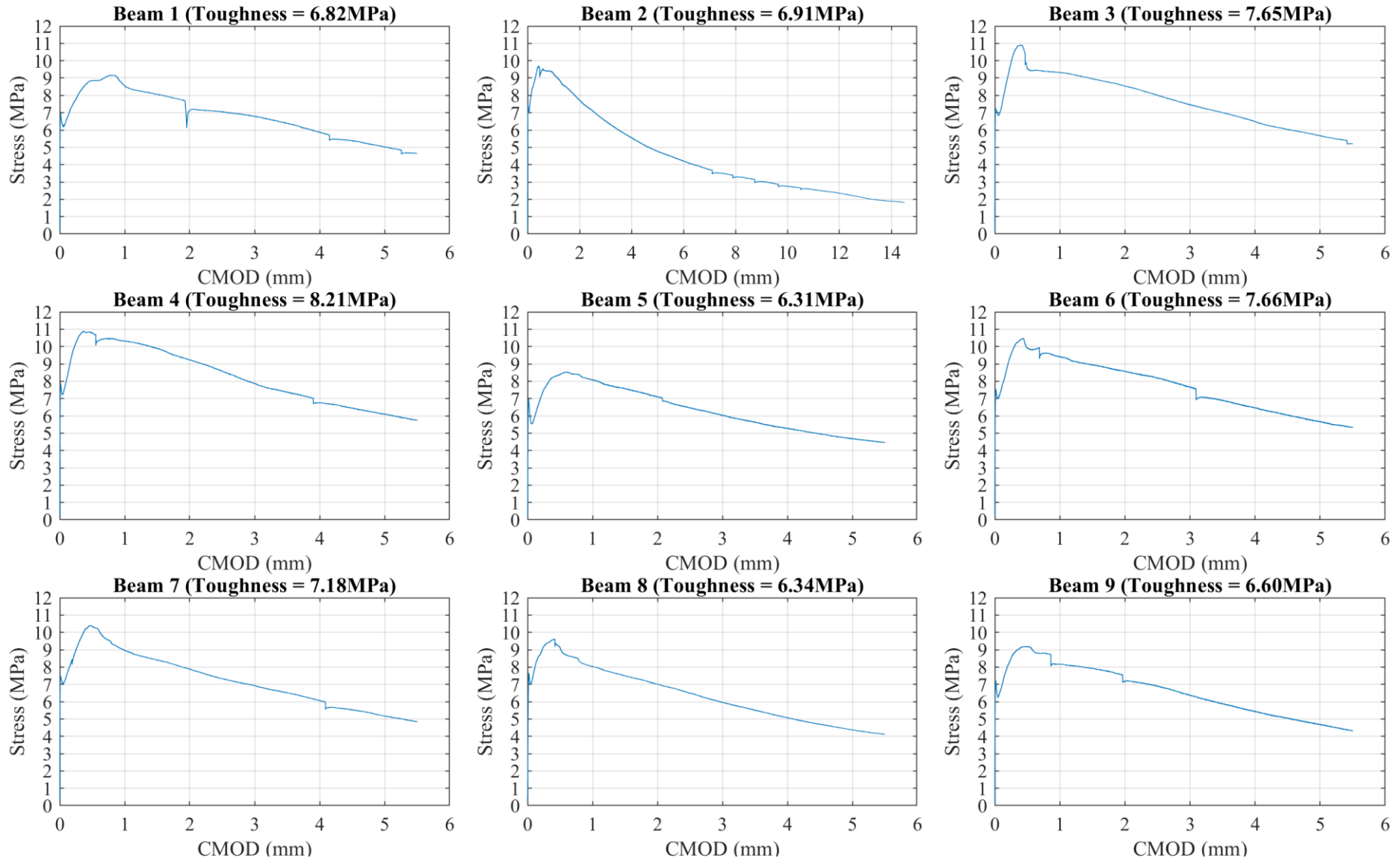


Figure A-5: Batch 100-30 individual Stress-CMOD curves

120-30-a

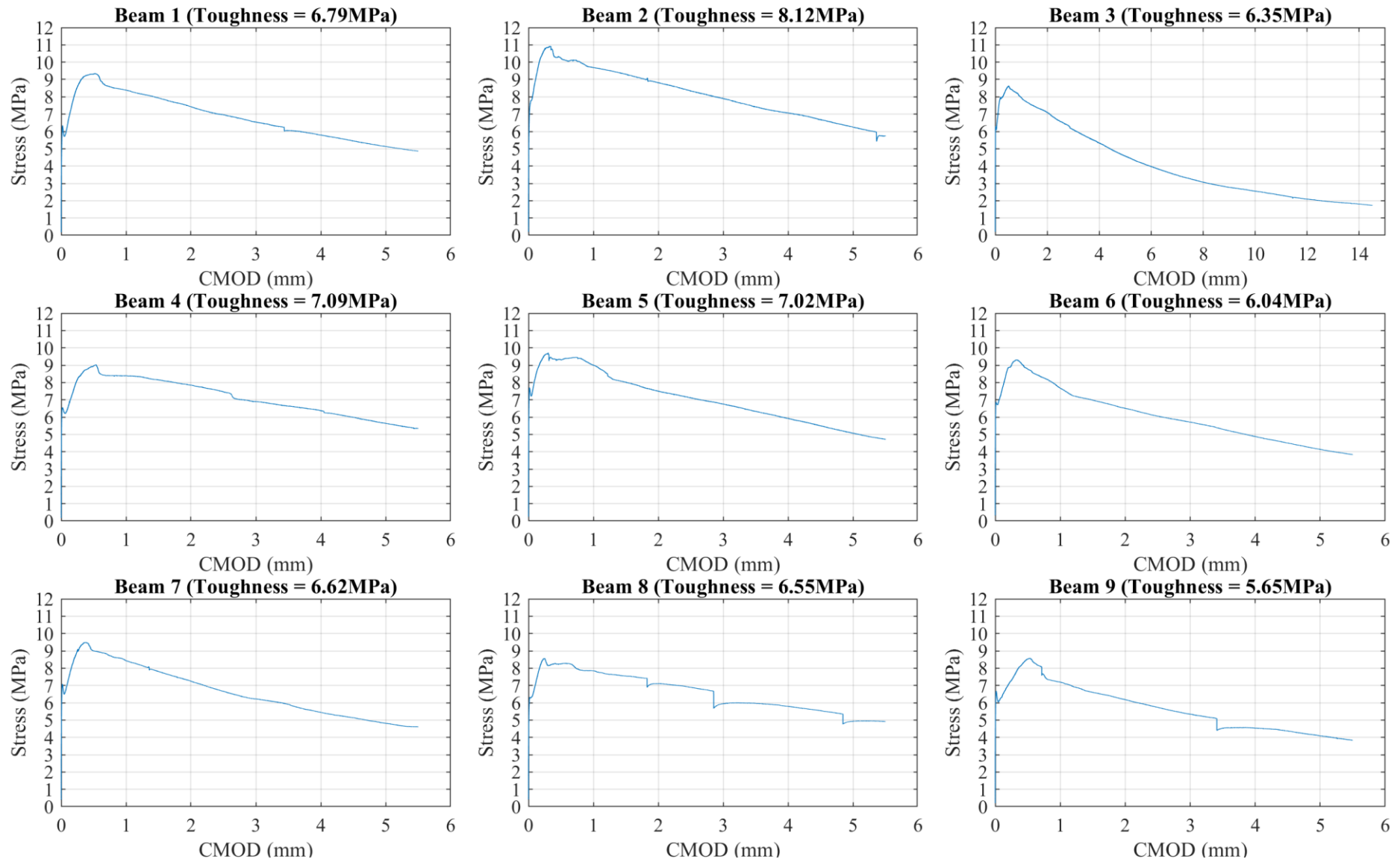


Figure A-6: Batch 120-30-a individual Stress-CMOD curves

120-30-b

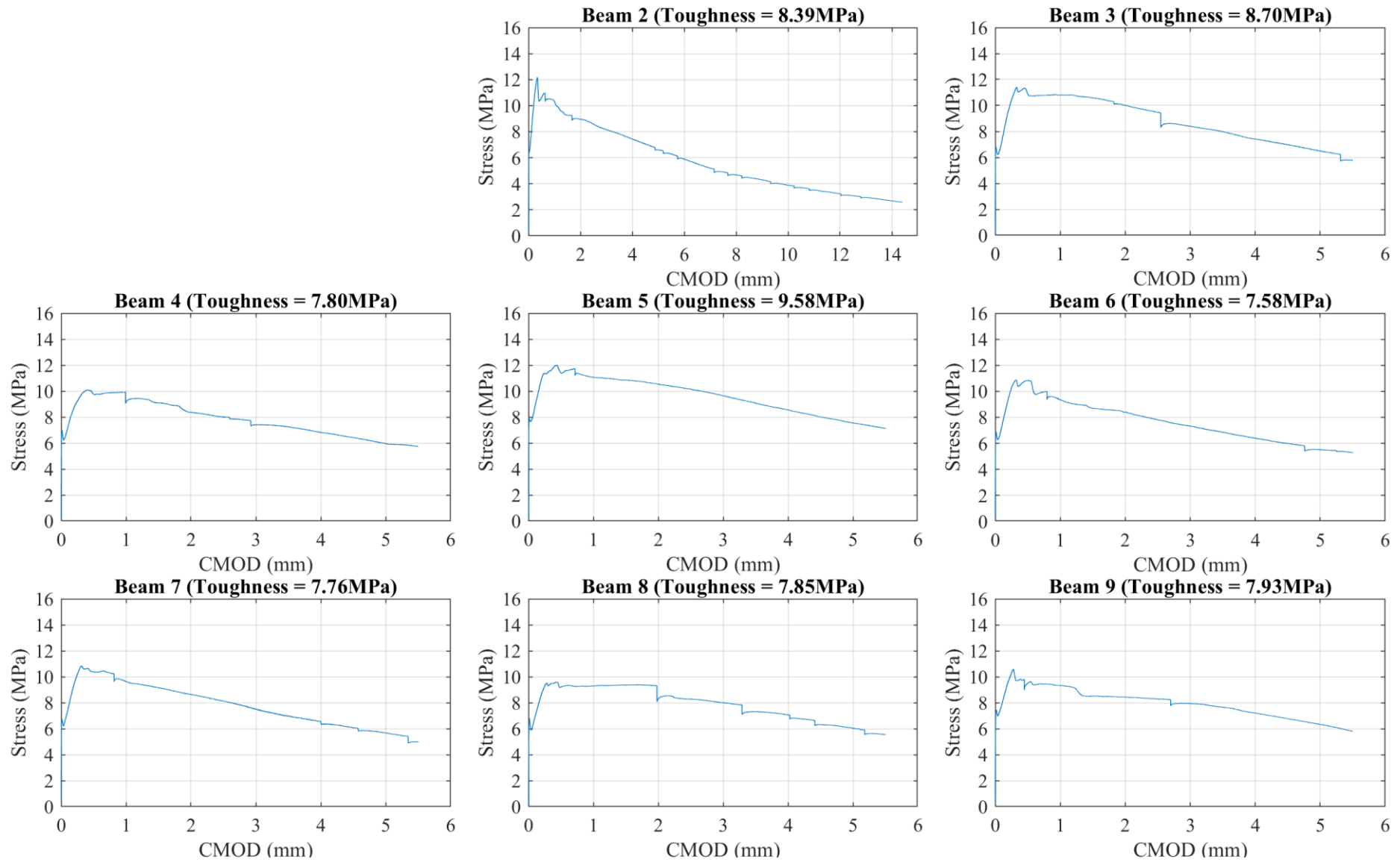


Figure A-7: Batch 120-30-b individual Stress-CMOD curves

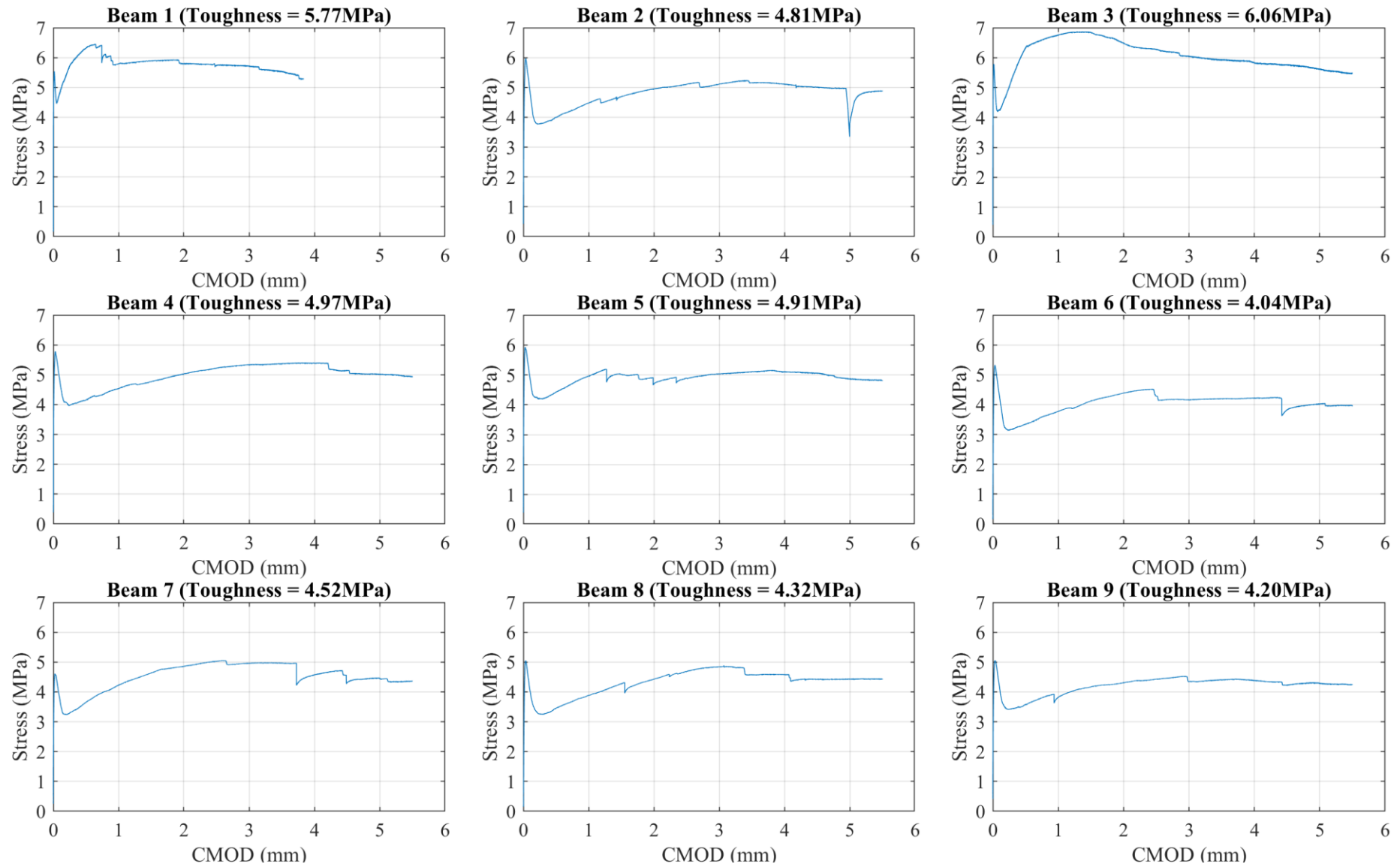
40-60

Figure A-8: Batch 40-60 individual Stress-CMOD curves

60-60

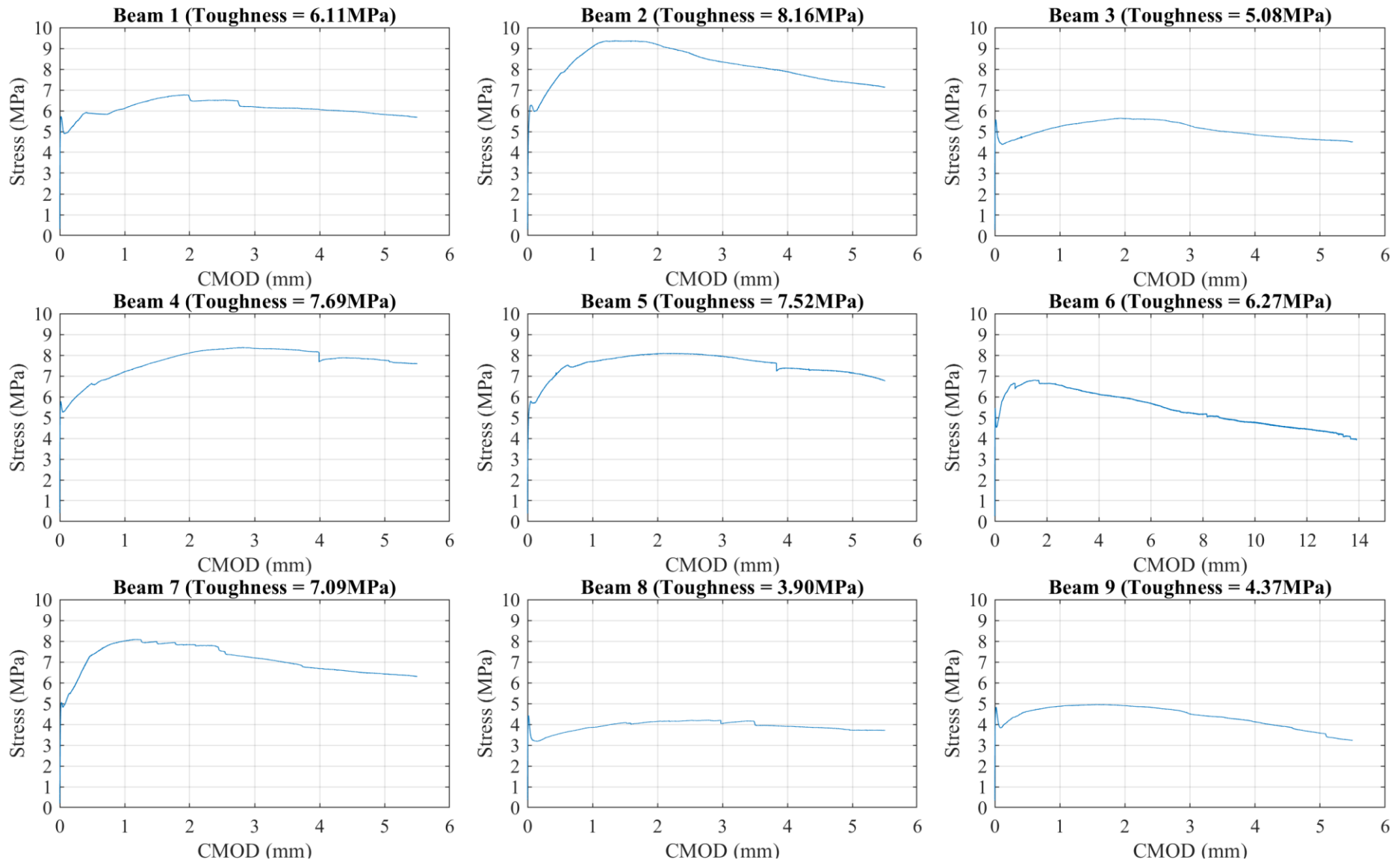


Figure A-9: Batch 60-60 individual Stress-CMOD curves

80-60-a

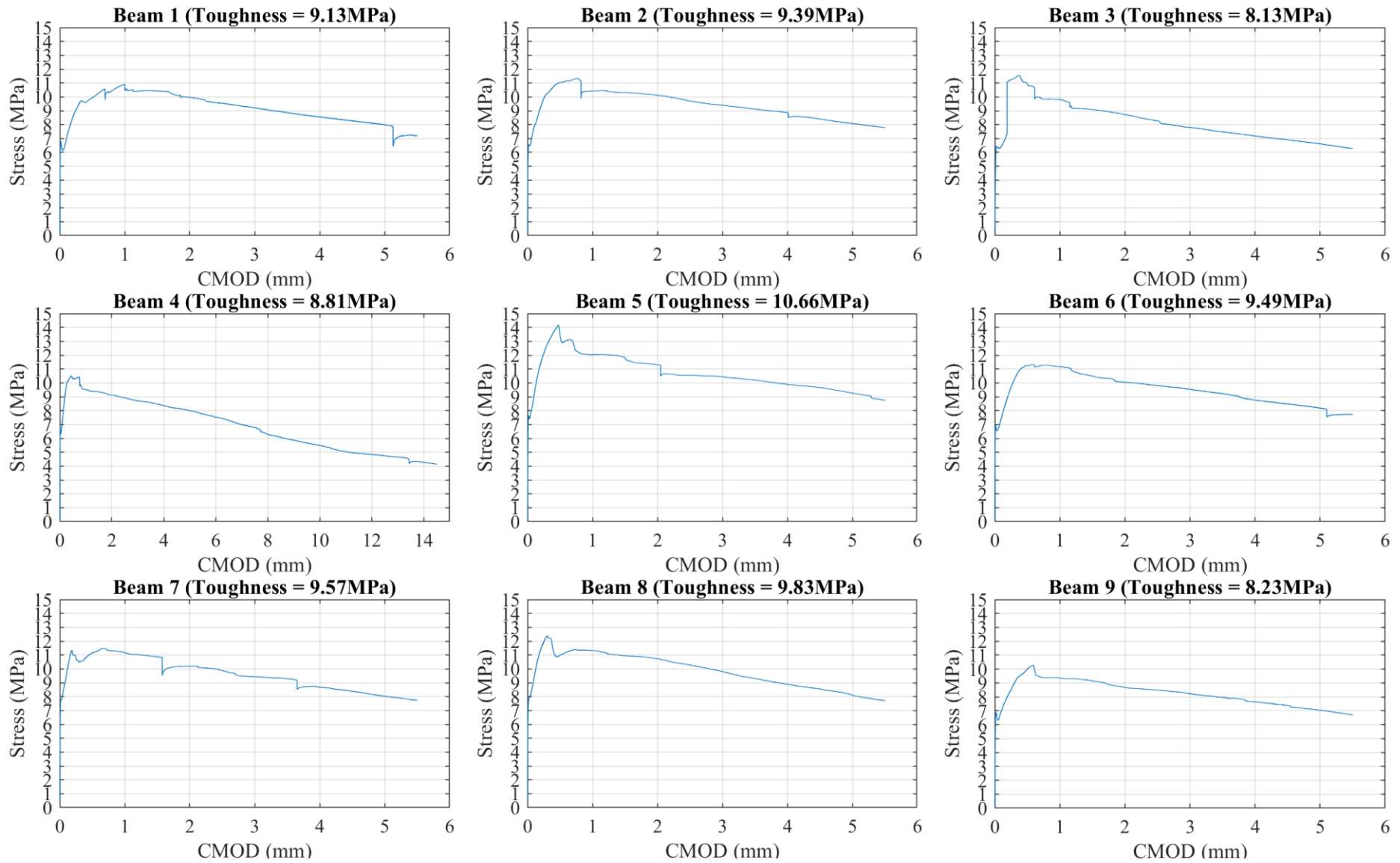


Figure A-10: Batch 80-60-a individual Stress-CMOD curves

80-60-b

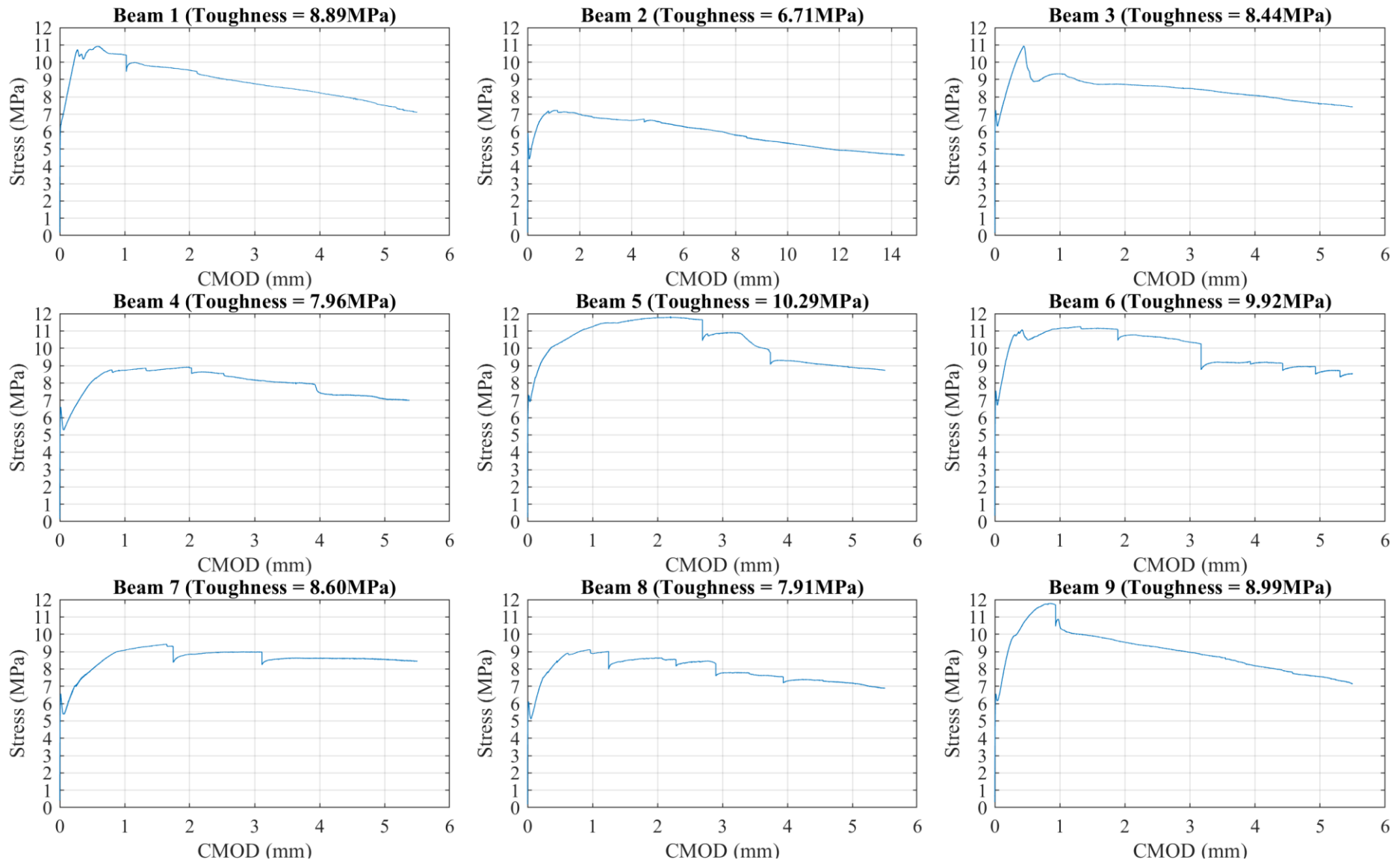


Figure A-11: Batch 80-60-b individual Stress-CMOD curves

100-60

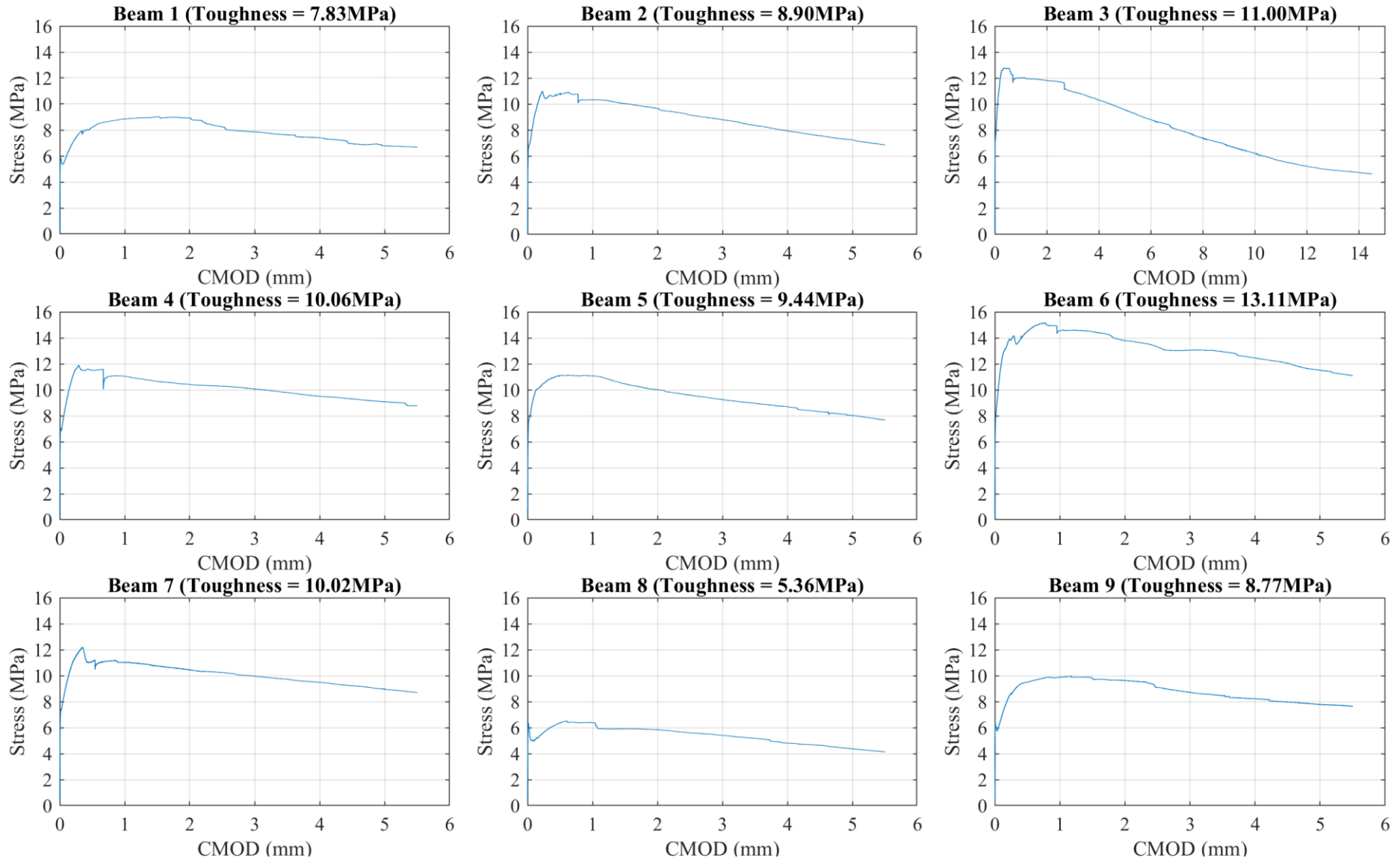


Figure A-12: Batch 100-60 individual Stress-CMOD curves

120-60-a

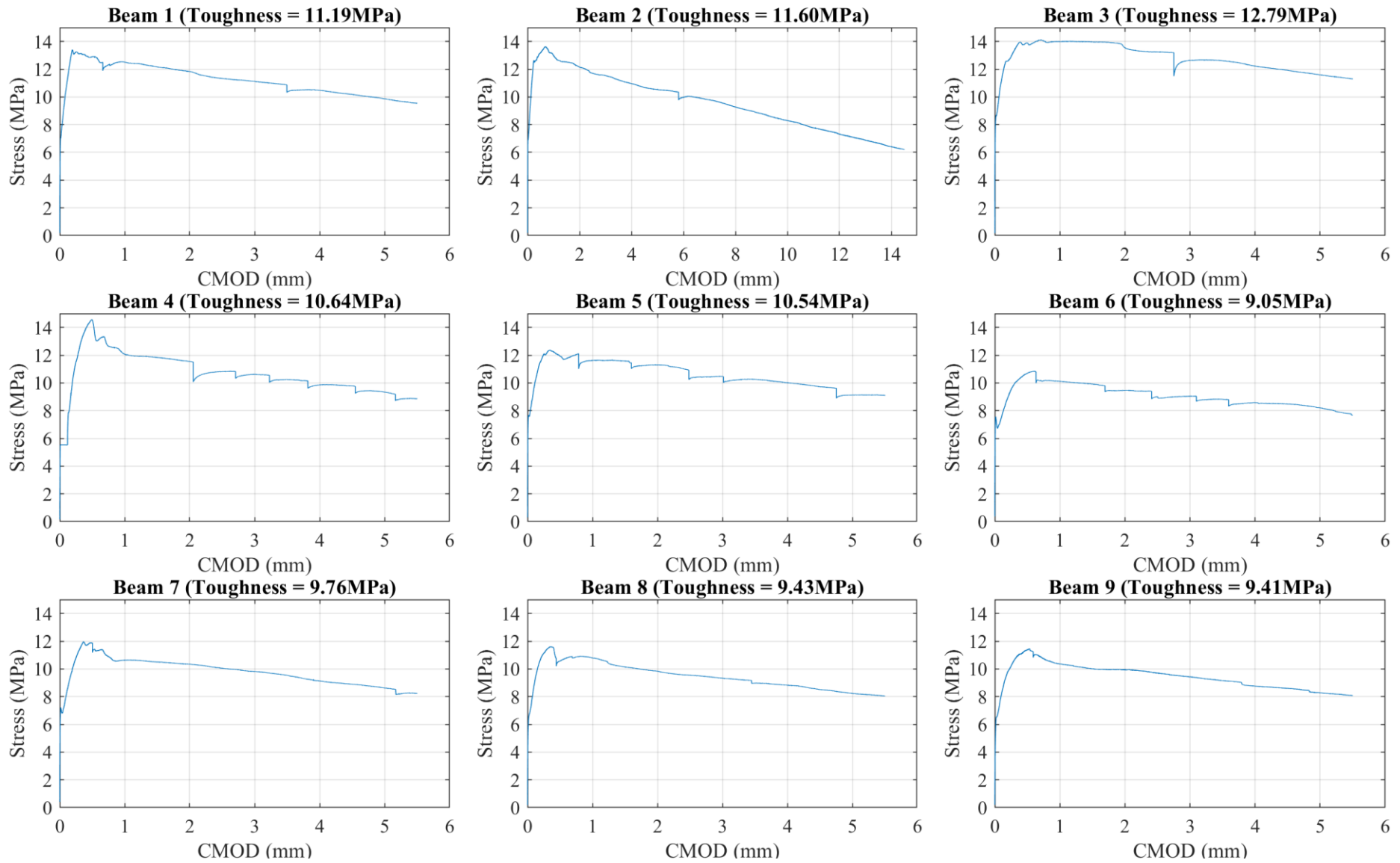


Figure A-13: Batch 120-60-a individual Stress-CMOD curves

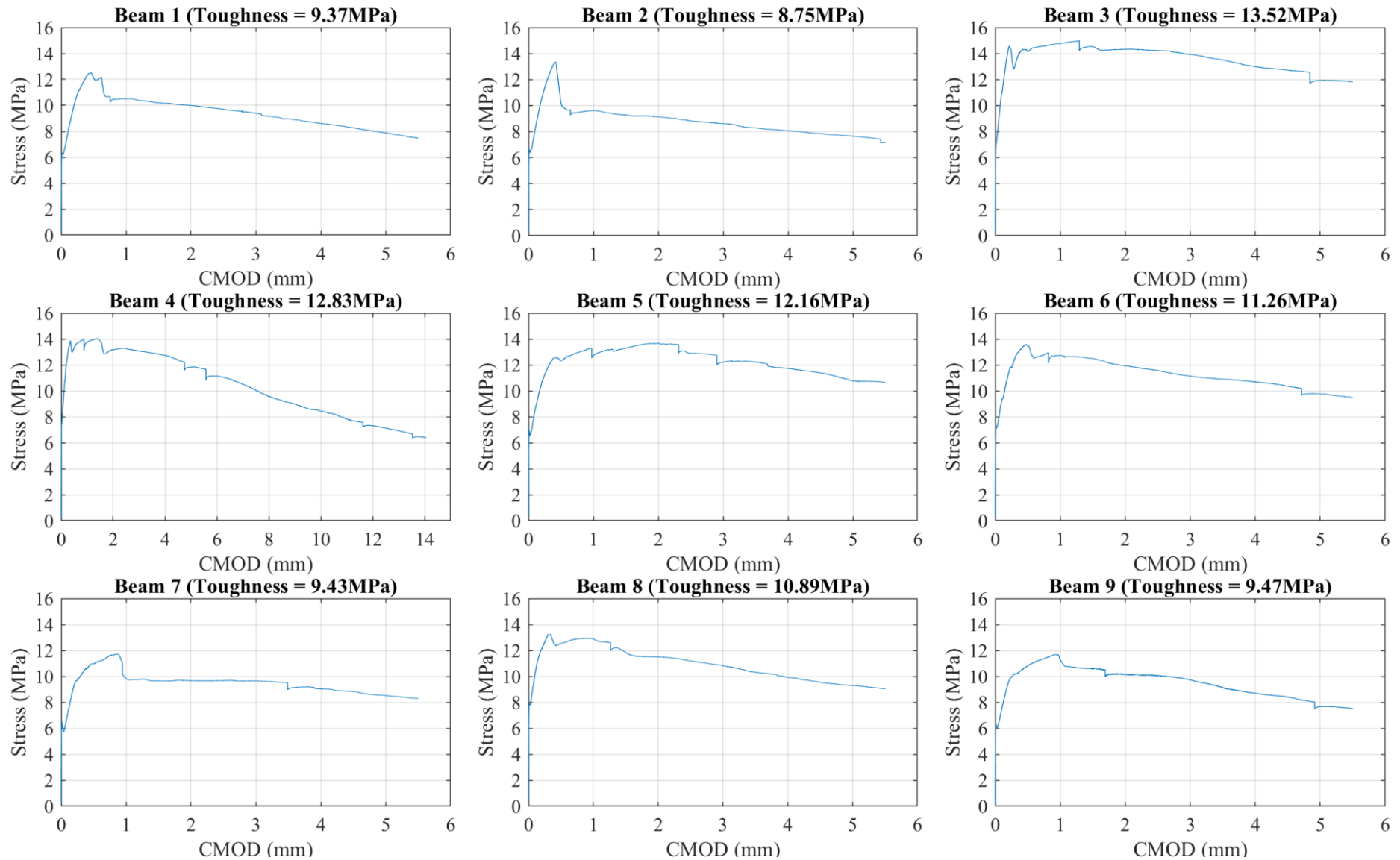
120-60-b

Figure A-14: Batch 120-60-b individual Stress-CMOD curves

A.2 Specimen Strength and Spatial Results: 30mm Mixtures

40-30

Table A-1: Batch 40-30 individual specimen results

Beam	$f_{R,1}$ (MPa)	$f_{R,4}$ (MPa)	$f_{eq,2}$ (MPa)	$f_{eq,3}$ (MPa)	Homogeneity	Dispersion	N_f	Nakagami Parameters	
								Shape	Scale
1	4.32	3.91	4.14	4.22	61.25	6.01	358	1.43	37.32
2	3.49	3.95	3.30	3.86	69.88	7.06	335	1.35	43.11
3	4.86	5.78	4.93	5.76	62.21	7.86	326	1.28	46.02
4	4.69	5.33	4.51	5.23	62.64	6.10	373	1.36	37.59
5	4.83	4.52	4.87	5.07	62.00	6.34	372	1.36	39.44
6	4.04	4.03	3.46	4.07	70.79	7.23	322	1.36	42.71
7	4.17	5.35	4.14	5.17	70.34	7.08	326	1.38	44.14
8	4.32	4.90	4.10	4.93	60.38	5.73	371	1.49	38.87
9	4.48	4.82	4.05	4.82	64.99	6.72	343	1.47	43.38
Average	4.36	4.73	4.17	4.79	64.94	6.68	347.33	1.39	41.40
CoV	9.96	14.37	13.37	12.94	6.53	10.34	6.16	4.70	7.58

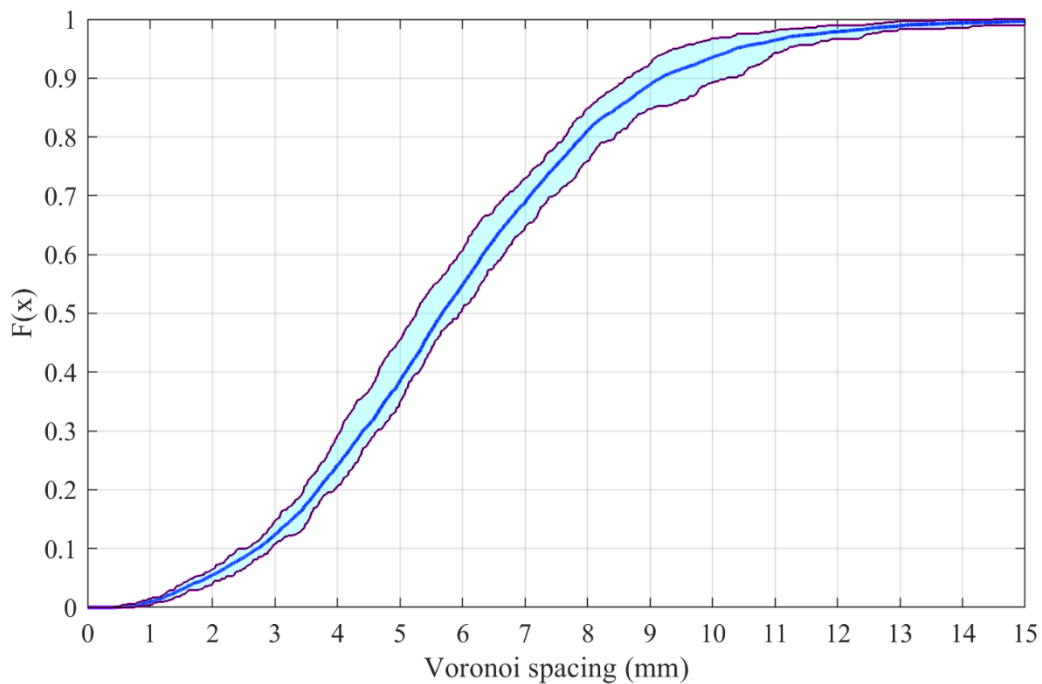


Figure A-15: Batch 40-30 average and envelope CDF of Voronoi spacing

60-30

Table A-2: Batch 60-30 individual specimen results

Beam	$f_{R,1}$ (MPa)	$f_{R,4}$ (MPa)	$f_{eq,2}$ (MPa)	$f_{eq,3}$ (MPa)	Homogeneity	Dispersion	N_r	Nakagami Parameters	
								Shape	Scale
1	8.01	6.47	7.24	7.36	63.93	4.96	529	1.20	27.35
2	5.99	6.25	6.18	6.57	52.26	4.20	575	1.30	24.92
3	5.11	4.38	4.65	4.94	52.34	4.83	525	1.35	29.25
4	7.85	5.91	6.60	7.45	54.34	4.31	575	1.26	24.60
5	6.35	4.59	5.28	5.78	59.51	5.26	441	1.28	29.85
6	5.17	4.40	4.45	4.96	68.49	6.25	455	1.16	31.98
7	8.14	5.51	7.31	7.00	65.06	5.67	470	1.18	31.26
8	6.91	5.17	6.01	6.20	51.99	4.94	478	1.35	31.09
9	6.58	4.80	6.20	5.96	58.46	5.18	462	1.38	31.67
Average	6.68	5.28	5.99	6.25	58.49	5.07	501.11	1.27	29.11
CoV	17.30	15.16	17.11	15.01	10.64	12.53	10.23	6.29	9.78

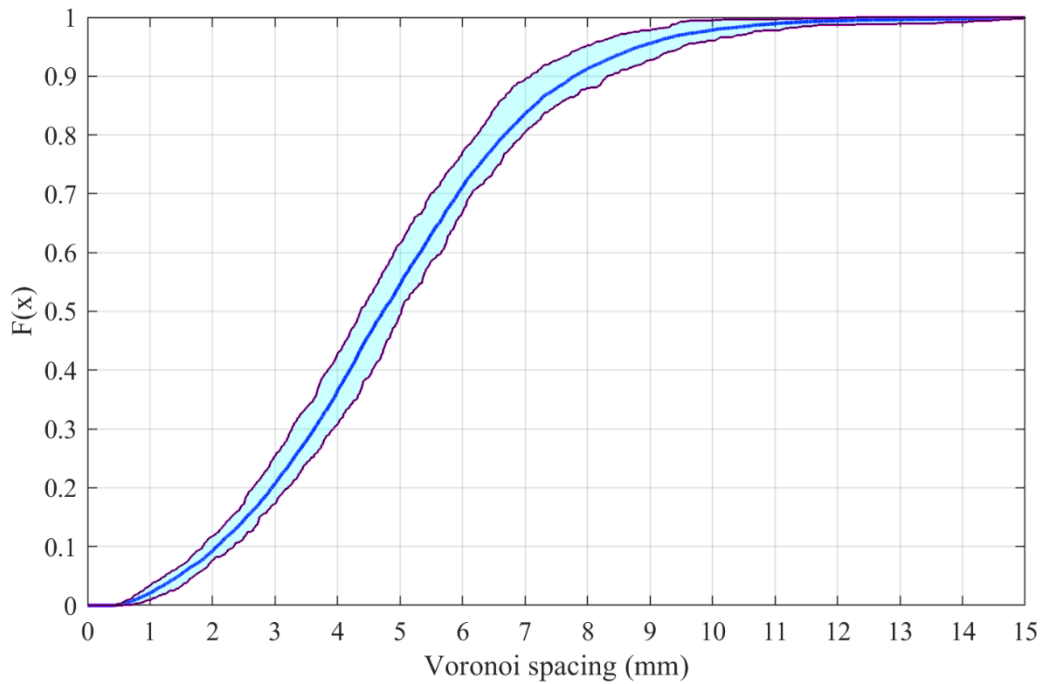


Figure A-16: Batch 60-30 average and envelope CDF of Voronoi spacing

80-30-a

Table A-3: Batch 80-30-a individual specimen results

Beam	$f_{R,1}$ (MPa)	$f_{R,4}$ (MPa)	$f_{eq,2}$ (MPa)	$f_{eq,3}$ (MPa)	Homogeneity	Dispersion	N_f	Nakagami Parameters	
								Shape	Scale
1	9.36	6.49	7.89	8.08	50.93	4.14	644	1.25	23.96
2	6.92	5.59	5.71	6.53	59.10	4.73	589	1.20	25.83
3	8.55	6.50	7.74	7.96	46.53	4.29	720	1.13	21.64
4	9.52	7.12	8.82	9.06	48.66	3.64	782	1.16	18.96
5	9.73	6.97	7.95	9.03	60.37	4.50	673	1.08	22.36
6	8.78	6.12	8.31	8.38	51.16	4.29	717	1.10	21.15
7	11.23	7.92	10.29	10.64	51.81	3.48	754	1.23	19.18
8	12.02	7.96	10.05	10.50	44.24	3.30	802	1.29	19.39
9	9.62	6.38	8.51	8.36	51.41	3.88	766	1.16	20.33
Average	9.53	6.78	8.36	8.73	51.58	4.03	716.33	1.18	21.42
CoV	15.54	11.65	16.14	14.65	10.22	12.02	9.73	6.07	10.85

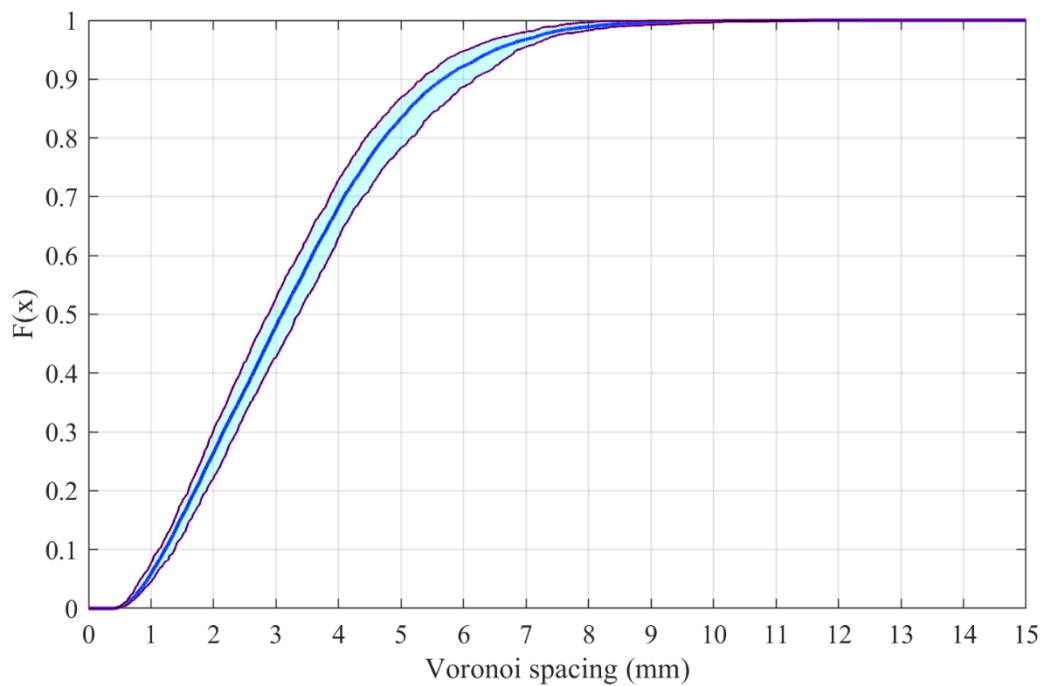


Figure A-17: Batch 80-30-a average and envelope CDF of Voronoi spacing

80-30-b

Table A-4: Batch 80-30-b individual specimen results

Beam	$f_{R,1}$ (MPa)	$f_{R,4}$ (MPa)	$f_{eq,2}$ (MPa)	$f_{eq,3}$ (MPa)	Homogeneity	Dispersion	N_f	Nakagami Parameters	
								Shape	Scale
1	10.35	6.83	8.11	8.79	52.57	3.93	677	1.21	21.74
2	8.35	5.42	7.07	7.18	58.31	3.86	695	1.21	21.03
3	9.20	7.49	7.32	8.24	56.97	4.11	633	1.32	24.26
4	8.14	7.57	7.52	8.15	52.03	4.41	590	1.30	26.04
5	7.93	6.65	6.61	7.64	53.67	4.06	642	1.29	23.31
6	9.67	6.11	8.12	7.89	61.44	4.36	746	1.03	20.42
7	8.67	6.61	7.49	7.80	56.15	3.97	765	1.06	19.36
8	7.84	5.31	6.22	7.01	49.69	3.97	654	1.28	23.02
9	8.74	6.67	7.09	7.82	51.53	4.08	699	1.20	21.69
Average	8.77	6.52	7.28	7.83	54.71	4.08	677.89	1.21	22.32
CoV	9.57	12.16	8.63	6.88	6.89	4.65	8.17	8.48	9.22

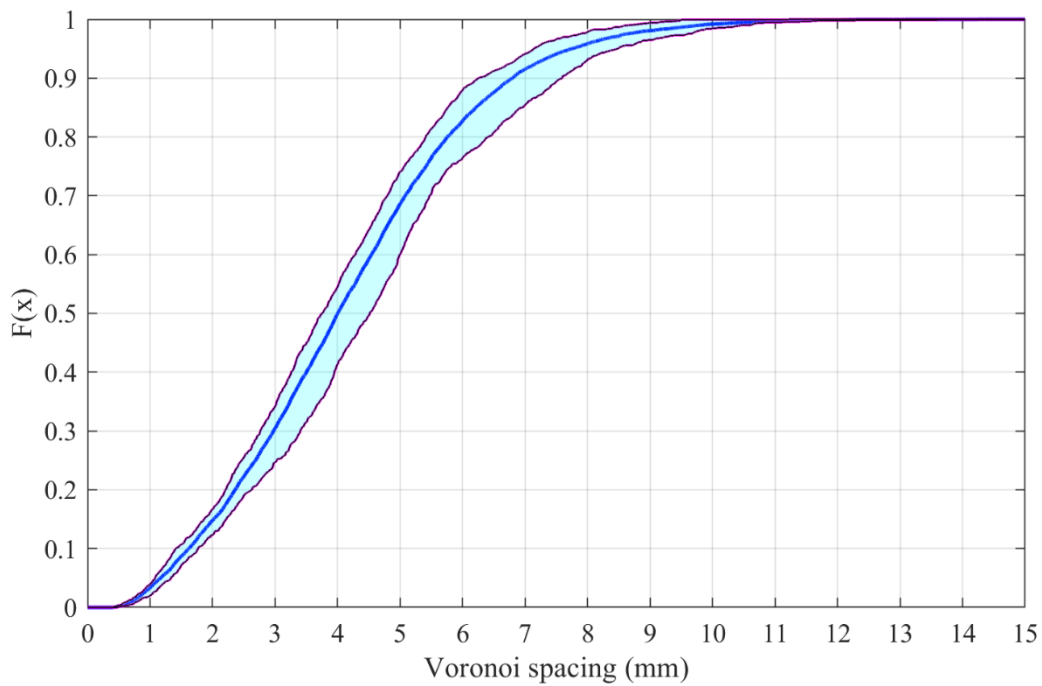


Figure A-18: Batch 80-30-b average and envelope CDF of Voronoi spacing

100-30

Table A-5: Batch 100-30 individual specimen results

Beam	$f_{R,1}$ (MPa)	$f_{R,4}$ (MPa)	$f_{eq,2}$ (MPa)	$f_{eq,3}$ (MPa)	Homogeneity	Dispersion	N_f	Nakagami Parameters	
								Shape	Scale
1	8.86	6.37	7.63	7.96	47.19	3.23	873	1.17	17.44
2	9.27	5.99	8.68	8.94	47.56	3.33	898	1.16	17.45
3	9.55	7.00	9.64	8.95	46.31	3.32	865	1.20	17.61
4	10.81	7.39	10.00	9.88	50.74	3.53	759	1.20	19.40
5	8.39	5.64	7.11	7.69	60.97	4.25	754	1.06	20.46
6	9.95	6.89	9.39	9.29	45.68	3.19	856	1.24	17.55
7	10.35	6.52	8.94	8.90	49.21	3.38	768	1.28	19.06
8	9.13	5.50	9.11	7.88	57.99	4.05	722	1.15	20.98
9	9.18	5.87	8.23	8.10	49.13	3.10	964	1.13	15.72
Average	9.50	6.35	8.75	8.62	50.53	3.49	828.78	1.18	18.41
CoV	7.96	10.26	10.81	8.66	10.60	11.43	9.79	5.36	9.15

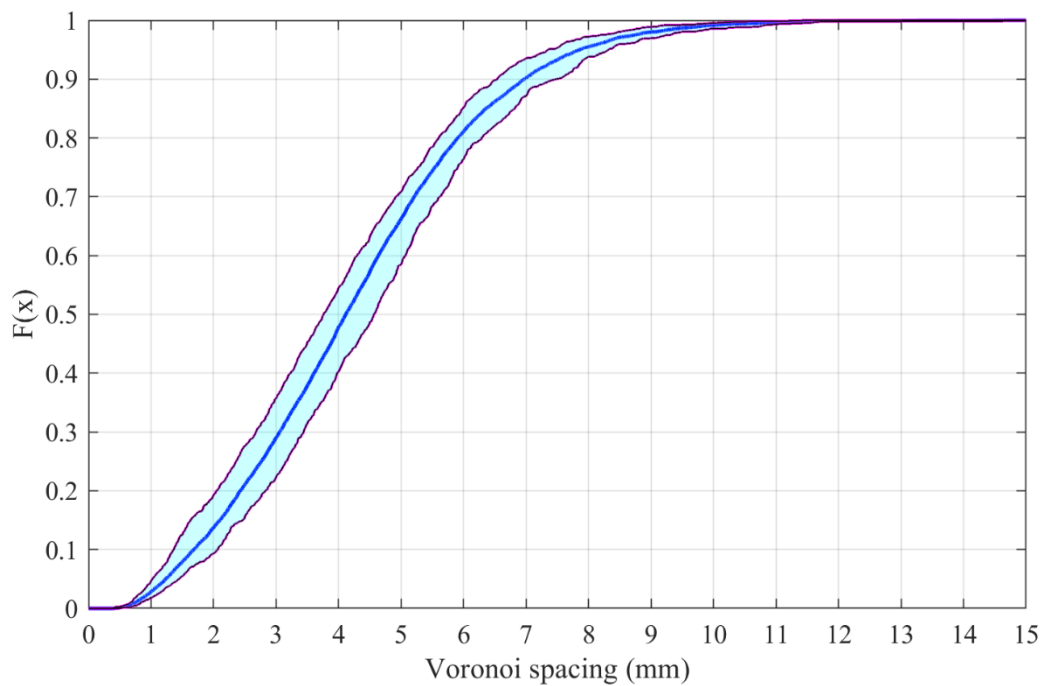


Figure A-19: Batch 100-30 average and envelope CDF of Voronoi spacing

120-30-a

Table A-6: Batch 120-30-a individual specimen results

Beam	$f_{R,1}$ (MPa)	$f_{R,4}$ (MPa)	$f_{eq,2}$ (MPa)	$f_{eq,3}$ (MPa)	Homogeneity	Dispersion	N_f	Nakagami Parameters	
								Shape	Scale
1	9.32	6.05	8.47	8.02	44.08	2.87	1077	1.14	14.71
2	10.23	7.41	10.85	9.67	45.91	2.73	1230	1.06	12.95
3	8.60	5.71	8.06	7.82	50.15	3.56	952	1.03	16.20
4	8.95	6.64	7.98	7.96	49.19	3.27	940	1.09	15.97
5	9.32	6.32	9.34	8.83	50.23	2.82	1038	1.13	14.68
6	8.76	5.29	8.96	7.81	57.95	3.45	932	1.01	15.83
7	9.00	5.90	8.82	8.04	54.73	3.23	982	1.03	15.15
8	8.24	5.96	8.28	7.83	48.17	2.85	1129	1.08	13.97
9	8.52	4.53	7.28	7.26	49.83	3.12	975	1.13	15.88
Average	8.99	5.98	8.67	8.14	50.03	3.10	1028.33	1.08	15.04
CoV	6.51	13.56	11.73	8.64	8.40	9.59	9.80	4.52	7.17

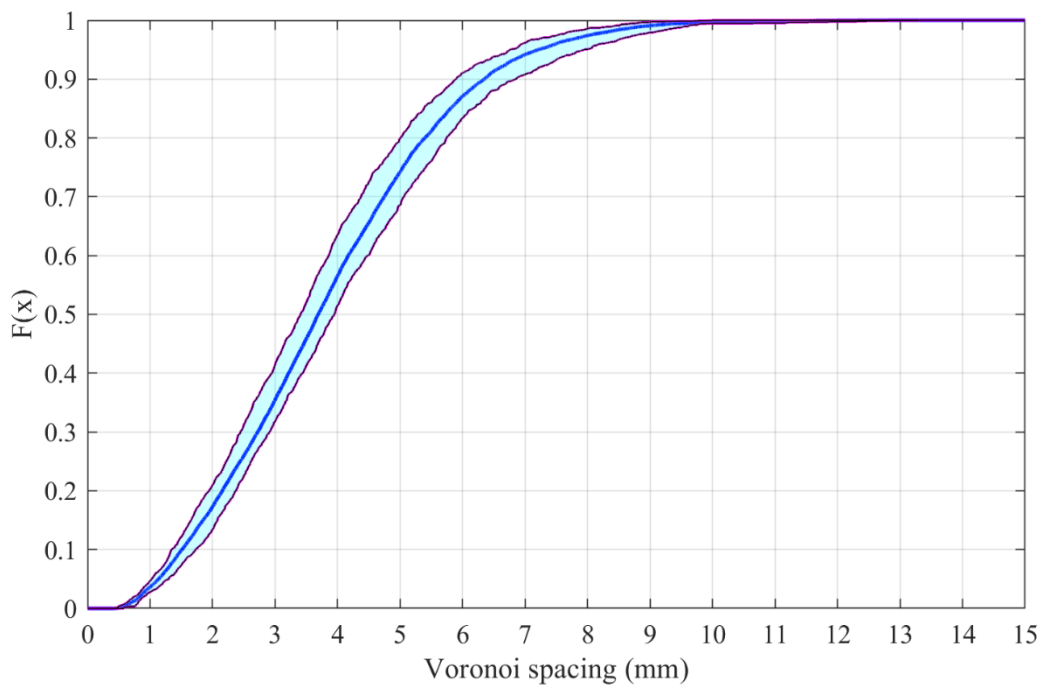


Figure A-20: Batch 120-30-a average and envelope CDF of Voronoi spacing

120-30-b

Table A-7: Batch 120-30-b individual specimen results

Beam	$f_{R,1}$ (MPa)	$f_{R,4}$ (MPa)	$f_{eq,2}$ (MPa)	$f_{eq,3}$ (MPa)	Homogeneity	Dispersion	N_f	Nakagami Parameters	
								Shape	Scale
1	-	-	-	-	-	-	-	-	-
2	10.60	7.83	10.57	9.86	50.58	3.50	989	1.03	16.16
3	10.88	7.97	9.98	10.02	44.08	2.96	1028	1.12	14.87
4	9.78	7.23	9.04	8.87	48.95	2.86	1226	1.01	12.78
5	11.42	9.07	11.15	10.87	49.30	2.63	1253	1.04	12.27
6	10.86	6.86	9.76	9.32	53.55	2.92	1024	1.01	12.89
7	10.38	6.98	9.86	9.57	49.21	3.15	986	1.05	14.98
8	9.21	7.32	8.88	8.82	45.41	3.17	1027	1.09	15.23
9	9.48	7.66	9.69	8.96	51.19	2.79	1176	1.04	12.58
Average	10.33	7.61	9.87	9.54	49.03	3.00	1088.63	1.05	13.97
CoV	7.43	9.28	7.53	7.36	6.22	9.00	10.16	3.67	10.71

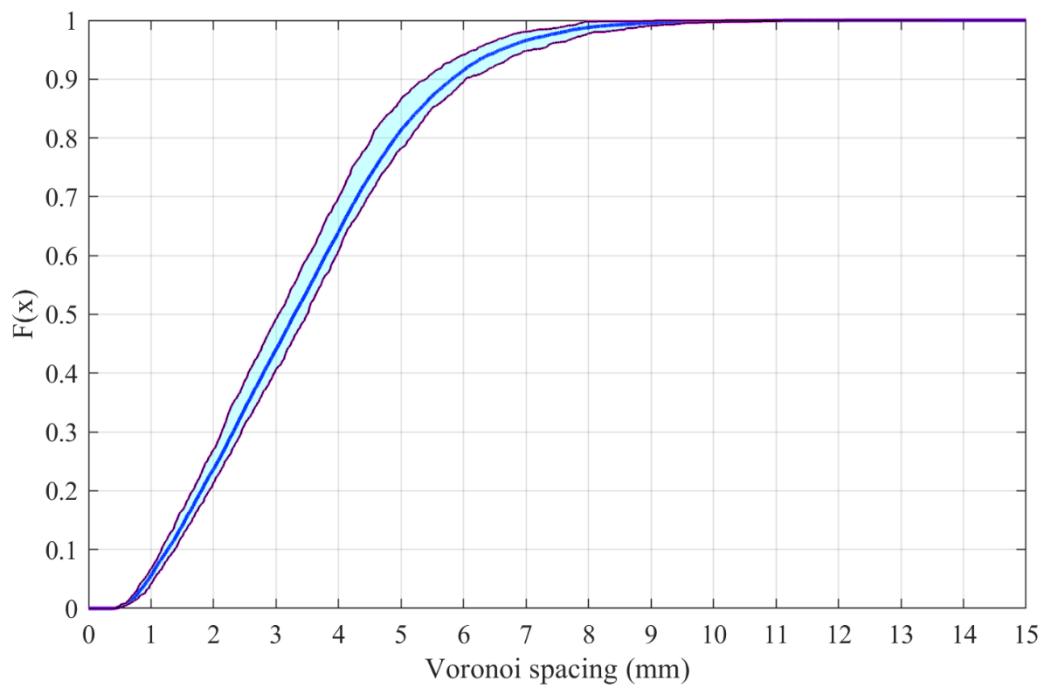


Figure A-21: Batch 120-30-b average and envelope CDF of Voronoi spacing

A.3 Specimen Strength and Spatial Results: 60mm Mixtures

40-60

Table A-8: Batch 40-60 individual specimen results

Beam	$f_{R,1}$ (MPa)	$f_{R,4}$ (MPa)	$f_{eq,2}$ (MPa)	$f_{eq,3}$ (MPa)	Homogeneity	Dispersion	N_f	Nakagami Parameters	
								Shape	Scale
1	6.31	5.55	6.38	6.04	83.28	13.54	156	1.61	93.98
2	3.99	5.17	3.74	4.73	94.21	16.33	96	2.05	143.05
3	6.33	5.93	5.00	6.13	106.81	14.96	111	1.81	124.20
4	4.14	5.38	4.00	4.91	93.80	17.55	134	1.42	109.45
5	4.41	5.11	4.31	4.87	113.38	14.34	134	1.46	95.84
6	3.35	4.20	3.11	3.99	127.19	24.74	95	1.36	144.22
7	3.65	4.97	3.46	4.53	126.83	29.85	92	1.32	164.54
8	3.45	4.58	3.27	4.27	96.23	20.13	122	1.41	117.49
9	3.58	4.41	3.43	4.16	97.44	17.95	128	1.42	110.83
Average	4.36	5.03	4.08	4.85	104.35	18.82	118.67	1.54	122.62
CoV	26.73	11.12	25.55	15.87	14.72	28.48	18.38	15.75	19.38

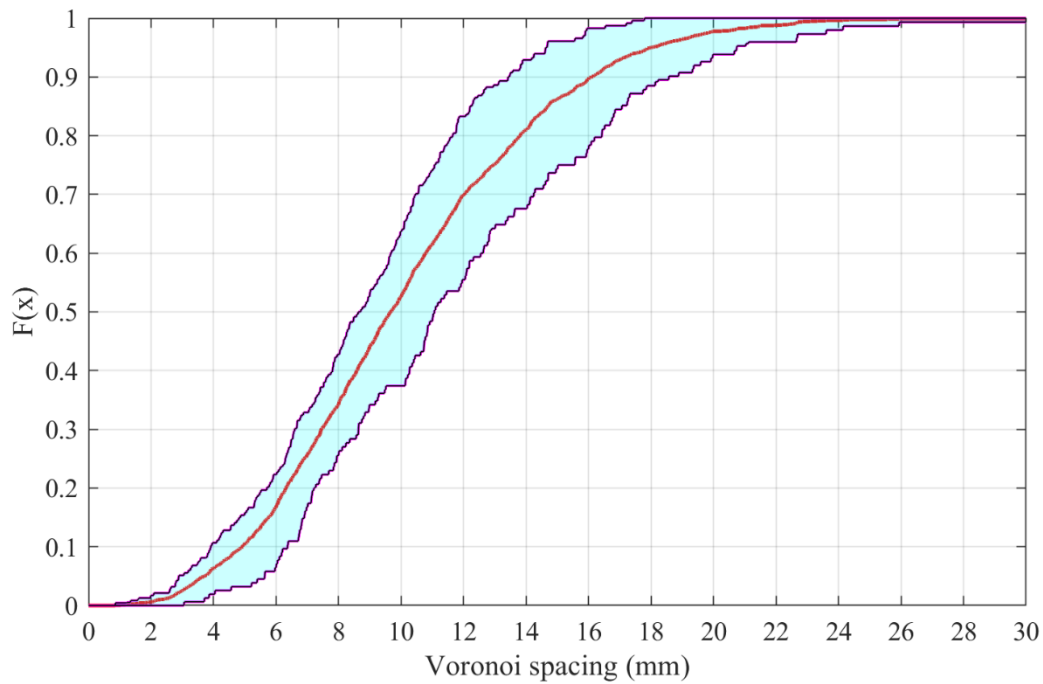


Figure A-22: Batch 40-60 average and envelope CDF of Voronoi spacing

60-60

Table A-9: Batch 60-60 individual specimen results

Beam	$f_{R,1}$ (MPa)	$f_{R,4}$ (MPa)	$f_{eq,2}$ (MPa)	$f_{eq,3}$ (MPa)	Homogeneity	Dispersion	N_f	Nakagami Parameters	
								Shape	Scale
1	5.87	6.12	5.43	6.17	100.44	16.70	133	1.46	102.60
2	7.77	8.11	8.21	8.61	92.70	11.17	209	1.38	68.86
3	4.81	5.03	4.60	5.21	110.34	19.46	136	1.38	116.34
4	6.59	8.28	6.59	7.76	86.33	13.53	226	1.10	65.84
5	7.25	7.72	7.59	7.81	91.66	12.83	177	1.37	76.96
6	6.31	6.24	5.58	6.36	76.53	10.56	205	1.49	72.64
7	7.37	6.97	6.25	7.34	96.65	14.32	179	1.26	76.90
8	3.56	4.02	3.18	3.88	89.59	11.41	160	1.66	83.06
9	4.61	4.35	4.17	4.64	86.74	17.10	142	1.49	105.62
Average	6.02	6.32	5.73	6.42	92.33	14.12	174.11	1.40	85.43
CoV	23.73	25.23	28.24	24.95	10.37	21.65	19.55	11.30	21.22

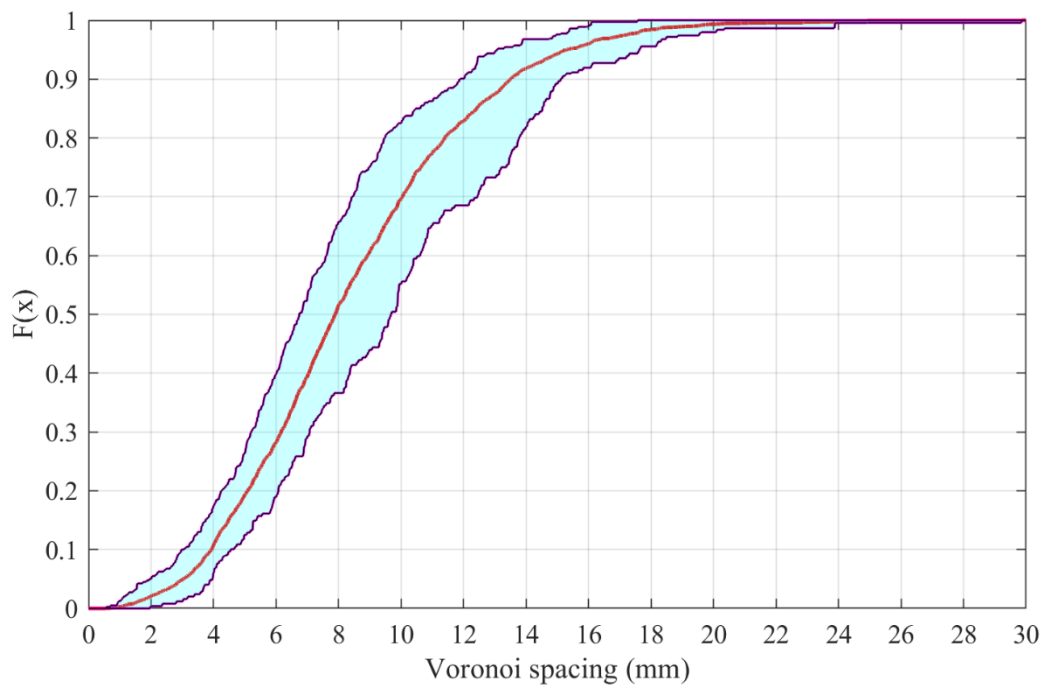


Figure A-23: Batch 60-60 average and envelope CDF of Voronoi spacing

80-60-a

Table A-10: Batch 80-60-a individual specimen results

Beam	$f_{R,1}$ (MPa)	$f_{R,4}$ (MPa)	$f_{eq,2}$ (MPa)	$f_{eq,3}$ (MPa)	Homogeneity	Dispersion	N_f	Nakagami Parameters	
								Shape	Scale
1	9.92	8.87	8.88	9.99	71.69	6.75	303	1.53	44.40
2	11.04	9.14	9.77	10.29	72.23	6.84	326	1.29	40.08
3	10.96	7.50	9.45	10.02	67.43	6.94	318	1.44	43.63
4	10.33	8.58	10.17	9.83	69.32	7.06	319	1.42	43.46
5	13.45	10.22	12.39	11.80	70.65	8.46	318	1.30	46.37
6	11.23	9.24	9.57	10.62	84.90	10.84	229	1.30	61.77
7	11.15	9.29	11.00	10.91	63.94	5.88	312	1.71	44.46
8	10.99	9.32	11.91	11.10	65.75	6.13	305	1.68	45.55
9	10.00	7.97	8.50	9.07	76.99	7.71	263	1.56	52.89
Average	11.01	8.90	10.18	10.40	71.43	7.40	299.22	1.47	46.96
CoV	9.47	9.02	13.07	7.73	8.89	20.31	10.74	10.91	13.89

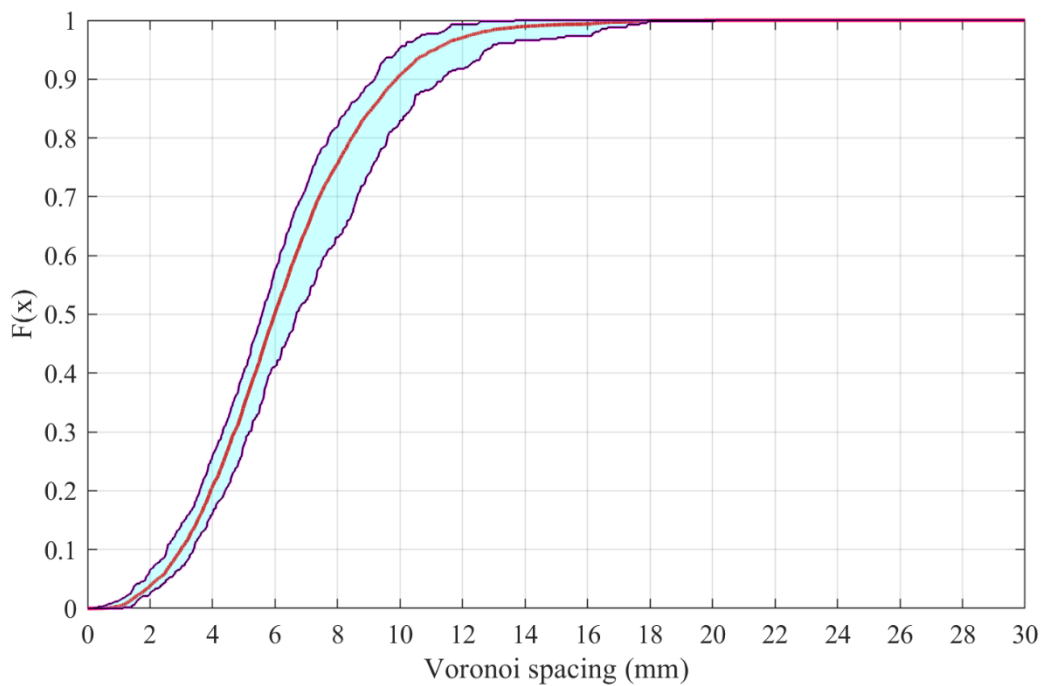


Figure A-24: Batch 80-60-a average and envelope CDF of Voronoi spacing

80-60-b

Table A-11: Batch 80-60-b individual specimen results

Beam	$f_{R,1}$ (MPa)	$f_{R,4}$ (MPa)	$f_{eq,2}$ (MPa)	$f_{eq,3}$ (MPa)	Homogeneity	Dispersion	N_f	Nakagami Parameters	
								Shape	Scale
1	10.73	8.51	10.04	10.13	78.36	8.92	306	1.21	48.17
2	6.70	6.69	5.31	6.67	93.10	11.78	168	1.48	77.43
3	9.71	8.26	9.14	9.05	79.05	11.60	186	1.42	74.74
4	8.09	8.03	6.53	8.17	86.62	12.62	190	1.35	76.73
5	10.32	10.15	9.63	10.91	88.07	11.98	227	1.17	59.95
6	10.48	9.18	10.17	10.72	77.67	10.19	273	1.26	55.03
7	7.97	8.62	6.86	8.44	95.68	10.26	220	1.31	59.25
8	8.57	7.65	7.35	8.47	94.15	12.92	173	1.46	86.34
9	10.93	8.66	9.42	10.21	76.98	7.78	282	1.40	48.56
Average	9.28	8.42	8.27	9.20	85.52	10.90	225.00	1.34	65.13
CoV	16.08	11.44	21.50	15.26	8.97	15.91	22.69	8.14	21.40

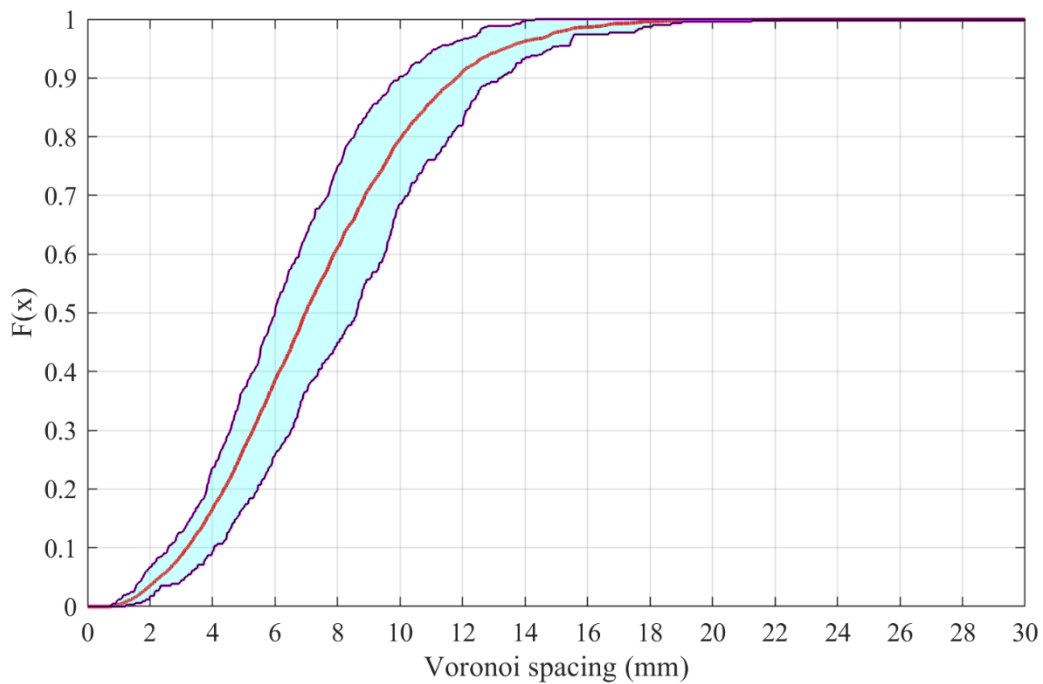


Figure A-25: Batch 80-60-b average and envelope CDF of Voronoi spacing

100-60

Table A-12: Batch 100-60 individual specimen results

Beam	$f_{R,1}$ (MPa)	$f_{R,4}$ (MPa)	$f_{eq,2}$ (MPa)	$f_{eq,3}$ (MPa)	Homogeneity	Dispersion	N_f	Nakagami Parameters	
								Shape	Scale
1	8.21	7.64	7.37	8.28	73.45	9.28	243	1.40	58.27
2	10.81	8.35	10.69	10.32	66.95	10.19	320	1.09	49.21
3	12.77	10.68	12.67	12.18	70.47	8.02	371	1.16	41.71
4	11.51	9.79	11.44	10.91	78.42	9.65	302	1.22	49.45
5	11.12	8.95	10.99	10.60	70.89	7.11	282	1.56	49.55
6	14.50	12.91	14.55	14.39	66.73	6.07	412	1.28	35.23
7	11.07	9.70	11.48	10.81	68.69	6.19	357	1.47	38.93
8	6.36	5.18	5.34	5.96	99.14	17.00	135	1.41	106.71
9	9.46	8.48	8.40	9.39	72.66	8.54	272	1.45	54.80
Average	10.64	9.08	10.32	10.31	74.15	9.12	299.33	1.34	53.76
CoV	22.60	23.46	27.36	22.94	13.54	36.18	27.14	11.75	39.40

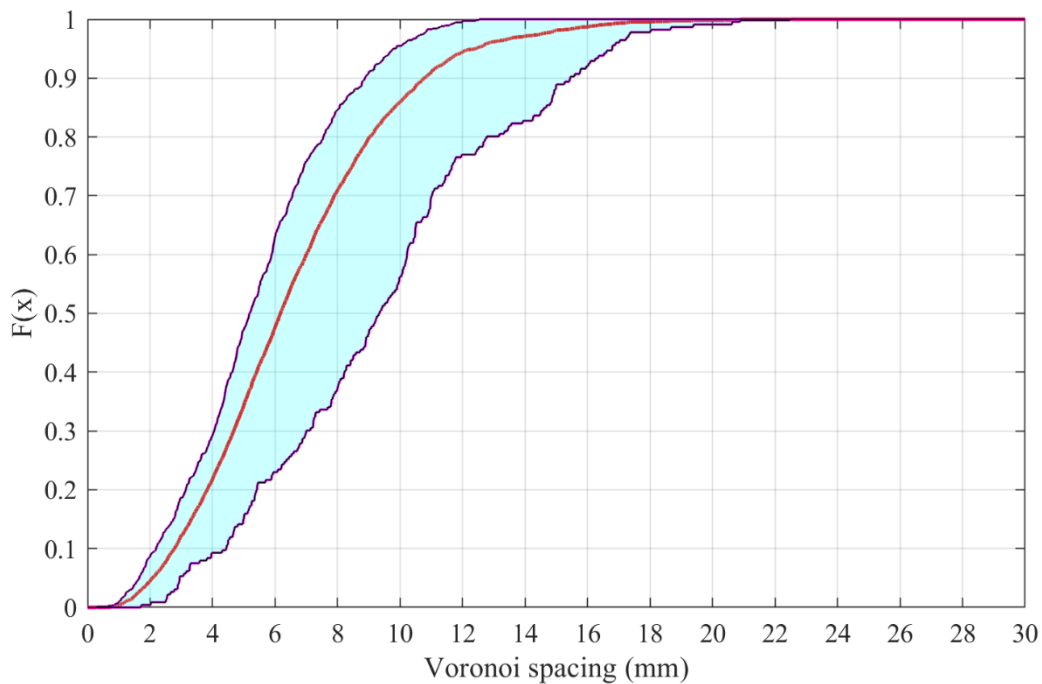


Figure A-26: Batch 100-60 average and envelope CDF of Voronoi spacing

120-60-a

Table A-13: Batch 120-60-a individual specimen results

Beam	$f_{R,1}$ (MPa)	$f_{R,4}$ (MPa)	$f_{eq,2}$ (MPa)	$f_{eq,3}$ (MPa)	Homogeneity	Dispersion	N_f	Nakagami Parameters	
								Shape	Scale
1	12.91	10.32	13.25	12.44	74.59	7.55	324	1.33	44.01
2	13.18	11.22	12.39	12.73	79.97	8.93	355	1.11	42.15
3	13.88	12.62	13.43	13.64	59.19	5.06	462	1.38	30.62
4	14.52	10.25	13.83	12.29	67.14	7.04	372	1.33	39.47
5	11.92	10.26	11.78	11.56	68.44	8.34	384	1.12	40.25
6	10.69	8.82	9.31	9.74	66.19	7.33	282	1.53	49.84
7	11.84	9.54	10.71	10.67	65.11	6.81	382	1.34	38.65
8	10.57	8.97	11.37	10.47	61.85	5.89	413	1.38	35.68
9	11.38	9.16	10.41	10.35	64.77	6.86	365	1.38	41.17
Average	12.32	10.13	11.83	11.54	67.47	7.09	371.00	1.32	40.20
CoV	11.24	12.00	12.93	11.34	9.41	16.49	13.73	10.09	13.26

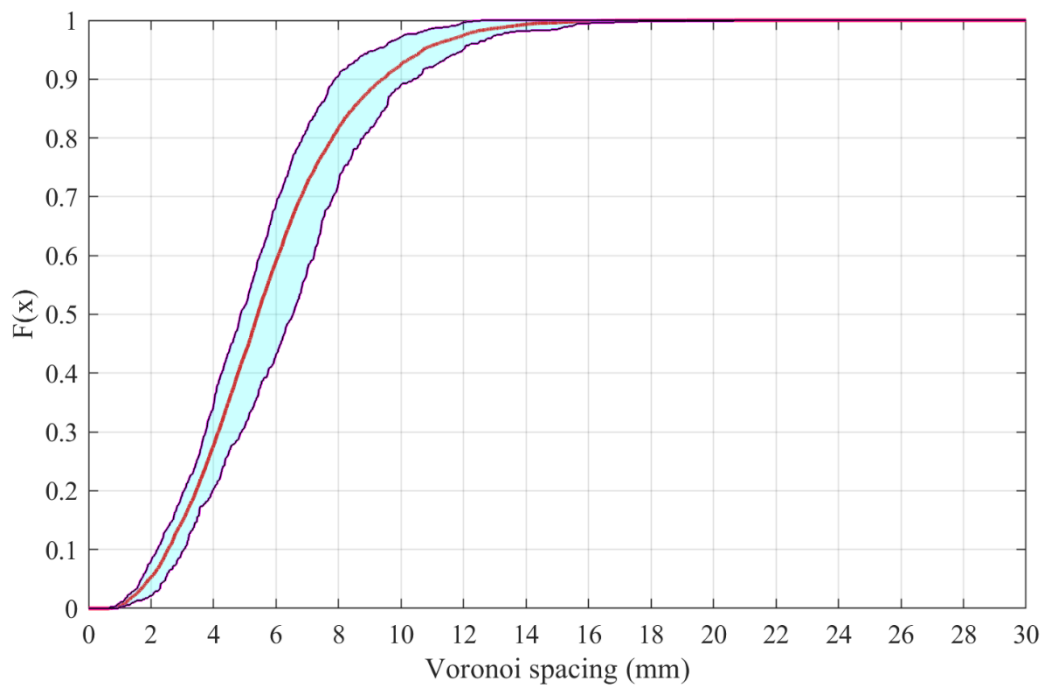


Figure A-27: Batch 120-60-a average and envelope CDF of Voronoi spacing

120-60-b

Table A-14: Batch 120-60-b individual specimen results

Beam	$f_{R,1}$ (MPa)	$f_{R,4}$ (MPa)	$f_{eq,2}$ (MPa)	$f_{eq,3}$ (MPa)	Homogeneity	Dispersion	N_f	Nakagami Parameters	
								Shape	Scale
1	12.14	8.94	10.87	10.72	69.87	7.54	261	1.62	53.45
2	10.24	8.27	11.32	9.80	75.49	7.35	354	1.29	40.35
3	14.14	13.51	14.02	14.27	62.40	5.24	425	1.46	33.57
4	13.30	12.90	12.84	13.28	72.43	6.52	423	1.15	33.99
5	12.34	12.23	11.12	12.62	72.22	6.88	357	1.30	39.53
6	13.51	10.89	12.17	12.36	56.90	5.63	426	1.38	32.51
7	10.95	9.03	9.46	10.05	82.56	9.31	245	1.35	54.15
8	12.54	10.30	12.72	11.87	70.03	6.61	401	1.19	35.32
9	10.83	9.11	10.05	10.12	60.82	5.82	407	1.43	35.55
Average	12.22	10.57	11.62	11.68	69.19	6.77	366.56	1.35	39.82
CoV	10.87	18.14	12.47	13.60	11.50	18.11	19.08	10.52	20.94

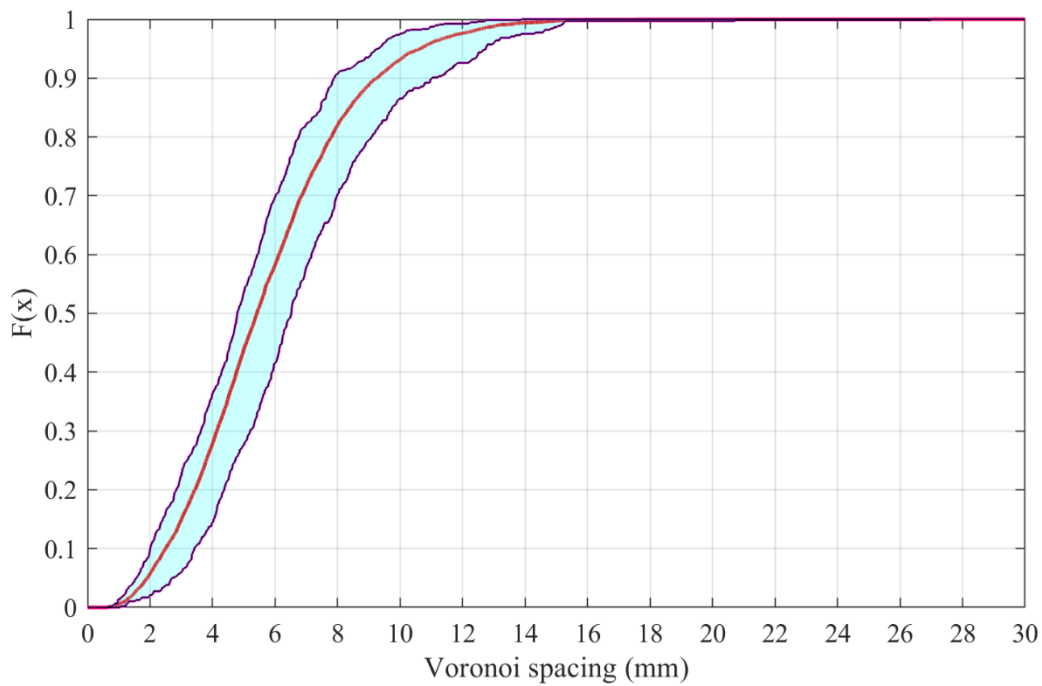


Figure A-28: Batch 120-60-b average and envelope CDF of Voronoi spacing

APPENDIX B - Batch 80-60-a Results

B.1 Chapter 4

Table B-1: Equivalent flexural strength and LOP results (Table 4-1)

$f_{ct,L}$		$f_{eq,2}$		$f_{eq,3}$	
Average (MPa)	CoV (%)	Average (MPa)	CoV (%)	Average (MPa)	CoV (%)
7.22	9.67	10.18	13.07	10.4	7.73

Table B-2: Residual flexural strength results (Table 4-2)

$f_{R,1}$		$f_{R,4}$	
Average (MPa)	CoV (%)	Average (MPa)	CoV (%)
11.01	9.47	8.9	9.02

Table B-3: Average of fibre count and spatial CDF parameter results (Table 4-3)

N_f	α_{95} (mm)	α_{50} (mm)	α_5 (mm)	Slope (ξ)
299	10.9	6	2.3	0.142

B.2 Chapter 5

Table B-4: Results from fibre distribution analysis using standardised grid spacing (Table 5-1)

Mean Grid Size	Mean $n_{f,std}$	Mean Variance of $n_{f,std}$	$n_{f,std}$ CoV (%)	Density (Fibres/mm ²)
8.8	3.8	6.1	64.4	0.0134

Table B-5: Results of fibre distribution analysis using grid sizes of 2x2 and 10x10 (Table 5-2)

2 x 2 Roster			10 x 10 Roster		
Mean n_f	Mean Variance of n_f	Mean n_f CoV (%)	Mean n_f	Mean Variance of n_f	Mean n_f CoV (%)
74.3	188.6	18	2.97	4.46	71.43

Table B-6: Variation in the fibre homogeneity of a batch of specimens (Table 5-3)

Standard deviation of homogeneity
6.35

Table B-7: Results of fibre dispersion and Nakagami fit parameters from Voronoi spacing data (Table 5-4)

N_f	Shape parameter	Scale parameter	Mean Voronoi spacing (mm)	Dispersion	Variance of dispersion
299	1.418	45.8	6.28	7.4	2.26

Table B-8: Mean degree of clustering for each batch (Table 5-5)

Degree of Clustering (CL_{Vor})	z
491	-1.64

B.3 Chapter 6

Table B-9: Mean equivalent fibre resistance for each batch (Table 6-1)

N_f	$N_{f,30}$	τ_{eq} (kPa/fibre)	Degree of Clustering (CL_{Vor})
299	862	11.88	491